STUDIES ON MYCOBACTERIAL GENES REQUIRED FOR GROWTH AND VIRULENCE

by

HAYLEAH PICKFORD

A thesis submitted to the

University of Birmingham

for the degree of

DOCTOR OF PHILOSOPHY

School of Biosciences

College of Life and Environmental Sciences

University of Birmingham

September 2019

DECLARATION

The work presented in this thesis was carried out in the School of Biosciences at The University of Birmingham, UK., B15 2TT during the period September 2016 to September 2019. The work in this thesis is original except where acknowledged by references.

No part of the work is being, or has been submitted for a degree, diploma or any other qualification at any other University.

ABSTRACT

Mycobacterium tuberculosis is the causative agent of tuberculosis, an infectious disease that is the cause of most deaths due to a single infectious pathogen. Approximately one quarter of the world's population is latently infected with *M. tuberculosis*, and may serve as a potential reservoir for reactivation and subsequent further infection**.** There is an increased prevalence in multidrug resistant tuberculosis, and a vulnerability of immunocompromised individuals to *M. tuberculosis* infection. Therefore, the need for to further knowledge on mycobacterial growth and virulence is imperative in the development of new antitubercular therapies and drugs.

Mycobacteria differ from some other well-studied rod-shaped bacteria, such as *E. coli* and *B. subtilis*, in that they incorporate new cell wall material at the cell poles, as opposed to the whole cell length. Additionally, mycobacteria lack homologues of numerous conserved cell division proteins present in laterally elongating rod-shaped bacteria. Research has begun to elucidate the role of these genes that drive and regulate cell elongation and division. In this study numerous deletion strains were constructed, based on sequence and structural homology with known cell growth and division proteins in other microorganisms, with the aim to delineate their potential roles in mycobacterial elongation and division. The deletion of *sepIVA*, encoding a DivIVA-domain containing protein, and the coiled-coil *MSMEG_4306* in *M. smegmatis* resulted in an elongated phenotype, suggesting a potential role in cell division. The *M. smegmatis* interacting partners of SepIVA were explored and were found to be involved in a variety of biosynthetic processes, including lipid biosynthesis and cell elongation and division.

This study also aimed to determine the potential immunological differences between wildtype *M. tuberculosi*s and an *M. tuberculosis* deletion strain, Δ*kasB*, which demonstrates an altered colony phenotype and mycolic acid profile upon deletion. Δ*kasB* is also highly attenuated in a mouse infection model. Cytokine production and mRNA expression analysis were utilised to investigate the innate immune response following bone marrow-derived macrophage infection with Δ*kasB*; IL-1β was produced in significantly greater quantities, yet IL-1β expression was significantly lower when compared to wildtype *M. tuberculosis*.

This thesis is dedicated to my family.

ACKNOWLEDGEMENTS

I would like to take this opportunity to thank all of the people who have made this thesis and the work behind it possible. Firstly, I would like to express my sincere gratitude to my supervisor, Dr Apoorva Bhatt, for welcoming me into his research lab, and granting me with the opportunity to carry out this project. I am thankful for his continual support, guidance and enthusiasm throughout my PhD journey. I would also like to thank Dr Luke Alderwick for the helpful input during my progress meetings, and Prof. Gurdyal Besra for the opportunity to be a member of the research group.

A very big thank you to every single Besra lab member, past and present; you welcomed me into the lab and provided a fun, supportive, food-filled environment throughout my three years at University of Birmingham. A special thank you goes to Albel Singh; thank you for being there whenever I need to utilise your wisdom and experience with my experiments, for never complaining, and for being cheerful every single day.

I would like to thank the BBSRC for funding my studies, and MIBTP for granting me a position in their 2015 cohort. I would also like to acknowledge collaborators of this work, for your help and wisdom; Gabriella Kelemen and Emily, for your work on the Δ*sepIVA* fluorescence microscopy and septation study. Also to Margarida Saraiva, Jeremy, Leandro, Kaori and Baltazar, for all of your help with the Δ*kasB* work, and the welcoming environment that you provided in the I3S laboratory.

A very special thank you to Richard for reminding me of what I am working so hard towards, and for your constant encouragement. I am immensely grateful to my family; none of this would have been possible without your ceaseless support and love.

TABLE OF CONTENTS

LIST OF FIGURES

CHAPTER 1

CHAPTER 2

CHAPTER 3

CHAPTER 4

CHAPTER 5

LIST OF TABLES

LIST OF ABBREVIATIONS

ACC – acyl-CoA carboxylase
ACCases – acyl-CoA carboxylases
AIM2 - absent in melanoma 2
APC- antigen presenting cells
BCG - Bacille Calmette-Guerin
BDL - below detection limit
BMDM - bone marrow derived macrophages
CDMEM - complete Dulbecco's Modified Eagle Medium
CFU - colony forming units
CoA – coenzyme A
DAT - diacyl trehalose
DTT – dithiothreitol
ELISA - enzyme-linked immunosorbent assay
FAS - fatty acid synthase
FBS - fetal bovine serum
HIV - human immunodeficiency virus
HSD - honestly significant difference
IFN-g - interferon-g
IL-1β - interleukin-1β
IL-12 - interleukin-12
IMD - intracellular membrane domain
iNOS – inducible nitric oxide synthase
LAMP - lysosome-associated membrane proteins
LB - Luria-Bertani
LCCM - L929-cell conditioned medium
LPS - lipopolysaccharide
mAGP - mycolyl arabinogalactan-peptidoglycan
Mincle - macrophage inducible C-type lectin
MDR-TB - multi-drug resistant tuberculosis
MOI - multiplicity of infection
MP - mycobacteriophage
MTBC - *Mycobacterium tuberculosis* complex
NK - natural killer
NI - non-infected
NLRP3 - NOD-, LRR and pyrin domain-containing protein 3
NO - nitric oxide
NTM - nontuberculous mycobacteria
OADC - oleic albumin dextrose catalase
PAMP - pathogen associated molecular pattern
PAT - polyacyl trehalose
PBP - penicillin-binding protein
PBS - phosphate buffered saline
PCR - polymerase chain reaction
PDIM – pthiocerol dimycocerosate
PG - peptidoglycan
PGL – phenolic glycolipid
PI - propidium iodide
PIMs - phosphatidylinositol mannosides

PRR – pattern recognition receptor
RNI – reactive nitrogen intermediates
ROI - reactive oxygen intermediate
RR-TB - rifampicin resistant tuberculosis
RT-PCR - real-time polymerase chain reaction
SCID - severe combined immunodeficient
Scy - *Streptomyces* cytoskeletal element S
DS - sodium dodecyl sulfate
SDS-PAGE - sodium dodecyl sulfate polyacrylamide gel electrophoresis
SEM - scanning electron microscopy
SL - sulfolipid
SL-1 - sulfolipid-1
SNP - single nucleotide polymorphism
SSC - saline-sodium citrate
TAE - Tris-acetate EDTA
TDM - trehalose dimycolate
TEM - transmission electron microscopy
TFB1 - transformation buffer 1
TFB2 - transformation buffer 2
Th1 - type 1 T helper
TIPOC - tip organising centre
TMM - trehalose monomycolate
TNF-α - tumour necrosis factor- α
TSB - tryptic soy broth
UV - ultraviolet
Van-FL - fluorescent vancomycin
XDR-TB - extensively drug resistant tuberculosis

PUBLISHED WORK ASSOCIATED WITH THIS THESIS

Pickford, H., Alcock, E., Singh, A., Kelemen, G. & Bhatt, A., 2020. A mycobacterial DivIVA domain-containing protein involved in cell length and septation. *Microbiology*. 2020 Sep;166(9):817-825

CHAPTER 1

General Introduction

1.1 Mycobacteriaceae

Mycobacteriaceae are a family of non-spore forming, aerobic rod-shaped bacteria, belonging to the Actinobacteria phylum, with a characteristically complex cell wall, conveying their hallmark acid-fast phenotype, and impervious nature to Gram-staining (Figure 1.1). Some lipids of the cell envelope are distinct to *Actinomycetes* members, such as *Corynebacterium*, *Rhodococcus* and *Nocardia*, all of which possess high genomic proportion of guanine and cytosine. Mycobacteria are typically divided into two groups, based on their growth rate; most mycobacterial species can be classified as rapidly growing, widespread, environmental soil-dwelling saprophytes. Some belong to the nontuberculous mycobacteria (NTM) species, defined as mycobacterial pathogens that do not belong to the *Mycobacterium tuberculosis* complex (MTBC), and also excluding *Mycobacterium leprae*, that are able to cause disease (Hoefsloot *et al*., 2013). NTMs have been well recognised as a cause of human disease since the 1950s (Lewis *et al*., 1960), yet they pose a serious risk to human health, due to their high level of innate antimicrobial resistance, and their prominence in patients with underlying disease (Tortoli, 2009). Slow growing mycobacteria include numerous human and veterinary pathogens, including the tuberculosis causing members of the MTBC, consisting of *Mycobacterium tuberculosis, Mycobacterium bovis, Mycobacterium africanum, Mycobacterium microti, Mycobacterium cannettii*, and the more recently recognised *Mycobacterium pinnipedii* and *Mycobacterium caprae* (Koch, 1882; Karlson & Lessel, 1970; Wells *et* al., 1937; Cousins *et al*., 2003; Aranaz *et al*., 2003). Whilst members of the MTBC display differential phenotypic characteristics, host preferences and pathogenicity, they share greater than 99.9% sequence similarity; between two members of the MTBC, there are no more than 2,500 single nucleotide polymorphism (SNPs). This suggests that members evolved from a single ancestor, resulting from an evolutionary bottleneck approximately 20,000 years ago (Sreevatsan *et al*., 1997). It has only recently been determined, through whole genome

comparative sequencing and genetic analysis that *Mycobacterium canetti* could represent the most ancestral lineage of the MTBC (Brosch *et al*., 2002; Fabre *et al*., 2004).

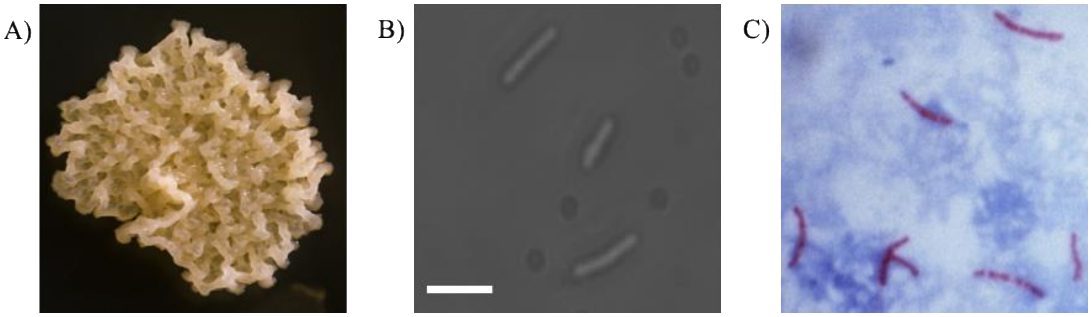

Figure 1.1. *Mycobacterium* growth phenotype. (A) A colony of *Mycobacterium smegmatis*. (B) Light micrograph of *M. smegmatis* (scale bar 5μm). (C) *M. tuberculosis* subject to acid-fast Ziehl-Neelson staining at magnification 1000X. Adapter from Centers for Disease Control and Prevention.

1.2 Tuberculosis and epidemiology

M. tuberculosis was discovered as the causative agent of tuberculosis by Robert Koch in 1882 (Koch, 1982). It is however, a disease of antiquity, with a prolific history; archaeological evidence documenting of tuberculosis in Egyptian mummies dates back over 5,000 years (Morse, 1964)**.** Since its discovery, tuberculosis has become the leading cause of death from a single infectious agent, resulting in approximately 10.4 million new cases in 2016, and an estimated 1.8 million deaths the year previous (World Health Organization, 2016). Tuberculosis is a disease associated with poverty, enhanced by poor living conditions such as overcrowding and poor hygiene, with areas such as these commonly lacking easily available drug therapy (Figure 1.2). Tuberculosis however is not a discriminatory pathogen, and is not restricted to these areas, with high population densities in developed countries also susceptible, due to the human-to-human transmission of *M. tuberculosis* via air droplets. Tuberculosis is predominantly a pulmonary disease, causing localised infection in the lungs. An individual

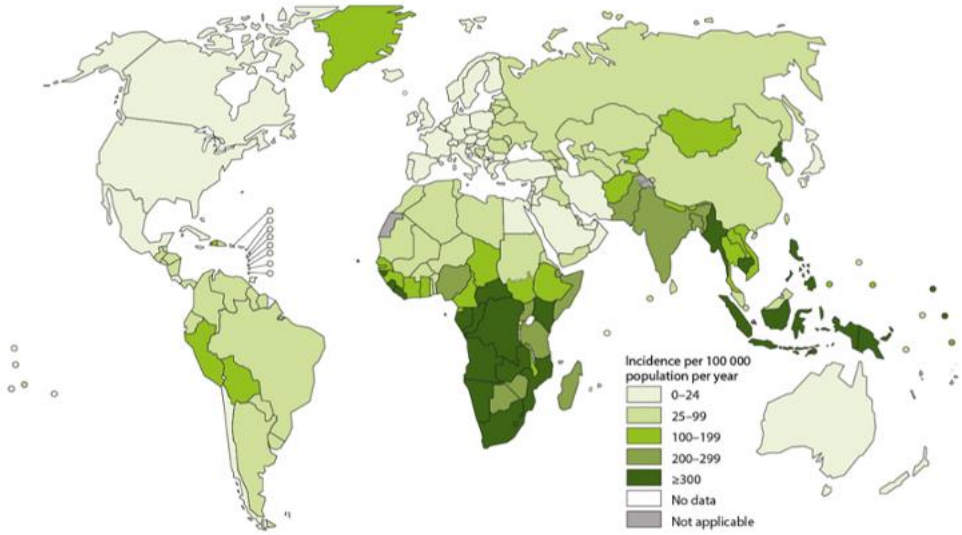

Figure 1.2. Map showing the global incidence of *M. tuberculosis* in 2017. Used with permission from World Health Organization Global Tuberculosis Report, 2017.

with active pulmonary tubercular disease will display non-specific general symptoms, such as weight loss, a productive cough, with or without haemoptysis, malaise and fever, and have the potential to spread disease. Tuberculosis can also affect sites other than the lungs (i.e., bones and joints, abdomen and lymph nodes) termed extrapulmonary tuberculosis. Tuberculosis can exist in two forms, latent or active disease. It has been estimated that 5-10% of individuals will develop active tubercular disease following the first exposure to *M. tuberculosis* (Lin & Flynn, 2010) (Figure 1.3); these individuals, unable to mount an effective immune response against the pathogen, then become a source of potential transmission of *M. tuberculosis*. The majority (approximately 90%) of individuals infected with *M. tuberculosis* are able to mount an immune response capable of eradicating or controlling bacilli growth. In the case of bacterial containment, a collection of immune cells are recruited to the site of infection, which are able to limit bacterial replication and subsequently prevents systemic infection. The bacilli held in check at the centre of this immune cell complex, termed the granuloma. The granuloma may

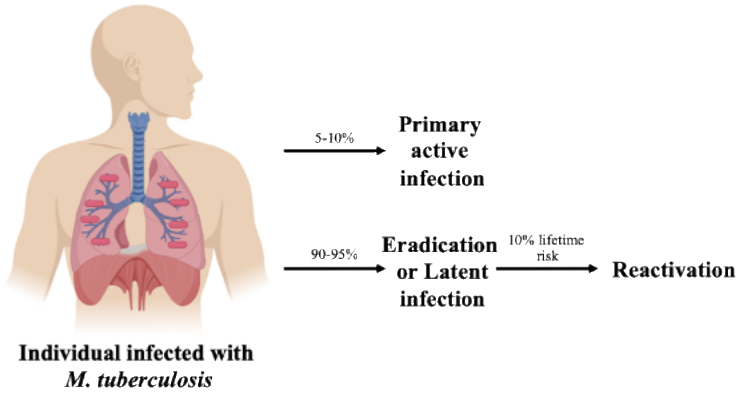

Figure 1.3. The potential outcomes following pulmonary infection with *M. tuberculosis*. Following inhalation of *M. tuberculosis* bacterial cells, bacilli are subsequently phagocytosed by resident alveolar macrophages. Of those infected, only 5-10% of infection cases will develop active disease. In the majority of cases, approximately 90% of healthy individuals infected, the host is capable of mounting an immune response that eradicates or controls bacilli growth. In the case of granuloma development, in which immune cells are recruited to the site of infection, bacterial cell replication is limited, as the granuloma is able to contain the bacilli, preventing subsequent systemic infection. *M. tuberculosis* bacilli are, however, not eradicated. These cells can serve as a reservoir for reactivation and the development of active disease; if there were an imbalance in the host's immune response to the containment of *M. tuberculosis* in the granuloma, bacilli may disseminate from this site and potentially cause tubercular disease.

serve as a reservoir for potential reactivation and the development of active disease; if there were an imbalance in the host's immune response, bacilli may disseminate from this site and potentially cause tubercular disease. Reactivation occurs in approximately 10% of individuals infected with *M. tuberculosis*.

Latency is a hallmark of tuberculosis infection, in which the individual remains asymptomatic and is not infectious. It is assumed that the bacilli are held in check by the host immune response, with an equilibrium established between pro- and anti- inflammatory factors (Lin & Flynn, 2010). It is approximated that 2 billion individuals worldwide are latently infected with *M. tuberculosis* (World Health Organization, 2014), with the risk of infection greatly increased in immuno-compromised individuals. Those latently infected will serve as a potential reservoir of disease if the infection were to re-activate, such as in the case of an individual receiving chemotherapy treatment, or a latently infected individual with a co-infection of human immunodeficiency virus (HIV), whereby the cell-mediated immune

response is compromised. HIV and *M. tuberculosis* co- infection results in an increased reactivation risk, with one quarter of HIV deaths as a result of tuberculosis (World Health Organisation, 2009).

1.3 The mycobacterial cell wall

The cell wall of mycobacteria are lipid-rich, and complex in the diverse genus-specific lipids that it contains; approximately 60% of the weight of the cell wall is composed of lipids, and conveys low permeability to hydrophilic agents, due to its hydrophobicity **(**Minnikin, 1982). The core cell wall structure of mycobacteria is termed the mycolyl arabinogalactan-peptidoglycan (mAGP) complex (Figure 1.4). The mAGP complex is composed of an inner peptidoglycan (PG) layer, covalently linked with arabinogalactan that is in turn esterified by long chain mycolic acids.

1.3.1 Mycolic acids

Mycolic acids are comprised of a β-hydroxyl fatty acid, termed the meromycolate branch, with a long α-alkyl side chain (Figure 1.5). Modifications within the meromycolate branch give rise to numerous mycolic acid subsets (Figure 1.5). This mycolic acid layer forms the inner leaflet of an outer lipid bilayer with a number of noncovalently bound glycolipids (Lea-Smith *et al*., 2007). Mycolic acids vary in length, ranging from C_{60} to C_{90} (Barry *et al*., 1998) and are highly abundant in the mycobacterial cell wall. The biosynthesis of mycobacterial mycolic acids is a complex process consisting of numerous sub-pathways,

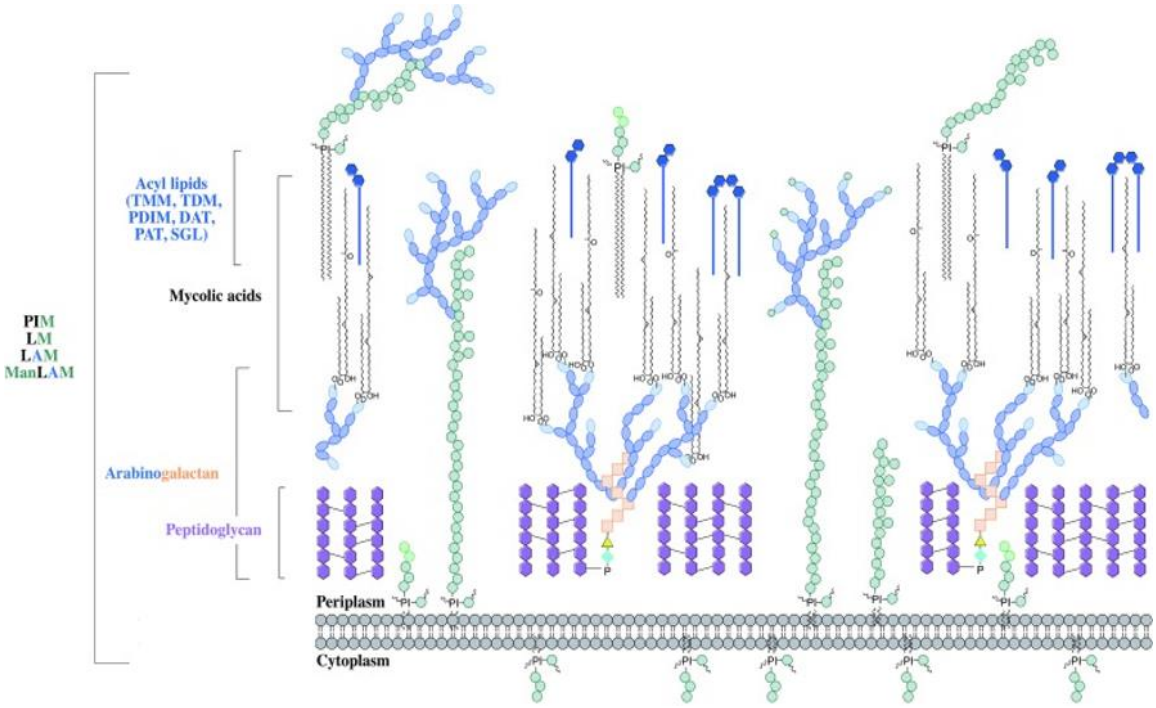

Figure 1.4. The mycobacterial cell envelope. The mycobacterial cell envelope is comprised of three major layers. The first innermost layer is the cytoplasmic membrane, a phospholipid bilayer. The core of the cell envelope, termed the mAGP is composed of the peptidoglycan layer, covalently bound to arabinogalactan, further esterified to the mycolic acid layer. This latter is the inner layer of the mycomembrane, with the outer section being the diverse, non-covalently bound glycolipids, in addition to carbohydrate and protein. TMM, trehalose monomycolate; TDM, trehalose dimycolate; PDIM:, phthiocerol dimycocerosates; DAT, diacyl trehalose; PAT, polyacyl trehalose; SGL, sulfoglycolipid; PIM, phosphatidyl-*myo*-inositol mannosides; LM, lipomannan; LAM, lipoarabinomannan; ManLAM, mannosylated lipoarabinomannan. Used with permission from Abrahams, K. A. *et al*., 2018.

producing key products that are ultimately utilised in the synthesis of mature MAs. Acetyl-CoA, produced as a result of carbohydrate and lipid breakdown, is carboxylated by acetyl CoA carboxylase, in an irreversible reaction, to form malonyl-CoA. Malonyl-CoA is an important substrate in fatty acid synthesis, and feeds into the two fatty acid synthase (FAS) systems, FAS- I and FAS-II. The FAS-I system is responsible for the *de novo* synthesis of fatty acids, key components for the subsequent biosynthesis of complex mycobacterial lipids. These chains can be further be extended by the FAS-II system, responsible for the elongation of these fatty acids to their full chain length of $C_{54\text{-}60}$ (Takayama *et al*., 2005). Condensation of the $C_{54\text{-}60}$ chain, with the shorter α-alkyl chain, catalysed by the polyketide synthase, Pks13 (Portevin, D. *et al*., 2004), results in mycolic acid precursors, which can then be further modified, for

example, through the introduction of functional group, or the insertion of double bonds, and finally reduced to produce mature MAs. Other members of the Actinomycetales order, such as *Nocardia* and *Corynebacteria*, also synthesise and produce mycolic acids, but at a much smaller length than mycobacterial mycolic acids, at $C_{40\text{-}60}$ and $C_{22\text{-}36}$ respectively (Tomiyasu, 1982; Collins *et al*., 1982). Additionally, whilst *Corynebacteria* mutant strains failing to synthesise mycolic acids grow at a reduced rate, their survival is not affected, indicating that they are non-essential (Portevin *et al*., 2005); in contrast, mycobacterial mycolic acids are essential for survival, confirmed in the inability to construct mutant mycobacterial strains that are devoid in mycolic acids (Vilchèze *et al.*, 2000; Portevin *et al*., 2004).

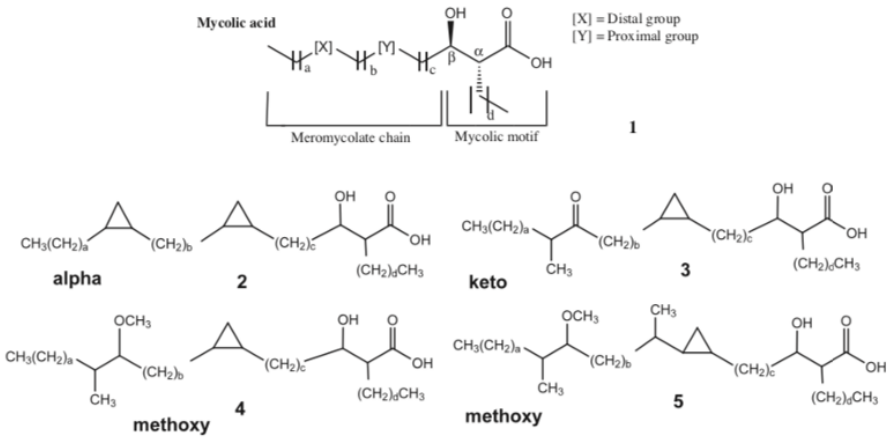

Figure 1.5. Mycolic acid structure and major mycolic acid classes. General mycolic acid structure with a-d representing methylene chains of various length; 2-5: The structure of major mycolic acid classes of *M. tuberculosis* complex members. Adapted with permission from Verschoor *et al*., 2012.

1.3.2 Trehalose dimycolate

Trehalose dimycolates (TDM), trehalose disaccharides esterified to two mycolic acids, have long been referred to as cord factor, due to serpentine arrangement of mycobacterial bacilli, as a result of TDM presence on the cell surface. TDM is present in all mycobacteria,

not limited to virulent strains only. Multiple research studies have demonstrated the importance of TDM in the protection of *M. tuberculosis* bacilli from the host response, via the inhibition of phagosome-lysosome fusion, and hence a protection from an acidic phagosome (Spargo *et al.*, 1991; Indrigo *et al.*, 2003). Work by Indrigo *et al.* (2002) utilised a delipidated *M. tuberculosis* strain, to show that the survival of bacilli in macrophages, which was decreased following delipidation, was restored upon reconstitution with TDM alone, hence TDM is recognised as a major factor in the innate macrophage response following *M. tuberculosis* infection. Purified TDM is capable of inducing nitric oxide (NO) secretion in mouse macrophages (Guillemard, E. *et al*., 1998), and inducing tumour necrosis factor- α (TNF- α) production, a potent proinflammatory cytokine in the development and maintenance of the granuloma, via the macrophage inducible C-type lectin (Mincle) receptor (Ishikawa *et al*., 2009), indicating a role of TDM in immuno-modulation as a result of *M. tuberculosis* infection. This is however unlikely to be the case *in vivo*, as TDM is not surface exposed (Ortalo-Magné *et al*., 1996). A study by Rao *et al.*(2005) demonstrated the importance of cyclopropyl modification to TDM, through the generation of a deletion strain unable to catalyse proximal cycloproponation of the alpha mycolate. This mutant strain demonstrated restricted bacterial growth *in vivo*, and a hypo-inflammatory response by macrophages, resulting in a less severe granulomatous inflammation. This result was expected, due to the absence of cyclopropyl modifications in non-pathogenic mycobacteria, and it highlights the importance of this modifications of mycolates on TDM to modify and influence the immune response following infection.

1.3.3 Sulfolipids

Due to the exclusivity of sulfolipids (SL) in pathogenic mycobacteria, much research has been carried out into the immunological properties of these lipids. Sulfolipid-1 (SL-1) is the most abundant SL in the outer membrane of *M. tuberculosis* (Middlebrook *et al.*, 1959). Goren *et al*. (1976) identified that *M. tuberculosis* derived SLs were capable of inhibiting phagolysosome formation in mouse macrophages. Additionally, it has been shown that *M. tuberculosis* derived SL is able to block priming in cultured human monocytes (Pabst *et al*., 1988), and therefore the potential of SL to limit macrophage activation, and subsequent phagocytosis and pathogen destruction.

1.3.4 Phthiocerol dimycocerosates

Phthiocerol dimycocerosates (PDIM) are highly abundant lipids also found in the cell wall of pathogenic mycobacteria (Onwueme *et al*., 2005) and have been shown to be necessary for virulence in a mouse model (Cox *et al*., 1999). Much research has been carried out into their functional role and in virulence in *M. tuberculosis.* Quigley *et al.* (2017) constructed a mutant in which a transcriptional repressor of the PDIM operon was deleted, resulting in an increase of PDIM production; upon macrophage infection, this strain demonstrated an increased ability to escape the phagosome, and subsequently, induce necrosis, suggesting a role of PDIM in host cell manipulation. Additionally, Camacho *et al*. (2001) identified that mutants unable to synthesise PDIMs demonstrated an increase in cell wall permeability, which may indicate a mechanism by which PDIMs contribute to the virulence of *M. tuberculosis*.

1.3.5 Phenolic glycolipids (PGLs)

Phenolic glycolipids (PGLs) are polyketide-derived factors that contribute greatly to mycobacterial virulence. PGLs are produced by pathogenic mycobacteria, with the exception of some *M. tuberculosis* strains, such as H37Rv, and CDC1551, due to a mutation within the polyketide synthase gene (Pks15) (Constant *et al*., 2002). *In vivo* research into the effect of PGL overproduction saw a decrease in the pro-inflammatory cytokine production, typically seen in the case of *M. tuberculosis* infection, and an increase in anti-inflammatory cytokine production (Reed *et al*., 2004; Sinsimer *et al*., 2008). Additionally, a PGL-deficient *M. bovis* strain was severely attenuated in a guinea pig infection model (Collins *et al*., 2005) suggesting that PGLs influence the host macrophages in an immunosuppressive manner.

1.4 M. tuberculosis pathogenesis

M. tuberculosis is a remarkable pathogen in its ability to cause human disease without the aid of secreted toxins. The mechanism of pathogenesis of *M. tuberculosis* lies in its ability to reside in alveolar macrophages, which engulf bacilli upon recognition of pathogen associated molecular pattern (PAMP) on the bacterial surface by pattern recognition receptors (PRR). *M. tuberculosis* are capable of resisting lysosomal fusion with the phagosome in which they reside, preventing their destruction through limiting exposure to the acidic contents of the lysosome, and the reactive nitrogen intermediates (RNI) produced during the process of phagosome-lysosomal fusion (Cooper & Khader, 2008). Instead, the bacteria remain intact in protective phagosomes, and are able to mount an infection if the hosts immune response is hindered. Infected macrophages release numerous proinflammatory cytokines, such as interferon-γ (IFN- γ), TNF-α, Interleukin-1β (IL-1β) and Interleukin-12 (IL-12), as a response to bacilli phagocytosis. This results in increased macrophage activation, and subsequently an

increase in phagocytosis, and the further recruitment of immune cells (i.e. lymphocytes, natural killer (NK) cells, dendritic cells and neutrophils) to the site of *M. tuberculosis* infection.

IFN-γ is primarily produced by NK cells and $CD4^+$ T lymphocytes following activation. The main role of IFN-γ is to induce macrophage activation, therefore macrophages are able to present antigen to $CD4^+$ T lymphocytes and induce further IFN-γ production. *M. tuberculosis* bacilli reside in infected macrophages, which are subsequently unable to exert mycobacterial mechanisms to eliminate the bacteria; when IFN-γ activates macrophages, it has been shown that this induces the transcription of more than 200 genes, including those for the production of antimicrobial molecules (Cooper, 2009). The importance of IFN-γ in *M. tuberculosis* infection has been demonstrated in IFN-γ knockout mice, which underwent sudden onset of tubercular infection (Cooper *et al*., 1993; Flynn *et al*., 1993). Additionally, Newport *et al*. (1996) identified that individuals lacking the IFN-γ receptor gene were highly susceptible to tubercular infection, due to an inability to form a successful granuloma (Ottenhoff *et al*., 2005).

TNF-α is a proinflammatory cytokine secreted by *M. tuberculosis* infected macrophages upon exposure to LPS (lipopolysaccharide) or other bacterial derived antigens. The multifunctional role of TNF-α, in apoptosis, cell recruitment and activation, highlights its importance in the immune response to *M. tuberculosis* infection. TNF-α is a regulator of chemokine production, highlighting its important role in driving immune cell migration to the site of infection, and subsequent granuloma formation. TNF-α hence maintains the granuloma integrity and confines the bacillus, preventing dissemination but without pathogen destruction (Petersen & Smith, 2013) and holding the bacilli growth in check. Although TNF-α is a crucial cytokine in the initial and also the long-term control of tuberculosis, due to its role in the apoptosis and stimulating cell migration to the site of infection, in addition to activating different populations of immune cells, there is a fine balance in the amount of TNF-α produced during tubercular infection; under-production would see the bacteria taking hold and resulting

in active disease, whereas over-production of TNF-α would result in systemic tissue damage. Multiple *in vivo* studies have associated the use of TNF-blockers with the progression of latent infection to active disease (Keane *et al.*, 2001; Núñez Martínez *et al.*, 2001). The employment of anti-TNF agents in inflammatory disorders such as Crohn's Disease has been found to cause tubercular disease reactivation in some patients who are latently infected (van Dullemen *et al.*, 1995), and similarly, latently infected mice rapidly develop tubercular disease and undergo granuloma disorganisation, shortly succumbing to death, following treatment with an anti-TNF antibody (Chakravarty *et al*., 2008). Additionally, TNF-α knockout mice are unable to form granulomas when infected with *M. tuberculosis* (Kaneko *et al*., 1999). All of these studies show the importance of TNF-α's role in controlling tubercular infection, and in the formation and maintenance of the granuloma during infection.

Another proinflammatory cytokine of great importance in the host's response to *M. tuberculosis* infection is IL-1β, a member of the IL-1 cytokine family. Initial recognition of PAMPs, results in the expression of pro-IL-1β. This priming step is an insufficient stimulus in driving the production of the active 17kDa IL-1β; an additional PAMP or damage associated molecular patterns (DAMP) is required to induce further processing (Lopez-Castejon & Brough, 2011) and the subsequent secretion of IL-1β (Krishnan *et al.*, 2013) (Figure 1.6). The recognition of additional DAMPs results in the assembly and activation of the inflammasome, a multimeric protein complex (Sharma & Kanneganti, 2016), which acts as a scaffold for inflammatory caspase, pro-caspase-1, which once activated, is required for the cleavage of pro-IL-1β into its active form, IL-1β, which is rapidly secreted from the phagocytic cell. It acts through the IL-1R1 receptor, found on numerous immune cells including monocytes, macrophages and T lymphocytes, resulting in the subsequent phagocytic cell activation via TNF-α production. IL-1β also has a role in the polarisation of $CD4^+$ helper T lymphocytes to the type 17 helper (Th17) subset (Chung *et al.*, 2009). Th17 lymphocytes play an important

role in the recruitment of immune cells to the site of infection; interleukin-17 (IL-17) secreted from activated Th17 lymphocytes further recruits neutrophils and macrophages to the site of infection. Juffermans *et al*. (2000) carried out a study, utilising mice lacking the IL-1 receptor; these animals were found to be more susceptible to *M. tuberculosis* infection, with an increased morbidity and bacterial burden in the lungs, when compared to wildtype mice. Additionally, there was a reduced number of infiltrating immune cells (macrophages and lymphocytes), and more areas of necrosis in these knockout mice, in conjunction with a reduced production of IFN-γ, highlighting the importance of IL-1 in the immune response against *M. tuberculosis* infection.

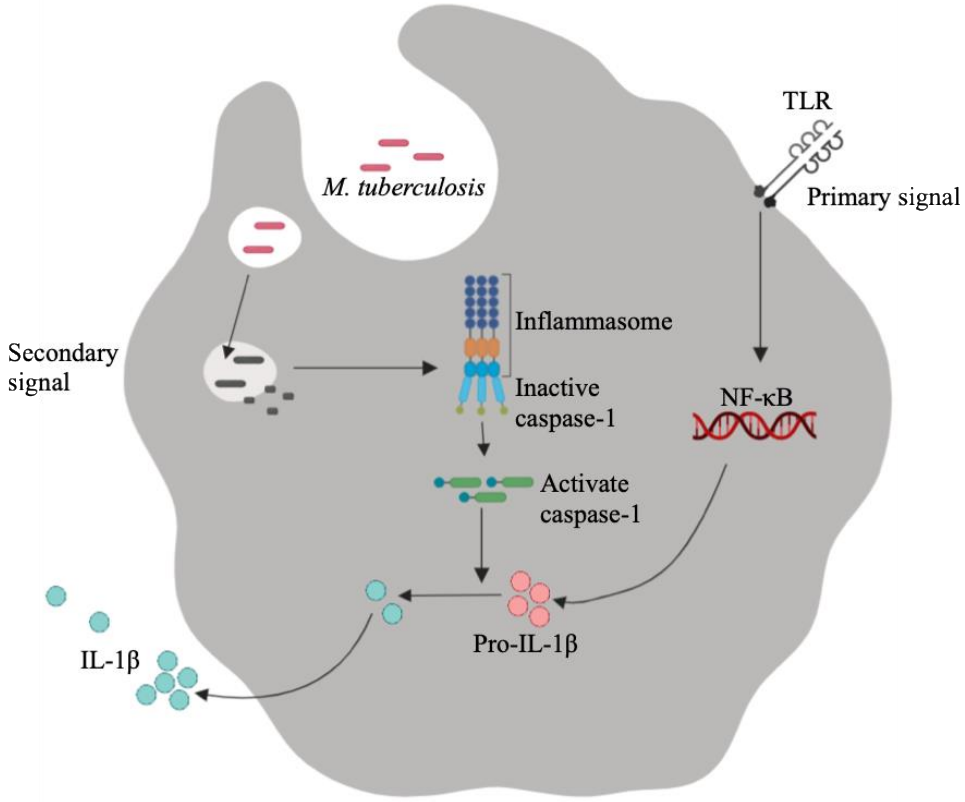

Figure 1.6. The biosynthesis and release of IL-1β from an *M. tuberculosis* infected macrophage. The primary signal of *M. tuberculosis* PAMP recognition by the macrophage TLR results in transcriptional processing to produce inactive pro-IL-1β; this priming signal is however insufficient in driving the production of active IL-1β. A secondary signal is required in the form of further DAMP recognition, which results in the assembly and activation of the multiprotein complex, the inflammasome. Subsequently, pro-caspase-1 is activated to its active form, which is able to cleave pro-IL-1β into its active form. Active IL-1β is rapidly secreted from the cell where it drives phagocytic cell activation.

IL-12 is a unique proinflammatory cytokine due to its heterodimeric structure, consisting of 40kDa (p40) and 35kDa (p35) subunits, linked by a disulfide bond (Zou *et al*., 1995). IL-12 is secreted by activated antigen presenting cells (APC), with IL-12 receptors located on naïve T cells, in addition to NK cells, dendritic cells and macrophages (Desai *et al*., 1992; Nagayama *et al.*, 2000; Grohmann *et al*., 2001) (Figure 1.7). IL-12 is a potent inducer of IFN-γ; *M. tuberculosis* activated APCs migrate to the draining lymph node, where antigen is presented to resident naïve $CD4^+$ T lymphocytes (Cooper *et al*., 2008). IL-12 is capable of polarising T cell differentiation towards a type 1 T helper (Th1) phenotype; Th1 cells are prolific Th1 cytokine producers (Berger, 2000), that are proinflammatory in nature, with the main cytokine produced by Th1 cells being IFN-g. Th1 cells migrate to the site of infection, with IFN-γ driving macrophage activation, and subsequently lowering the bacterial burden via bacilli destruction. The role of IL-12 in converting naïve $CD4^+$ T cells to T helper cells provides a link of the innate to the adaptive immune response to *M. tuberculosis.* The importance of IL-12 in the protection against tubercular infection has been explored in many studies; Cooper *et al*. (1997) generated IL-12p40 knockout mice, who were unable to control infection upon exposure to *M. tuberculosis.* Additionally, some individuals presenting with a deficiency in IL-12p40 and IL-12 receptor subunits, and additional cytokine receptors, are more susceptible to low virulence, or environmental mycobacteria, often resulting in mycobacterial disease (Filipe-Santos *et al*., 2006)**.**

1.5 Granuloma formation

The mobilisation of immune cells to the site of infection results in the formation of a highly organised structure termed the granuloma (Figure 1.8). Serving as a host mechanism to contain the infection and limit the systemic damage caused by the immune response mounted

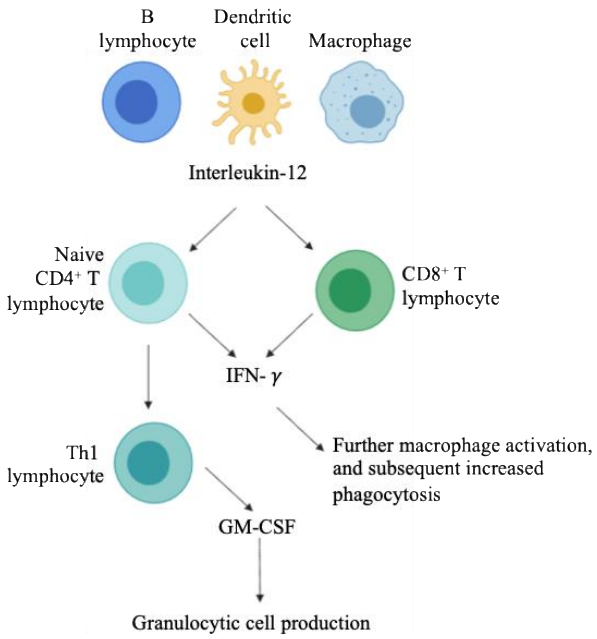

Figure 1.7. The release and action of IL-12 during *M. tuberculosis* infection. IL-12 is secreted from antigen presenting cells, with IL-12 receptors located on $CD8^+$ T lymphocytes, with IFN-gamma produced as a result of stimulation. IL-12 also drives the polarisation of naïve $CD4^+$ T cell polarisation towards Th1 differentiation; Th1 lymphocytes are prolific cytokine producers, with one of these cytokines being IFN-γ. This combined increase in IFN- γ production drives further macrophage activation and a subsequent increase in bacilli phagocytosis and *M. tuberculosis* elimination. Th1 cells also produce a glycoprotein, granulocyte macrophage colony stimulating factor (GM-CSF), which promotes the production of granulocytic cells, such as neutrophils, which migrate to the granuloma.

against the bacilli, the granuloma is also advantageous to the bacteria; *M. tuberculosis* is able to reside at the core, surrounded by immune cells, and serving as a reservoir for potential reactivation if conditions become favourable, such as in the case of immunosuppression. In this case, uncontrolled cell death, and bacilli replication can occur. The granuloma centre may become necrotic, upon which it can be termed the caseum, meaning “cheese” in Latin, due to its appearance, a mass of necrotic macrophages as a result of an inability to limit bacilli replication. The caseum is also lipid-rich, which can be utilised by residing bacilli (Daniel *et al.*, 2011). Infected cells further recruit immune cells to the site of infection, such as differentiated macrophages, dendritic cells and lymphocytes, via cytokine and chemokine production. Some infected macrophages fuse to form multinucleated Langhans giant cells, specific to tubercular infection, that whilst their ability to phagocytose bacteria is lost, they are

still able to present antigen (Lay *et al*., 2007). Macrophages are also able to differentiate into lipid- rich macrophages, termed foamy macrophages, due to its high lipid content. A study by Peyron *et al.*, (2008) determined the phagosome containing mycobacteria, of infected foamy macrophages, migrate towards the lipid bodies resulting in the engulfment of the bacilli into the lipid droplets and with the accumulation of lipids within the microbe; this suggests a role of foamy macrophages in the long-term persistence of mycobacteria. Multinucleated giant cells and foamy cells surround the infected macrophages at the core of the granuloma. Another differentiated macrophage subset often found in the granuloma are epithelioid cells; Turk & Narayanan (1982) identified that these mononuclear cells had lost their phagocytic capability, yet were able to secrete fibroblast activating factor, a protein that stimulates fibroblast proliferation, often found as a fibrotic capsule that surrounds the granuloma's necrotic core (Cyktor *et al*., 2013).

Neutrophils are also recruited to the site of infection during this time, one of the first cells to migrate to this site (Appelberg & Silva, 1989). Neutrophils are activated by *M. tuberculosis* products, such as lipoarabinomannan (Riedel & Kaufman, 1997), and they secrete numerous cytokines, such as IL-1β and TNF-α, hence the further cell recruitment to the granuloma. NK cells also localise to the granuloma, where they produce IFN-γ subsequently activating macrophages, and inducing apoptosis in infected macrophages (Bancroft, 1993; Oshimi *et al*., 1996; Vankayalapati *et al*., 2002;Smyth *et al*., 2005).

The highly proficient antigen presenting dendritic cells, present in the lungs, are able to migrate to the nearby lymph nodes, where antigen is presented to naïve T lymphocytes, resulting in activation and proliferation. Dendritic cells, provide a bridge between the innate and the adaptive immune response against *M. tuberculosis.* The activated T lymphocytes migrate to the granuloma where they are located on the periphery, along with B lymphocytes.

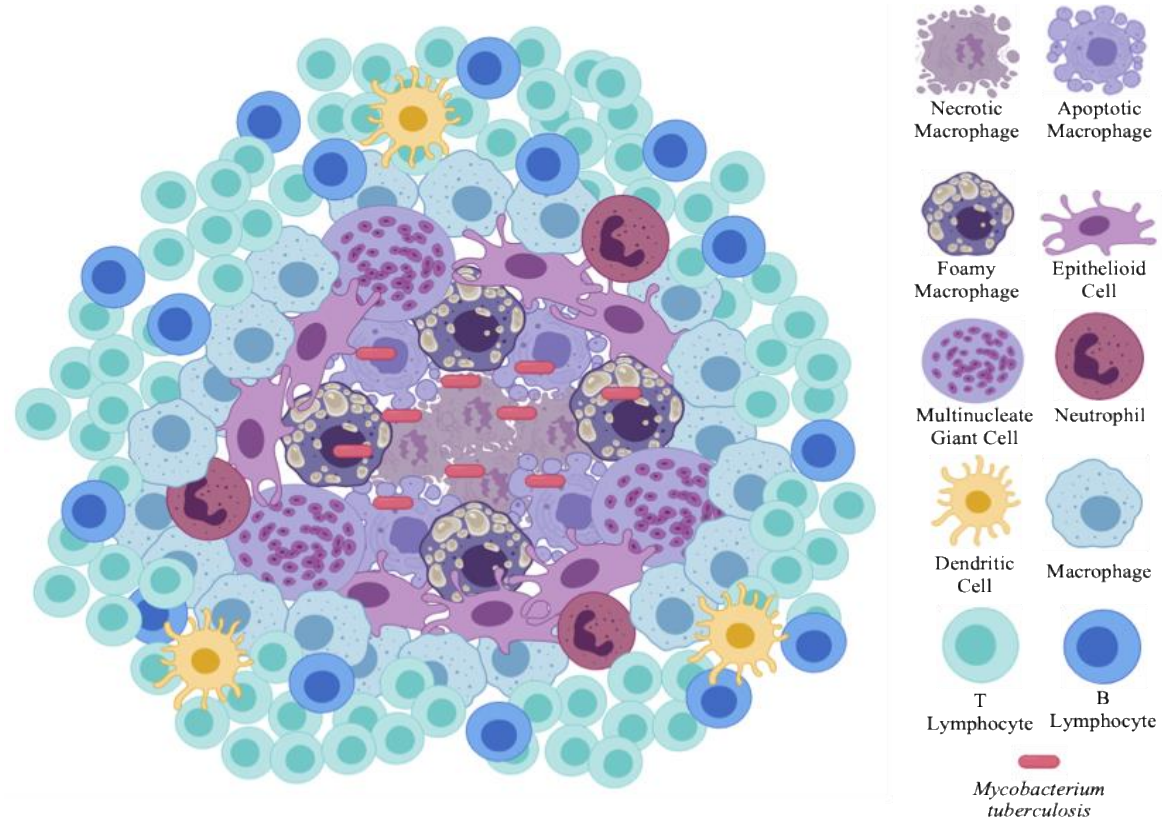

Figure 1.8. The granuloma following mycobacterial infection. *M. tuberculosis* bacilli are contained at the centre of the granuloma, which may become necrotic in the case of bacilli replication and cell death. Macrophages, located at the granuloma centre, can exist in many stages of health (healthy and phagocytosing, apoptotic and necrotic). Surrounding the macrophages are a plethora of differentiated macrophages (foamy macrophages, multinucleate giant cells and epithelioid cells) and an abundance of immune cells, including cytokine-producing neutrophils, capable of activating macrophages, and dendritic cells, which shuttle *M. tuberculosis* antigen to nearby lymph nodes to drive T lymphocyte differentiation and proliferation. Activated T lymphocytes are located on the periphery of the granuloma, along with B lymphocytes, which are also recruited to the site of infection.

1.6 Vaccines against tuberculosis

The Bacille Calmette-Guerin (BCG) vaccine remains the only vaccination against tuberculosis currently in use. Since its first use in 1921, the BCG vaccine has been used to immunise over 4 billion individuals worldwide (Zhang *et al.*, 2016). Discovered by Albert Calmette and Camille Guérin, this virulent *M. bovis* strain was attenuated through continual passage. This vaccine is the world's most widely used vaccine (Dye, 2013), and the 7 years following its first utilisation, over 100,000 children were immunised against tuberculosis

(Daniel, 2006). It has been shown that the BCG vaccine is safe to use with stable mutations, as since its first use, there have been no reversions back to virulence, in animals, observed in animals (Mahairas *et al*., 1996).

Whilst the BCG vaccine remains widely used, immunisation efficiency remains a questionable topic. Distribution of the original BCG vaccine worldwide and subsequent subculture and passage has resulted in variable strains used in vaccination campaigns, with names based upon the location in which they are used (Zhang *et al*., 2013). A number of studies have confirmed BCG's effectivity, yet estimate its ability to reduce the risk of tuberculosis by an average of 50% (Coldlitz *et al*., 1994). There lacks a consistent worldwide BCG vaccination programme, with vaccination regime differing between countries, due to the variable protection that the immunisation provides, and the individual risk of a person developing tuberculosis. Failure to establish a uniform worldwide immunisation programme, as well as usage of multiple difference strains of the BCG vaccine, may have resulted in the differential efficacy observed by BCG vaccination.

1.7 Treatment of tuberculosis

Tuberculosis treatment remains extensive and complex, one reason for this being the heterogeneity of the mycobacterial population at any one time during an infection; a person may be infected with both actively replicating bacterial cells, in addition to those that have entered a dormant state (non-replicating). The overall aim of successful tuberculosis treatment is to cure the individual of the disease, and minimising the transmission to others. In addition, the key to tuberculosis chemotherapy for successful treatment is compliance to the treatment regime; failure to do so increases the risk of the emergence of drug resistant strains, leading to treatment failure, and the requirement for more complex therapy, such as second-line

antibiotics that are more expensive than first-line drugs, and are capable of producing unfavourable adverse side effects in patients. Monitoring during treatment regime is therefore required. The current treatment regime for pulmonary tuberculosis is a six-month course of isoniazid and rifampicin in combination, along with pyrazinamide and ethambutol for the initial two months. The World Health Organization (2018) have predicted that 53 million lives have been saved by effective tuberculosis diagnosis and the treatment that is currently in place, showing that although extensive, the treatment is highly effective.

1.8 Multi-drug resistant tuberculosis (MDR-TB) and extensively drug resistant tuberculosis (XDR-TB)

Whilst the current pulmonary tuberculosis treatment is a combination of potent first-line antibiotics that are well tolerated and produce few side effects, decades of their use has undoubtedly led to the development of drug resistance; contributors of which, are inappropriate prescription by health care professionals, availability of poor quality drugs, or failure on the patients part to complete the prescribed treatment regime. The diagnosis of drug resistant tuberculosis is dependent on the number of drugs, which are no longer effective. Multi-drug resistant tuberculosis (MDR-TB) is used to describe cases of tuberculosis in which isoniazid and rifampicin are no longer effective, two very powerful first-line drugs. Further drug resistance can develop however, resulting in extensively drug-resistant tuberculosis (XDR-TB), assigned to tuberculosis cases in which some second-line drugs are no longer effective. The success rates for treatment of MDR-TB and XDR-TB are very low, at 54% and 30% respectively (World Health Organization, 2018), due to the drastically reduced treatment options that remain effective. In 2016, it was estimated that around 5% of new cases of diagnosed tuberculosis, approximately 600,000 cases, were in fact MDR-TB (World Health

Organization, 2016), with 6.2% of these cases actually classified as XDR-TB (World Health Organization, 2018) (Figure 1.9).

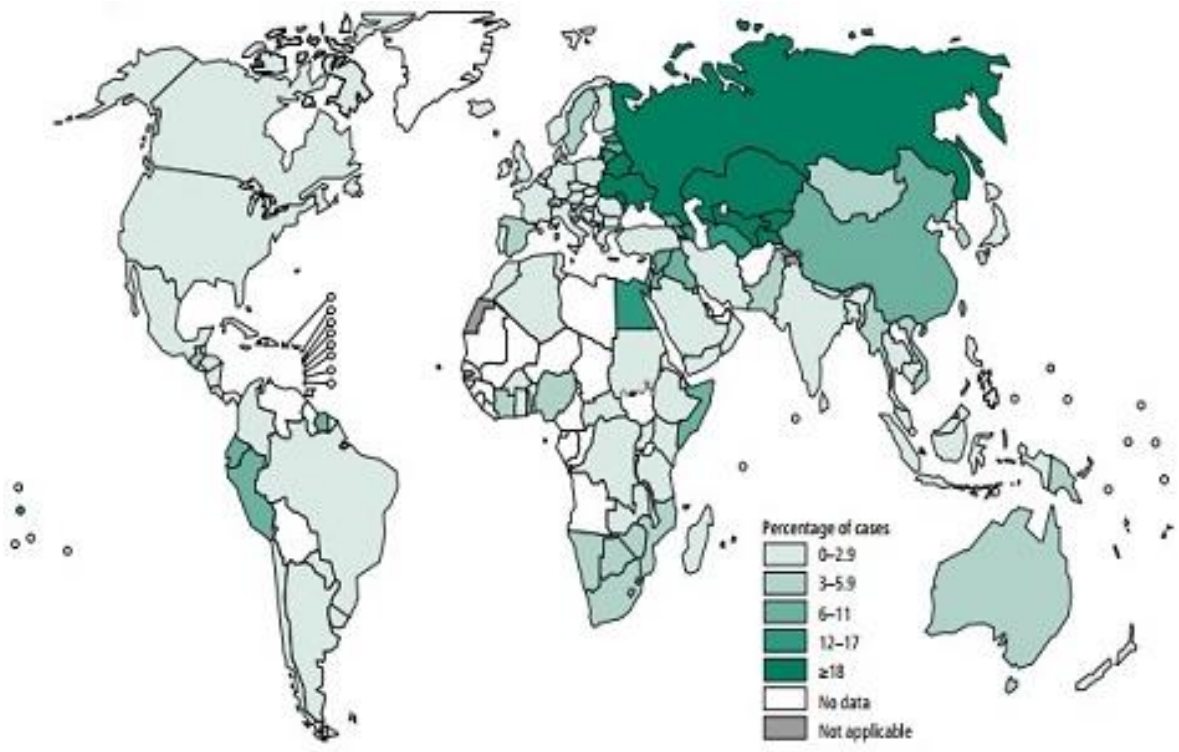

Figure 1.9. Map showing the global incidence of new tuberculosis cases that are classified as MDR-TB or rifampicin resistant tuberculosis (RR-TB). Used with permission from World Health Organization Global Tuberculosis Report, 2017.

1.9 Cell growth and division

Whilst the growth and cell division of rod-shaped bacteria has been widely studied, especially in *Escherichia coli* and *Bacillus subtilis*, the mechanisms involved differ greatly than those in *Actinobacteria*. *E. coli* and *B. subtilis* elongate via the lateral deposition of new cell wall material along their side walls, whereas mycobacteria insert new cell wall material at the poles. Additionally, the resultant daughter cells of mycobacteria are phenotypically distinct, often asymmetric in cell length (Aldridge *et al.*, 2012), whereas the daughter cells of laterally growing rod-shaped bacteria are almost identical.

1.9.1 Cell division in laterally growing *E. coli* and *B. subtilis,* and polar growing actinobacteria

The highly conserved tubulin homolog FtsZ (Lutkenhaus, 1993) is considered the "ringleader" of bacterial cell division (Baranowski *et al*., 2019). With the ability to polymerise into protofilaments, that associate to form the Z-ring, the assembly of this complex at the mid-cell is the first indicator of septation occurrence. FtsZ is essential in almost all bacteria, due to its role in cytokinesis. The Z-ring is capable of recruiting a number of other proteins to complete septation, acting as a docking site for the recruitment of PG synthetic machinery, involved in the construction of the septa.

Z-ring positioning in *E. coli* and *B. subtilis* is highly regulated to ensure that its positioning is restricted to the mid-cell, and inhibited from assembling at the cell poles. A highly studied system in *E. coli* and *B. subtilis*, termed the Min system, functions in preventing Z-ring assembly and placement at any site other than the mid-cell; this is maintained by an inhibitor of Z-ring formation, MinC (Figure 1.10). MinC concentration remains highest at the cell poles, by interacting with MinD, an ATPase that binds to the polar membrane in the presence of ATP, and becoming active in preventing FtsZ polymerisation. In *E. coli*, MinE is able to release MinD from the membrane through ATP hydrolysis, where MinD oscillates to the opposing poles. In this oscillatory manner, MinC is always maintained at the cell poles, preventing Z-ring formation. In *B. subtilis,* MinC and MinD are anchored at the cell poles by DivIVA, utilising MinJ as a bridge between DivIVA and the MinCD complex, hence preventing Z-ring assembly. DivIVA is recruited to sites of negative curvature (Lenarcic *et al*., 2009), and depletion of DivIVA in *B. subtilits* produced filamentous cells, with the presence of minicells, indicating an inhibition of cell division, with the divisions that do occur aberrantly assembling close to the cell poles (Edwards & Errington, 1997).

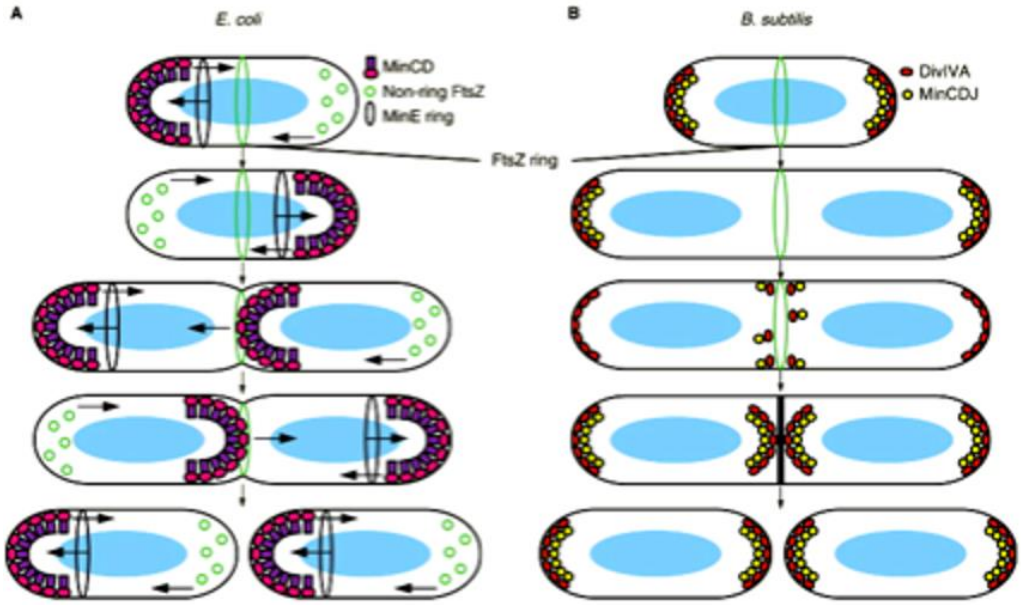

Figure 1.10. The Min systems of *E. coli* and *B. subtilis.* (A) In *E. coli*, the FtsZ assembly inhibitor, MinC, remains at its highest concentration at the cell poles, preventing septa formation at these sites. MinC is maintained at the poles due to its interaction with, and the action of MinD, an ATPase that binds to the pole membrane. MinE is able to release MinD, and subsequently MinC, from the membrane by ATP hydrolysis where it oscillates to the opposing poles. (B) In *B. subtilis*, DivIVA, which binds to the membrane at the sites of negative curvature, such as the poles, anchors MinC and MinD, via a MinJ bridging protein, to the cell poles, and subsequently hinders FtsZ assembly at these sites. Used with permission from Rowlett *et al*., 2013.

Cell division in *B. subtilis* and *E. coli* has been widely studied, with the characterisation of numerous proteins important in division, ultimately forming a complex termed the divisome (Goehring & Beckwith, 2005; Harry *et al*., 2007). These include candidates that anchor FtsZ to the cell membrane and recruit cell wall biosynthetic machinery to the septa site, in the case of SepF and FtsA (Hamoen *et al*., 2006; Jensen *et al*., 2005). Divisome components also promote FtsZ polymerisation, in the case of ZapA (Gueiros-Filho & Losick, 2002). Other members of the divisome include PBP2B, a penicillin binding protein (PBP). GpsB is found to shuttle another penicillin binding protein, PBP1, between the elongation and division complexes, where it is involved in the assembly of the bacterial cell wall at the sites or elongation and the septa respectively (Claessen *et al*., 2008). A divisome component present in *E. coli*, but not *B. subtilis*, ZipA, has also been found to stabilise the Z ring upon formation (Hale & de Boer, 1997).

Mycobacteria lack Min homologues, suggesting an alternate mechanism for FtsZ assembly and septation. Z-ring positioning is speculative, with most research showing that cell division occurs at a range across the mid-cell; Singh *et al.* (2012) showed that the assembly of the Z-ring in exponentially growing mycobacterial strains (*Mycobacterium marinum* and *M. smegmatis*) occurs randomly across a mid-cell range. Aldridge *et al.* (2012) also demonstrated that the mycobacteria divided less symmetrically when compared to *E. coli.* Mycobacteria lack numerous divisome components identified in *B. subtilis* and *E. coli*; no homologs of FtsA or ZapA are present in the mycobacterial divisome. They do, however, possess many divisome proteins that have been shown as having a role in FtsZ anchoring and polymerisation, including FtsX, FtsE and FtsW (Vicente *et al.*, 2006; Datta *et al.*, 2002) (Figure 1.11). A key cell division factor is the FtsZ interacting protein, CrgA, that localises to the cell pole; the deletion of which results in inefficient cell division (Plocinski *et al.*, 2011). Another FtsZ interactor, SepF, is an essential component of the core machinery that drives cell division in mycobacteria, with thedepletion of which resulting in a complete block of cytokinesis (Gola *et al.*, 2015).

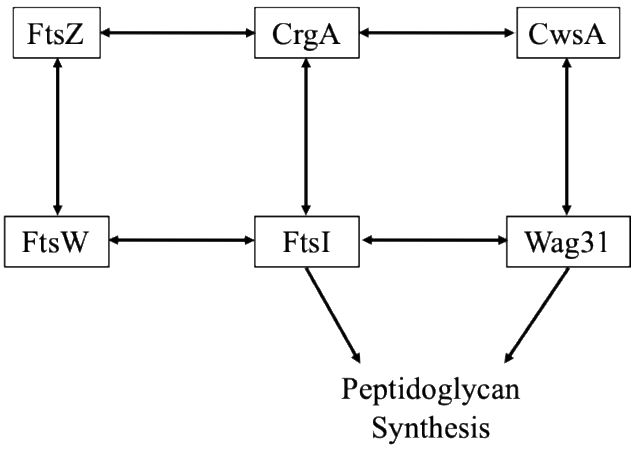

Figure 1.11. Interactions of proteins involved in mycobacterial cell division and cell elongation. Interactions between numerous Fts proteins involved in cell division, which also interact with proteins involved in the regulation of the biosynthesis of cell wall material, contributing to cell wall synthesis at the septa and the poles. Adapted with permission from Plocinski *et al.*, 2012.

1.9.2 Cell elongation in laterally growing *E. coli* and *B. subtilis*, and in polar growing Actinobacteria

The laterally extending *E. coli* and *B. subtilis* possess an actin homologue, MreB, (Jones *et al*., 2001) that functions in tethering PG synthetic machinery to the cell membrane (Carballido-López, 2006) (Figure 1.12). Previously thought to span the whole length of the cell in the form of helical cables (Shih *et* al., 2003; Jones *et al*., 2001; Figge *et al*., 2004), it has now been shown that instead, MreB assembles into patches along the sidewalls (Domínguez-Escobar *et al*., 2011). MreB inactivation in *E. coli* and *B. subtilis* results in the formation and coccoid, rounded cell, due to a loss of rod-shape (Varma & Young, 2009; Formstone & Errington, 2005).

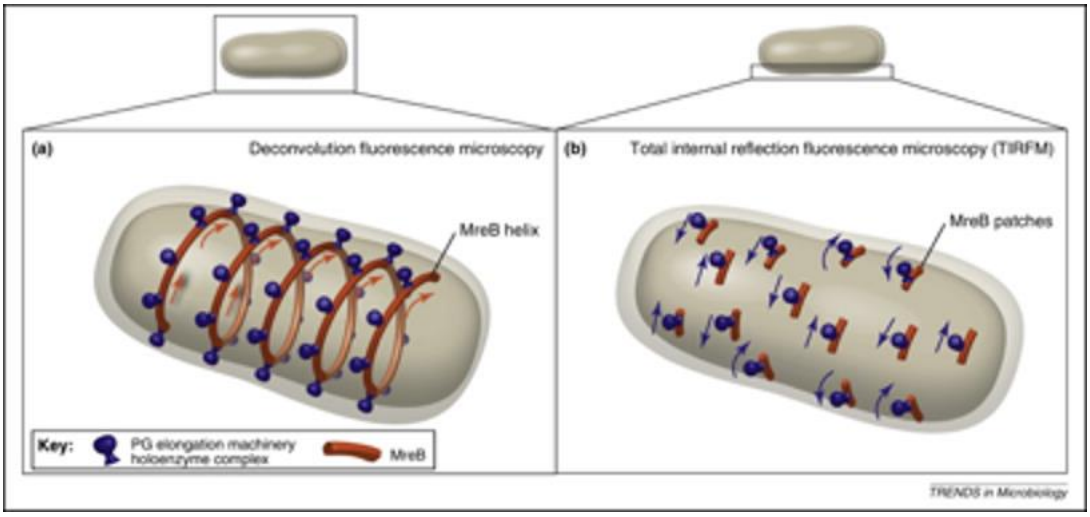

Figure 1.12. Simplified diagrams showing the two theories of MreB movement and localisation within the *B. subtilis* cell. MreB tethers peptidoglycan biosynthetic machinery to the cell membrane. (A) previous studies, using deconvolution fluorescence microscopy, showed that MreB assembles into helical cables, spanning the whole length of the cell (Shih *et al*., 2003; Jones *et al*., 2001; Figge *et al*., 2004). (B) Work by Domínguez-Escobar *et al.* (2011) employed total internal reflection fluorescence microscopy, and were able to visualise MreB patches which assemble along the sidewall. Used with permission from White & Gober, 2011.

Actinobacteria lack an MreB homologue (Jones *et al*., 2001), with the exception of *S. coelicolor*; in this case however, its role is dispensable in apical growth (Heichlinger *et al*.,

2011). The filamentous *S. coelicolor* elongates via the deposition of cell wall material at the hyphal tips. Unlike the role of DivIVA in *B. subtilis*, which is crucial in successful septation, the coiled-coil DivIVA in *S. coelicolor* is involved in hyphal polar growth, with the overexpression of *divIVA* causing the formation of multiple new sites of cell wall incorporation, in the form of hyperbranching (Flärdh, 2003). DivIVA in *S. coelicolor* interacts with numerous coiled-coil proteins that have been shown to play a role in *Streptomyces* polar growth (Figure 1.13). Holmes *et al.* (2013) provide evidence that *Streptomyces* cytoskeletal element (Scy), a large coiled-coil protein, interacts with DivIVA. The role of Scy lies in controlling and limiting the number of polar growth assembly sites; the deletion of Scy from *S. coelicolor* resulted in aberrant branching compared to the wildtype strain, and fluorescent vancomycin (Van-FL), used for visualising the incorporation of new PG material, stained the apical tips of the mutant strain more intensely, indicating a role in determining the future sites for tip formation, and also the sites of PG incorporation. DivIVA and Scy also interact with the *in vivo* filament-forming protein, FilP (Bagchi *et al*., 2008; Holmes *et al*., 2013). FilP is found to convey mechanical strength to the hyphae, and maintains cell shape, with a FilP mutant in *S. coelicolor* producing additional non-uniform branching (Bagchi *et al*., 2008). Holmes *et al*. (2013) have hypothesised that the polar growth and subsequent tip extension of *S. coelicolor* is governed by a complex assembly, consisting of these three coil-coil interacting partners, plus additional components that are yet to be identified, termed the tip organising centre (TIPOC).

Whilst a mycobacterial TIPOC has not been identified, the role of an essential DivIVA homolog, Wag31, in mycobacteria has a similar role to its *Streptomyces* counterpart, in establishing and maintaining polar growth and cell shape. Wag31 localises to the cell poles (Kang, *et al*., 2008), where it interacts with numerous proteins involved in the regulation of cell shape and cell wall synthesis. Plocinski *et al.* (2012) identified an *M. tuberculosis* small membrane protein, named CwsA, that interacts with Wag31, and causes cell wall biosynthesis

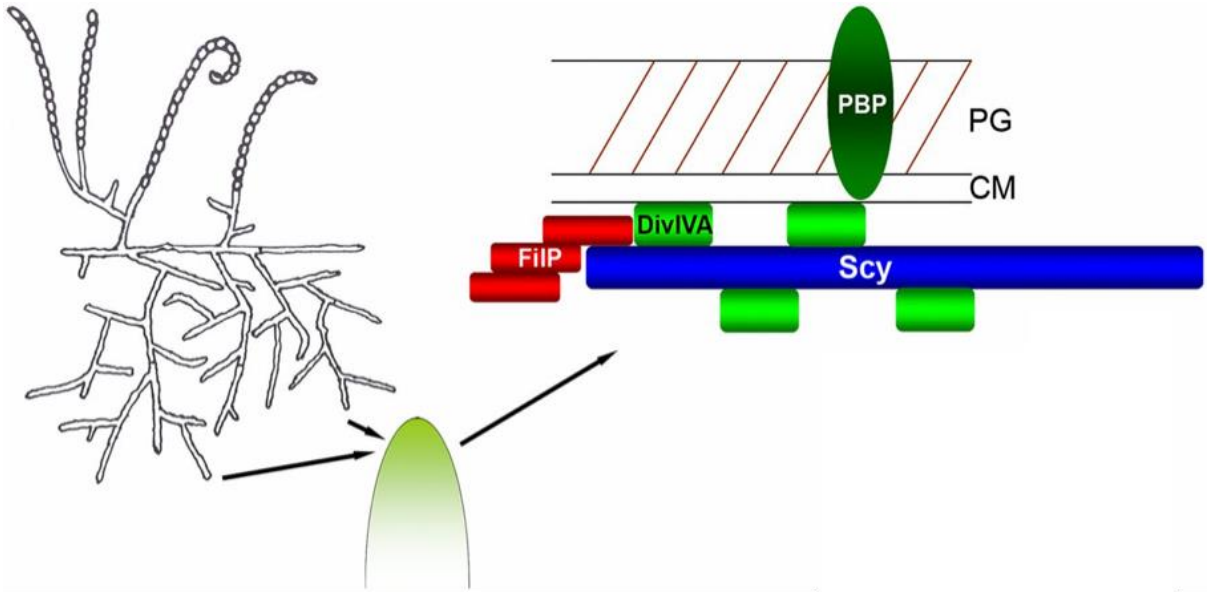

Figure 1.13. The TIPOC of the filamentous polar growing *S. coelicolor*. DivIVA has been shown to interact with cell wall biosynthetic machinery, at the cell membrane. DivIVA also interacts with the coiled-coil proteins FilP, and Scy, which convey mechanical strength to the hyphal branch, and controls the number and sites of future branching, respectively. PG, peptidoglycan; CM, cell membrane. Adapted with permission from Holmes *et al*., 2013.

defects and a bulged phenotype upon deletion. Xu *et al*. (2014) identified that Wag31 also interacts with AccA3, a subunit of a fatty acid biosynthesis complex that is utilised in the elongation of fatty acids and mycolic acids (Wakil *et al*., 1983). Wag31 has also been shown to interact with MtrB, a known regulator of cell division and cell wall biosynthesis; deletion of *mtrB* from *M. smegmatis* resulted in filamentous cells, with very few septa (Plocinska *et al*., 2012). Mukherjee *et al*. (2009) demonstrated that Wag31 is able to interact with FtsI, a PBP hypothesised to play a crucial role in the biosynthesis of septa PG (Datta *et al*., 2006). The depletion of Wag31 in *M. smegmatis* resulted in an abnormal phenotype of cellular bulging with abundant cell lysing present (Kang *et al*., 2008). With the known interactors of Wag31, and the effect of depletion, the function of Wag31 is proven to be in the regulation of cell shape and cell wall biosynthesis.

The given population of mycobacteria at any one time is phenotypically heterogenous in terms of cell length (Santi *et al*., 2013). As previously mentioned, cytokinesis occurring over a range at the mid-cell will produce daughter cells of different lengths. Many research studies have also demonstrated differential bipolar growth in mycobacteria (Joyce *et al*., 2012; Singh *et al*., 2013). Aldridge *et al.* (2012) identified that mycobacteria preferentially elongate at one pole, formed in the previous generation, termed the old pole (Figure 1.14). Following cytokinesis, the cell which inherits the original old pole will be faster growing, as compared to the cell inheriting the new old pole. Additionally, Aldridge *et al*. (2012) found that the cell that inherits the mother's old pole is more susceptible to antibiotics which act against the cell wall. It is however these cells which have been shown to have an increased tolerance to rifampicin (Richardson, K. *et al*., 2016). This preferential growth at the old pole may be due to the higher concentration of certain cell elongation determining proteins to this site; Meniche *et al.*, (2014) determined that Wag31 was concentrated at the old pole. Rego *et al*. (2017) identified *lamA*, a divisome member and highly conserved gene across mycobacterial species, yet not in other microorganisms; upon deletion of *lamA* from *M. smegmatis*, cell elongation was more symmetric than the wildtype, with the growth at each pole occurring at a similar rate, leading to the hypothesis that LamA inhibits growth at the new pole. Interestingly, cells lacking LamA were found to be more susceptible to cell wall targeting antibiotics (Rego *et al*., 2017). Numerous studies have identified the differential susceptibility of the heterogenous mycobacterial population to antibiotics, suggesting that the heterogeneity observed may convey a survival advantage against anti-mycobacterial agents. PonA1 is a PBP that incorporates new PG subunits into the polar cell wall (Kieser & Rubin, 2014); Kieser *et al.* (2015) identified that elongation rates of mycobacteria are modulated by the phosphorylation of PonA1. Changes in PonA1 levels induce growth defects and abnormal rates of cell

elongation. Additionally, excess PonA1 resulted in the production of ectopic poles, indicating PonA1 as a central determinant of mycobacterial polar growth (Kieser *et al*., 2015).

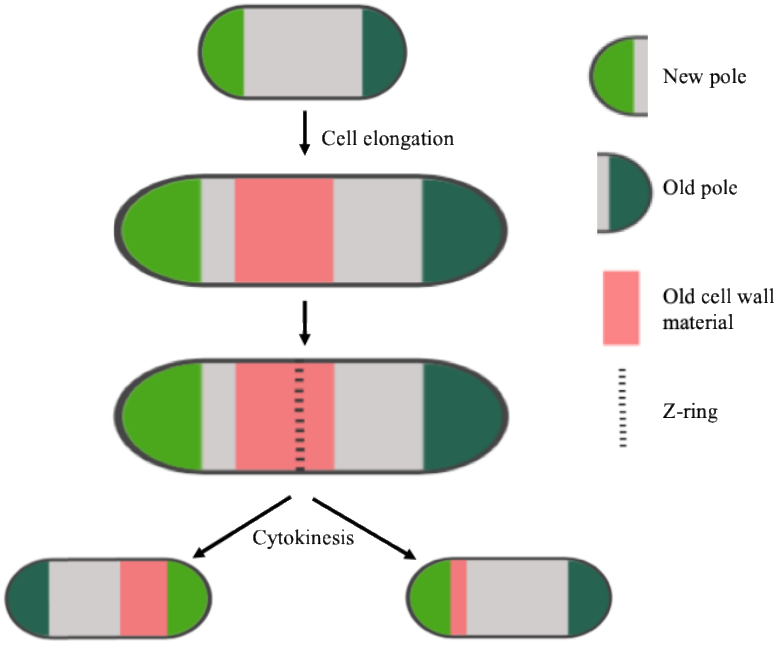

Figure 1.14. Mycobacterial polar growth and division. Mycobacteria grow preferentially at the old pole, inherited from the previous generation. Following cytokinesis, the cell inheriting the original old pole will grow quicker than the other cell, containing a new old pole. Adapted from Logsdon, M. M. & Aldridge, B. B., 2018.

1.10 Aims and objectives

The overall aim of this thesis is to study polar growth and division in mycobacteria, and its possible integration into cell wall biosynthesis. Whilst the vast majority of this work will focus on the role of selected coiled-coil proteins in mycobacterial growth, part of the project will involve the study of innate immune response of an attenuated *M. tuberculosis* deletion strain, the mycolic acid profile of which is severely altered.

In order to identify and study candidates that may have a role in mycobacterial polar elongation and division, a number of approaches will be employed:

1) Comparative bioinformatic analysis will be employed to identify potential candidates, based on conserved protein domains, and sequence and structural homology.
2) Specialised Transduction will be utilised to generate deletion strains of these identified genes, and essentiality will be determine through growth analysis.
3) Following on, a phenotypic analysis will be performed, to determine the effect of gene deletion on cell morphology and lipid profiling. This will include a colony morphology study, followed by a full lipidomic analysis, if a change in colony morphology is observed. A cell length analysis will also be carried out, to determine if the gene deletion resulted in a change in average cell length. Where possible, fluorescence microscopy will also be employed to identify and differences in septation and chromosomal material partitioning as a result of the gene deletion.
4) Finally, in order to begin to delineate the role of the candidates in mycobacterial polar growth and division, the determination of interacting partners will be attempted.

Additionally, I will also investigate the role of cell wall biosynthesis in *M. tuberculosis* virulence, using a Δ*kasB* mutant with truncated cell wall mycolic acids. This mutant is highly attenuated in mice infection and fails to cause disease, yet is still detectable in the lungs. Due to the similarity of this deletion strain to latent tubercular infection, immunological assays will be employed to identify differences in the innate immune response compared to wildtype *M. tuberculosis.*

CHAPTER 2

A Mycobacterial DivIVA Domain-Containing Protein Involved in Cell Length and Septation

2.1 INTRODUCTION

Two of the most widely studied rod-shaped bacteria, *Escherichia coli* and *Bacillus subtilis* elongate via the lateral deposition of cell wall material along the whole length of the cell. The cell wall biosynthetic machinery is recruited to these sites by MreB, an actin-like protein which drives peptidoglycan synthetic machinery to the lateral cell walls (Jones *et al.*, 2001). Both of these bacteria possess an inhibitory system, termed the Min system, which ensures FtsZ protofilaments assembly into the Z-ring occurs only at the mid cell. Alike to mycobacteria, *Streptomyces coelicolor* grows via polar elongation, and is widely studied; both lack Min homologues, and therefore utilise a different mechanism for the correct assembly and placement of the Z-ring. Additionally, the mechanism for polar elongation is MreB-independent, indicating that an alternative pathway and potentially, complex of proteins, is employed in polar growth.

DivIVA, first identified in *B.* subtilis, is a tropomyosin-like protein, having weak similarities to the eukaryotic cytoskeletal proteins, tropomyosins (Edwards, *et al.*, 2000). The role of $DivIVA_{BS}$ is as a scaffold protein that is able to recruit cell division machinery to the respective site (Edwards & Errington, 1997). The coiled-coil protein, DivIVA in *S. coelicolor*, is essential and has been found to possess a different role of $DivIVA_{BS}$. In *S. coelicolor*, DivIVA is localised to the hyphal tips, in addition to being the earliest marker of future branching sites (Flärdh, 2003; Hempel *et al.*, 2008). A study by Flärdh (2003) showed that $DivIVA_{SC}$ overexpression results in hyperbranching, indicating the differential role of DivIVA in *S. coelicolor,* in the recruitment of components required for branching, compared to its role in *B. subtilis.* Other actinobacteria possess homologues of DivIVA. A study by Letek *et al.* (2008) found that upon depletion of DivIVA from *Corynebacterium glutamicum*, cells took on a coccoid morphology, with inhibited polar growth; this was restored upon the introduction of DivIVA from *Streptomyces* or *Mycobacterium*, but not from *B. subtilis*, indicating a conserved

function of actinomycete DivIVA in cell growth and also the maintenance of rod or filamentous shape. In *S. coelicolor*, DivIVA interacts with many coiled-coil proteins, including the novel protein Scy and the filament-forming FilP, that are involved in the control of branch number and location, and in conveying mechanical strength to the cell tips respectively (Holmes *et al*., 2013; Bagchi *et al*., 2008). These three proteins are components of the tip organising centre (TIPOC) in *S. coelicolor*, a complex that drives tip extension (Holmes *et al*., 2013).

Mycobacteria possess numerous proteins that carry the conserved DivIVA domain, in addition to a DivIVA homolog itself, termed Wag31 in *Mycobacterium tuberculosis*; its role, having been explored in *Mycobacterium smegmatis*, is in the maintenance of cell shape and in the ability to direct nascent peptidoglycan biosynthesis to the cell poles (Kang *et al*., 2008). Wag31 appears to be a leading protein in the maintenance of cell elongation, due to its interacting partners, including both AccA3 and AccD5, members of the acyl-CoA carboxylase (ACC) complex, a key complex in the biosynthesis of lipid and mycolic acids, interact with Wag31 (Xu *et al*., 2014; Meniche *et al*., 2014). Wag31 also interacts with CwsA, required for cell wall synthesis and maintenance of cell shape, and ParA, a protein important in chromosomal segregation respectively (Plocinski *et al*., 2012; Ginda *et al*., 2013). Lee *et al*. (2014) also found that Wag31 interacts with a serine/threonine kinase, PknA, a signal transduction pathway component which regulates cell shape. Whilst research, such as these interaction studies, is beginning to determine a link between the division and elongation machinery of mycobacteria, further work is required to identify other potential components in a yet to be established potential mycobacterial TIPOC.

This study focusses on a putative coiled-coil protein encoded by the *M. tuberculosis* gene *Rv2927c* and its homologue in *M. smegmatis*, *MSMEG_2416*, with the interest in probing the function of this protein in terms of mycobacterial growth and cell division. MSMEG_2416 was chosen as it shares a conserved DivIVA domain with the septum forming protein DivIVA.

Previous studies have shown that MSMEG_2416 (termed SepIVA) associated with the septum in the later stages of cell division, localising to the division site and the intracellular membrane domain (Wu *et al.*, 2018). This study aimed to determine the effect of the loss of *sepIVA* on growth of *M. smegmatis* by generating a strain lacking *sepIVA* function. *Rv2927c*, the *M. tuberculosis* homologue of *sepIVA*, was predicted to be an essential gene (Griffin *et al.*, 2011), and we anticipated that likewise, *sepIVA* would be essential gene in *M. smegmatis*, as other studies have failed to generate a knockout (Wu *et al.*, 2018; Jain *et al.*, 2018). However, surprisingly, we were able to generate a null mutant of *sepIVA* indicating that the gene is not essential for growth of *M. smegmatis* in laboratory media. Furthermore, the mutant strain showed altered colony morphology, cell length, and septation patterns, indicating a potential role in mycobacterial division. This work also began to elucidate the potential interacting partners of SepIVA.

2.2 RESULTS

2.2.1 Homologues of SepIVA in other bacteria

The amino acid sequence of SepIVA was utilised in a BLASTP search, and sequence alignment analysis to identify homologous proteins within the mycobacterial species, and within other polar growing *Actinomycetale* suborders. Homologues were found in environmental non-pathogenic mycobacteria, members of the tuberculosis causing *Mycobacterium tuberculosis* complex (MTBC), and also the decaying genome of *Mycobacterium leprae* (Figure 2.1A). This indicates that SepIVA is conserved across the mycobacterial species. Although with slightly lower identity/ similarity scores, SepIVA homologues were also identified in other saprophytic mycolate producing *Corynebacterianea*, such as *Nocardia, Gordonia, Tsukamurella, Rhodococcus, Hoyosella, Segniliparus, Dietzia* and *Corynebacteria* (Figure 2.1B). Additionally, lower identity scoring homologues were also identified in *Streptomyces,* a genus of the Actinobacteria phylum. When the amino acid sequence of SepIVA was used as a query in a BLASTP search against any potential similar proteins in *E. coli* and *B. subtilis*, no potential candidates were identified. This suggests that SepIVA homologues are conserved across polar growth progenitors of the *Actinomycetales.* Figure 2.2 shows a phylogenetic analysis of the mycobacterial and *Corynebacteriaceae* species members included in the multiple sequence alignment. Additionally, a lower identity scoring homologue was also identified in *Streptomyces*, a genus of the Actinobacteria phylum.

TMHMM v. 2.0 (http://www.cbs.dtu.dk/services/TMHMM/) and TMpred https://embnet.vital-it.ch/software/TMPRED_form.html) were utilised to predict transmembrane regions of SepIVA. According to these bioinformatic analysis tools, SepIVA lacks transmembrane regions (Figure 2.3).

The amino acid sequence of SepIVA was analysed in a structural assessment, in regard to its coiled-coil conformation, using the online tool COILS (Lupus *et al.*, 1991)

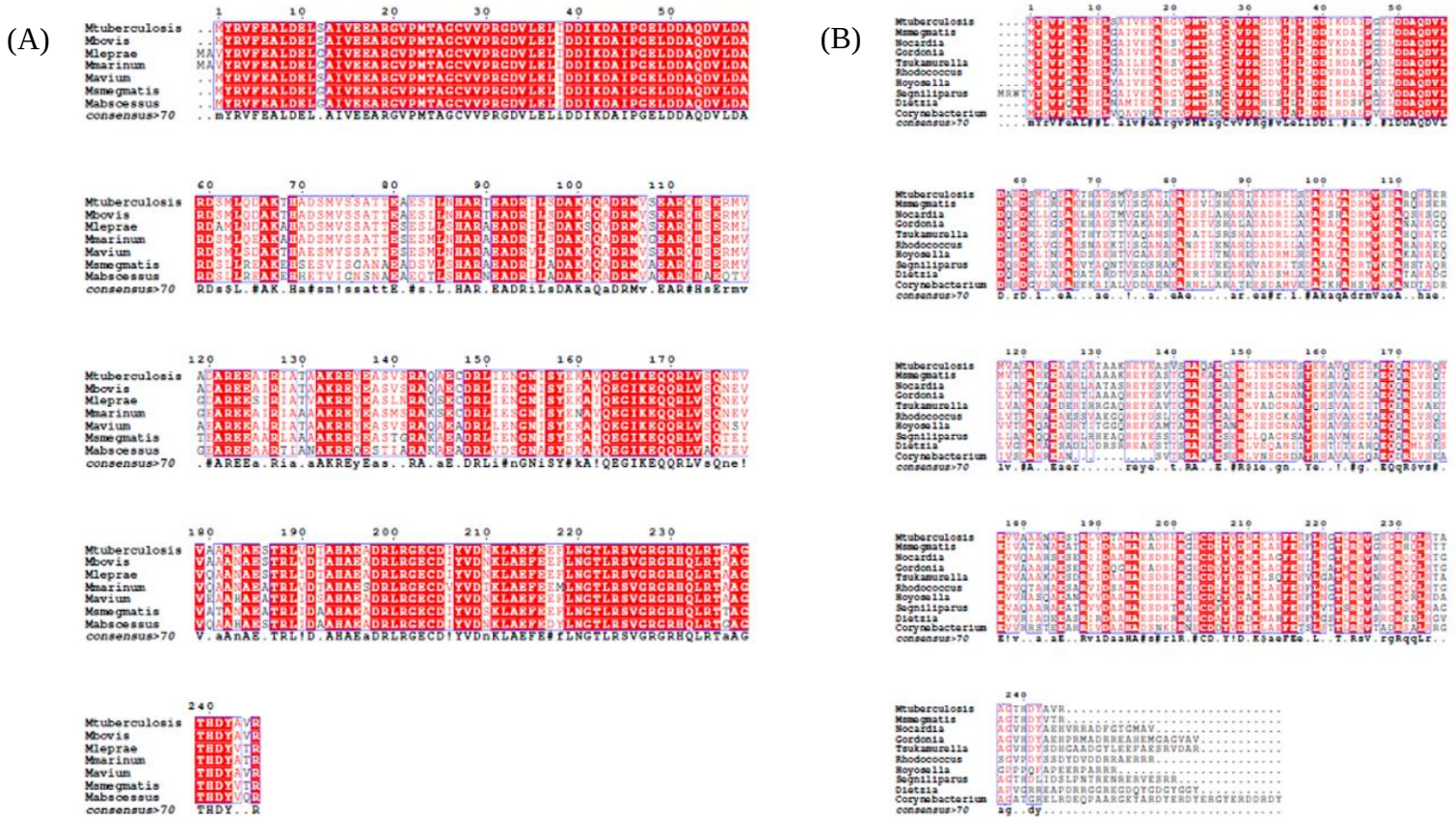

Figure 2.1. Multiple sequence alignment of the *M. smegmatis* SepIVA with Actinobacterial homologues. Homologues were identified using the SepIVA amino acid sequence and a BLASTP search. Multiple sequence alignment with hierarchical clustering was performed using Multalin (http://multalin.toulouse.inra.fr/multalin/multalin.html). Alignment of the *M. smegmatis* SepIVA amino acid sequence with homologues in other mycobacterial species (A) and with genera from the suborder *Corynebacterianea* (B).

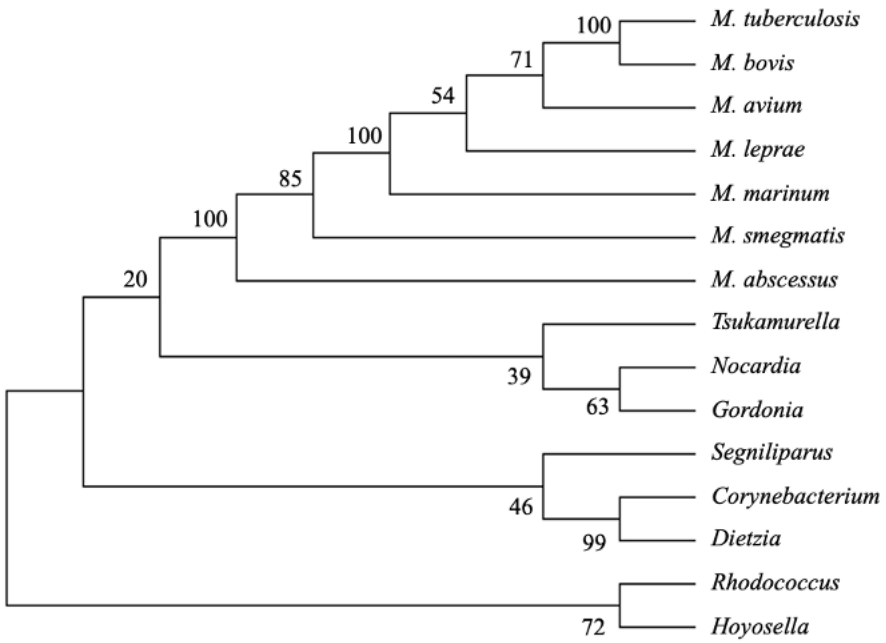

Figure 2.2. Phylogenetic tree of *Corynebacteriaceae* species constructed using MEGA software . The phylogenetic tree was generated on MEGA Software using the amino acid sequences of proteins with high identity and similarity to *M. smegmatis* SepIVA. The methodology used was maximum likelihood, and the phylogram stability was analysed by bootstrapping 100 replications. Nodes with bootstrap values are indicated

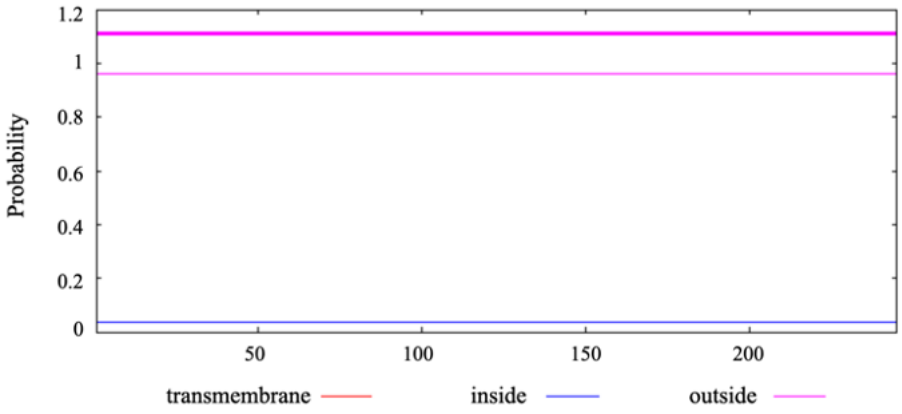

Figure 2.3. TMHMM predictions for *M. smegmatis* SepIVA. No transmembrane domains were predicted by TMHMM.

(https://embnet.vital-it.ch/software/COILS_form.html). COILS determines the probability that a residue within a protein is part of a coiled-coil structure, based upon the comparison with sequences of known coiled-coil proteins. SepIVA from *M. smegmatis* was

predicted to have two coiled-coil domains (Figure 2.4A). Using the online tool MULTICOILS (http://cb.csail.mit.edu/cb/multicoil/cgi-bin/multicoil.cgi), which identifies the probability of trimeric and dimeric coiled-coils, the oligomerisation status of SepIVA of *M. smegmatis* was explored (Wolf *et al*., 1997). The dimerization probability of the first coiled-coil domain was above the threshold (Wolf *et al*., 1997), indicating that SepIVA of *M. smegmatis* is predicted as a dimeric coiled-coil protein (Figure 2.4B).

A paralog of SepIVA has been identified as MSMEG_4217, the *M. smegmatis* homologue of Wag31.

(A)

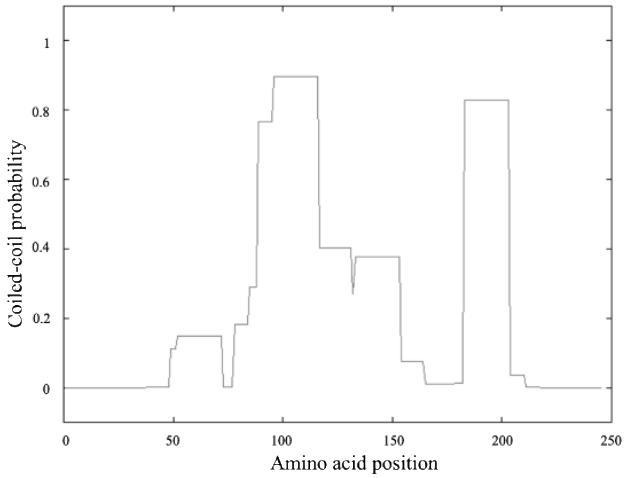

(B)

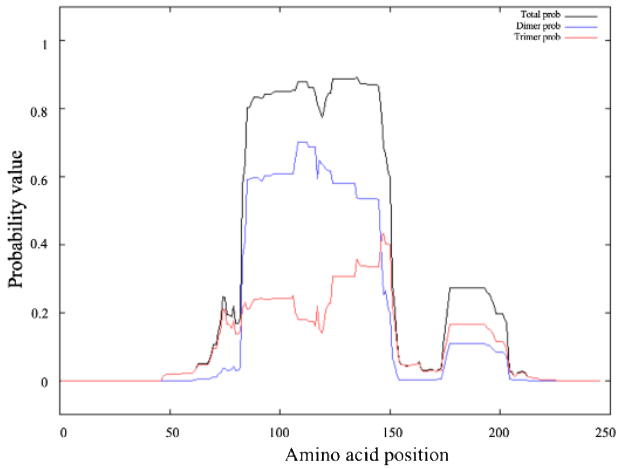

Figure 2.4. Predicted coiled-coil regions of *M. smegmatis* SepIVA, based on its amino acid sequence. The coiled-coil probabilities of SepIVA were predicted using COILS (A), and its dimerization and trimerization probabilities using MULTICOILS (B). SepIVA is predicted to possess two coiled-coil domains, the former of which is predicted as a dimer.

2.2.2 Generation of a *M. smegmatis* mc^2 155 Δ*sepIVA* null knockout

To determine whether *sepIVA* is essential in the survival and growth of *M. smegmatis* mc^2 155, an allelic exchange substrate was constructed, and Specialised Transduction was performed, to replace *sepIVA* with a hygromycin resistance cassette (Figure 2.5). The gene deletion was confirmed by whole genome sequencing. This null knockout strain was designated Δ*sepIVA*. The ability to generate a gene deletion strain indicated that *sepIVA* is a non-essential gene in *M. smegmatis* mc^2 155. Following confirmation of gene deletion, *sepIVA*, along with its native promoter, was cloned into the integrative plasmid pMV306, using the primer pair SepIVA_Comp_F and SepIVA_Comp_R, and was introduced into *M. smegmatis* mc^2 155 Δ*sepIVA*, to generate a complemented strain (Δ*sepIVA*C). In addition to complementation with *sepIVA*, Δ*sepIVA* was also complemented with the *M. tuberculosis* homologue *Rv2927c*. *Rv2927c*, along with its native promoter, was cloned into pMV306 using the primer pair Rv2927c_Comp_F and Rv2927c_Comp_R, and introduced into *M. smegmatis* mc^2 155 Δ*sepIVA*, to generate a complemented strain (Δ*sepIVA*CRv). To confirm complementation, PCR was carried out using the primer pairs listed above, which were utilised in the construction of the complemented strains (Figure 2.6).

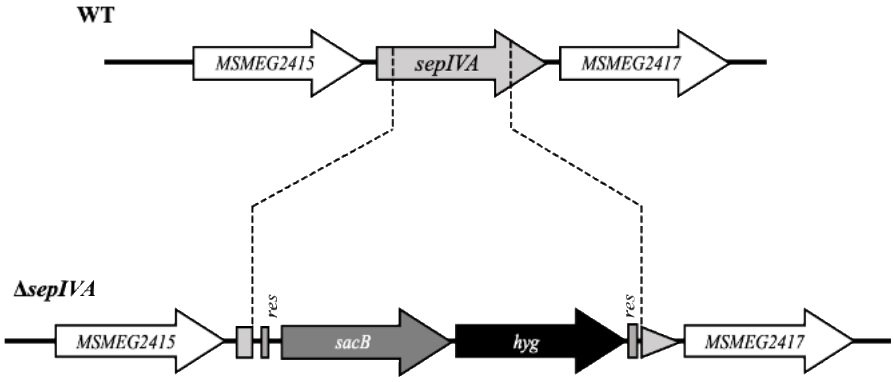

Figure 2.5. Construction of a *M. smegmatis sepIVA* deletion mutant. A schematic representation showing the removal of the gene of interest *sepIVA*, from *M. smegmatis*, and its replacement with a hygromycin resistance cassette. WT, wildtype. sacB - sucrose counter-selectable gene from *Bacillus subtilis*; *hyg* - hygromycin resistance gene; *res* - γδ-resolvase site.

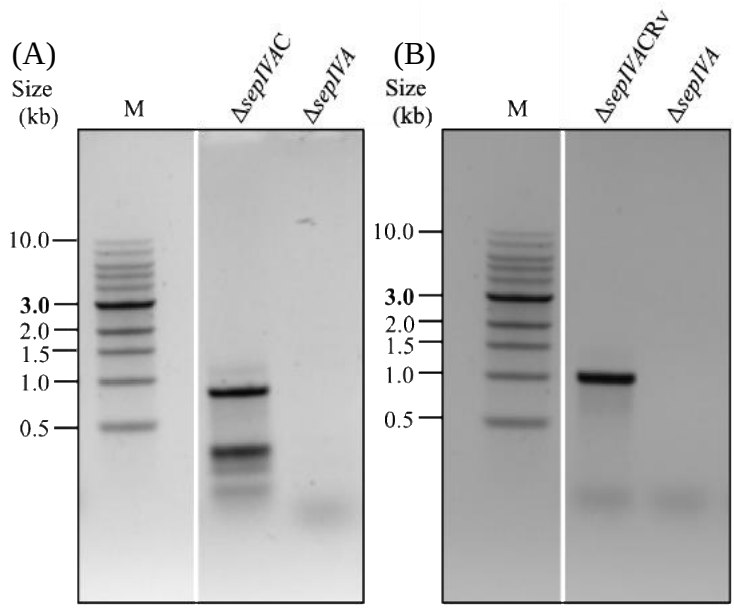

Figure 2.6. Confirmatory PCR of Δ*sepIVA* complementation with *sepIVA* and *Rv2927c*. *sepIVA* (A) and Rv2927c (B) were cloned into pMV306 and was introduced into Δ*sepIVA* separately. Complementation was verified by confirmatory PCR, with an expected band size of approximately 1kb. M, DNA ladder marker.

2.2.3 The effect of *sepIVA* deletion in *M. smegmatis* mc^2 155 on growth in liquid media

To determine whether the deletion of *sepIVA* had any effect on growth and replication, a growth rate analysis was carried out, including *M. smegmatis* mc^2 155 WT, Δ*sepIVA* and Δ*sepIVA*C. All bacterial strains were cultured, in triplicate, in TSB broth, supplemented with 0.05% Tween-80 and grown at 37°C, with agitation. At each time point, an aliquot was taken, and diluted in sterile PBS, with dilutions plated, and colony forming units counted subsequently. No significant difference in the growth rate of the mutant strain when compared to the parental WT *M. smegmatis* mc^2 155 (Figure 2.7).

Upon culturing *M. smegmatis* mc^2 155 Δ*sepIVA* in liquid media, the cells were noticeably clumpy (Figure 2.8), when compared to both wildtype *M. smegmatis*. A wildtype phenotype was restored upon complementation of Δ*sepIVA* with *sepIVA*.

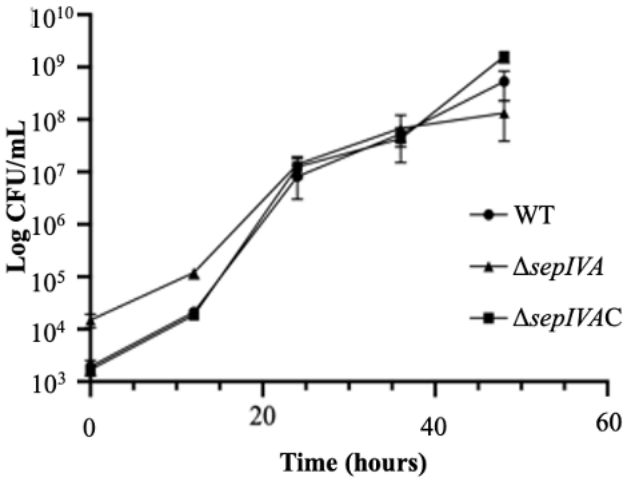

Figure 2.7. Growth curve of wildtype *M. smegmatis*, Δ*sepIVA* and Δ*sepIVA*C. All strains were cultured in TSB supplemented with 0.05% Tween-80, and grown at 37°C with agitation. Aliquots were taken at each time point and serial dilutions were plated to determine CFU/ml. There was no significant difference in growth rate as a result of the loss of *sepIVA* from *M. smegmatis* mc^2 155. WT, wildtype.

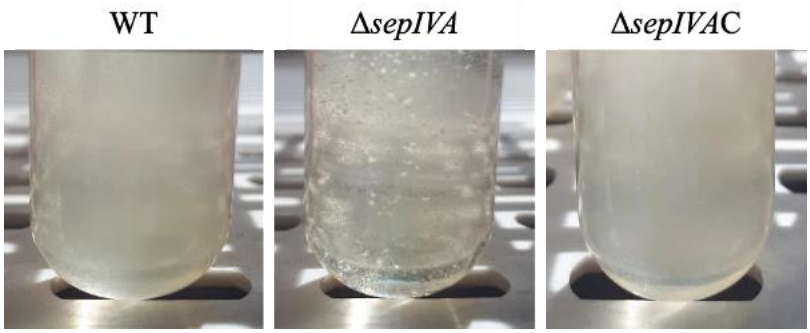

Figure 2.8. Growth phenotype of wildtype *M. smegmatis*, Δ*sepIVA* and Δ*sepIVA*C when cultured in liquid media. All strains were cultured in TSB supplemented with 0.05% Tween-80, and grown at 37°C with agitation. Photographs were taken 36 hours post inoculation. Δ*sepIVA* was noticeably clumpy compared with wildtype *M. smegmatis* and Δ*sepIVA*C. WT, wildtype.

2.2.4 The effect of *sepIVA* deletion in *M. smegmatis* mc^2 155 on colony morphology

To determine whether the deletion of *sepIVA* had any effect on bacterial morphology, a colony morphology and pellicle formation study was carried out. Bacterial strains were plated onto TSB agar plates with and without 0.05% Tween-80. Upon deletion of *sepIVA* from *M. smegmatis* mc^2 155, there was a striking difference in the appearance of colonies, as compared

to the parental WT strain (Figure 2.9); colonies appeared more 'dry' and convoluted compared to the WT strain, with the phenotype more apparent when cultured on tryptic soy agar supplemented with 0.05% Tween-80. Introduction of an integrating plasmid-borne copy of *sepIVA* with its native promoter into Δ*sepIVA* restored colony morphology to that of the WT strain indicating that the observed changes were solely due to the loss of *sepIVA*. Colony morphology could also be restored in Δ*sepIVA* transformed with a plasmid-borne copy of *Rv2927c* indicating that the *M. tuberculosis* homologue could functionally complement the Δ*sepIVA* mutant.

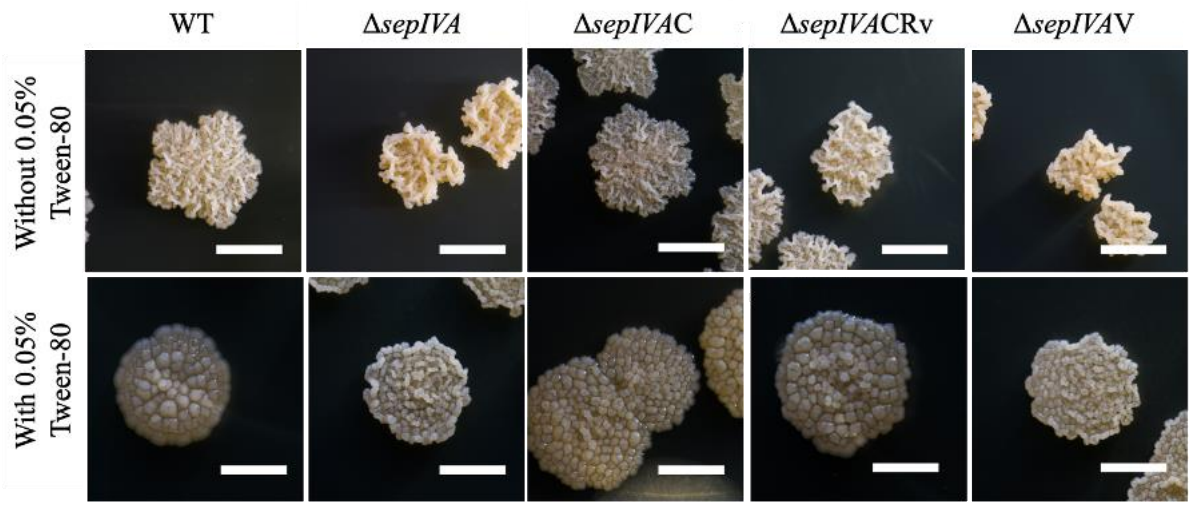

Figure 2.9. Colony morphology of wildtype *M. smegmatis*, Δ*sepIVA* and Δ*sepIVA*C. Single colonies of WT *M. smegmatis*, Δ*sepIVA*, Δ*sepIVA*C, Δ*sepIVA*CRv and Δ*sepIVA*V were cultured on TSB agar with and without the supplementation of 0.05% Tween-80. The loss of *sepIVA* resulted in a more wrinkled, convoluted colony morphology, which was more apparent in the presence of 0.05% Tween-80. WT, wildtype. Scale bar – 5mm.

2.2.5 The effect of *sepIVA* deletion in *M. smegmatis* mc^2 155 on pellicle formation

A pellicle is a biofilm that forms on the air-water interface. The pellicle forming ability of the strains was studied, to determine whether the loss of *sepIVA* from *M. smegmatis* mc^2 155 impaired the strains ability to form an intact pellicle. The mutant demonstrated an impaired

ability to form a pellicle, with native formation restored in the complemented strain (Figure 2.10).

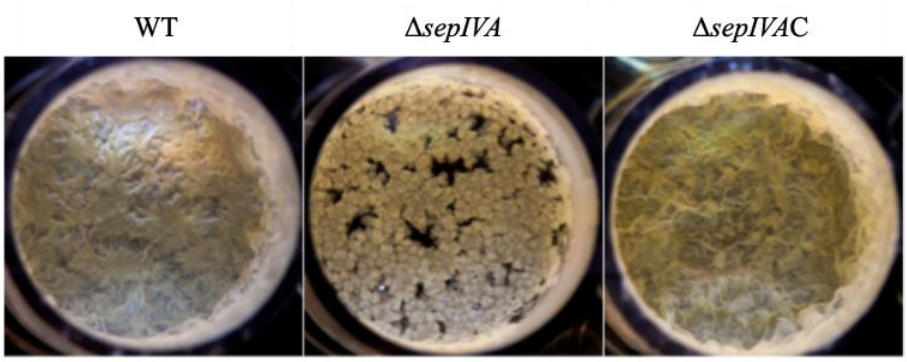

Figure 2.10. Pellicle forming ability of wildtype *M. smegmatis*, Δ*sepIVA* and Δ*sepIVA*C. Pellicle formation of wildtype *M. smegmatis*, Δ*sepIVA* and Δ*sepIVA*C, when cultured in Sauton's media. The loss of *sepIVA6* resulted in a defect in ability to form an intact pellicle. WT, wildtype.

2.2.6 The lipid profile of *M. smegmatis* mc^2 155 Δ*sepIVA*

A change in colony morphology from wildtype phenotype following a gene deletion is frequently indicative of a change in the cell envelope lipid content. Additionally, cell wall lipid biosynthesis enzymes are known to interact with the cytoskeletal machinery to coordinate cell wall biogenesis with polar growth (Kang *et al*., 2008; Jani *et al*., 2008) For these reasons, the lipid profile of Δ*sepIVA* and its respective WT and complemented strain were analysed, when strains were grown on solid media, supplemented with and without 0.05% Tween-80. The lipid profiles of *M. smegmatis* mc^2 155 WT, Δ*sepIVA* and Δ*sepIVA*C were analysed by thin layer chromatography. Figure 2.11 and Figure 2.12 show that there are no obvious differences in the lipid content of the cell wall of Δ*sepIVA*, when compared to WT or Δ*sepIVA*C, in terms of both polar and apolar lipids, and also fatty acid and mycolic acid methyl esters (FAMEs and MAMEs) respectively; therefore, the change in colony morphology is not as a result of a change in cell envelope lipid content.

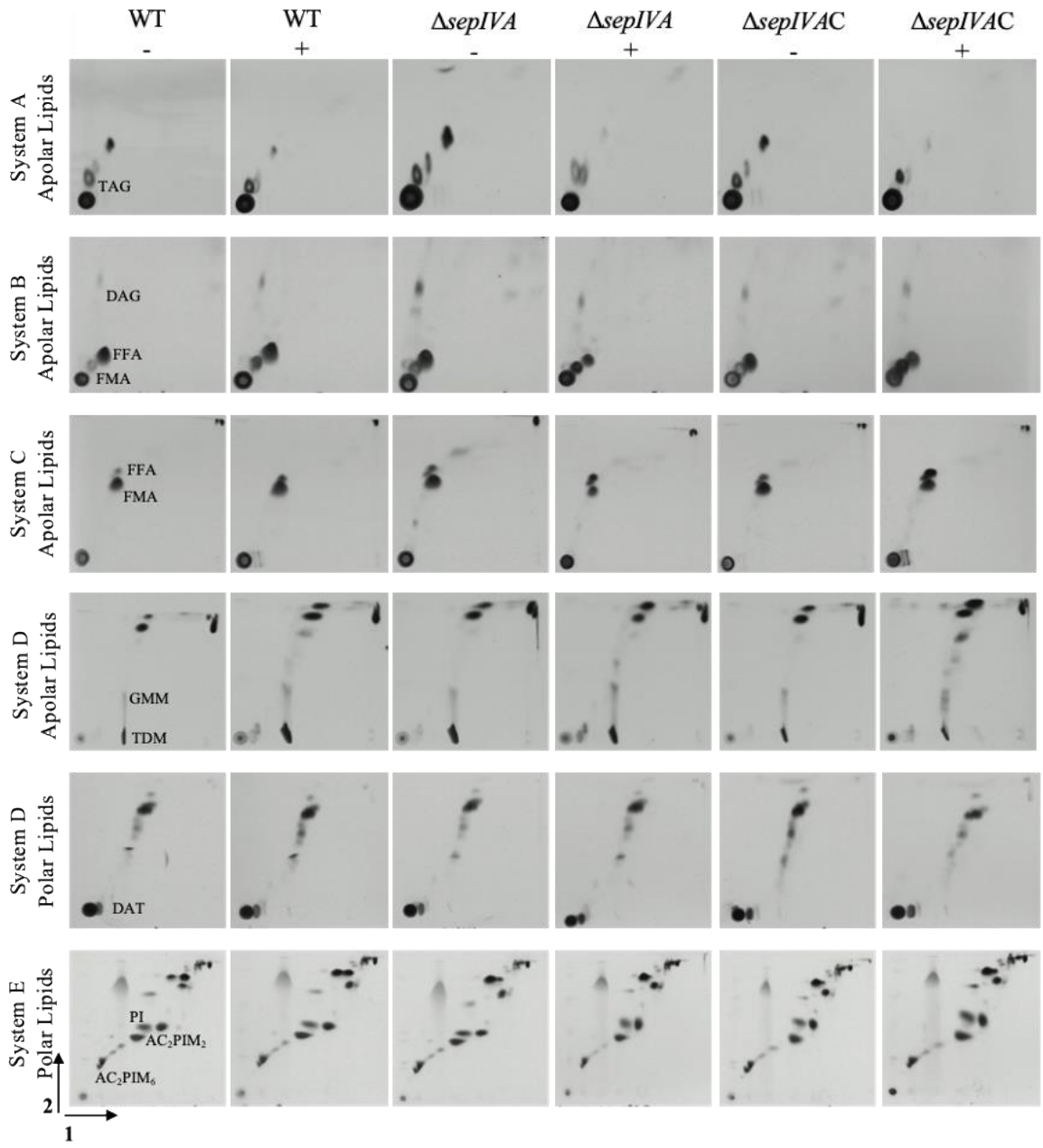

Figure 2.11. Lipid analysis of wildtype *M. smegmatis*, Δ*sepIVA* and Δ*sepIVA*C. 2D-TLC analysis of [^{14}C]-labelled lipids extracted from strains that were cultured on ^{14}C-acetic acid labelled TSB agar, with and without the supplementation of 0.05% Tween-80. Colony material was collected and a full lipid extraction was carried out. 20,000cpm of extracted lipids were spotted onto a silica plate, then separated using different solvent systems (see General Materials and Methods Chapter for full protocol of lipid extraction and solvent systems). No difference in lipids profiles was identified following the loss of *MSMEG2416*, regardless of the 0.05% Tween-80 supplementation, in terms of polar and apolar lipid content. WT, wildtype. TAG, triacylglycerols; DAG, diacylglycerols; FFA, free fatty acid; FMA, free mycolic acid; GMM, glucose monomycolate; TDM, trehalose dimycolate; DAT, diacyltrehalose mycolate; PI, phosphatidylinositol; AC_2PIM_2, diacyl phosphatidylinositol dimannoside ; AC_2PIM_6, diacyl phosphatidylinositol hexamannoside

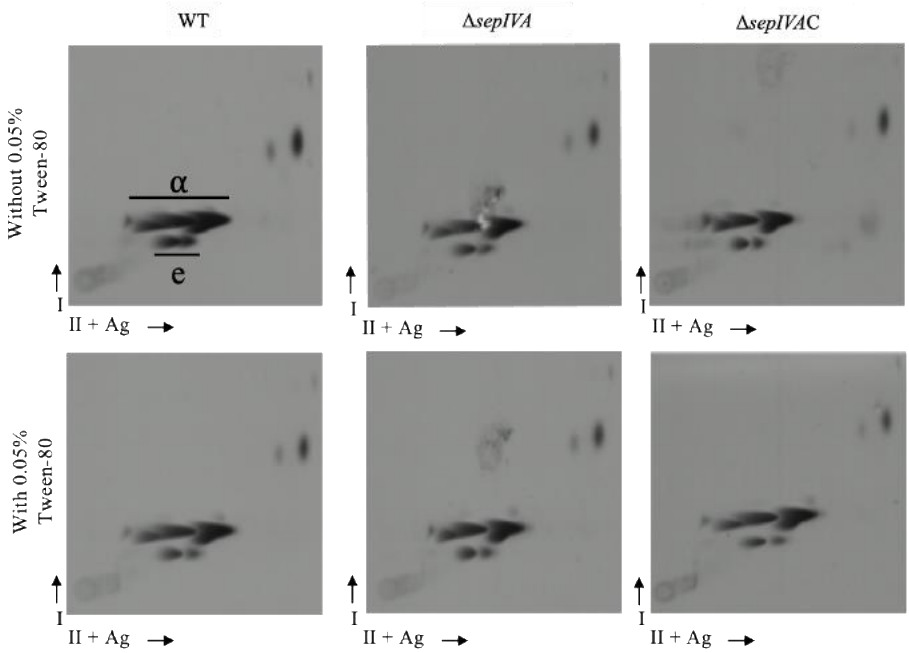

Figure 2.12. Mycolic acid analysis of wildtype *M. smegmatis*, Δ*sepIVA* and Δ*sepIVA*C. FAMEs and MAMEs were extracted from the delipidated cell pellet following previous full lipid extraction. 20,000cpm of each lipid extract was spotted onto a silica plate and was analysed by 2D-Ag^+-argentation TLC (see General Materials and Methods for protocols of lipid extraction, 2D-Ag^+-argentation TLC and the solvent system used). No difference was observed following the loss of *sepIVA*, regardless of 0.05% Tween-80 supplementation, in terms of mycolic acid content. WT, wildtype. α, alpha-mycolates; e, epoxy-mycolates

2.2.7 The effect of *sepIVA* deletion on cell length

As there were no observed changes in lipid content of Δ*sepIVA* compared to WT and *sepIVA*C, the cell phenotype was studied microscopically to determine if the change in colony morphology was as a result in differing cell morphology. A population of 250 cell were measured to determine variation in cell length. It was found that Δ*sepIVA* cells were significantly longer than WT and Δ*sepIVA*C cells, from the population sampled (Figure 2.13); the average cell length of WT, Δ*sepIVA* and Δ*sepIVA*C were 5.4μm, 8.8μm and 6.5μm, respectively, suggesting that a loss of *sepIVA* impacted average cell length.

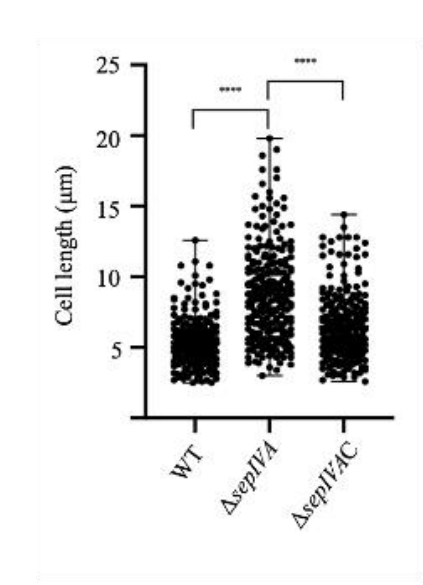

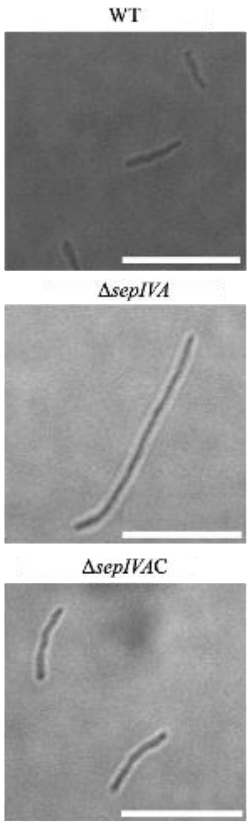

Strain	Average Length (µm)	Standard Deviation (µm)
WT	5.4	1.7
Δ*sepIVA*	8.8	3.3
Δ*sepIVA*C	6.5	2.3

Figure 2.13. Microscopy and cell length analysis of wildtype *M. smegmatis*, Δ*sepIVA* and Δ*sepIVA*C. Strains were cultured in TSB supplemented with 0.05% Tween-80, and visualised at 100X magnification. A sample of 250 cells were measured to determine average cell lengths. The deletion of *sepIVA* resulted in the production of significantly longer cells, when compared to wildtype *M. smegmatis* and Δ*sepIVA*C. WT, wildtype; ****, $P<0.0001$. (Scale bar, 10µm). Panel on the left shows a bar graph of all measurements taken.

2.2.8 The effect of *sepIVA* deletion on septation and chromosomal segregation in *M. smegmatis* mc^2 155

Δ*sepIVA* cells were significantly longer when compared to WT and Δ*sepIVA* cells. To further query the long phenotype that was observed in the Δ*sepIVA* strain, the formation of septa in the mutant strain was investigated using fluorescent vancomycin staining. As seen inFigure 2.14, more irregular, frequent septation pattern was observed in the mutant strain compared to the WT strain; the longer cells of Δs*epIVA* had more crosswalls and often generated mini-compartments. Septation phenotypes were restored to WT patterns in the

complemented strain. This finding shows that the loss of *sepIVA* dysregulated patterns of septum formation in *M. smegmatis.*

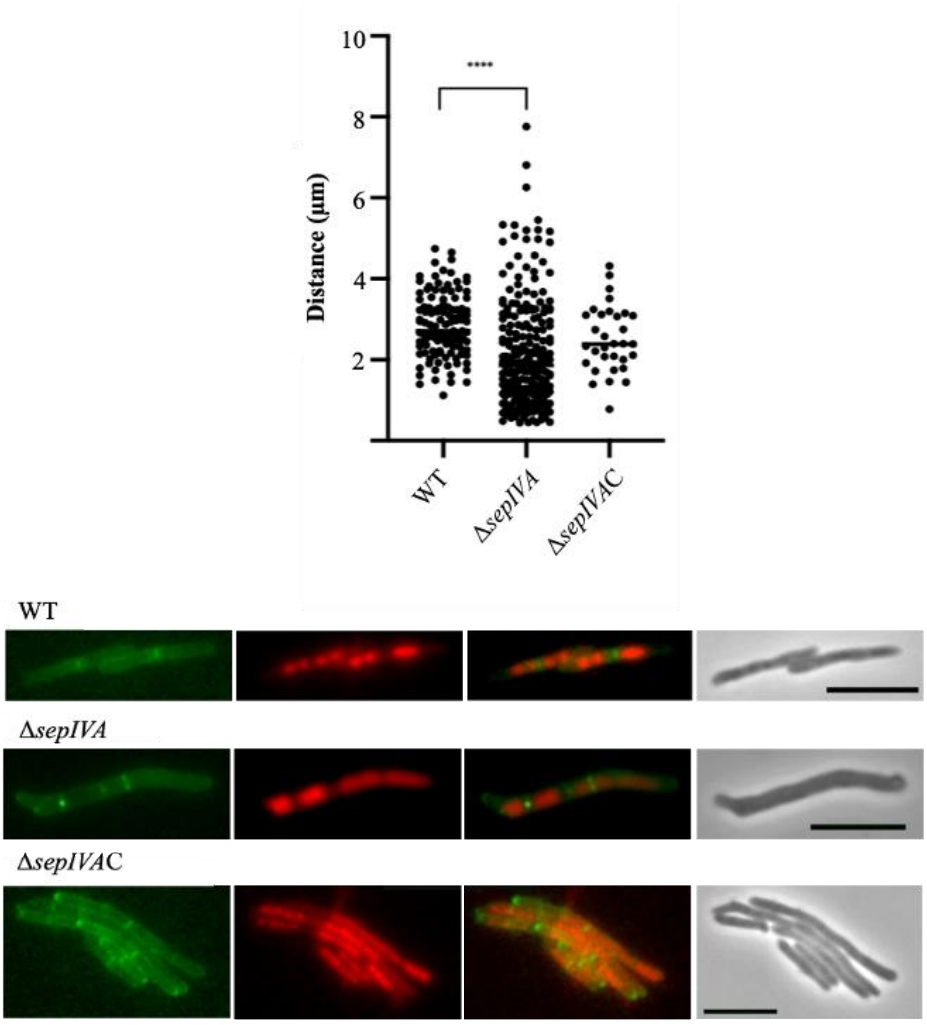

Figure 2.14. Fluorescence microscopy and analysis of septation of wildtype *M. smegmatis*, Δ*sepIVA* and Δ*sepIVA*C. Strains were cultured in TSB supplemented with 0.05% Tween-80, and the cell membrane and chromosomal matter was stained using fluorescent vancomycin and propidium iodide, respectively. The distance between septa of a population of cells was recorded and analysed statistically. *sepIVA* deletion resulted in aberrant septation, with the distance between septa to septa, or cell end statistically shorter than wildtype M. smegmatis. WT, wildtype. ****, P<0.0001. (Scale bar, 10µm).

2.2.9 The *in vitro* assembly of SepIVA

SepIVA is coiled-coil in nature, and displays the basic intermediate filament-like protein architecture, of a central rod domain of alternating coiled-coil segments and linkers (Herrmann & Aebi, 2004). Additionally, SepIVA bears similarity to the *S. coelicolor* protein

Scy, which, as an intermediate filament-like protein, is able to self-assemble into filaments *in vitro*. For these reasons, SepIVA was purified, and its ability to form filaments *in vitro* was investigated.

SepIVA was cloned into the expression vector, pET28b, using the primer pair SepIVA_pET28b_F and SepIVA_pET28b_R, to generate the construct pET28b- *sepIVA*. This construct was transformed into *E. coli* BL21, and overexpression was induced, once an OD_{600} of 0.5 was reached (following incubation at 37°C), with the addition of 1mM IPTG. The culture was further incubated at 16°C, 180rpm overnight. Following a wash with PBS, the pellet was resuspended in lysis buffer (25mM Tris, 250mM NaCl, pH 7, 5% glycerol + protease inhibitor), and the cell suspension was lysed by sonication (30 seconds on, 30 seconds off for 10 cycles on ice. Following centrifugation at 15,000rpm for 1 hour at 4°C, the soluble fraction was filtered through 0.22μm filters. A 1ml HisTrap HP column (loaded with Ni sepharose high performance affinity resin) was washed with sterile double distilled H_2O, followed by lysis buffer. The column was then equilibrated with lysis buffer + 10mM imidazole. The filtered soluble fraction was applied and immobilised to the column and the column was washed with lysis buffer with increasing concentrations of imidazole (20mM, 100mM, 200mM, 300mM, 500mM, 1M and 2M). The flow through from each wash was collected, and samples were boiled for 10 minutes in 1X protein loading buffer. Samples were loaded onto SDS-PAGE and ran for 1 hour at 20V, 300mA (Figure 2.15A), followed by a Western blot to confirm His-tagged protein.

The purified protein was dialysed into 20mM Tris, 150mM NaCl, pH 8, and was negatively stained with freshly prepared 2% ammonium molybdate (pH 8) on a 400-mesh copper grid with a carbon coated pyroxylin support film. The grids were viewed by transmission electron microscopy (TEM), to determine the *in vitro* characteristics of SepIVA,

in terms of the ability to form filaments. SepIVA failed to form an organized filamentous structure *in vitro* (Figure 2.15).

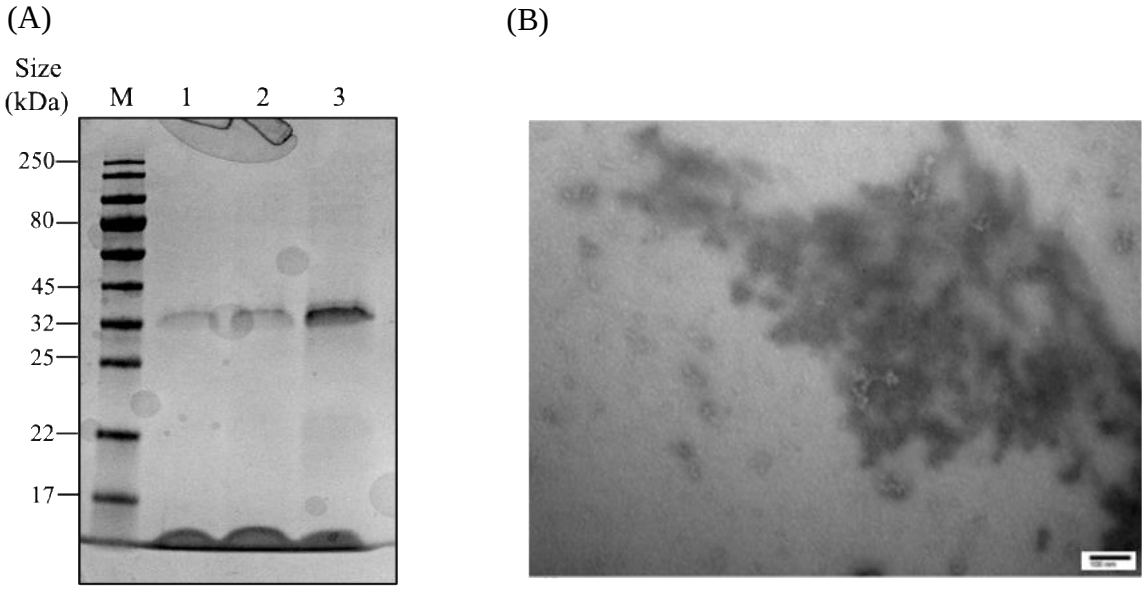

Figure 2.15. SDS-PAGE and negative staining of purified His-tagged SepIVA. His-tagged SepIVA was overexpressed in *E. coli* BL21. Cells were lysed and the lysate was centrifuged at 15,000rpm for 1 hour at 4°C. the soluble fraction was purified using Ni-NTA affinity chromatography and increasing concentrations of imidazole were used to elute the bound purified protein. Samples were loaded onto SDS-PAGE to confirm protein presence and assess purity (A). Purified protein was dialysed into the appropriate buffer for negative staining. Negatively stained protein was applied to a grid, and protein was viewed using TEM microscopy, to assess filament formation (B).

2.2.10 Identifying potential interacting partners of SepIVA

To identify potential interacting partners of SepIVA in *M. smegmatis*, and its *M. tuberculosis* homologue, Rv2927c, the bacterial adenylate cyclase-based two-hybrid (BACTH) assay was utilised. This assay is based upon the reconstitution of separated components of the adenylate cyclase of *Bordetella pertussis* when proteins, cloned into BACTH vectors, are brought into close proximity due to protein interaction. The resultant cyclic AMP production, and subsequent increased expression of the *lac* and *mal* operons, allows for distinction and confirmation of protein interaction, upon plating on selective media. Additionally, the β-galactosidase assay was utilised to quantify the strength of the interaction between the proteins.

The bait protein, in this case SepIVA or Rv2927c, were cloned into pKNT25, whilst the prey protein (potential interacting partners), were cloned into pUT18. Due to the conserved DivIVA domain of SepIVA, the potential interacting partners chosen were those with roles in mycobacterial polar growth and septation, including the cell division proteins FtsZ and FtsI, and the DivIVA homologue, the cell wall synthesis protein Wag31. Figure 2.16 shows that there were no positive interactions identified between the bait and prey proteins studied.

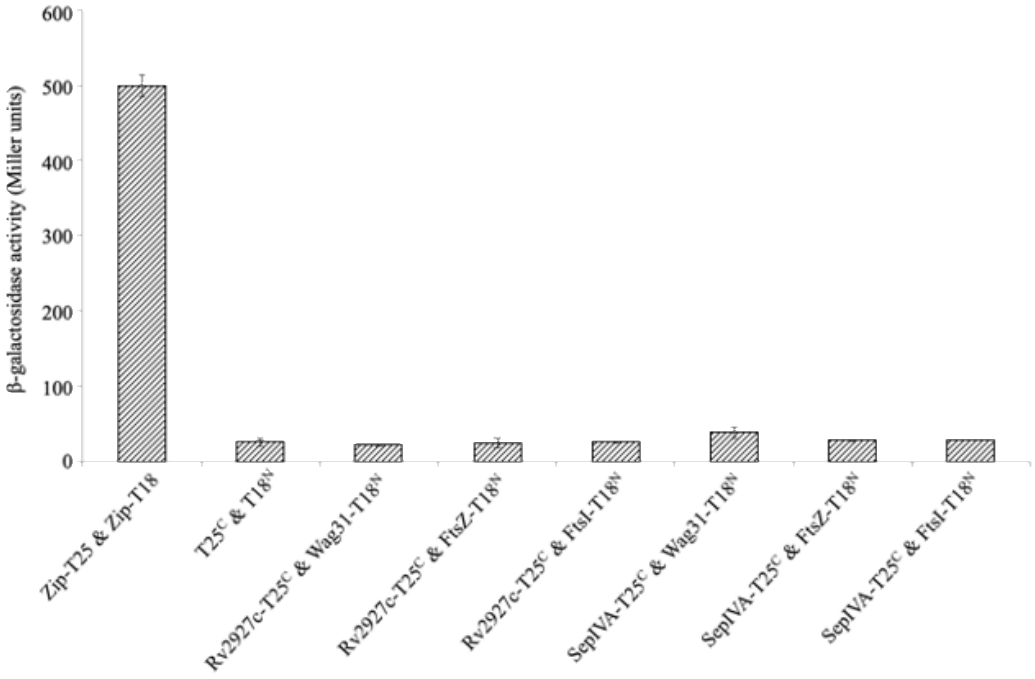

Figure 2.16. BACTH analysis of interactions between *M. tuberculosis* Rv2927c and *M. smegmatis* SepIVA and potential *M. tuberculosis* interactors. All genes encoding full length proteins were cloned into pUT18 and pKT25, fused in frame with adenylate cyclase T25 or T18 fragments. Resultant plasmids were co-transformed into *E. coli* BTH101. The efficiencies of functional complementation between the hybrid proteins were quantified by measuring β-galactosidase activities in toluene-treated *E. coli* BTH101 harbouring the corresponding plasmids. A strain expressing T25 and T18 fragments fused to a leucine zipper domain were used as a positive control (Zip-T25 & Zip-T18). The empty vectors pKT25-pUT18 were used as a negative control ($T25^C$ & $T18^N$). Results are expressed in Miller units and are the mean ± standard deviation of three independent experiments, in triplicate.

An alternative method was utilised to determine potential interacting partners of SepIVA in *M. smegmatis*. *sepIVA* was cloned into the vector pMyNT, which carries a kanamycin resistance, an N-terminal His tag and an acetamidase regulon, using the primer pair

SepIVA_pMyNT_F and SepIVA_pMyNT_R. *M. smegmatis* transformed with the recombinant plasmid was cultured at 37°C for until an OD_{600} 1.0 was reached. Protein overexpression was induced with the addition of 34mM acetamide, and cells were incubated for a further 24 hours at 37°C. Cells were washed, resuspended in PBS 0.05% Tween-80, 0.13% paraformaldehyde, to crosslink interacting protein and incubated for 1 hour at 37°C. The cell suspension was resuspended in lysis buffer (100mM Tris, 150mM NaCl, 1mM EDTA, pH 7 + protease inhibitor). Cells were lysed by sonication, and the cell lysate was centrifuged at 18,000rpm for 45 minutes at 4°C. The cell lysate was incubated with Ni-NTA resin for 2 hours at 4°C, with agitation. Protein was eluted using an imidazole gradient. Fractions were collected for each elution and visualised by SDS-PAGE, to identify potential interacting partners of SepIVA. *M. smegmatis* mc^2 155 transformed with the empty vector pMyNT was used as a control. Approximately 8 bands were observed following SDS-PAGE of samples (Figure 2.17). Identified in the interaction study were numerous proteins involved in the various stages of the biosynthesis of mycobacterial lipids and mycolic acids (Pks16, Pks13 AccA3, PanK and FadD35), in addition to proteins that have shown to be, or may be, involved in cell growth and division (Wag31, WhiA and FtsE).

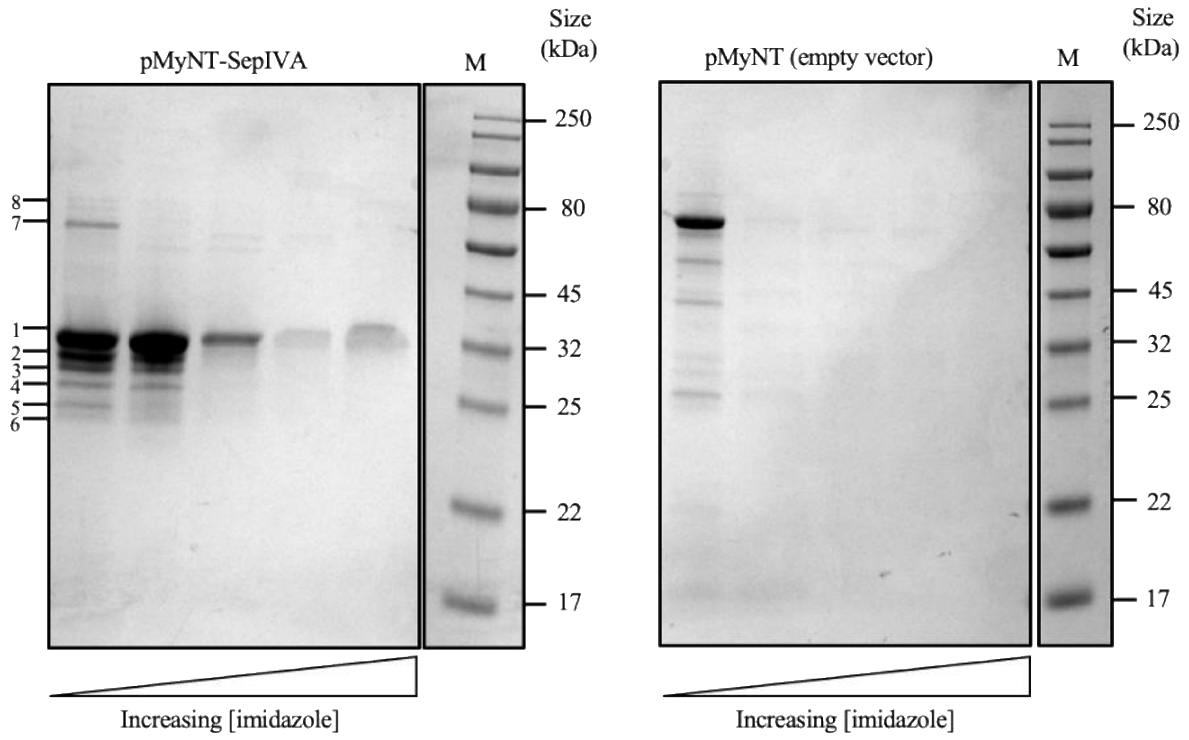

Band No.	Protein	Gene	Description	Coverage (%)	Unique Peptides
1	MSMEG2416			41	2
	MSMEG5252	*coaA*	Pantothenate Kinase	25	2
2	MSMEG4217	*wag31*	Cell wall synthesis protein	64	13
	MSMEG	*fadD32*	Long chain fatty acid AMP ligase	44	15
	MSMEG2416			25	2
	MSMEG5252	*coaA*	Pantothenate Kinase	18	4
	MSMEG1583	*groEL1*	Chaperonin	2	14
3	MSMEG2416			41	2
4	MSMEG3894	*prcA*	Proteasome alpha subunit	46	8
	MSMEG2416			37	2
	MSMEG3895	*prcB*	Proteasome beta subunit	36	6
5	MSMEG2089	*ftsE*	Cell division ATP-binding protein	38	6
	MSMEG2416			1	6
6	MSMEG2750	*ideR*	Iron-dependent repressor IdeR	64	11
	MSMEG2416			26	2
	MSMEG4891	*ahpC*	Alkylhydroperoxide reductase	1	6
7	MSMEG1583	*groEL1*	Chaperonin	63	14
	MSMEG1401	*tuf*	Elongation factor Tu	45	3
	MSMEG0880	*groEL2*	Chaperonin	17	25
	MSMEG5435	*pks16*	Acyl-CoA synthase	13	4
	MSMEG5892	*otsA*	Alpha-trehalose-phosphate synthase (UDP-forming)	8	3
8	MSMEG1582	*groeS*	Chaperone protein	36	7
	MSMEG0709	*dnaK*	Chaperone protein	29	7
	MSMEG6393	*fadD32*	Long chain fatty acid AMP ligase	24	13
	MSMEG1807	*accA3*	Acetyl-/propionyl-coenzyme A carboxylase alpha chain	8	4
	MSMEG6392	*pks13*	Polyketide synthase	5	4
	MSMEG4254	*fadD15*	Long chain fatty acid CoA ligase	4	2

Figure 2.17. SDS-PAGE analysis of protein samples that are present following the overexpression of SepIVA in *M. smegmatis*, following nickel affinity purification. SepIVA was fused to a His-tag and overexpressed in *M. smegmatis*, in the acetamide inducible vector, pMyNT. Interacting proteins were crosslinked following incubation with paraformaldehyde. Cells were lysed and centrifuged prior to incubation with Ni-NTA resin for 2 hours at 4°C. Protein was eluted using an imidazole gradient. Fractions were collected and analysed by SDS-PAGE. Bands of interest were excised and submitted for mass spectrometry.

2.3 DISCUSSION

In the widely studied *E. coli* and *B. subtilis*, nascent cell wall material is incorporated along the length of the cell in a lateral manner and septation occurs at a precise mid-point, giving rise to identical daughter. Actinobacteria elongate from the poles in an asymmetric manner (Dahl, 2004), with Z-ring assembly and more dispersed when compared to the laterally growing *E. coli* (Singh *et al*., 2013), resulting in a highly heterogenous population. Mycobacteria lack the expected homologs, found in laterally growing bacteria, that drive cell growth, shape maintenance and division, indicating that actinobacteria may possess a unique pathway and set of proteins that may have a role in polar elongation or in organising biosynthetic machinery to the site of cell wall material incorporation, whether this be the cell poles, of the septa. SepIVA was selected for investigation in this study, as it is a coiled coil protein similar to other coiled coil proteins involved in polar growth in other bacteria.

2.3.1 SepIVA is conserved across the *Actinomycetale* order, and is absent from laterally growing rod-shaped bacteria, such as *E. coli* and *B. subtilis*

SepIVA was utilised in a BLASTP search, as a query against many rod-shaped bacterial species. SepIVA was found to be conserved across mycobacterial species, with homologues identified in pathogenic, opportunistic and non-pathogenic environmental mycobacteria. SepIVA homologues were also identified in numerous *Corynebacterianea* members, such as saprophytic soil-dwelling, mycolate producing *Nocardia*, *Rhodococcus* and *Tsukamurella*. Within the order of *Actinomycetales*, many proteins were identified, which share similarity/identity to SepIVA, including the filamentous *Streptomyces* sp., which also elongates via the polar deposition of new cell wall material at the cell tips; SepIVA was found to have approximately 43% similarity to the *S. coelicolor* coiled-coil protein, Scy, which has

been characterised as a molecular assembler, marking the sites of future branching and tip formation in addition to localising and promoting polar growth at the hyphal tips (Holmes *et al*., 2013). Interestingly, there were no significant matches following a BLASTP search using SepIVA as a query against the laterally elongating *E.coli* and *B. subtills.* These findings would suggest that *sepIVA*, and the *M. tuberculosis* homologue, *Rv2927c*, represent conserved coiled-coil proteins within the polar growth progenitors of *Actinomycetales*, yet is absent from other well studied rod-shaped bacteria, such as *E. coli* and *B. subtilis*, that elongate via the incorporation of cell wall material along the cell length.

2.3.2 *sepIVA* is not essential in the growth and survival of *M. smegmatis*

This study has begun to delineate the role of a protein, SepIVA, and its involvement in mycobacterial growth and septation; this was through the successful construction of a deletion strain, in which *sepIVA* in *M. smegmatis* was replaced with a hygromycin resistance cassette, and which demonstrated cell viability following gene replacement. This research has shown that *sepIVA* is a non-essential gene in *M. smegmatis*, contradictory to previous work by Wu *et al*. (2018) and Jain *et al.* (2018), who were unable to generate a strain in which *sepIVA* was which transcriptionally depleted.

2.3.3 The loss of *sepIVA* resulted in alterations in phenotype, including a change in colony morphology and pellicle forming ability, which was not as a result in the changes cell envelope lipid composition

Upon the deletion of *sepIVA* from *M. smegmatis*, phenotypic differences observed, when compared to WT *M. smegmatis* and Δ*sepIVA*C, including growth characteristics in liquid

media, a change in colony morphology and pellicle formation. Upon culture in liquid media, Δ*sepIVA* cells distinctly clumped more readily, compared to wildtype *M. smegmatis*. This phenotype was corrected upon complementation with *sepIVA*. Due to the waxy cell wall of mycobacteria, clumping during growth in liquid media is a common phenotype, when a detergent or surfactant is absent. Even in the presence of a 0.05% Tween-80 however, *M. smegmatis* Δ*sepIVA* cells appeared to clump more readily than wildtype *M. smegmatis.* This phenotype is one that has also been observed by Healy *et al*. (2020). Upon the deletion of RipA from *M. tuberculosis*, cells were noticeably clumpy when cultured in liquid media. RipA is a peptidoglycan hydrolase in *M. tuberculosis* that has been shown to have a role in cell division crucial during both *in vitro* growth and infection (Healy *et al*., 2020). *M. tuberculosis* cells in which RipA was deleted demonstrated an elongated multiseptated phenotype, indicative of a cell division defect; cells continue to elongate and incorporate septa, yet fail to successfully divide. Due to the similarity in the clumpy phenotype observed by both *M. smegmatis* Δ*sepIVA* and *M. tuberculosis* Δ*ripA*, and the known role of RipA in cell division, this study continued investigation into the potential role of SepIVA in mycobacterial cell division.

Although colony morphology is a complex phenotype to draw hypotheses from, subtle changes in the surface components of the cell wall can present as major colony morphology differences. Chen *et al*. (2006) constructed a mutant strain of *lsr2* in *M. smegmatis,* a previously uncharacterised cytosolic protein, which resulted in an altered colony morphology as a result in the loss of two apolar mycolate-containing lipids, as well as an inability to form a full intact pellicle. Additionally, Alexander *et al.* (2004) generated a *Mycobacterium marinum* strain in which a mutation in PimF caused a change in colony morphology; as an enzyme involved in the biosynthesis of phosphatidylinositol mannosides (PIMs) and also LAM and LM, all key mannose-containing glycolipids of the mycobacterial cell wall, the change in certain products of lipid biosynthesis pathways is the causative factor for the altered colony morphology. A

change in the surface components of a cell population may alter the cell-to-cell interactions observed; an obvious difference in growth when cultured in liquid media (increased clumping from Δ*sepIVA*) in conjunction to the changes in colony morphology and defective pellicle forming ability, further corroborated the theory that these findings were as a result of the deletion of *sepIVA*, causing an unknown change to cell surface. For that reason, a full lipid analysis was carried out, to determine any potential differences between Δ*sepIVA*, WT *M. smegmatis* and Δ*sepIVA*C. Cell wall lipid components analysed by thin layer chromatography revealed no changes in the apolar or polar lipids, or the mycolic acids. This directed the study towards investigation of individual cells, in terms of the shape and architecture.

2.3.4 The loss of *sepIVA* resulted in an elongated phenotype, due to increased aberrant septation

An analysis of cell length found that the Δ*sepIVA* cell population sampled were significantly longer than WT *M. smegmatis* and Δ*sepIVA*C. This filamentous nature, following *sepIVA* deletion, in addition to maintaining viability, may indicate an inability of cells to divide. The study by Wu *et al.* (2018), which depleted *sepIVA* from *M. smegmatis*, also found that cells displayed a filamentous phenotype, with a failure to divide. Other studies have identified an elongated phenotype in mycobacteria following the depletion of certain cell division and elongation factors. Dziadek *et al*. (2003) depleted FtsZ, the tubulin homologue that assembles into protofilaments, forming the Z-ring, a recruiter of cell division and cell wall biosynthetic machinery, and also the earliest marker of future site of division (Erickson, 1995), from *M. smegmatis*; cells, in which FtsZ production was blocked, were longer in length and demonstrated a decreased viability, yet no excessive nucleoid segregation was observed, as multiseptate cells were not identified. Numerous studies have depleted PknA and PknB, serine/

threonine kinases that are part of an operon involved in the maintenance of cell shape and also cell elongation; Wag31, the mycobacterial cell wall and shape regulator (Kang *et al.*, 2008), is a substrate of these kinases (Kang *et al.*, 2005). Strains depleted of PknA and PknB demonstrated an elongated phenotype also (Kang *et al.*, 2005; Nagarajan *et al.*, 2015). Located in the same cluster as *pknA* and *pknB* is *pstP*, encoding a serine/ threonine protein phosphatase. Sharma *et al*. (2016) were able to generate elongated cells of *M. smegmatis*, with multiple septa, as a result of the depletion of PstP. Also located downstream of *pstP*, in the same operon, is *rodA* and *pbpA*, which encode RodA and PbpA respectively, two proteins required for the regulation of mycobacterial cell length and peptidoglycan synthesis (Arora *et al.*, 2018). Studies have identified that *rodA* and *pbpA* are co-transcribed with *pstP*, (Kang *et al*., 2005; Arora *et al.*, 2018), demonstrating its regulatory role in cell growth and division. The approximately 6-fold increase in multiseptate cells, compared to wildtype *M. smegmatis*, would suggest that PstP has a critical role in both cell elongation and cell division. The proteins mentioned above are found to localise with the mycobacterial divisome, the complex of cell division machinery. With research by Wu *et al* (2018) identifying that SepIVA localisation coincides with that of the divisome also, and the elongated phenotype observed upon SepIVA deletion, like that seen following the depletion of these mentioned proteins, it may be likely that SepIVA interacts with the divisome.

Following *sepIVA* deletion, and visualisation of the cell membrane and septa using fluorescent vancomycin, it was observed that the distance between septa was significantly less than when compared to WT *M. smegmatis* and Δ*sepIVA*C. Although the septa number per cell was not quantified, septa visualisation highlighted the multiple septa present per cell, as a result of the gene deletion; aberrant septation was clear when compared to WT *M. smegmatis* and Δ*sepIVA*C, with the uniform presence of a single mid cell septa.

In the case of *sepIVA* deletion, aberrant septation was observed, in a population of elongated cells. A study by Healy *et al.* (2020) determined that upon the deletion of RipA, an *M. tuberculosis* peptidoglycan hydrolase, the median cell length was also significantly increased compared to the wildtype and complemented cells. Additionally, over half of the Δ*ripA* population contained more than one septum indicating continuous elongation without successful cell division. This division defect was exacerbated upon the deletion of Ami1, a peptidoglycan amidase, in a Δ*ripA* background. The importance of these enzymes in survival and growth is demonstrated in the increased sensitivity of a RipA depleted *M. tuberculosis* strain to cell wall-targeting and mycobactericidal frontline drugs, such as isoniazid and vancomycin, and rifampicin, respectively (Healy *et al*., 2020). Additionally, during bone marrow derived macrophage (BMDM) infection, *ripA* silencing resulted in halted replication, and bacterial clearance during a mouse infection. This further demonstrates the requirement of this peptidoglycan hydrolase in *in vivo* cell division (Healy *et al*., 2020). A clumpy phenotype observed (when grown in liquid media) in both *M. tuberculosis* Δ*ripA*, and in *M. smegmatis* Δ*sepIVA*, in addition to the similarity of increased median cell length and septum number per cell. It would be interesting to continue future work in the direction of investigating a role of SepIVA in peptidoglycan modification and synthesis, necessary for cell elongation and division. Whilst SepIVA does not have an apparent enzymatic domain (Wu *et al*., 2018), this is similar to the major role of Wag31. As a regulator in cell wall, Wag31 is crucial for maintaining mycobacterial cell shape and cell wall synthesis by localizing peptidoglycan synthesis machinery to the sites of nascent cell wall material incorporation (Kang *et al*., 2008). It may be hypothesised that SepIVA may have a regulatory role in contributing to the construction of the cell septa, via yet to be determined interactions with cell wall precursor enzymes (Wu *et al*., 2018).

The changes observed in septa formation, as a result of *sepIVA* deletion from *M. smegmatis* mc^2 155 indicates that SepIVA may be controlling and limiting the frequency of septa synthesised in the cell. Research by Wu *et al.* (2018) identified that SepIVA localises to the pole and also the cell septa, in a dynamic manner throughout the cell cycle. These are sites of cell wall biosynthesis, and hence the sites where biosynthetic machinery is recruited, to drive cell elongation (the poles) and septa formation. This finding, of SepIVA localisation to sites of cell wall biosynthesis, in addition to the finding from this study showing more frequent septa formation in Δ*sepIVA* further solidifies the potential role of SepIVA in controlling septa biosynthesis and the coordination of biosynthetic machinery at the cell poles, the sites of nascent cell wall incorporation.

2.3.5 Purified SepIVA failed to form a higher order filamentous structure *in vitro*

Similarity to the Scy protein to *S. coelicolor* led to a brief study of the *in vitro* assembly of SepIVA, to identify whether it was able to self-assemble into filaments, a characteristic observed by purified Scy (Holmes *et al.*, 2013) and other intermediate filament-like proteins. SepIVA purified from *E. coli* failed to form filaments *in vitro*. In addition to the cytoskeletal filament forming actin and tubulin superfamilies (such as FtsZ and MreB), coiled coil proteins, that assemble into intermediate filaments are widely distributed proteins that typically function as cellular scaffolds, often with a structural role or as recruiters of other proteins (Wagstaff & Löwe, 2018).

The inability of purified SepIVA to assemble into higher ordered filamentous structures *in vitro*, whilst it doesn't rule out a potential structural role of SepIVA in *M. smegmatis* mc^2 155, it does provide valuable information on the behaviour of this protein, more specifically in the buffer defined in this study. Prior to hypothesising that SepIVA does not spontaneously

self-assemble into a filamentous structure *in vitro*, alike to that of intermediate filament-like proteins, alternative buffer conditions must be explored. Optimal conditions, in terms of buffer pH, buffering compound and potential additive, are crucial in ensuring protein solubility and stability during experimentation. Work should continue to trial a range of buffers and assessing SepIVA ability to self-assemble into a filamentous structure *in vitro* prior to concluding its inability to do so.

2.3.6 SepIVA potentially interacts with mycobacterial proteins of varying function, including lipid biosynthesis, cell division and cell growth

The first approach to determine interacting partners of *M. smegmatis* SepIVA was to utilise the BACTH This assay is based upon the reconstitution of separated components of the adenylate cyclase of *Bordetella pertussis* when proteins, cloned into BACTH vectors, are brought into close proximity due to protein interaction. The resultant cyclic AMP production, and subsequent increased expression of the *lac* and *mal* operons, allows for distinction and confirmation of protein interaction, upon plating on selective media. Additionally, the β-galactosidase assay was utilised to measure the transcriptional activity and hence, quantify the strength of the interaction between the proteins. (Serebriiskii & Golemis, 2000) This approach failed to identify the chosen candidates as interactors of both *M. smegmatis* SepIVA and *M. tuberculosis* Rv2927c. This does not negate the possibility of a potential interaction between these putative interacting proteins, as limitations in the BACTH method do exist, and may have hence resulted in a false negative. The first downfall in this system is that, unlike a yeast two-hybrid system, in which a prey library can be prepared and interactors can be identified from this, the BACTH depends upon the determination of a single prey candidate. Subsequent cloning of multiple prey candidates into the BACTH vectors is labour intensive and time

consuming, compared the construction of a full prey library to be assayed at once with a single bait construct in the yeast two hybrid system. Additionally, a known limitation of two hybrid assays is the lack of detection, due to the improper folding of certain proteins intracellularly. This is especially true for membrane proteins. Lack of detection may also be due to the inability of a protein to enter the nucleus; if this is the case, transcription-based assays become redundant (Mehla *et al*., 2017). Whilst the BACTH system is a popular, well developed two hybrid method, due to the limited research on *M. smegmatis* SepIVA and its known interactors, an alternative widespread screening approach would be more beneficial at this early stage of determining the role of SepIVA.

Following the inability to determine interactors of SepIVA using the BACTH system and the limitations that it presents, an alternative method of interaction study was utilised. This involved the overexpression of the protein of interest in its native host, followed by crosslinking to preserve the interacting partners. SepIVA was overexpressed in *M. smegmatis* mc^2 155, with potential interacting partners crosslinked and purified, via the His-tagged SepIVA. Of the proteins identified in mass spectrometry analysis of the individual bands following purification, numerous of these appear to have roles in lipid and glycolipids biosynthesis, cell division and cell growth.

In this study, two proteins involved in cell growth and division were identified to interact with SepIVA, Wag31 and FtsE. As previously discussed, Wag31 is the mycobacterial DivIVA homologue, and a cell wall and shape regulator (Kang *et al*., 2008) which localises to the cell poles. The depletion of Wag31 resulted in a rounded tip phenotype, indicating an essential role of Wag31 in polar peptidoglycan synthesis, with aberrant peptidoglycan synthesis as a result of Wag31 depletion, and maintenance of cell shape. In mycobacteria, FtsE's role is somewhat speculative and based on the role of other FtsE homologues. Whilst FtsE has been shown to localise to the cell membrane (Mir *et al*., 2006), its specific location is not yet fully

understood; in *E. coli* however, FtsE localises to the septa where it interacts with FtsZ, and has a role in cell division, due to the filamentous nature of cells following the deletion of FtsE (Schmidt *et al*., 2004; de Leeuw *et al*., 1999) . Du *et al*. (2016) showed that FtsE failed to localise to septa in the absence of FtsX, speculating that FtsX provides a linker between FtsE and the divisome. What is known about FtsE in mycobacteria is that it is able to form a complex, termed FtsEX, with FtsX, which has also been shown to have a role in cell division. Based on previous research, and research of their homologues, the potential interaction of SepIVA with both Wag31 and FtsE further suggests a possible role of SepIVA in cell growth and division.

One potential interesting interacting partner of SepIVA, identified in this study, was AccA3 (MSMEG_1807). Due to the complex lipid profile of the mycobacterial cell envelope, mycobacteria possess numerous acyl-CoA carboxylases (ACCases), biotin-dependent enzymes that generates the metabolite, malonyl-CoA, catalysed from acetyl-CoA, for subsequent acyl chain elongation and *de novo* fatty acid biosynthesis, carried out by the FAS-I and FAS-II complexes (Schweizer & Hofmann, 2004). Mycobacterial acyl-CoA carboxylase (ACC) consist of three subunits, the α-subunit, β-subunit and the ε-subunit; Cole *et al*. (1998) identified that the *M. tuberculosis* genome possesses three α-subunit genes (*accA1-3*), and six β-subunit genes (*accD1-6*). Most organisms possess only one or two ACCases (Cronan & Waldrop, 2002), with it thought that mycobacteria possess so many β-subunits for the synthesis of the many unique lipids and glycolipids found in the mycobacterial cell wall. Portevin *et al.* (2005) found that AccA3 copurified with AccD4 and AccD5, and identified a potential model for the final condensation reaction of the biosynthesis of mycolic acids, including this ACC, along with two other genes, *pks13* and *faD32*; Pks13 is required for the final condensation reaction in the assembly of mycolic acids (Portevin *et al*., 2004), Fad32 links the fatty acid

synthase pathway to the polyketide synthase pathway, via transfer of fatty acids to polyketide synthase proteins, required for mycolic acid biosynthesis (Mohanty *et al*., 2011).

Interestingly, in a co-immunoprecipitation study by Xu *et al.* (2014), Wag31, which localises to the cell poles, the sites of elongation and cell wall material incorporation, has also been shown to co-immunoprecipitate with AccA3, in addition to AccD4 and AccD5, although the interaction is exclusively between Wag31 and AccA3. This further highlights the strong interaction between AccA3, AccD4 and AccD5, showing that both β-subunit could be pulled-down via the α-subunit, AccA3. Due to this interaction, it could be assumed that AccA3 also localises with Wag31. With the known interaction of AccA3 with Wag31, a regulator of cell shape and growth, it is not inappropriate to hypothesise that there is a true interaction, as seen in this study, between SepIVA and AccA3, or any other ACC subunit; like the cell poles, cell wall material synthesis and incorporation is required at the septa, where SepIVA has been shown to localise (Wu *et al.*, 2018). With the proposed role of SepIVA in potentially regulating and controlling septa biosynthesis, it would be interesting to see both the expression and localisation of AccA3 in WT mc^2 155 *M. smegmatis* in comparison to Δ*sepIVA*C; if AccA3 were to interact with SepIVA and localise to the sites of cell wall biosynthesis, it may be likely that AccA3 could be observed at the aberrant septa formed as a result of SepIVA deletion, in addition to an increased expression, due to the multiple septa observed per cell.

In the interaction study, SepIVA was found to interact with MSMEG_3081, the *M. smegmatis* mc^2 155 homologue of the *M. tuberculosis* protein, WhiA. Whilst little research has been carried out on the mycobacterial WhiA, it is predicted to be essential for growth and survival in *M. tuberculosis* H37Rv (DeJesus *et al.*, 2017). WhiA is somewhat well studied in other actinobacteria, including *Streptomyces*, where it was first characterised (Ainsa *et al.*, 2000). It has been described as a transcription factor that functions as an activator of the expression of many cell division machinery genes, including *ftsZ*, *ftsW* and *ftsK* (Bush *et al.*,

2016). The deletion of WhiA in *Streptomyces venezuelae* produced elongated cells that were unable to divide, potentially due to the repressive activity that WhiA has on the cell division proteins, especially FtsZ, which drives sporulation septation (Bush *et al*., 2016). WhiA is also present in *Corynebacteria*, where numerous proteins recruited to the divisome during septation are under its control, including FtsZ and SepF (Lee *et al*., 2018). Extrapolating research from closely related *Actinomycetales* may indicate that the role of WhiA in mycobacteria is in cell division. The potential interaction of WhiA with SepIVA, along with the aberrant septation as a result of SepIVA deletion further strengthens the hypothesis that SepIVA is mycobacterial candidate in the regulation of division.

In addition to identifying the interaction between Wag31 and AccA3, Xu *et al.* (2014) determined the expression of *accA3* to be the highest of the ACC α-subunit genes, during exponential growth phase of *M. tuberculosis*. Pawelczyk *et al*. (2011) identified that the expression of *accD4-6* by *M. smegmatis* during exponential phase, was lower when compared to *M. tuberculosis* expression of these β-subunit genes. Whilst SepIVA was found to interact with AccA3 during the interaction study, it may be that the expression levels of other β-subunit genes found to interact with AccA3, and hence, were pulled-down by Wag31, via the Acca3 interaction, may be too low for identified in this study with SepIVA. Additionally, it must be taken into consideration that AccA3 is a highly expressed protein in mycobacterial growth; further experimentation is required for the confirmation of this interaction, as the high expression of this protein (Wang *et al.*, 2005) may be enough to cause a false positive interaction in this study.

Other interacting partners of SepIVA, which have various roles in lipid biosynthesis pathways, identified in this study were Pks13 (MSMEG_6392), FadD32 (MSMEG_6393), Pks16 (MSMEG_5435) and PanK (MSMEG_5252). FadD32 and Pks13 belong to a putative operon involved in the synthesis of mycolic acids. Research has shown that the long-chain acyl

AMP ligase, FadD32, activates the meromycolic chain, prior to condensation with the shorter α-chain, which is carried out by the polyketide synthase, Pks13 (Portevin *et al.*, 2004; Trivedi *et al*., 2004; Portevin *et al.*, 2005). Both FadD32 and Pks13 are essential mycobacterial enzymes, as mycolic acid biosynthesis is an essential pathway for mycobacterial survival (Portevin *et al*., 2005; Portevin *et al*., 2004). The inhibition of FadD32 compromises the growth of *M. tuberculosis in vitro* and also intracellularly (in macrophages) (Carroll *et al*., 2011), with depletion of Pks13 in *M. smegmatis* arresting growth 6 hours post initiation of depletion (Fay *et al*., 2019).

The other two potentially interaction partners of SepIVA are Pks16 and PanK. Limited research has been carried out on the putative polyketide synthase Pks16. Vilchèze *et al.* (2014) identified that Pks16 was upregulated in a KasB phosphomimetic strain of *M. tuberculosis*, KasB being the β-ketoacyl-ACP synthases responsible for the last elongation steps of the growing acyl-ACP chains of mycolic acids, to their final length (Bhatt *et al*., 2007). This indicates an anticipated role of Pks16 in lipid biosynthesis. PanK, an essential panotothenate kinase, is encoded by *coaA*, catalyses the rate-limiting step in the coenzyme A (CoA) biosynthetic pathway (Reddy *et al*., 2014), with CoA essential for lipid biosynthesis.

With the hypothesis that SepIVA is involved in the synthesis of cell septa, it is expected that SepIVA may interact with proteins that are involved in lipid biosynthesis. Its function, however, and the role that it has in lipid biosynthetic machinery crosstalk remains somewhat unknown, and further interaction studies would determine strong interactors. As crosslinking took place in the cells, it may be likely that a number of the proteins, identified as interacting with SepIVA, may in fact be a component of a larger interacting complex, as opposed to rather directly interacting with SepIVA. Also, it has previously been shown that SepIVA interacts with FtsQ (Wu *et al*., 2018), a protein which localises to the septa, with overexpression resulting in multiseptate elongated cells, indicating a role in cell length maintenance and

division (Jain *et al.*, 2018). It may have been expected that in this study, FtsQ would have been identified as an interacting partner of SepIVA through the pulldown assay utilised. FtsQ is however, found in small abundance within the cell (Guzman *et al*., 1992). Whilst FtsQ was not identified in this mass spectrometry analysis of SepIVA interacting partners, this interaction should not be dismissed, as previous research has proven this, further contributing to the knowledge established in this study, that SepIVA interacts with this division protein, and has role is in mycobacterial cell division and septation.

SepIVA has a conserved DivIVA domain, a domain first identified in *B. subtilis*. $DivIVA_{BS}$ is a cell division initiation protein that, upon its depletion, resulted in filamentous cells, with the presence of minicells, due to aberrant division located close to the cell poles, as opposed to the mid-cell (Mendelson, 1975; Edwards & Errington, 1997), indicating a role of DivIVA in septa positioning. The *divIVA* homolog in mycobacteria, *wag31*, has a differing role to $DivIVA_{BS}$; Wag31 is involved in the maintenance of cell shape and growth, essential for peptidoglycan synthesis at its sites of localisation, the cell poles and the septa (Kang *et al*., 2008). Despite the reasonable similarity and identity of SepIVA with Wag31, 29.4% and 19.7% respectively (Wu *et al*., 2018), it would appear from this study that the role of SepIVA is similar to that of $DivIVA_{BS}$; DivIVA depletion results in filamentous cells, due to the inhibition of cell division initiation. The deletion SepIVA from *M. smegmatis* also produced an elongated cell phenotype, yet an increase in septation was observed. It may be hypothesized from this research that whereas DivIVA in *B. subtilis* is an initiator of cell division, SepIVA in *M. smegmatis* may function in regulating and controlling septa synthesis, as upon *sepIVA* deletion, aberrant septation occurred.

CHAPTER 3

Investigating the Role of an Uncharacterised Mycobacterial DivIVA Domain-Containing Coiled-Coil Protein

3.1 INTRODUCTION

The eukaryotic cytoskeleton composition and organisation is well understood, with the characterisation of the three major cytoskeletal systems which are responsible for maintaining cell shape and integrity; microfilaments are assembled from actin, the most abundant protein in eukaryotes, that drives cell motility and intracellular trafficking and is found underlying the plasma membrane (Svitkina & Borisy, 1999; Tilney & Portnoy, 1989). Similarly, microtubules, composed of polymerised tubulin, also function in intracellular transport and cell division. Finally, unlike microfilaments and microtubules, intermediate filament proteins play a structural role, in conveying mechanical strength to the cell (Herrmann *et al.*, 2009). Homologues of these three highly complex cytoskeletal elements are prevalent in bacteria. MreB has been identified as an actin homologue, found in many rod-shaped bacteria such as *Escherichia coli* and *Bacillus subtilis*, in addition to other non-coccoid bacterial species (Figge *et al.*, 2004). Its assembly into filaments, that move dynamically around the cell diameter (Domínguez *et al*., 2011), is vital for PG biosynthesis, due to its ability to act as a scaffold for PG-synthesising machinery (White & Gober, 2011). MreB has an important role in cell shape determination (Doi *et al.*, 1988; Jones *et al*., 2001). FtsZ is the most ubiquitous and well-studied tubulin homologue found in almost all bacterial cells. It is paramount in cell division, assigning the site of future septation through the assembly of protofilaments into a contractile ring, in addition to acting as a scaffold for the recruitment of other cell division proteins.

Intermediate filaments have been shown to play an important cytoskeletal role in cell shape maintenance in eukaryotes. Intermediate filaments are α-helical rods that are able to assemble into higher order rope-like structures (Wilk *et al.*, 1995). A unique feature of intermediate filaments is their ability to self-assemble to form filaments *in vitro* (Ausmees *et al*., 2003). The intermediate filament protein structure consisting of a rod domain, essential for filament formation, which is composed of a coiled-coil confirmation, that may be continuous

or interrupted with short non-coiled-coil sequences (Herrmann *et al*., 2009). Crescentin was the first discovered bacterial intermediate filament-like protein, named due to its shared identity to numerous eukaryotic intermediate filaments (Ausmees *et al*., 2003), and is found in the rod-shaped *Caulobacter crescentus*, localised along one lateral side, resulting in concave cell curvature at the location (Ausmees *et al*., 2003). Crescentin is found underlying and attached to the cell membrane, where it is in a stretched configuration (Cabeen *et al*., 2009); the absence of which results in cells that are straight rods, with the loss of vibroid shape, and the detachment of crescentin from the cell membrane results in its condensation into a helical structure (Charbon *et al*., 2009). Crescentin shares identity with numerous eukaryotic intermediate filaments, such as cytoskeletal protein keratin 19 (25%), and nuclear protein lamin A (24%) (Esue *et al*., 2010).

Scy and FilP are coiled-coil intermediate filament-like proteins in *Streptomyces coelicolor*, and both are required for normal growth; the deletion of *scy* resulted in aberrant over-branching, indicating the importance of Scy in the assembly of the *S. coelicolor* multiprotein complex controlling polar growth, the tip organising centre (TIPOC), and hence the number of tips established (Holmes *et al*., 2013). The deletion of *filP* from *S. coelicolor* resulted in the accumulation of cell biomass at the hyphae, but an inability to elongate in a polar manner, as typically seen in wildtype *S. coelicolor* (Bagchi *et al*., 2008). Additionally, it was shown that the hyphae of *S. coelicolor* of *filP* deleted cells were highly susceptible to pressure and shear forces when compared to wildtype hyphae. The role of FilP was therefore attributed to providing mechanical strength and support to the hyphae of *S. coelicolor*. Scy and FilP share approximately 27% and 25% identity to crescentin, respectively. Scy and FilP have been shown to interact with one another, and also both interact with DivIVA, the positional marker for future branching site and the driver of polar growth (Holmes *et al*., 2013); together,

all three proteins have been assigned as components of the *S. coelicolor* TIPOC, crucial for successful polar elongation of this filamentous bacteria.

The coiled-coil Rv1682 of *Mycobacterium tuberculosis* possesses a DivIVA domain. Currently, its function is unknown, yet it is predicted to be non-essential to mycobacterial survival and growth. This chapter will begin to elucidate the role of *Rv1682* in mycobacterial growth. Work began with the generation of a *Rv1682* knockout in the attenuated, category 2 *M. bovis* BCG Pasteur. Although no changes were observed during the phenotypic analysis of the knockout strain, in comparison to the wildtype and complemented counterparts, this work demonstrated the non-essentiality the *Rv1628* homologue in *M. bovis* BCG Pasteur.

3.2 RESULTS

3.2.1 Homologues of *Rv1682* in other bacteria

The amino acid sequence of Rv1682 was used as a query in a BLASTP search, to identify homologous proteins. A multiple sequence alignment analysis with hierarchical clustering was performed using the online tool MultAlin (http://multalin.toulouse.inra.fr/multalin/multalin.html) (Figure 3.1). Homologues with 100% identity were identified in the members of the *Mycobacterium tuberculosis* complex (MTBC), including in *Mycobacterium bovis, Mycobacterium africanum, Mycobacterium canetti* and *Mycobacterium microti*. Homologues were also identified in other opportunistic mycobacterial strains, with only slightly lower identity scores. Additionally, a homologous protein was found in the decaying genome of *Mycobacterium leprae.* A high identity was observed between the lipid binding domain in the N terminal of the septum site-determining protein, $DivIVA_{BS}$, the *M. tuberculosis* cell wall synthesis protein, Wag31, and Rv1682.

A point of interest is that homologous proteins were not identified in many fast-growing non-pathogenic mycobacterial strains, including *Mycobacterium smegmatis*, *Mycobacterium fortuitum* and *Mycobacterium gilvum*, and the fast-growing pathogenic *Mycobacterium terrae* and *Mycobacterium peregrinum*. No homology was also found in the pathogenic strains *Mycobacterium ulcerans* and *Mycobacterium marinum*, which was unsuspected, due to the high identity (approximately 85%) of these strains to *M. tuberculosis* (Rogall *et al*., 1990). This indicates that Rv1682 is somewhat conserved, yet not fully, across the mycobacterial genus.

Although with slightly lower identity/ similarity scores, Rv1682 homologues were also identified in other saprophytic mycolate producing *Corynebacterianea*, such as *Nocardia*, *Gordonia, Tsukamurella, Rhodococcus, Hoyosella, Dietzia* and *Corynebacteria* (Figure 3.1B). Figure 3.2 shows a phylogenetic analysis of the mycobacterial and *Corynebacteriaceae* species

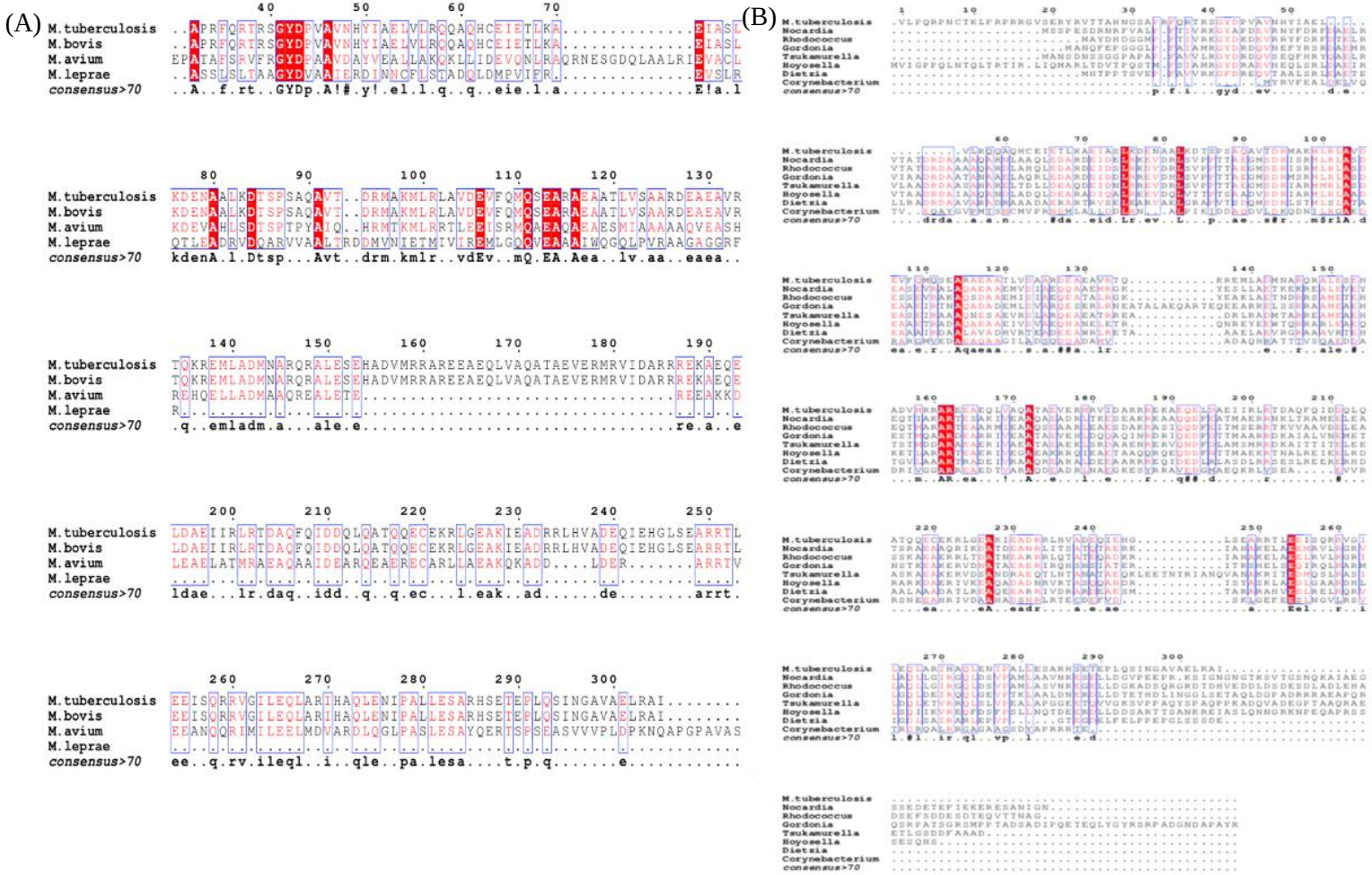

Figure 3.1. Multiple sequence alignment of *M. tuberculosis* H37Rv Rv1682 with Actinobacterial homologues. Homologues were identified using the Rv1682 amino acid sequence and a BLASTP search. Multiple sequence alignment with hierarchical clustering was performed using MultAlin (http://multalin.toulouse.inra.fr/multalin/multalin.html). Alignment of the *M. tuberculosis* Rv1682 amino acid sequence with homologues in other mycobacterial species (A) and with genera from the suborder *Corynebacterianea* (B)

members included in the multiple sequence alignment. Additionally, a lower identity scoring homologue was also identified in *Streptomyces*, a genus of the Actinobacteria phylum.

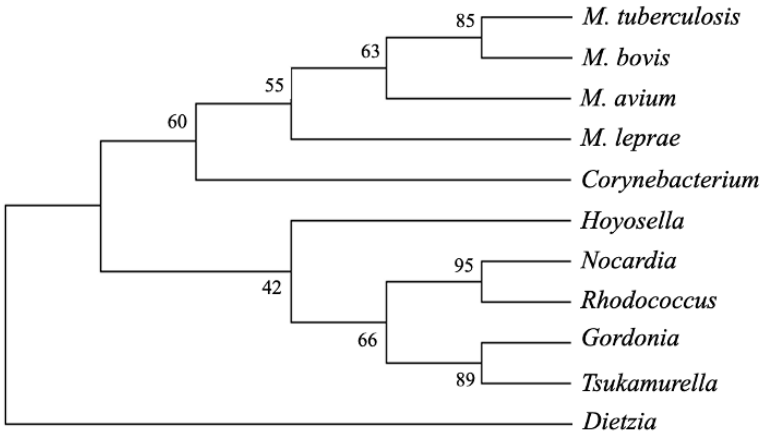

Figure 3.2. Phylogenetic tree of *Corynebacteriaceae* species constructed using MEGA software . The phylogenetic tree was generated using the amino acid sequences of proteins with high identity and similarity to *M. tuberculosis* H37Rv Rv1682. The methodology used was maximum likelihood, and the phylogram stability was analysed by bootstrapping 100 replications. Nodes with bootstrap values are indicated

When the amino acid sequence of Rv1682 was utilised as a query in a BLASTP search against potentially similar proteins in *E. coli* and *B. subtilis*, no candidates were identified. This suggests that Rv1682 homology is conserved across the polar growing progenitors of Actinomycetales.

TMHMM v. 2.0 (http://www.cbs.dtu.dk/services/TMHMM/) and TMpred (https://embnet.vital-it.ch/software/TMPRED_form.html) were utilised to predict transmembrane regions of Rv1682. According to these bioinformatic analysis tools, Rv1628 lacks transmembrane regions (Figure 3.3).

The amino acid sequence of Rv1682 was analysed in a structural assessment, in regards to its coiled-coil conformation, using the online tool COILS (Lupas *et al*., 1991) (https://embnet.vital-it.ch/software/COILS_form.html). COILS determines the probability that a residue within a protein is part of a coiled-coil structure based upon the comparison with

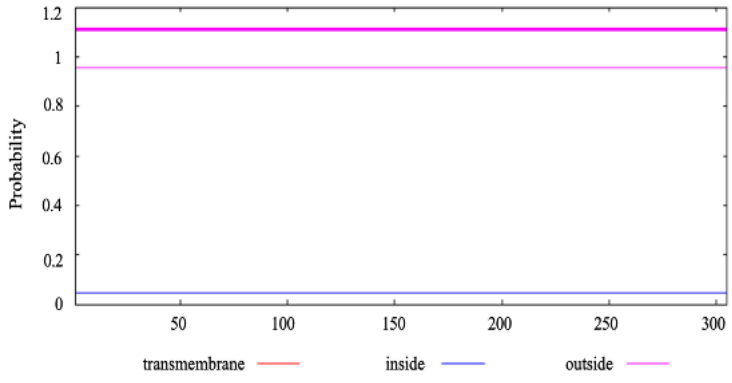

Figure 3.3. TMHMM predictions for *M. tuberculosis* H37Rv Rv1682. No transmembrane domains were predicted by TMHMM.

sequences of known coiled-coil proteins. Rv1682, from *M. tuberculosis* H37Rv was predicted to have numerous coiled-coil domains (Figure 3.4A). Using the online tool MULTICOILS (http://cb.csail.mit.edu/cb/multicoil/cgi-bin/multicoil.cgi), which identifies the probability of trimeric and dimeric coiled coils, the oligomerisation status of Rv1682 was explored (Wolf *et al*., 1997). The dimerization probability was above the threshold (Wolf *et al*., 1997), indicating that Rv1682 is predicted as a dimeric coiled-coil protein (Figure 3.4B).

As Scy is a coiled-coil filament protein that shares sequence similarity with other intermediate filaments, such as the eukaryotic keratin (33%) and nuclear lamin (40%), and also the bacterial crescentin (44%), the mycobacterial Rv1682, was utilised in a pairwise sequence alignment analysis (EMBOSS Water) to determine its sequence similarity to eukaryotic and prokaryotic intermediate filaments. Rv1682 has 39% similarity to crescentin, 39% similarity to keratin, and 40% similarity to nuclear lamin.

Numerous paralogs of *Rv1682* were identified in *M. tuberculosis;* these include *Rv2927c*, *Rv1278, Rv2229c* and *Rv1493.*Work beginning to elucidate the roles of the *M. smegmatis* homologues of *Rv2927c* and *Rv2229c*, *MSMEG_2416* and *MSMEG_4306* respectively, can be found in chapter 2 and chapter 4.

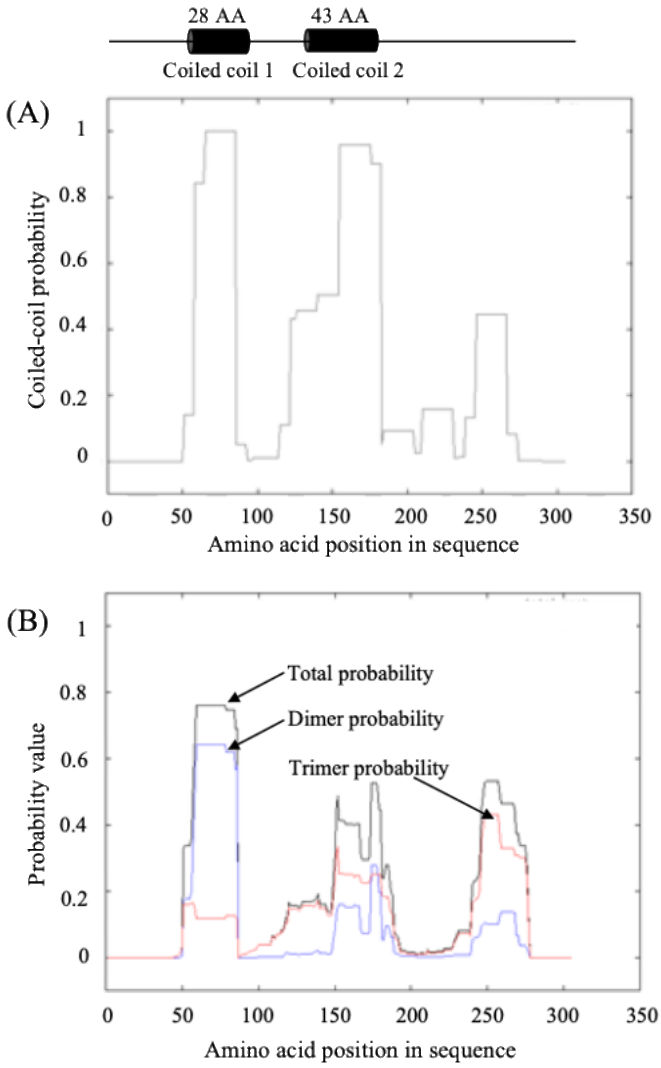

Figure 3.4. Predicted coiled-coil regions of *M. tuberculosis* H37Rv Rv1682, based on its amino acid sequence. The coiled-coil probabilities of Rv1682 were predicted using COILS (A), and its dimerization and trimerization probabilities using MULTICOILS (B). Rv1682 is predicted to possess two coiled-coil domains, the former of which is predicted as a dimer.

3.2.2 Generation of a *M. bovis Mb1709* knockout strain

To determine whether *Rv1682* is essential in the survival and growth of *M. tuberculosis*, the model strain *M. bovis* BCG Pasteur was utilised, an allelic exchange substrate was constructed. Specialised Transduction was performed, to replace *Mb1709*, the homologue of *Rv1682*, with a hygromycin resistance cassette (Figure 3.5). The gene deletion was confirmed by confirmatory PCR using the primers pairs Mb1709_KO_F and HL, and Mb1709_KO_R

and HR (Figure 3.5); this strain was designated Δ*Mb1709*. The ability to generate a gene deletion strain indicates that *Mb1709* is a non-essential gene of *M. bovis* BCG Pasteur.

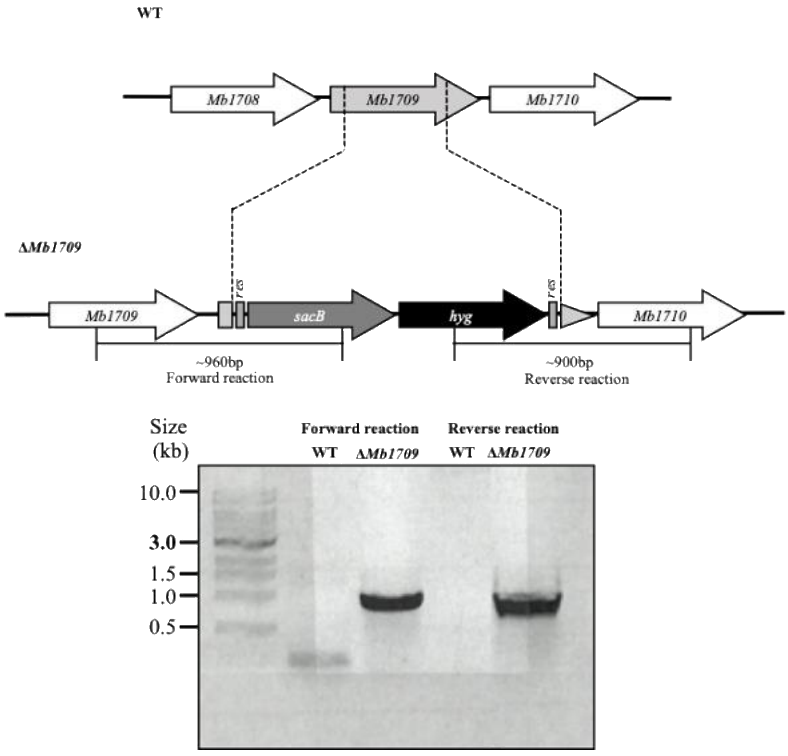

Figure 3.5. Construction and confirmation of a *M. bovis* BCG Pasteur *Mb1709* deletion mutant. A schematic representation showing the removal of the gene of interest *Mb1709*, from *M. bovis* BCG Pasteur, and its replacement with a hygromycin resistance cassette. To confirm the deletion of *Mb1709*, confirmatory PCR was employed, using primers located within the hygromycin resistance cassette, and in the neighbouring genes, to generate PCR products of approximately between 900 and 960bp in the case of successful gene deletion. WT, wildtype. M, DNA marker ladder. sacB - sucrose counter-selectable gene from *Bacillus subtilis*; *hyg* - hygromycin resistance gene; *res* - γδ-resolvase site.

Following confirmation of gene deletion, *Rv1682*, along with its native promoter, was cloned into the integrative vector, pMV306, using the primer pair Rv1682_Comp_F and Rv1682_Comp_R. This plasmid was designated pMV306-*Rv1682*. This construct was introduced into *M. bovis* BCG Δ*Mb1709*, to generate a complemented strain (Δ*Mb1709*C). Confirmatory PCR was carried out to determine successful complementation with *Rv1682*, using the primer pair Rv1682_Comp_F and Rv1682_Comp_R (Figure 3.6). The empty vector, pMV306, was also introduced into *M. bovis* BCG Δ*Mb1709*, to generate the control strain Δ*Mb1709*V.

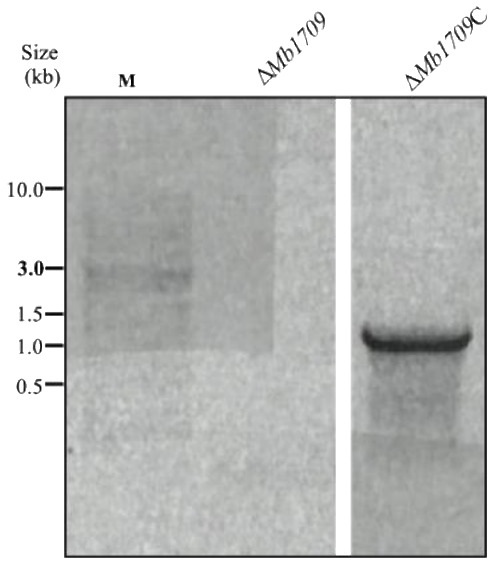

Figure 3.6. Confirmatory PCR of Δ*Mb1709* complementation with *Rv1682*. *Rv1682* was cloned into pMV306 and was introduced into Δ*Mb1709*. Complementation was verified by confirmatory PCR, with an expected band size of approximately 1kb. M, DNA ladder marker.

3.2.3 The effect of *Mb1709* deletion in *M. bovis* BCG on growth in liquid media

To determine whether the deletion of *Mb1709* had any effect on growth and replication, a growth rate analysis was carried out, including *M. bovis* BCG wildtype, Δ*Mb1709* and Δ*Mb1709*C. All strains were cultured, in triplicate, with an aliquot taken at each time point, and cell density measured. The growth rate of all three strains were similar and no significant difference was observed (Figure 3.7), following statistical analysis using the means from two biological replicate experiments. There did not appear to be any significant difference in the growth rate of the mutant strain, when compared to the parental wildtype strain.

3.2.4 The effect of *Mb1709* deletion in *M. bovis* BCG on colony morphology

To determine whether the deletion of *Mb1709* from *M. bovis* BCG Pasteur has any effect on morphology, a colony morphology study was carried out. Bacterial strains were

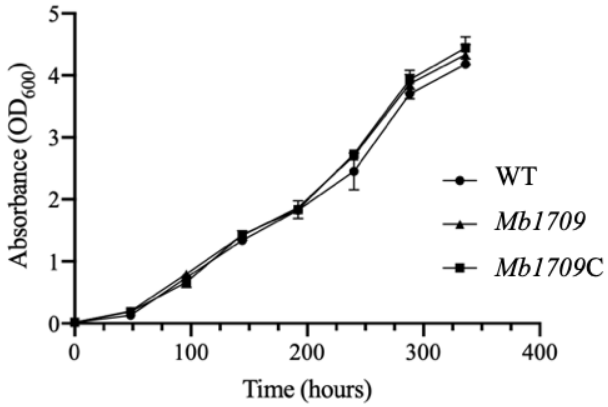

Figure 3.7. Growth curve of wildtype *M. bovis* BCG Pasteur, *ΔMb1709* and Δ*Mb1709*C. All strains were cultured in Middlebrook 7H9 broth supplemented with 10% OADC and 0.05% Tween-80. Cultures were grown statically, at 37°C. Aliquots were taken at each time point, with cell density measured. There was no significant in growth rate as a result of the loss of *Mb1709* from *M. bovis* BCG Pasteur. WT, wildtype.

grown in Middlebrook 7H9 supplemented with 10% OADC and 0.05% Tween-80, and were spotted onto Middlebrook 7H9 agar plates, supplemented with 10% OADC, with and without 0.05% Tween-80. Upon the deletion of *Mb1709*, no difference was observed when compared to wildtype *M. bovis* BCG Pasteur and Δ*Mb1709*C (Figure 3.8).

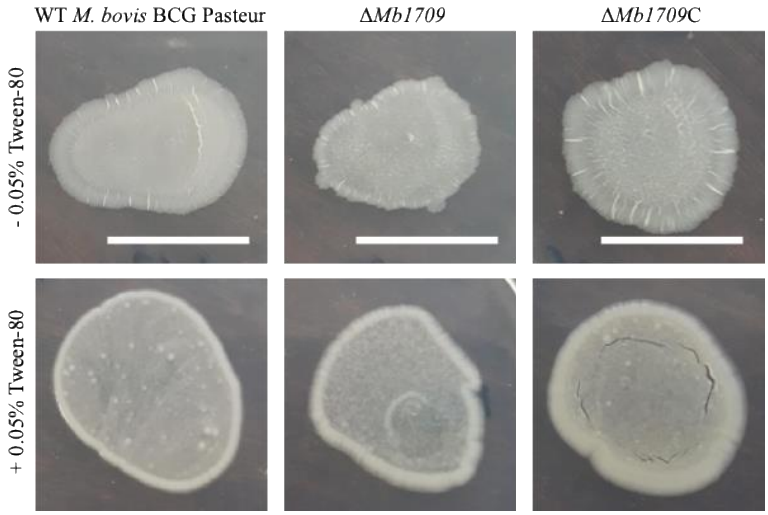

Figure 3.8. Colony morphology of wildtype *M. bovis* BCG Pasteur, *ΔMb1709* and Δ*Mb1709*C. Spot colonies of WT *M. bovis* BCG Pasteur, Δ*Mb1709* and Δ*Mb1709*C were cultured on Middlebrook 7H9 agar with and without the supplementation of 0.05% Tween-80. The loss of *Mb1709* did not show a change in colony, even in the presence of 0.05% Tween-80. Scale bar – 5mm.

3.2.5 The effect of *Mb1709* deletion in *M. bovis* BCG on pellicle formation

To study the ability of these strains to form pellicles following *Mb1709* deletion, cultures were grown, in Middlebrook 7H9 broth, supplemented with 10% OADC and 0.05% Tween-80 until an OD_{600} of 0.8-1.0 was reached. Cultures were diluted to an OD_{600} of 0.05 in Sauton's broth, and 1.5mL of diluted cell culture was added to 24-well plates. Plates were incubated at 37°C, 5% CO_2, until pellicles had formed. The pellicle forming ability of *M. bovis* BCG Δ*Mb1709* did not appear to be defective, compared to wildtype *M. bovis* BCG Pasteur and Δ*Mb1709*C (Figure 3.9).

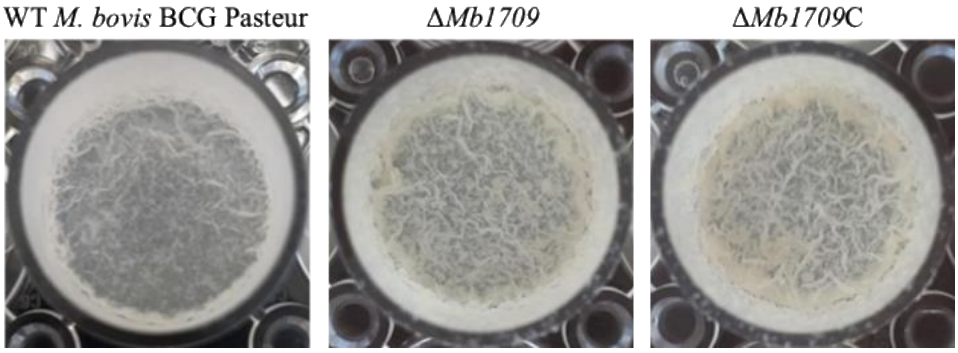

Figure 3.9. Pellicle forming ability of wildtype *M. bovis* BCG Pasteur, *ΔMb1709* and Δ*Mb1709*C. Pellicle formation of WT *M. bovis* BCG Pasteur, Δ*Mb1709* and Δ*Mb1709*C, when cultured in Sauton's media. The loss of *Mb1709* did not appear to cause a defect in ability to form a pellicle.

3.2.6 Lipid profile of *M. bovis* BCG Δ*Mb1709*

Although no change in colony morphology was observed following *Mb1709* deletion from *M. bovis* BCG Pasteur, a full lipid analysis was carried out to determine whether the mutant strain demonstrated a differing lipid profile compared to wildtype *M. bovis* BCG Pasteur and Δ*Mb1709*C. Cultures were grown in Middlebrook 7H9 broth, supplemented with 10% OADC and 0.05% Tween-80, and were labelled with ^{14}C-acetic acid. A full lipid

extraction was carried out, to profile the polar and apolar lipids (see General Materials and Methods). The lipid profiles of *M. bovis* BCG wildtype, Δ*Mb1709* and Δ*Mb1709*C were analysed by thin layer chromatography. Figure 3.10 and Figure 3.11 show that there are no obvious differences in the lipid content of the cell wall of Δ*Mb1709*, in regards to apolar lipids, polar lipids, or mycolic acids.

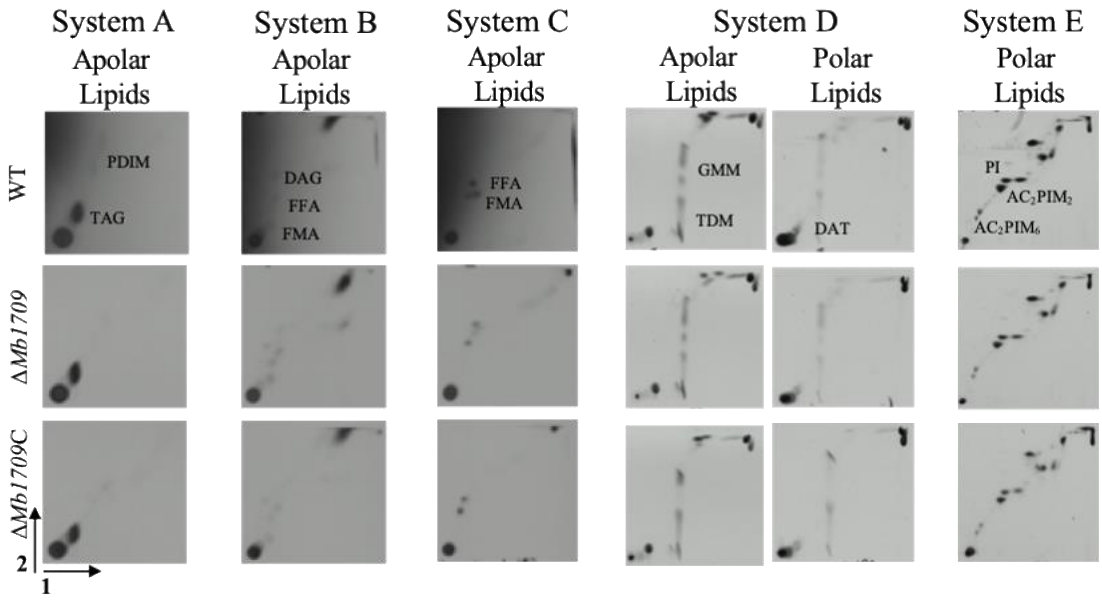

Figure 3.10. Lipid analysis of wildtype *M. bovis* BCG Pasteur, Δ*Mb1709* and Δ*Mb1709*C. 2D-TLC analysis of [^{14}C]-labelled lipids extracted from strains that were cultured In Middlebrook 7H9 broth supplemented with 10% OADC and 0.05% Tween-80. Labelled lipids were extracted and 20,000cpm of extracted lipids were spotted onto a silica plate, then separated using different solvent systems (see General Materials and Methods for full protocol of lipid extraction and solvent systems). No difference in lipid profiles were identified following the loss of *Mb1709*, in terms of polar and apolar lipids. WT, wildtype. TAG, triacylglycerols; PDIM, phthiocerol dimycocerosates; DAG, diacylglycerols; FFA, free fatty acid; FMA, free mycolic acid; GMM, glucose monomycolate; TDM, trehalose dimycolate; DAT, diacyltrehalose mycolate; PI, phosphatidylinositol; AC_2PIM_2, diacyl phosphatidylinositol dimannoside ; AC_2PIM_6, diacyl phosphatidylinositol hexamannoside

3.2.7 The effect of *Mb1709* deletion on cell length *M. bovis* BCG

As no changes were observed in the lipid profile of Δ*Mb1709,* the cell phenotype was studied microscopically to determine if the deletion of *Mb1709* resulted in a change in cell

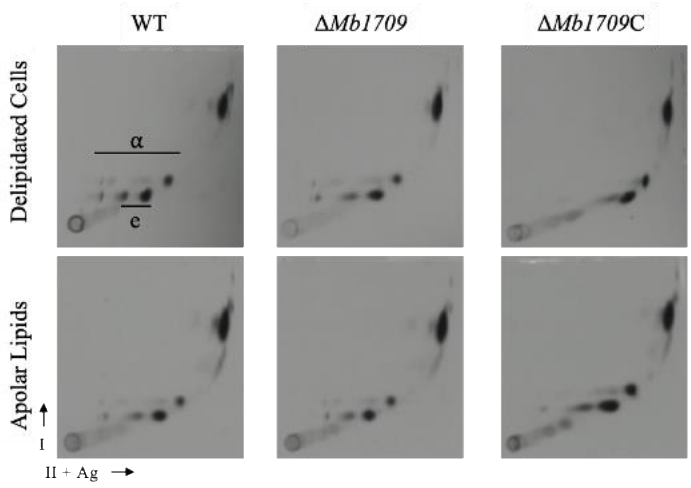

Figure 3.11. Mycolic acid analysis of wildtype *M. bovis* BCG Pasteur, Δ*Mb1709* and Δ*Mb1709*C. FAMEs and MAMEs were extracted from the delipidated cell pellet, and the inner and outer apolar lipid extracts, following previous full lipid extraction. 20,000cpm of each lipid extract was spotted onto a silica plate and was analysed by 2D-Ag^+-argentation TLC (see General Materials and Methods for protocols of lipid extraction, 2D-Ag^+-argentation TLC and the solvent system used). No difference was observed following the loss of *Mb1709*, in terms of mycolic acid content. WT, wildtype. α, alpha-mycolates; e, epoxy-mycolates.

length, compared to wildtype *M. bovis* BCG Pasteur and Δ*Mb1709*C. Cells were visualised using phase contrast microscopy, and a population of 250 cells were measured to determine variation in cell length (Figure 3.12). It was found that there was no significant difference in the cell lengths of the strains in this study.

During the microscopic analysis, it was noted that Δ*Mb1709* displayed an uncharacteristic phenotype, with what looked like patchy accumulations along the cell length at varying intervals (Figure 3.13). This phenotype was absent in the wildtype and complemented counterparts**.**

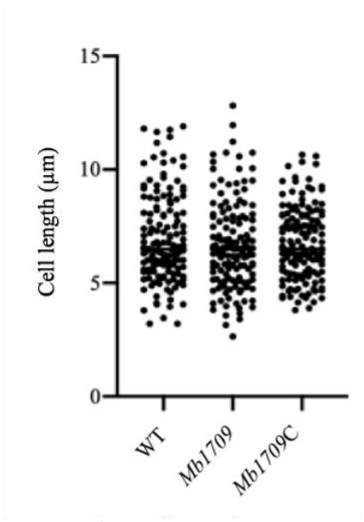

Strain	Average (µm)	Standard Deviation (µm)
WT	7.0	1.9
Δ*Mb1709*	6.9	1.9
Δ*Mb1709*C	6.6	1.6

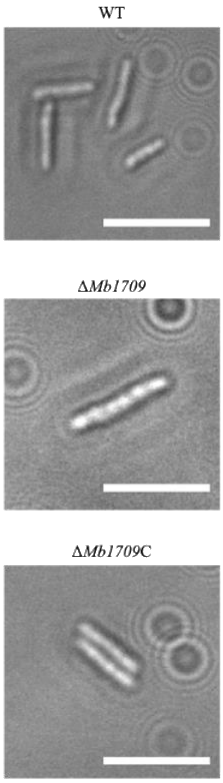

Figure 3.12. Microscopy and cell length analysis of wildtype *M. bovis* BCG Pasteur, Δ*Mb1709* and Δ*Mb1709*C. Strains were cultured in Middlebrook 7H9 broth supplemented with 10% OADC and 0.05% Tween-80, and visualised at 100X magnification. A sample of 250 cells were measured to determine average cell lengths. The deletion of *Mb1709* did not result in any changes in cell length when compared to wildtype *M. bovis* BCG Pasteur and Δ*Mb1709*C. WT, wildtype. Scale bar, 10µm.

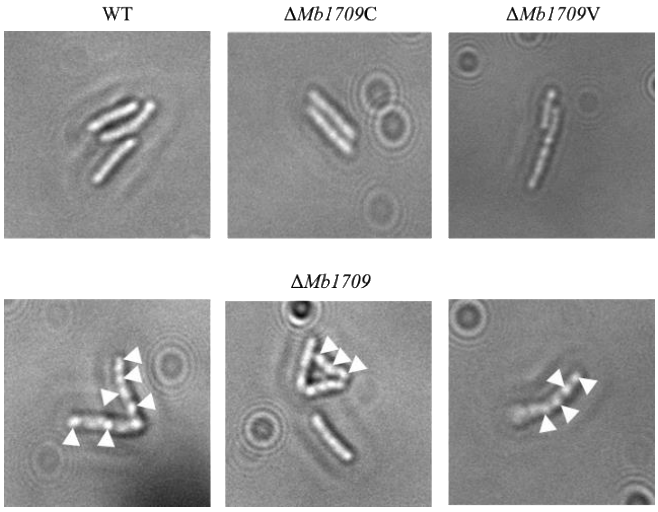

Figure 3.13. Microscopy of the *M. bovis* BCG Δ*Mb1709* mutant. Strains were cultured in Middlebrook 7H9 broth supplemented with 10% OADC and 0.05% Tween-80, and visualised at 100X magnification. A sample of 250 cells were photographed. Patchy accumulations can be seen along the cell length of Δ*Mb1709* cells (indicated with white arrow head), but are absent in wildtype and Δ*Mb1709*C cells. WT, wildtype.

3.3 DISCUSSION

Intermediate filament proteins have been widely studied in eukaryotic cells, and are found in all cells, except for plants and fungi (Lodish *et al*., 2000). Their role in eukaryotic cells has been delineated, with great structural importance in reinforcing cells in the form of mechanical support to the plasma membrane (Charrier & Janmey, 2016). Their stability is due to the longitudal and lateral interactions that exist between individual protofilaments producing high tensile strength intermediate filament bundles, hence the ability of intermediate filament like proteins to assemble into a higher ordered filamentous structure *in vitro*. Intermediate filament like proteins have been widely studied in *C. crescentus* and *Streptomyces*, in the case of crescentin, which spans the cell length and plays a role in maintaining the cells vibroid shape (Ausmees *et al*., 2003), and FilP, a protein that has been shown to convey mechanical strength to the hyphal tips (Bagchi *et al*., 2008), respectively. Little research has been carried out in identifying and characterising potential intermediate filament like proteins in other actinobacteria, such as mycobacteria. This study aimed to begin to elucidate the function of the previously uncharacterised mycobacterial protein, Rv1682, a DivIVA domain containing coiled-coil protein. Through the construction of a Δ*Mb1709* deletion strain, with *Mb1709* being the *M. bovis* BCG homologue of *Rv1682*, and the employment of growth and phenotypic analysis, this work has begun to delineate the role of Δ*Rv1682*.

3.3.1 *Mb1709* is not essential in the growth and survival of *M. bovis* BCG Pasteur

It was demonstrated that *Mb1709* is a non-essential gene of *M. bovis* BCG Pasteur. The deletion of *Mb1709* from *M. bovis* BCG Pasteur showed no significant changes in growth rate, or phenotypic characteristics, such as colony morphology, the ability to form a higher structured pellicle, or the length of cells. In certain eukaryotic cells lines lacking cytoplasmic

intermediate filaments, a change in growth or cell morphology is not discernable (Venetianer *et al*., 1983; Hedberg & Chen, 1986), indicating the redundancy of some intermediate filaments to the growth and proliferation of these cell lines. In the case of the well-studied crescentin and FilP of *C. crescentus* and *S. coelicolor*, respectively, growth defects can be observed upon the generation of mutant strains; crescentin depletion results in cells that demonstrate a straight morphology, as opposed to the characteristic vibroid shape (Ausmees *et al*., 2003), and FilP depletion slows the rate of growth of *S. coelicolor* and hyphae become distorted and weakened to shear forces (Bagchi *et al*., 2008). It would seem that the depletion/ deletion of intermediate filament like proteins from prokaryotic cells results in a growth defect as a result of this loss. Based on its amino acid sequence, Rv1682 displays homology to multiple intermediate filament-like proteins. Bagchi *et al*. (2008) also showed that Mb1709, the *M. bovis* homologue, is capable of self-assembling into a filamentous structure *in vitro*, demonstrating an intermediate filament-like property of this protein following purification. It could therefore be assumed that Rv1682, the *M. tuberculosis* homologue of Mb1709, is also capable of self-assembling into a filamentous structure *in vitro*, hence, possessing an intermediate filament-like property. Despite the homology of Rv1682 to certain intermediate filament-like proteins, based on its amino acid sequence, the lack of changes in growth rate and morphology upon the deletion of *Mb1709* from *M. bovis* BCG Pasteur indicates the need for further investigation into its potential role as an intermediate filament-like protein.

3.3.2 Rv1682 possesses two coiled-coil domains, the former of which is predicted to be dimeric

Using the online tools COILS, it was predicted that Rv1682 possess two coiled-coil domains. Coiled-coil protein assembly is complex; 2-7 alpha helices (Lupus & Gruber, 2005;

Liu *et al*., 2006) are coiled to one another in either a parallel or anti-parallel orientation, in a rope-like manner. Based on the amino acid sequence of Rv1682, the online tool MULTICOILS, which predicts dimeric or trimeric nature of coiled-coil domains within a protein, predicted that Rv1682 possess a dimeric (consisting of two alpha-helices) N-terminal coiled-coil domain. $DivIVA_{BS}$, which also possesses a dimeric N-terminal domain, and dimerises via the coiled-coil region of its C-terminal domain (van Baarle *et al*., 2013). The study by van Baarle *et al.* (2013) has shown that the interaction of $DivIVA_{BS}$ with MinJ, a linker protein between DivIVA and the septum determining machinery (Patrick & Kearns, 2008), and RacA, a chromosomal anchoring protein that ensures proper chromosome segregation (Ben-Yehuda *et al*., 2003), is terminal specific; the C-terminal of $DivIVA_{BS}$ interacts with RacA, whereas the N-terminal binds to the transmembrane MinJ; hence the role of $DivIVA_{BS}$ as scaffold protein cell wall biosynthetic and chromosomal segregation machinery (Thomaides *et al*., 2001). The N-terminal also possesses a lipid binding domain, suggesting that the lipid binding domain of the N-terminal is located close to the cell membrane, whilst the C-terminal is able to reach into the cytoplasm (Van Baarle *et al.*, 2013). Future study of the terminal specific interactions of Rv1682 would provide crucial evidence on the potential role of Rv1682.

3.3.3 Rv1682 is conserved across the *Actinomycetale* order, and absent from laterally growing rod-shaped bacteria, such as *E. coli* and *B. subtilis*

With a failure to identify crescentin homologues in other bacteria, based on sequence similarity a study by Bagchi *et al.* (2008) investigated the widespread presence of intermediate filament like proteins in other bacteria, based on the conserved domain organisation observed in intermediate filament like proteins**.** One candidate protein was identified in *M. bovis*;

Mb1709 is a probable coiled-coil structural protein that shares the typical structural plan, consisting of a central rod domain of alternating coiled segments and linkers, flanked by more globular head and tail domains (Bagchi *et al.*, 2008; Herrmann & Aebi, 2004). When purified, Mb1709 was capable of form filaments *in vitro*, a characteristic property of intermediate filament like proteins. The 100% identity between this protein and the *M. tuberculosis* homologous protein, Rv1682, would imply that like Mb1709, Rv1682 would behave like other intermediate filament like proteins, in relation to its capability of forming filaments *in vitro*. Additionally, Rv1682 possesses a DivIVA domain, similar to Wag31, the DivIVA homologue in *M. tuberculosis.* Wag31 possesses ability to form filaments *in vitro* (Choukate *et al*., 2018), showing the conserved characteristic of intermediate filament forming proteins. This finding, in addition to the filament-forming ability of Rv1682's *M. bovis* homolog, would further suggest that Rv1682 may be an intermediate filament like protein, with filament forming capability (*in vitro*).

Interestingly, there were no significant matches following a BLASTP search using Rv1682 as a query against the laterally elongating *E.coli* and *B. subtills.* These findings would suggest that *Rv1682,* represents a conserved coiled-coil proteins within the polar growth progenitors of *Actinomycetales,* yet is absent from other well studied rod-shaped bacteria, such as *E. coli* and *B. subtilis*, that elongate via the incorporation of cell wall material along the cell length.

This study began the construction of a His-tagged Rv1682, with the aim to purify this protein, and determine a crystal structure. Despite developing a construct in which Rv1682 was tagged with an N-terminal polyhistidine tag, time constraints limited the opportunities to tailor protein purification. Whilst this work would have provided concrete evidence in the structure of Rv1682, time constraints hindered this project; work on this study will continue.

3.3.4 The loss of *Mb1709* from *M. bovis* BCG Pasteur did not show any alteration in phenotype, including a change in colony morphology, pellicle forming ability, cell envelope composition, or a change in cell length

Despite the thorough analysis of *M. bovis* BCG Pasteur following *Mb1709* deletion, it was difficult to identify phenotypic changes as a result of the loss of this gene; the loss of *Mb1709* did not show an alteration in the colony morphology, the pellicle forming ability, the cell envelope lipid composition, or in the average cell length. An altered phenotype observed following the loss of *Mb1709* from *M. bovis* BCG Pasteur was the presence of patchy accumulations along the cell length, that were absent in the wildtype and complemented strains. Whilst this work did not begin to delineate the cause of this phenotype, further work is necessary to determine the nature of these patchy accumulations, and also if the loss of *Mb1709* results in this phenotype.

Observed in *M. tuberculosis* during latency or exposure to stress conditions (such as hypoxia), lipid bodies are cytoplasmic triacylglycerol (TAG) accumulations that are utilised as an energy source (Shi *et al*., 2010). Shi *et al*., (2010) also identified that carbon flow, during stress, is rerouted from the synthesis of biosynthetic precursors to that of the synthesis of storage compounds. Although TAG was not found to be produced at greater quantities by the deletion strain, and whilst unable to visualise lipid bodies through phase contrast microscopy alone, it would be interesting to visualise the patchy accumulations observed during this study, and how lipids localise with these. Utilising a lipid stain, such as Nile red, would provide information on whether lipids are accumulating along the cell length. Additionally, a study into exposing the strains to stress conditions (i.e. hypoxia, nutrient scarcity, or pH alterations for example) would shed light on whether this deletion strain readily forms lipid bodies, when compared to wildtype *M. bovis* BCG Pasteur, and Δ*Mb1709*C.

For this reason, and the somewhat limited research previously carried out on Rv1682, or its orthologs, hinders the ability to draw hypotheses on the potential role of Rv1682 in *M. tuberculosis* growth. Predictions on the function of Rv1682 remain speculative until further research has been performed. As carried out in chapter 2, performing an interaction study utilising a His-tagged, with inducible overexpression in *M. bovis* BCG Pasteur, would provide valuable insight into the potential interacting partners of Rv1682, further contributing to delineating the role of Rv1682. Additionally, studying the localisation of Rv1682 during the cell cycle, both independently and relative to other proteins whose functions are known, would provide further evidence to then build upon the current speculative role that Rv1682 may be an intermediate filament like protein, based on its amino acid, and the function of its orthologs.

CHAPTER 4

Investigating the Role of an Uncharacterised Mycobacterial Zinc-Ribbon Domain-Containing Coiled-Coil Protein

4.1 INTRODUCTION

Research carried out in chapter 2 and chapter 3 investigated the role of the SepIVA and Rv1682, a *Mycobacterium smegmatis* and *Mycobacterium tuberculosis* coiled-coil protein, respectively, that both possess a DivIVA domain, and possess sequence similarity to *Streptomyces coelicolor* coiled-coil proteins, with cytoskeletal roles in polar growth. Interest in Rv1682, due to its sequence similarity to *S. coelicolor* proteins, and conserved domains led to a bioinformatic analysis, and identification of a paralog, the uncharacterised *M. tuberculosis* protein, Rv2229c, and its *M. smegmatis* homologue, MSMEG_4306. Paralogous genes arise as a duplication event from the same genome, in which multiple copies of the same gene develop. Typically, as only one gene is required for functioning, the other copies are able to take on and accumulate changes; this can sometimes arise in gene which can produce a protein of changed function, a pseudogene, or the retention of a function similar to the original gene. A report by Nehrt *et al.* (2011) claimed that paralogues within the same organism are more closely related in terms of function, than orthologues in different organisms at the same level of divergence. In this case, the study of these paralogues may help in assigning a function and understanding the role of these proteins in mycobacterial growth.

There are contradictory reports of the essentiality of *Rv2229c* for *M. tuberculosis* growth; Sassetti *et al*. (2003) predicts the gene to be essential whereas DeJesus *et al.* (2017) suggests that it is a non-essential gene. The *M. smegmatis* homologue, *MSMEG_4306*, is predicted to be non-essential for survival (DeJesus *et al*., 2017). Not much is known about *Rv2229c* and its *M. smegmatis* homologue, with this only exacerbated by the fact that there are no proteins in other microorganisms, of known function, with amino acid sequence similarity; this makes it extremely difficult to extrapolate and assign a potential function to MSMEG_4306/ Rv2229c, based on the research of similar known proteins.

Similar to the proteins studied in previous chapters, SepIVA and the Rv2229c paralog, Rv1682, MSMEG_4306 possess a coiled-coil domain, confirmed recently by Kumar & Karthikeyan (2018). This study also determined that MSMEG_4306 displays a C-terminal conserved C4-type zinc-ribbon domain (belonging to the zf-RING_7 Pfam family). Very little research has been carried out on proteins with this conserved domain, yet it has been shown that the zinc binding finger protrusions are also able to bind numerous macromolecules, such as DNA, RNA, proteins and lipids (Klug, 1999; Hall, 2005; Gamsjaeger *et al*., 2007; Matthews & Sunde, 2002).

The lack of widely studied proteins, which could be used as templates for preliminary knowledge for a similar protein, limits that which can be predicted as a function for the query for the protein. Although research has begun to delineate the structure of MSMEG_4306 (Kumar & Karthikeyan, 2018), in an attempt to predict its role in *M. smegmatis* growth and survival, its function still remains speculative, based on structural and comparative analysis.

This chapter has begun to elucidate the role of *MSMEG_4306* and *Rv2229c* in the growth of *M. smegmatis* and *M. tuberculosis*, respectively, through the construction of gene deletion strains, and phenotypic analysis. The *M. bovis* homologue of *Rv2229c*, *Mb2254c*, was used as a surrogate to study the genes in the slow growing *M. bovis* BCG. The ability to generate deletion strains of *MSMEG_4306* and *Mb2254c* in *M. smegmatis* and *M. bovis* BCG Pasteur, respectively, indicates the non-essentiality of these genes for growth and survival. The loss of *MSMEG_4306* in *M. smegmatis* resulted in a change in colony morphology and pellicle forming ability, with pellicle forming ability also affected following the deletion of *Mb2254c* from *M. bovis* BCG Pasteur. Additionally, the loss of *MSMEG_4306* from *M. smegmatis* resulted in an elongated cell phenotype. Minor alterations in the production of trehalose dimycolate (TDM) and a lipid species which co-migrates with triacylglycerol (TAG) were also observed following the deletion of *MSMEG_4306* from *M. smegmatis*. Further lipidomic

investigation and additional fluorescent staining (i.e. of the cell membrane and septa, and the nuclear material) would provide knowledge in assigning a role to the previously uncharacterised MSMEG_4306.

4.2 RESULTS

4.2.1 Homologues of MSMEG_4306 in other bacteria

The amino acid sequence of MSMEG_4306 was utilised in a BLASTP search, to identify homologous proteins. A multiple sequence alignment analysis with hierarchical clustering was performed using the online tool MultAlin (http://multalin.toulouse.inra.fr/multalin/multalin.html). Homologues were found in most mycobacterial species, including in environmental non-pathogenic saprophytes, members of the tuberculosis causing *Mycobacterium tuberculosis* complex (MTBC), and also in the decaying genome of *Mycobacterium leprae* (Figure 4.1A). This indicates that MSMEG_4306 is conserved across the mycobacterial genus.

Although with slightly lower identity/ similarity scores, MSMEG_4306 homologues were also identified in other saprophytic mycolate producing *Corynebacterianea*, such as *Nocardia, Gordonia, Tsukamurella, Rhodococcus, Hoyosella, Segniliparus, Dietzia* and *Corynebacteria* (Figure 4.1B). Figure 4.2 shows a phylogenetic analysis of the mycobacterial and *Corynebacteriaceae* species members included in the multiple sequence alignment. Additionally, lower identity scoring homologues were also identified in *Streptomyces*, a genus of the Actinobacteria phylum.

When the amino acid sequence of MSMEG_4306 was used as a query in a BLASTP search against potentially similar proteins in *E. coli* and *B. subtilis*, no candidates were identified. This suggests that MSMEG_4306 homologues are conserved across polar growth progenitors of the Actinomycetales.

TMHMM v. 2.0 (http://www.cbs.dtu.dk/services/TMHMM/) and TMpred (https://embnet.vital-it.ch/software/TMPRED_form.html) were utilised to predict transmembrane regions of MSMEG_4306. According to these bioinformatic analysis tools, MSMEG_4306 lacks transmembrane regions (Figure 4.3).

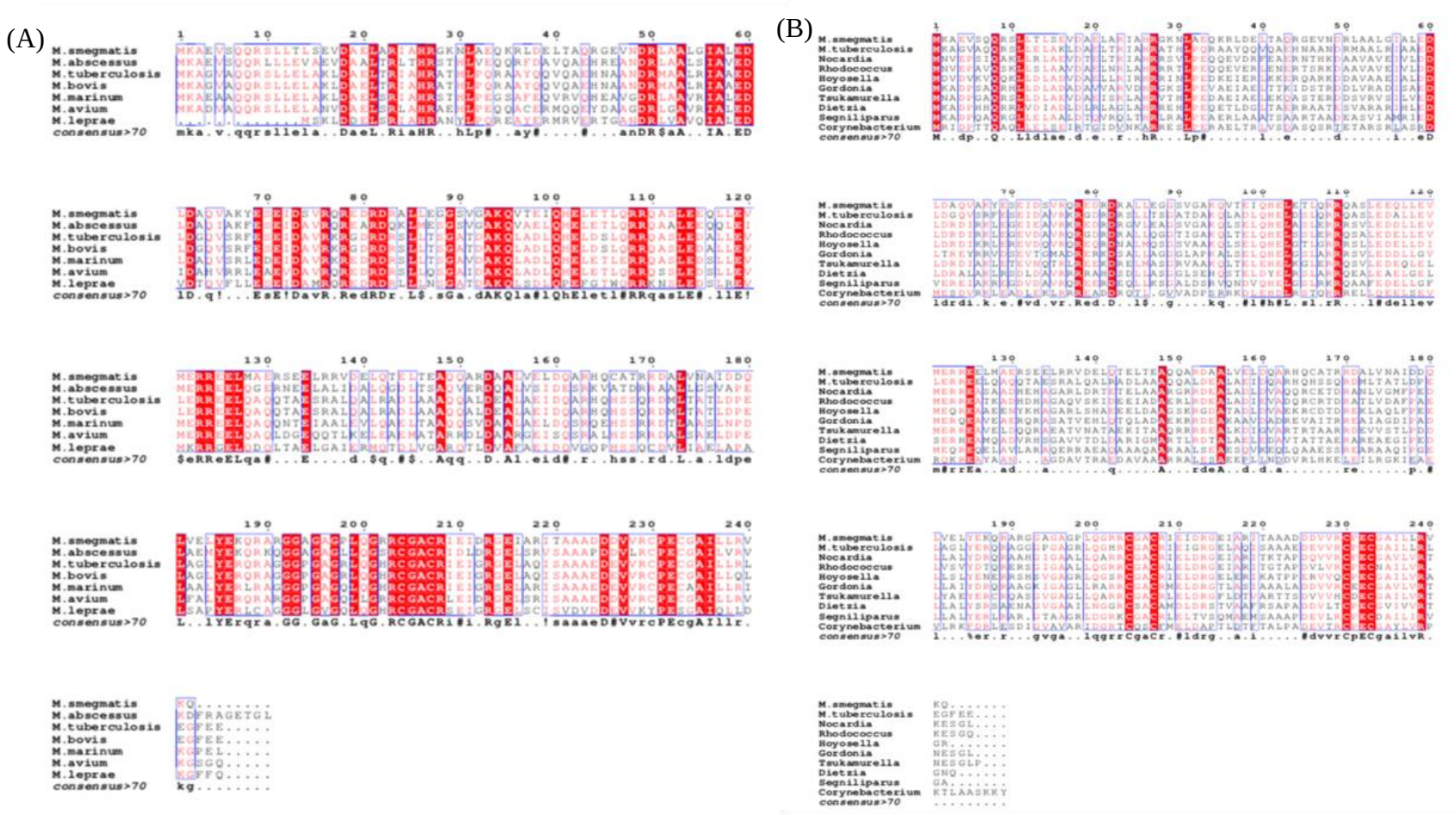

Figure 4.1. Multiple sequence alignment of *M. smegmatis* MSMEG_4306 with Actinobacterial homologues. Homologues were identified using the MSMEG_4306 amino acid sequence and a BLASTP search. Multiple sequence alignment with hierarchical clustering was performed using MultAlin (http://multalin.toulouse.inra.fr/multalin/multalin.html). Alignment of the *M. smegmatis* MSMEG_4306 amino acid sequence with homologues in other mycobacterial species (A) and with genera from the suborder *Corynebacterianea* (B).

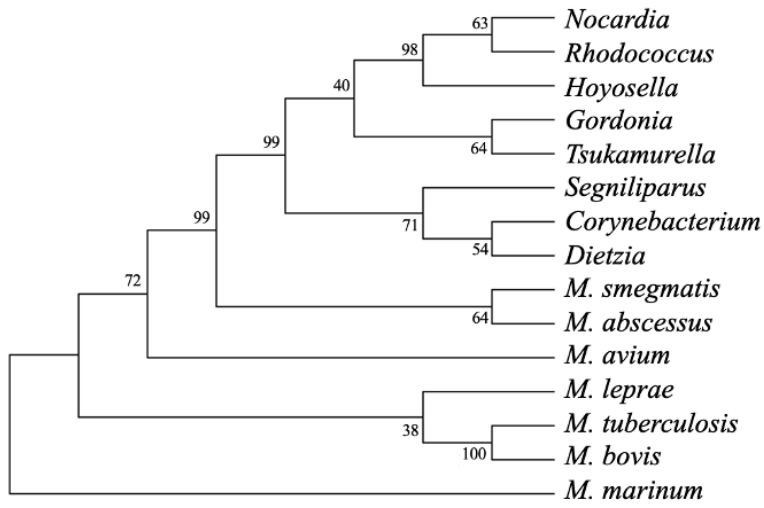

Figure 4.2. Phylogenetic tree of *Corynebacteriaceae* species constructed using MEGA Software . The phylogenetic tree was generated using the amino acid sequences of proteins with high identity and similarity to *M. smegmatis* MSMEG_4306. The methodology used was maximum likelihood, and the phylogram stability was analysed by bootstrapping 100 replications. Nodes with bootstrap values are indicated

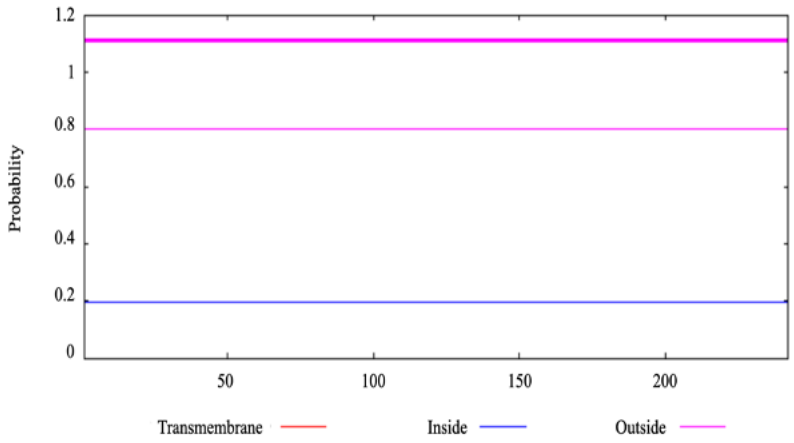

Figure 4.3. TMHMM predictions for *M. smegmatis* MSMEG_4306. No transmembrane domains were predicted by TMHMM.

The amino acid sequence of MSMEG_4306 was analysed in a structural assessment, in regard to its coiled-coil conformation, using the online tools COILS (Lupus *et al*., 1991) (https://embnet.vital-it.ch/software/COILS_form.html). COILS determines the probability that a residue within a protein is part of a coiled-coil structure, based upon the comparison with

sequences of known coiled-coil proteins. MSMEG_4306 from *M. smegmatis* was predicted to have two coiled-coil domains (Figure 4.4A). Using the online tool MULTICOILS (http://cb.csail.mit.edu/cb/multicoil/cgi-bin/multicoil.cgi), which identifies the probability of trimeric and dimeric coiled-coils, the oligomerisation status of MSMEG_4306 of *M. smegmatis* was explored (Wolf *et al*., 1997). The trimerisation probability of both coiled-coil domains was above the threshold (Wolf *et al*., 1997), indicating that MSMEG_4306 of *M. smegmatis* is predicted as a trimeric coiled-coil protein (Figure 4.4B).

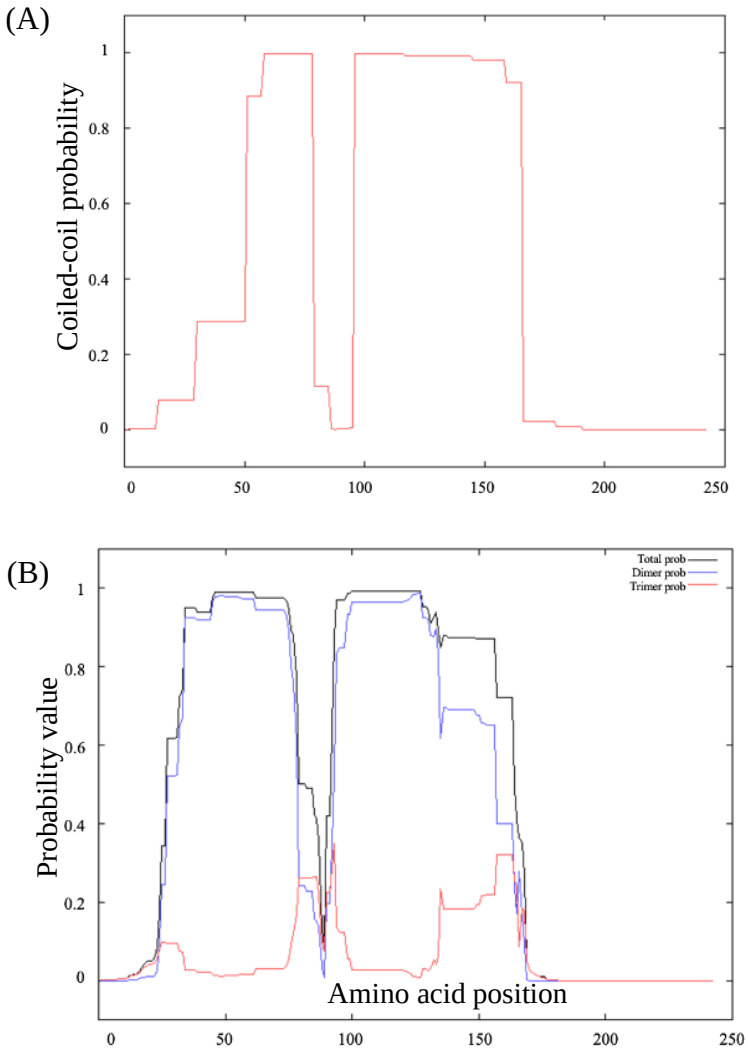

Figure 4.4. Predicted coiled-coil regions of *M. smegmatis* MSMEG_4306. The coiled-coil probabilities of MSMEG_4306 were predicted using COILS (A), and its dimerization and trimerization probabilities using MULTICOILS (B). MSMEG_4306 is predicted to possess two coiled-coil domains, which are predicted as a dimer.

The amino acid sequence of *M. smegmatis* MSMEG_4306 was modelled by I-TASSER (Iterative Threading Assembly Refinement, https://zhanglab.ccmb.med.umich.edu/I-TASSER/) to predict protein structure and function. The structure with the higher C-score (a confidence score for estimating the quality of predicted models, typically in the range of -5 to 2, where a model of a high C-score is of greater confidence) is shown in Figure 4.5A. The amino acid sequence of *M. smegmatis* MSMEG_4306 was also used to identify structural analogues. Figure 4.5B shows the highest ranked structural analogue, CT398 of *Chlamydia trachomatis*.

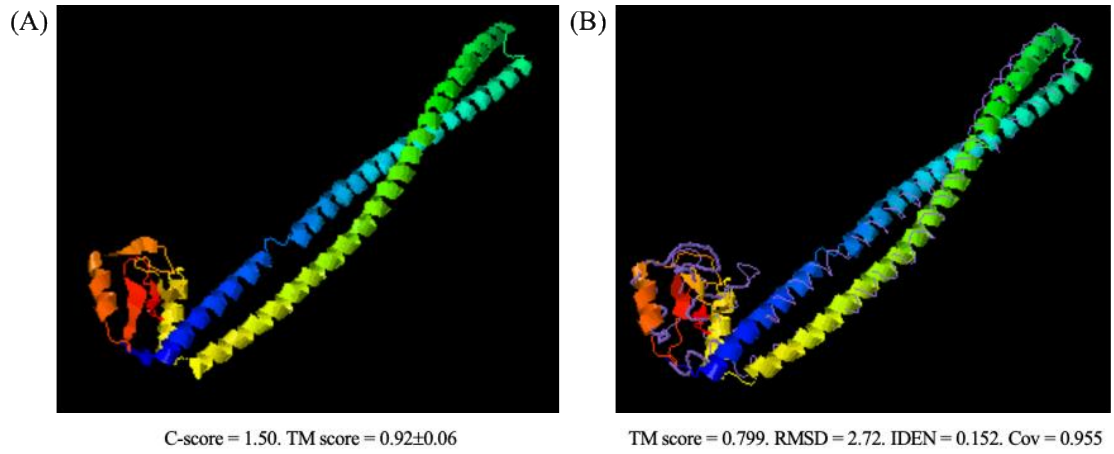

Figure 4.5. Modelling of *M. smegmatis* MSMEG_4306 via I-TASSER, and the identification of a structural analogue. The amino acid sequence of MSMEG_4306 was modelled using I-TASSER (AS). A structural analogue of MSMEG_4306, *Chlamydia trachomatis* CT398, was also identified (B) (MSMEG_4306 displayed as a cartoon model; CT398 displayed as backbone trace). C-score, a confidence score for estimating the quality of predicted models; TM-score and RMSD, known standards for measuring structural similarity between two structures; IDEN, the percentage sequence identity in the structurally aligned region; Cov, the coverage of the alignment by TM-align and is equal to the number of structurally aligned residues divided by length of the query protein.

4.2.2 Generation of a *M. smegmatis* mc^2 155 Δ*MSMEG_4306*, and *M. bovis* BCG Pasteur Δ*Mb2254c* knockout strain

To determine whether *MSMEG_4306* and *Mb2254c* are essential in the survival and growth of *M. smegmatis* mc^2 155 and *Mycobacterium bovis* BCG (respectively), allelic exchange substrates were constructed. Specialised Transduction was performed, to replace *MSMEG_4306* and *Mb2254c* with a hygromycin resistance cassette (Figure 4.6). Successful gene deletion of *MSMEG_4306* from *M. smegmatis* mc^2 155 was confirmed by Southern blot analysis, and this null knockout strain was designated Δ*MSMEG_4306*. Successful gene deletion of *Mb2254c* from *M. bovis* BCG Pasteur was confirmed by confirmatory PCR using the primer pairs Mb2254c_KO_F and HL, and Mb2254c_KO_R and HR (Figure 4.7) this strain was designated Δ*Mb2254c*. The ability to generate gene deletion strains indicates that both *MSMEG_4306* and *Mb2254c* are non-essential genes in *M. smegmatis* mc^2 155 and *M. bovis* BCG, respectively.

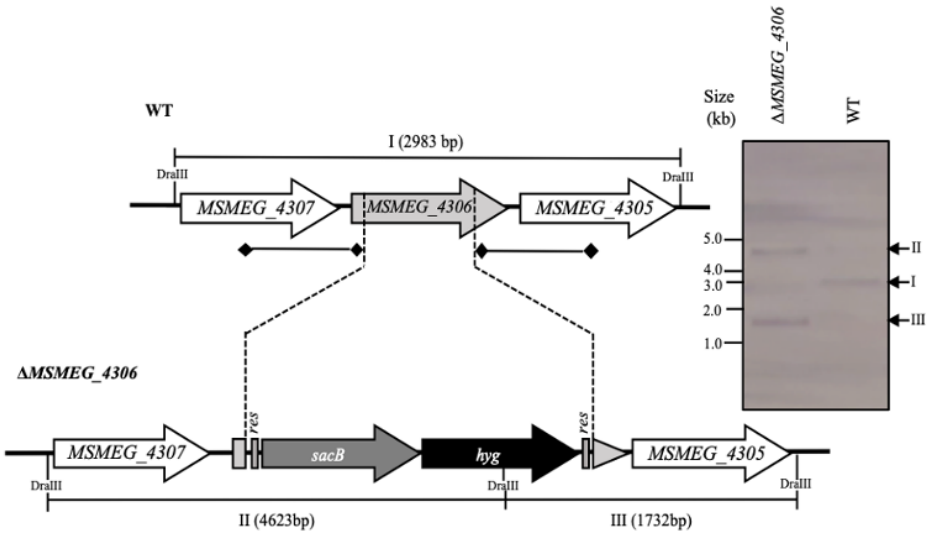

Figure 4.6. Construction and confirmation of a *M. smegmatis MSMEG_4306* deletion mutant. A schematic representation showing the removal of the gene of interest, *MSMEG4306,* from *M. smegmatis*, and its replacement with a hygromycin resistance cassette. To confirm the deletion of *MSMEG_4306,* Southern blot analysis was employed, using digoxigenin labelled probes indicated by the thick lines with square ends. The expected bands following Southern Blot analysis, following *DraIII* digestion, are indicated (I, II, III). WT, wildtype. sacB - sucrose counter-selectable gene from *Bacillus subtilis*; *hyg* - hygromycin resistance gene; *res* - γδ-resolvase site.

Following the confirmation of gene deletion, *MSMEG_4306* and *Mb2254c*, along with their native promoter, were cloned into the integrative plasmid pMV306, using the primer pairs MSMEG_4306_Comp_F and MSMEG_4306_Comp_R, and Mb2254c_Comp_F and Mb2254c_Comp_R, respectively. The plasmids were designated pMV306-*MSMEG_4306* and pMV306-*Mb2254c*. The subsequent plasmids were introduced into *M. smegmatis* mc^2 155

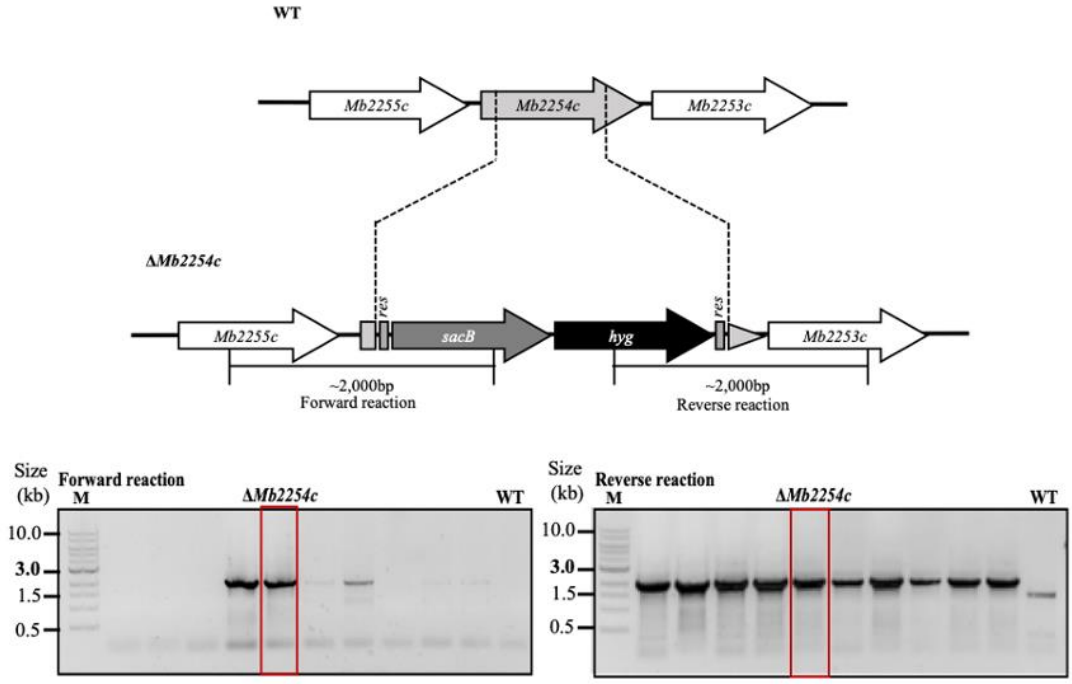

Figure 4.7. Construction and confirmation of a *M. bovis* BCG Pasteur *Mb2254c* deletion mutant. A schematic representation showing the removal of the gene of interest, *Mb2254c*, from *M. bovis* BCG Pasteur, and its replacement with a hygromycin resistance cassette. To confirm the deletion of *Mb2254c*, confirmatory PCR was employed, using primers located within the hygromycin resistance cassette, and in the neighbouring genes, to generate PCR products of approximately 2,000bp in the case of successful gene deletion. The bands outlined in red indicate successful gene deletion and the strain that was used throughout the study. WT, wildtype. M, DNA ladder marker. sacB - sucrose counter-selectable gene from *Bacillus subtilis*; *hyg* - hygromycin resistance gene; *res* - γδ-resolvase site.

Δ*MSMEG_4306* (pMV306-*MSMEG_4306*), and *M. bovis* BCG Δ*Mb2254c* (pMV306-*Mb2254c*), to generate complemented strains, Δ*MSMEG_4306*C and Δ*Mb2254c*C, respectively. Confirmatory PCR was carried out to determine successful complementation, using the primer pair MSMEG_4306_Comp_F and MSMEG_4306_Comp_R, and Mb2254c_Comp_F and Mb2254c_Comp_R (Figure 4.8 and Figure 4.9). The empty vector,

pMV306, was also introduced into *M. smegmatis* Δ*MSMEG_4306* and *M. bovis* BCG Δ*Mb2254c*, to generate the control strains Δ*MSMEG_4306*V and Δ*Mb2254c*V.

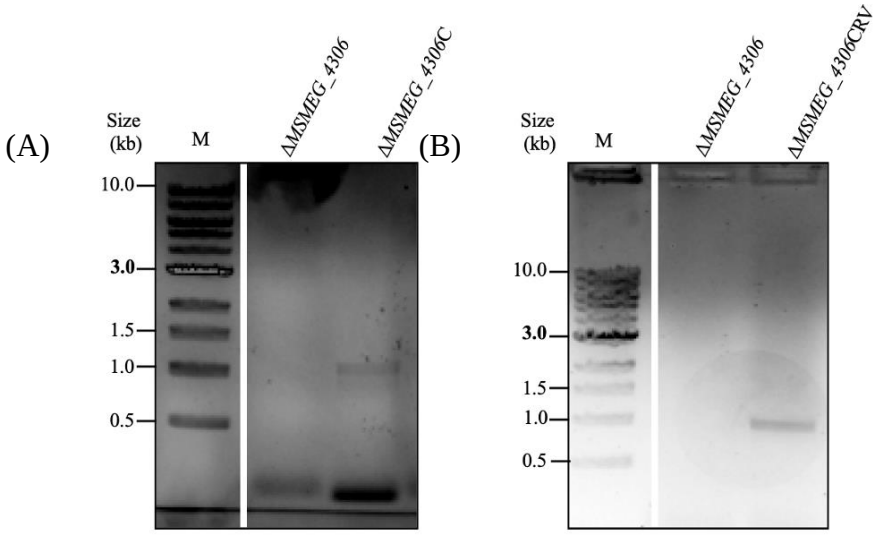

Figure 4.8. Confirmatory PCR of Δ*MSMEG_4306* complementation with *MSMEG_4306* and *Rv2229c*. *MSMEG_4306* and *Rv2229c* were cloned into pMV306 and were introduced into Δ*MSMEG_4306*, resulting in (A) Δ*MSMEG_4306*C and (B) Δ*MSMEG_4306*CRv, respectively. Complementation was verified by confirmatory PCR, with an expected band size of approximately 1kb. M, DNA ladder marker.

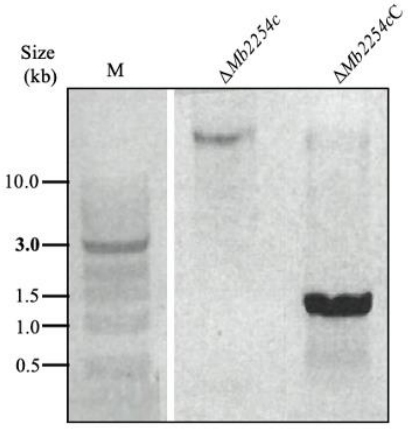

Figure 4.9. Confirmatory PCR of Δ*Mb2254c* complementation with *Rv2229c*. *Rv2229c* was cloned into pMV306 and was introduced into Δ*Mb2254c*. Complementation was verified by confirmatory PCR, with an expected band size of approximately 1kb. M, DNA ladder marker.

4.2.3 The effect of *MSMEG_4306* and *Mb2254c* deletion in *M. smegmatis* mc^2 155 and *M. bovis* BCG growth, respectively, in liquid media

To determine whether the deletion of *MSMEG_4306* and *Mb2254c* had any effect on growth and replication, a growth curve analysis was carried out. All strains were cultured in triplicate with aliquots taken at each time point, from which cell density was measured, along with colony forming units (in the case of Δ*MSMEG_4306*). The growth rate of all strains employed in each growth analysis study were similar and no significant difference was observed (Figure 4.10A, Figure 4.10B, andFigure 4.11), following statistical analysis using the means from two biological replicate experiments. There was no significant difference observed in the growth rate of the mutant strains when compared to the wildtype parental strains.

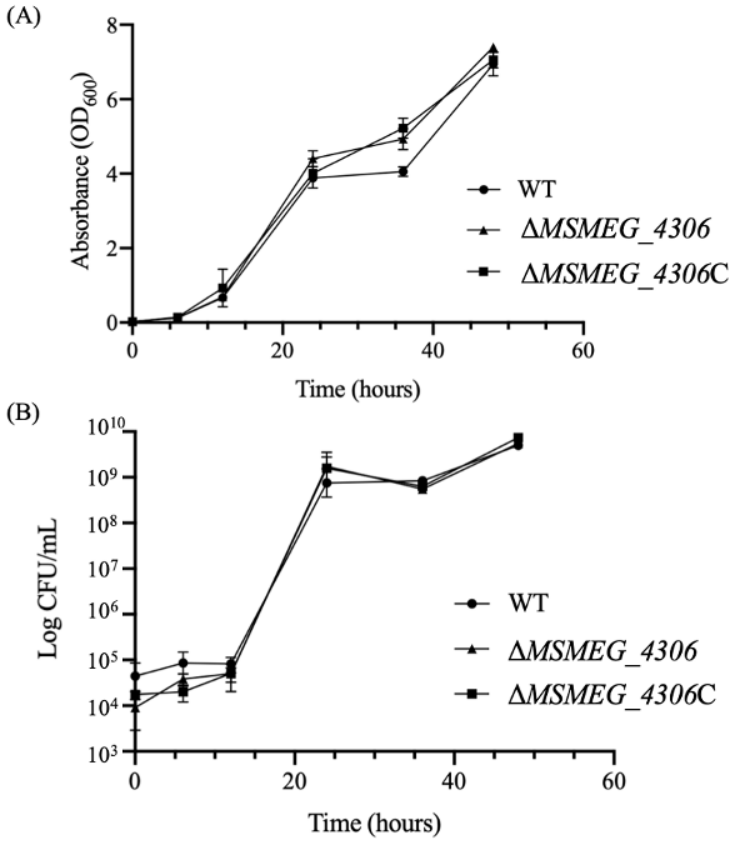

Figure 4.10. Growth curves of wildtype *M. smegmatis* mc^2 155, Δ*MSMEG_4306* and Δ*MSMEG_4306*C. All strains were cultured in TSB supplemented with 0.05% Tween-80, and grown at 37°C with agitation. Aliquots were taken at each time point, with cell density measured (A), and samples serially diluted and plated to determine colony forming units (B). There was no significant difference in growth rate as a result of the loss of *MSMEG_4306* from *M. smegmatis*. WT, wildtype.

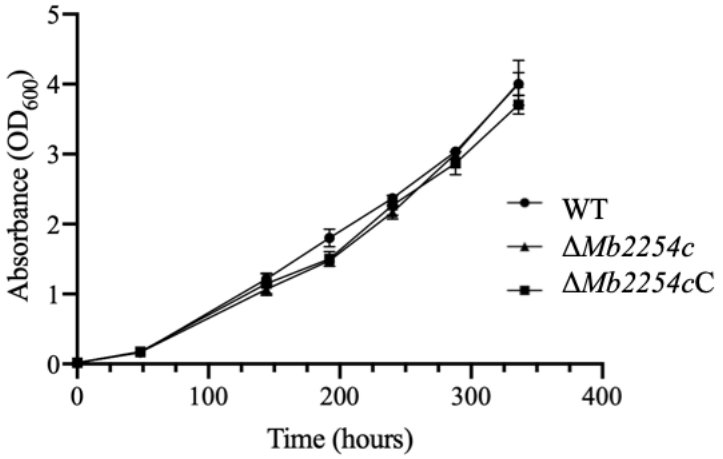

Figure 4.11. Growth curve of wildtype *M. bovis* BCG Pasteur, Δ*Mb2254c* and Δ*Mb2254c*C. All strains were cultured in Middlebrook 7H9 broth supplemented with 10% OADC and 0.05% Tween-80. Cultures were grown statically, at 37°C. Aliquots were taken at each time point, with cell density measured. There was no significant in growth rate as a result of the loss of *Mb2254c* from *M. bovis* BCG Pasteur. WT, wildtype.

4.2.4 The effect of *MSMEG_4306* and *Mb2254c* deletion in *M. smegmatis* mc^2 155 and *M. bovis* BCG on colony morphology

To determine whether the deletion of *MSMEG_4306* or *Mb2254c* from *M. smegmatis* mc^2 155 and *M. bovis* BCG Pasteur, respectively, had any effect on bacterial morphology, a colony morphology study was carried out. Bacterial strains were plated onto their respective agar plates with and without 0.05% Tween-80. Upon the deletion of *MSMEG_4306* from *M. smegmatis* mc^2 155, the colony morphology was less rugose and with less aerial growth (Figure 4.12). The native colony morphology was restored in Δ*MSMEG_4306*C, indicating that the change in colony morphology is solely due to the loss of *MSMEG_4306*. The loss of *Mb2254c* from *M. bovis* BCG Pasteur did not appear to show any changes in colony morphology (Figure 4.13).

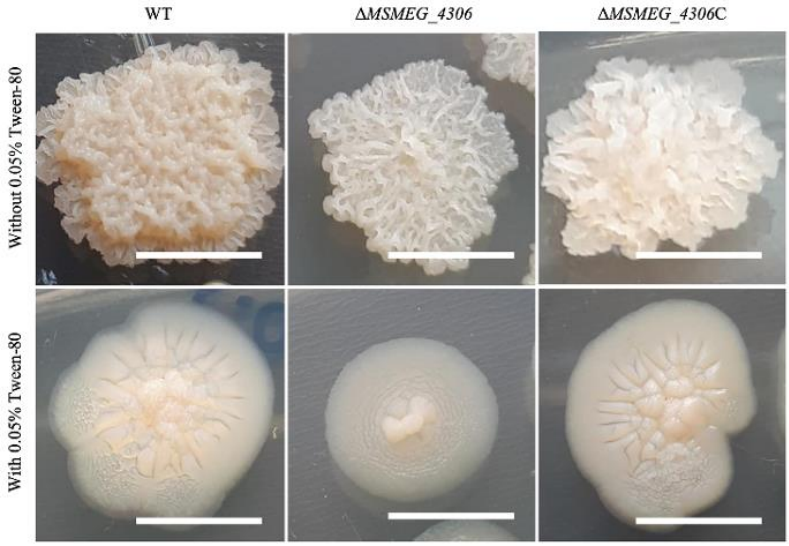

Figure 4.12. Colony morphology of wildtype *M. smegmatis* mc^2 155, Δ*MSMEG_4306* and Δ*MSMEG_4306*C. Single colonies of wildtype *M. smegmatis*, Δ*MSMEG_4306* and Δ*MSMEG_4306*C cultured on TSB agar with and without the supplementation of 0.05% Tween-80. The loss of *MSMEG4306* resulted in a less rugose colony morphology, showing less aerial growth, when compared to wildtype *M. smegmatis* and Δ*MSMEG_4306*C. WT, wildtype. Scale bar – 5mm.

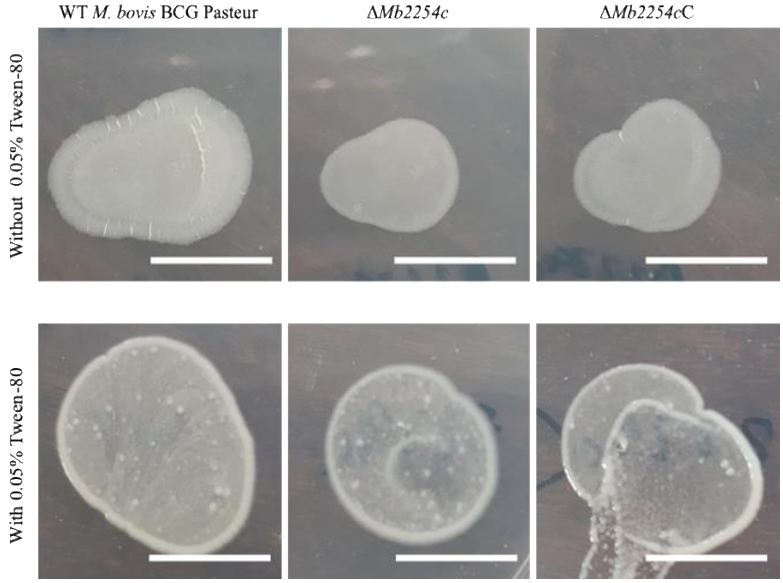

Figure 4.13. Colony morphology of wildtype *M. bovis* BCG Pasteur, Δ*Mb2254c* and Δ*Mb2254c*C. Spot colonies of wildtype *M. bovis* BCG Pasteur, Δ*Mb2254c* and Δ*Mb2254c*C were cultured on Middlebrook 7H9 agar, with and without the supplementation of 0.05% Tween-80. There appeared to be no difference in colony morphology. WT, wildtype. Scale bar – 5mm.

4.2.5 The effect of *MSMEG_4306* and *Mb2254c* deletion in *M. smegmatis* mc^2 155 and *M. bovis* BCG on pellicle formation

The pellicle forming ability of the strains was studied, to determine whether the loss of *MSMEG_4306* from *M. smegmatis* mc^2 155, or *Mb2254c* from *M. bovis* BCG impaired the strains ability to form an intact pellicle. Δ*MSMEG_4306* demonstrated an impaired ability to form a pellicle, as the pellicle appeared to be less intact when compared to wildtype (Figure 4.14). Δ*Mb2254c* was severely defective at forming a pellicle, when compared to wildtype *M. bovis* BCG Pasteur (Figure 4.15). This characteristic was restored back to wildtype phenotype following complementation with *Mb2254c*, indicating that the impaired ability to form a pellicle is as a result of the loss of *Mb2254c.*

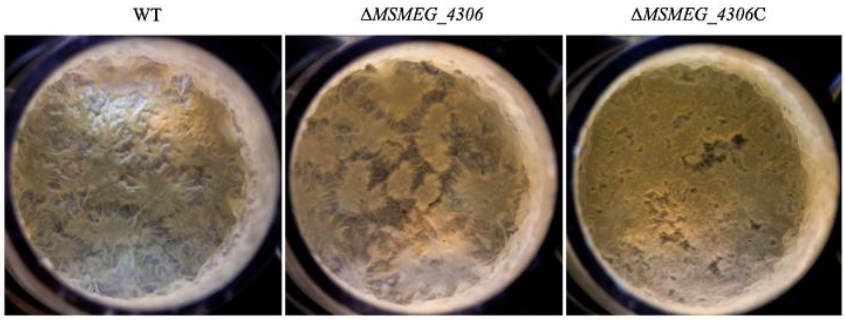

Figure 4.14. Pellicle forming ability of wildtype *M. smegmatis* mc^2 155, Δ*MSMEG_4306* and Δ*MSMEG_4306*C. Pellicle formation of wildtype *M. smegmatis,* Δ*MSMEG_4306* and Δ*MSMEG_4306*C, when cultured in Sauton's media. The loss of *MSMEG_4306* resulted in a defect in ability to form an intact pellicle, as the pellicle looked less intact when compared to wildtype *M. smegmatis* and Δ*MSMEG_4306*C. WT, wildtype.

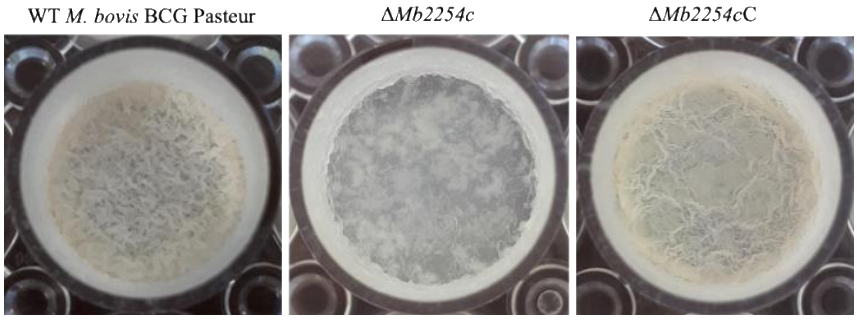

Figure 4.15. Pellicle forming ability of wildtype *M. bovis* BCG Pasteur, Δ*Mb2254c* and Δ*Mb2254c*C. Pellicle formation of wildtype *M. bovis* BCG Pasteur, Δ*Mb2254c* and Δ*Mb2254c*C, when cultured in Sauton's media. The loss of *Mb2254c* resulted in a defect in the ability to form an intact pellicle, when compared to wildtype *M. bovis* BCG Pasteur and Δ*Mb2254c*C. WT, wildtype.

4.2.6 Lipid profile of *M. smegmatis* mc^2 155 Δ*MSMEG_4306*

A change in colony morphology from wildtype characteristics is frequently indicative of a change in the cell envelope lipid content. Additionally, the cell wall lipid biosynthesis machinery are frequently known to interact with the cytoskeletal factors to coordinate cell wall biogenesis with polar growth (Kang *et al.*, 2008; Jani *et al.*, 2008). Hence, the lipid profiles of *M. smegmatis* mc^2 155 wildtype, Δ*MSMEG_4306* and Δ*MSMEG_4306*C were analysed by thin layer chromatography. Lipids were extracted from bacteria cultured on solid media, supplemented with and without 0.05% Tween-80. The lipid profiles of *M. smegmatis* mc^2 155 wildtype, Δ*MSMEG_4306* and Δ*MSMEG_4306*C were analysed by thin layer chromatography. Figure 4.16A and Figure 4.16B show that there are no major differences in the lipid content of the cell wall of Δ*MSMEG_4306*, when compared to wildtype and Δ*MSMEG_4306*C, in terms of both polar and apolar lipids. A lipid species, which appears to co-migrate with trehalose dimycolate (TDM) and triacylglycerol (TAG) (indicated with a white arrow head in Figure 4.16A) was however produced in greater quantities by Δ*MSMEG_4306* when compared to wildtype *M. smegmatis* and Δ*MSMEG_4306*C.

4.2.7 The effect of *MSMEG_4306* deletion on cell length of *M. smegmatis* mc^2 155

As only a minor change were observed in the lipid profile of Δ*MSMEG_4306* compared to wildtype and Δ*MSMEG_4306*C, the cell phenotype was studied microscopically to determine if the change in colony morphology and pellicle forming ability was as a result in differing cell morphology. Cells were visualised using phase contrast microscopy, and a population of 250 cells were measured to determine variation in cell length. It was found that Δ*MSMEG_4306* cells were significantly longer than wildtype and Δ*MSMEG_4306*C cells,

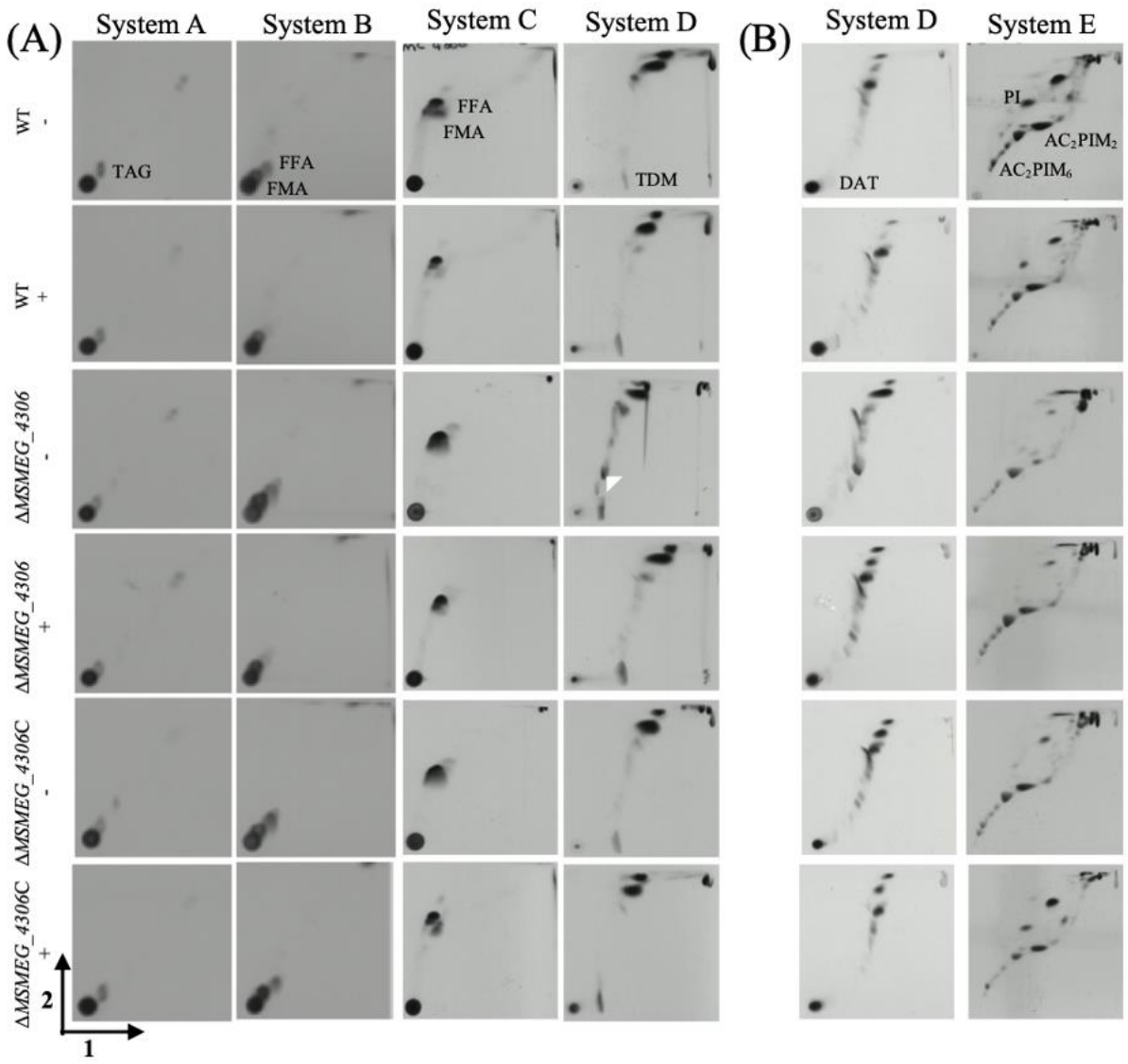

Figure 4.16. Lipid analysis of wildtype *M. smegmatis* mc^2 155, Δ*MSMEG_4306* and Δ*MSMEG_4306*C. 2D-TLC analysis of [^{14}C]-labelled lipids extracted from strains that were cultured on ^{14}C-acetic acid labelled TSB agar, with and without the supplementation of 0.05% Tween-80. Colony material was collected and a full lipid extraction was carried out. 20,000cpm of extracted lipids were spotted onto a silica plate, then separated using different solvent systems (see General Materials and Methods Chapter for full protocol of lipid extraction and solvent systems). TDM appeared to be produced at higher quantities by the mutant, with a co-migrating lipid species absent from wildtype *M. smegmatis* and the complemented strain, indicated with the white arrow head. Apolar (A) and polar (C) lipids. WT, wildtype. TAG, triacylglycerols; FFA, free fatty acid; FMA, free mycolic acid; TDM, trehalose dimycolate; DAT, diacyltrehalose mycolate; PI, phosphatidylinositol; AC_2PIM_2, diacyl phosphatidylinositol dimannoside; AC_2PIM_6, diacyl phosphatidylinositol hexamannoside

from the population sampled (Figure 4.17). The average lengths of wildtype, Δ*MSMEG_4306* and Δ*MSMEG_4306*C were 6.9μM, 7.8μM and 7.2μM respectively, suggesting that the loss of *MSMEG_4306* impacted the average cell length.

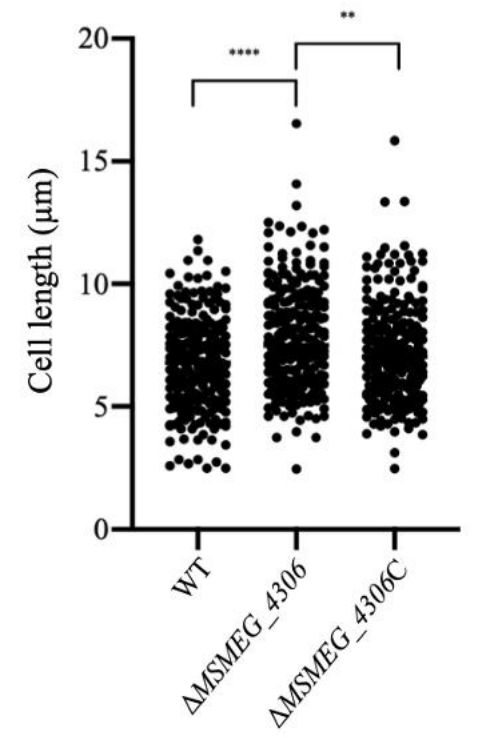

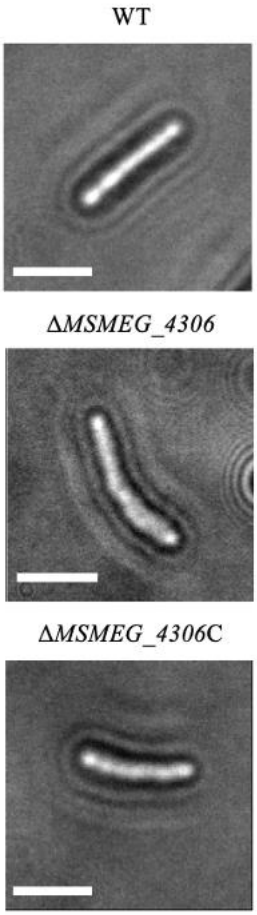

Strain	Average (µm)	Standard Deviation (µm)
WT	6.1	1.7
Δ*MSMEG_4306*	7.8	2.1
Δ*MSMEG_4306*C	7.2	2.0

Figure 4.17. Microscopy and cell length analysis of wildtype *M. smegmatis* mc^2 155, Δ*MSMEG_4306* and Δ*MSMEG_4306*C. Strains were cultured in TSB supplemented with 0.05% Tween-80, and visualised at 100X magnification. A sample of 250 cells were measured to determine average cell lengths. The deletion of *MSMEG_4306* resulted in the production of significantly longer cells, when compared to wildtype *M. smegmatis* and Δ*MSMEG_4306*C. WT, wildtype. **, $P<0.01$; ****, $P<0.0001$. (Scale bar, 10µm). Panel on the left shows a bar graph of all measurements taken.

4.3 DISCUSSION

Uncharacterised proteins of bacterial genomes represent a void in the understanding of a microorganism's virulence, metabolism and growth. Approximately 50% of the *M. tuberculosis* genome is comprised of uncharacterised or hypothetical proteins (Mazundu & Mulder, 2012). The requirement of assigning a function to these uncharacterised proteins would contribute greatly to the understanding of not just the roles of these gene products, but also in the broader sense, their potential interacting partners and the complexes that they may be a component of. This study has begun to delineate the role of MSMEG_4306, a previously uncharacterised *M. smegmatis* protein, through the construction of a gene deletion strain, and its application in various phenotypic analysis studies, to determine the effect of loss of *MSMEG_4306* on mycobacterial growth.

4.3.1 MSMEG_4306 is conserved across the Actinomycetale order, and is absent from laterally growing rod-shaped bacteria, such as *E. coli* and *B. subtilis*

The amino acid sequence of MSMEG_4306 was utilised in a BLASTP search to identify homologous proteins within other bacterial species. MSMEG_4306 homologues were identified in most mycobacterial species, including both environmental saprophytes, and pathogenic mycobacteria capable of causing human disease, indicating that MSMEG_4306 homologues are conserved across the mycobacterial genus. MSMEG_4306 homologues were also identified in other species of the *Corynebacteriaceae* family, in addition to other families within the Actinomycetale order, albeit with lower identity scores. A BLASTP search utilising MSMEG_4306 as a query against other laterally growing, rod-shaped bacteria, such as *E. coli* and *B. subtilis* found no homologous proteins. It could therefore be hypothesised that MSMEG_4306 homologous proteins are present in polar growth progenitors of the

Actinomycetale order, with a conserved function, involved in a mechanism that is specific to these actinobacteria.

4.3.2 *MSMEG_4306* and *Mb2254c* are not essential in the growth and survival of *M. smegmatis* mc^2 155 and *M. bovis* BCG Pasteur, respectively

This study has shown that both *MSMEG_4306* and *Mb2254c* are non-essential genes in *M. smegmatis* and *M. bovis* BCG Pasteur, respectively, due to the successful replacement of each gene with a hygromycin resistance cassette, and the subsequent viability. Previous work by DeJesus *et al*. (2017) predicted that *Rv2229c* is an essential gene in *M. tuberculosis* H37Rv. This study utilised the BSL-2 *M. bovis* BCG Pasteur as a model for the slow-growing virulent *M. tuberculosis* H37Rv. Whilst *M. bovis* BCG Pasteur and *M. tuberculosis* H37Rv do possess physiological differences (Mahairas *et al*., 1996; Rehren *et al*., 2008), the identity between *Rv2229c* and *Mb2254c* is >99.5% identity. Due to the almost identical nature of these homologues, in which the deletion of *Mb2254c* was successful, it can therefore be assumed that *Rv2229c* is a non-essential gene of *M. tuberculosis* H37Rv.

4.3.3 MSMEG_4306 demonstrates high similarity, in terms of domain organisation, with CT398 of *C. trachomatis* and HP0958 of *Helicobacter pylori*

A search of the Protein Data Bank, using MSMEG_4306's amino acid sequence, as a template initially identified no statistically similar proteins, whose functions were known and characterised. MSMEG_4306 was then used as a template to identify potential structurally similar proteins (SWISS MODEL ExPASY). The crystal structure of CT398, from *C. trachomatis*, presented with the highest identity to MSMEG_4306, with an identity score of

approximately 15.5%. Both CT398 and MSMEG_4306 possess a C-terminal zinc-ribbon domain. Whilst zinc-finger structural motif is present in a wide variety of proteins with varying function, the majority typically bind DNA, RNA or protein; the C4 RING-type zinc finger motif (possessing four cysteine residues in the consensus sequence CXXC-X_{20}-CXXC; where X is any amino acid), identified in CT398, and in MSMEG_4306 (a slight difference of CXXC-X_{22}-CXXC), is often involved in DNA-binding regions, based on the research on the presence of C4-type zinc fingers located within the DNA-binding regions of some nuclear receptor families (Rigden, 2011). Further study into the DNA binding capabilities of MSMEG_4306 should take place to delineate the role of this uncharacterised protein; the employment of experiments, such as DNA electrophoretic mobility shift assay, or chromatin immunoprecipitation (ChIP) assay, would contribute to further knowledge on the potential DNA binding ability of MSMEG_4306, as opposed to purely speculative assumption based on common functions of conserved protein structural domains.

Work by Kumar & Karthikeyan (2018) verified this finding, and confirmed that a remarkable similarity is observed between the zinc-ribbon domains of MSMEG_4306 and CT398. Additionally, they identified another protein, HP0958 of *Helicobacter pylori*, as having high structural similarity, in terms of the C-terminal zinc-ribbon domain, to MSMEG_4306, yet a low overall poor sequence identity, with an identity score of only 15% (Kumar & Karthikeyan, 2018). HP0958 also possesses the C4 RING-type zinc finger motif (CXXC-X_{20}-CXXC), as observed in CT398, and to some extent, MSMEG_4306. CT398 and HP0958, in their respective pathogens, have been shown to bind to the sigma factor RpoN, and the ATPase regulator FliH (Barta *et al*., 2015; Rain *et al*., 2001)**,** with HP0958 essential for normal motility in *Helicobacter pylori* (Ryan *et al*., 2005), and both HP0958 and CT398 comprise part of the type III secretion systems (T3SS) in their respective pathogens, a complex structure that injects effector proteins into the eukaryotic host cell, as an effective virulence mechanism (Coburn *et*

al., 2007; Barta *et al*., 2015). Mycobacteria are non-motile bacilli, and lack T3SS's, showing a lack of conserved function between the structurally similar proteins of these distant strains. Kumar and Karthikeyan (2018) however speculated that the similarity in the domain organisation between these strains may suggest that MSMEG_4306 is involved in a mycobacterial secretion system. With only little previous research carried out on delineating the function of MSMEG_4306, the assumptions made on the role of MSMEG_4306 remain highly speculative, and further study is required to confirm any current hypotheses on potential function.

4.3.4 The loss of *MSMEG_4306* resulted in alterations in phenotype, including a change in colony morphology and pellicle forming ability, which may be as a result in the changes of cell envelope lipid composition

Although no difference in growth rate was identified between Δ*MSMEG_4306*, and wildtype *M. smegmatis* mc^2 155 and Δ*MSMEG_4306*C, a phenotypic analysis of colony morphology, when grown on TSB agar supplemented with the detergent Tween-80, identified a differential colony morphology upon *MSMEG_4306* deletion, when compared to wildtype *M. smegmatis* mc^2 155 and Δ*MSMEG_4306*C; the mutant colony appeared to show less aerial growth, with a less rugose appearance more obvious when growth media was supplemented with 0.05% Tween-80. Additionally, the ability to form a pellicle when grown in Sauton's media appeared to be impacted following *MSMEG_4306* deletion, with the pellicle appearing less intact, in the mutant strain. Both the colony morphology and pellicle appearance were restored to that observed in wildtype *M. smegmatis* mc^2 155, upon complementation with *MSMEG_4306*. The pellicle forming ability of Δ*Mb2254c* was severely impacted when compared to wildtype *M. bovis* BCG Pasteur and Δ*Mb2254c*C, with a very sparse pellicle that

was less corrugated, signifying a defect in the progression of pellicle formation. An alteration in the morphology phenotype (colony or as a more complex structure like a pellicle) is often indicative of cell surface lipid changes, which may have an effect on the way that cells interact with one another. A full lipid profiling was carried out to determine if there was a different in the outer or inner lipids, when bacteria were grown on solid media, with and without the supplementation of 0.05% Tween-80, as the change in colony morphology was more severe when grown in the presence of the detergent. It appeared that a lipid species that co-migrated with TDM and triacylglycerol (TAG) was produced in greater quantities by the mutant strain, with this lipid species less dense in the analysis of wildtype and complemented strain lipids. Without further experimentation, it is difficult to determine if this lipid species if an increased accumulation of TDM, TAG or solely a lipid which comigrated with these. One hypothesis of the difference observed in the lipid profile of Δ*MSMEG_4306* compared to wildtype *M. smegmatis* and Δ*MSMEG_4306*C could be due to the development of lipid bodies. Lipid bodies are small structures, found in bacilli, containing accumulated TAG, a. major energy source for some actinomycetes (Olukoshi & Packter, 1994; Alvarez *et al*., 2000). These arise due to stress responses, such as in the case of hypoxia (Daniel *et al*., 2011). The application of stress-induction studies followed by subsequent lipid analysis and electron microscopy could shed light on the potential formation of lipid bodies, which may be the cause of the altered lipid profiling of Δ*MSMEG_4306*. It would be interesting to identify, and further work will begin to, determine the nature of this lipid through mass spectrometry, to identify its presence and accumulation upon the deletion of *MSMEG_4306.* Additionally, confirmation of the accumulating lipid species, suspect to be TDM, would provide direction for the further investigation into assigning a role to MSMEG_4306.

4.3.5 The loss of *MSMEG_4306* resulted in an elongated phenotype

As change in colony morphology and pellicle forming ability may be indicative of a cellular morphology change further investigation was carried out into the cause of the change in colony morphology, leading to a study on the average cell length of cells following *MSMEG_4306* deletion. It appeared that, among a population of 250 sampled cells, the deletion of *MSMEG_4306* caused cells to be significantly longer when compared to wildtype *M. smegmatis* mc^2 155 and Δ*MSMEG_4306*C. Numerous studies have demonstrated an elongated phenotype in mycobacteria following the deletion or depletion of genes whose products interact with cell wall biosynthetic machinery, or have roles in cell division; one example is SepF, an FtsZ interacting protein that demonstrates sequence similarity to SepF of *B. subtilis*, where its role is in the regulation of the Z-ring assembly, with deletion resulting a *B. subtilis* cells showing deformed septa (Hamoen *et al.*, 2005). In mycobacteria, SepF is essential; the knockdown of which resulted in a failure of FtsZ to localise to the septa, leading to a distinct elongated phenotype (Gola *et al*., 2015), alike to that observed in *M. smegmatis*, following *MSMEG_4306* deletion. It was also observed that SepF is able to interact with MurG, a peptidoglycan synthesizing enzyme, indicating that SepF has a regulatory role in the coordination of cell division and peptidoglycan biosynthesis, based on its known interacting partners FtsZ and MurG (Gupta *et al*., 2015). Another study in which an elongated phenotype was observed upon the depletion of proteins with roles as division machinery was by Wu *et al.* (2018); they confirmed that the depletion of numerous cell division proteins resulted in elongated cells with aberrant branching. These proteins included FtsZ, the septation initiating protein, FtsQ, which has been shown to modulate cell length and division, and FtsL and FtsB, homologous to proteins in *E. coli* that function as a trimer with FtsQ to initiate cell division (Jain *et al*., 2018; Tsang & Bernhardt, 2014). It would be interesting to determine the site of localisation of MSMEG_4306 in *M. smegmatis*, relative to known division machinery such as

FtsZ and other Fts proteins that have roles in cell division, as well as identifying a potential interacting relationship between these proteins. Identifying any subsequent changes in the localisation of interacting partners, following *MSMEG_4306* deletion would greatly contribute to delineating a potential role of MSMEG_4306 in cell division, hypothesised due to the elongated phenotype observed following its loss from *M. smegmatis.*

The study carried out by Kumar and Karthikeyan (2018) concluded with the prediction that MSMEG_4306 might have a role in mycobacterial secretion systems, based on the finding that structural similarity exists, in terms of the domain organisation, between MSMEG_4306, CT398 and HP0958. Additionally, they hypothesised that, due to the presence of Rv2229c, a close homologue, in the cell wall and membrane fractions (Mawuenyega *et al*., 2005; Målen *et al*., 2010; de Souza *et al*., 2011), the role of MSMEG_4306 may be in lipid biosynthetic pathways or the synthesis or secretion of certain macromolecules. Using the online prediction tools, TMHMM v. 2.0 and TMpred, it is likely that MSMEG_4306 lacks transmembrane regions. The hypothesis make by Kumar and Karthikeyan (2018), that MSMEG_4306 may be a membrane bound protein involved in a secretion system, is likely to be inaccurate.

The hypothesis from this study, that MSMEG_4306 is involved in cell division, due to the elongated phenotype observed following its deletion from *M. smegmatis* mc^2 155, is purely speculative due to the need for further research to confirm this. As carried out in chapter 2, examination of septation, utilising a fluorescent membrane dye, such a fluorescent vancomycin, along with a nucleoid stain, such a propidium iodide, will provide further evidence on whether a deletion of *MSMEG_4306* had an effect on cell division, as suspected, due to significantly longer Δ*MSMEG_4306* cells. Additionally, identifying sites of MSMEG_4306 localisation within the cell during the cell cycle would also further enhance the research into the function of MSMEG4306 in mycobacterial growth. The localisation of MSMEG_4306, relative to other proteins that are known to localise to the septa, and are vital

in successful cell division, such as FtsZ and FtsQ, would provide further evidence on the speculative role of MSMEG_4306 in mycobacterial cell division. Similarly, as in chapter 2, the construction of an *M. smegmatis* strain in which the overexpression of His-tagged MSMEG_4306 is inducible, would provide valuable insight into the potential interacting partners of MSMEG_4306; time constraints limited the study, so interacting protein partners could not be determined**.** This study will continue to further delineate the potential role of MSMEG_4306 in mycobacterial division. Whilst this study has begun to characterise the current hypothetical *M. smegmatis* protein, MSMEG_4306, identifying interactors, whose roles have been assigned and researched substantially, would further contribute to the delineation of MSMEG_4306's role in mycobacterial growth and cell division.

CHAPTER 5

Utilising *M. tuberculosis* Δ*kasB* as a Model of Latent Infection, to Determine Differing Host Immune Responses Between Active and Latent Tubercular Infection

5.1 INTRODUCTION

The growth and division of mycobacteria is extremely challenging to decipher, due to the complex multi-layered cell envelope. Mycobacteria, and other actinobacteria such as *Streptomyces coelicolor* do not possess an MreB ortholog, an actin homologue found in laterally growing bacteria, such as *Escherichia coli* and *Bacillus subtilis* that acts as a scaffold for peptidoglycan synthesising machinery at the sites of wall growth (Carballido-López *et al*., 2006). This indicates that an alternative coordination process is present in mycobacteria that drives the synthesis and incorporation of the complex cell wall components at the sites of cell wall assembly, the cell poles and the septa.

In mycobacteria, the DivIVA homologue, Wag31, is considered the coordinator of polar growth (Kang *et al*., 2008); it interacts with enzymes require for cell wall precursor biosynthesis. This highlights the importance of Wag31 in directing these enzymes to the sites of cell wall biosynthesis, the septa and the cell tips, for the incorporation of their products. Research shows that Wag31 is able to interact with an essential component of the acetyl-CoA carboxylase (ACC) complex, AccA3, involved in the synthesis of the C_{22}-C_{26} mycolate precursor (Gande *et al*., 2007). Wag31 has also been shown to interact with FtsI, also known as penicillin-binding protein 3 (PBP3), a transpeptidase thought to be necessary for optimal peptidoglycan cross-linking at its localisation site, the septa (Plocinska *et al*., 2014; Plocinski *et al*., 2011).

Mycolic acids constitute a large portion (40%) of the dry cell weight of the *M. tuberculosis* cell envelope, and have been shown to be essential for viability (Takayama *et al*., 1972; Vilchèze *et al*., 2000; Portevin *et al*., 2004). The FAS-II system is a fatty acid synthesising system that utilises the acyl CoA (C_{16}) substrate from the FAS-I system, and produces the meromycolate backbone chain (C_{56}) of mature mycolic acids (Qureshi *et*

al.,1984). KasA and KasB are condensing enzymes that elongate this substrate by two carbon units with each successive cycle, to form the meromycolate chain (Kremer *et al*., 2000). Mycolic acid biosynthesis is a prominent target for antitubercular therapy, due to their essentiality for survival.

The mycolate containing glycolipid, trehalose dimycolate (TDM), also referred to as cord factor, has long been considered an immunomodulatory lipid component of the mycobacterial cell wall; in mice, TDM alone is capable of eliciting the production of numerous proinflammatory cytokines, including TNF-α, IFN-γ, IL-10 and IL-12 (Behling *et al*., 1993; Lima *et al*., 2001). TDM is also found to be responsible for the recruitment of a large number of activated macrophages around the lesion during mycobacterial infection (Lima *et al*., 2001). Research has shown that TDM alone is capable of modulating the immune response during intracellular infection. Indrigo *et al*. (2002) found that the attenuation of delipidated *M. tuberculosis* bacilli was lost upon the reconstitution of TDM alone, with virulence restored to normal levels, during infection of mouse derived macrophages. Additionally, research into the mycolate modification of cyclopropionation on the meromycolate chain have been shown to influence the virulence of strains, and hence, the outcome of disease progression. Studies have shown that the deletion of the proximal cyclopropane rings of alpha, methoxy or keto mycolic acids results in strain attenuation in mice (Glickman *et al*., 2000; Dubnau *et al*., 2000). From these studies, it can be observed that not only are mycolic acids essential for viability, and forming a significant component of the mycobacterial cell wall, but they also possess immunostimulatory properties and are capable of directing the host immune response.

The initial interaction of *M. tuberculosis* pathogen associated molecular patterns (PAMP) with immune cell pathogen recognition receptors (PRR) results in the production of numerous inflammatory cytokines. Some of these cytokines are proinflammatory in nature, and demonstrate crucial roles in the containment and eradication of the bacilli. IFN-γ is a potent

macrophage activator. Activation drives the induction of the transcription of over 200 genes involved in the production of antimicrobial molecules (Cooper, 2009), in addition to infected activated macrophages displaying mycobactericidal capabilities. Activated macrophages are also capable of driving T lymphocyte polarisation towards a type I T helper (Th1) phenotype by the production of the proinflammatory Th1 cytokines (Berger, 2000), such as IL-12 and IL-1β. IL-12 is a prolific inducer of IFN-γ and hence drives the cycle of polarisation of Th1 cells through the presentation of antigen on antigen presenting cells, the further macrophage activation through the production of IFN-γ and the subsequent intracellular bacilli destruction. IL-1β, secreted by activated macrophages, is also capable of driving T cell polarisation to the type 17 helper (Th17) phenotype, able to secrete the proinflammatory IL-17. IL-17 further recruits macrophages and other immune cells, such as neutrophils, to the site of infection, to drive the assembly of the granuloma, the complex structure formed to attempt to contain the bacilli at a focal point. TNF-α is another proinflammatory cytokine of great importance during tubercular infection. Through the regulation and production of chemokines, TNF-α drives the recruitment and migration of immune cells to the site of infection. This ensures the formation and maintenance of a successful granuloma, in which the bacilli reside at the centre.

An efficient proinflammatory response as a result of *M. tuberculosis* results in mycobacterial eradication, or the control of replication, where the bacilli may be held in check by the immune response, yet fails to be eradicated fully. These cells may serve as a potential reservoir for reactivation, if the hosts immune system were to be compromised; due to the dormancy of these cells, and the potential for progression to active disease, this disease state is termed latent tuberculosis. Developing an understanding of the proinflammatory immune response to *M. tuberculosis* would provide vital information on the key modulators of the outcome of tubercular disease, active or latent.

A study by Bhatt *et al.* (2005) established the essentiality of *kasA* in mycobacteria, with a conditional depletion strain inducing cell lysis. The depletion of KasA also resulted in the accumulation of α' mycolates, and a reduction in the production of α and epoxy mycolates (Bhatt *et al*., 2005). In contrast, *kasB* has successfully been deleted from *M. tuberculosis*, indicating that it is non-essential for mycobacterial growth (Bhatt *et al*., 2007). The deletion of *kasB* from *M. tuberculosis* drastically altered the colony morphology, in addition to abolishing cording ability; this was due to the synthesis and accumulation of mycolates with shorter chain lengths, confirming the role of KasB as an accessory gene in the elongation of mero-mycolic acids to their full length (Bhatt *et al.*, 2007). The most profound finding was that the *kasB* deletion strain was able to persist in immunocompetent mice, without causing morbidity or death; *M. tuberculosis* Δ*kasB* was still detected in the lungs of mice, but the infected models remained healthy, with all of the Δ*kasB* infected mice alive 356 days post infection, compared to the wildtype and complemented strain infected mice, in which all had succumbed to infection. Infection of severe combined immunodeficient (SCID) mice with *M.* tuberculosis Δ*kasB* also resulted in death, indicating that the ability of the mouse to control bacterial replication, in terms of the Δ*kasB* mutant, was dependent on the cell mediated immunity of the infected host.

The deletion of *kasB* from *M. tuberculosis* resulted in an attenuated strain that demonstrated long term persistence without causing active disease. The ability to detect bacilli approximately 450 days post infection in otherwise healthy mice suggests that the employment of *M. tuberculosis* Δ*kasB* may provide a good model in the study of latent infection. The knowledge on immunological difference between latent and active disease, and the immune response involved in the establishment and maintenance of latent tuberculosis remain limited. The employment of *M. tuberculosis* Δ*kasB* as an infection model for latent tuberculosis may

begin to elucidate how the hosts immune response is able to prevent bacterial replication and active disease, yet fails to completely eradicate the bacilli, in the case of latency.

The aim of the study outlined in this chapter was to begin to delineate the immunological differences observed in the innate immune response towards a strain representing active disease, *M. tuberculosis* CDC1551, and a strain representing latent infection, *M. tuberculosis* CDC1551 Δ*kasB*. More specifically, these strains were utilised in various assays to determine immunological differences, upon infection of bone marrow derived murine macrophages (BMDM), in terms of assessing cytokine production and quantification, employing enzyme-linked immunosorbent assay (ELISA) and real-time polymerase chain reaction (RT-PCR). BMDMs infected with *M. tuberculosis* CDC1551 Δ*kasB* produced significantly greater TNF-α and IL-1β when compared to BMDMs infected with wildtype *M. tuberculosis* CDC1551. Additionally, upon infection with *M. tuberculosis* Δ*kasB*, the mRNA expression of IL-1β was significantly reduced, compared to both wildtype *M. tuberculosis* and the complemented strain, *M. tuberculosis* Δ*kasB*C. Whilst the use of *M. tuberculosis* Δ*kasB* as a model for latent tuberculosis is somewhat limited currently, this work has begun to elucidate the differences in the innate immune response following BMDM infection with the attenuated strain *M. tuberculosis* Δ*kasB*, and the virulent *M. tuberculosis* CDC1551.

5.2 RESULTS

5.2.1 Bacterial uptake and intracellular survival of *M. tuberculosis* strains in murine BMDMs

To examine intracellular survival, murine BMDM's were infected separately, with wildtype *M. tuberculosis* CDC1551, Δ*kasB* and the complemented strain, (Δ*kasB*C), at a MOI (multiplicity of infection) of 2 (two bacterial cells to one target BMDM). The intracellular bacterial count was determined by lysing cells and plating serial dilutions. BMDM's were infected with each strain in triplicate, and the means of two technical replicates were compared by means of one-way ANOVA with Tukey's post-test. There was a greater initial uptake of *M. tuberculosis* Δ*kasB* and Δ*kasB*C by BMDMs when compared to the wildtype strain, *M. tuberculosis* CDC1551, but this difference was not significant (Figure 5.1). Following washing of BMDMs and further incubation to determine intracellular bacterial survival at 72 hours post infection, the number of intracellular bacteria reached a similar level for all strains.

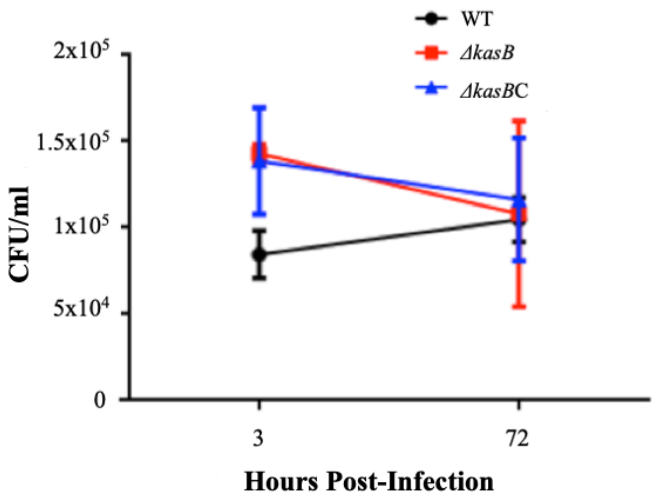

Figure 5.1. Intracellular counts of bacteria in BMDMs following 3 hours and 3 days post infection. BMDMs were infected with each strain (wildtype *M. tuberculosis* CDC1551, Δ*kasB* and Δ*kasB*C) in triplicate, with the mean of two technical replicates analysed. No significant difference was observed in the initial uptake of any of the strains, or in the intracellular survival of these strains within BMDMs, following 72 hours of infection. WT, wildtype.

5.2.2 Pro-inflammatory cytokine release by urine BMDMs upon infection with *M. tuberculosis* strains

Murine BMDMs were infected with wildtype *M. tuberculosis* CDC1551, Δ*kasB* or Δ*kasB*C, at a MOI of 2. At 24 hours post infection, the supernatants from all wells were collected and assayed for pro-inflammatory cytokine (TNF-α and IL-1β) release. BMDM's were infected with each strain in triplicate, and the means of two technical replicates were compared by means of one-way ANOVA with Tukey's post-test. Murine BMDMs infected with Δ*kasB* released a significantly higher concentration of TNF-α compared to wildtype *M. tuberculosis* CDC1551 (Figure 5.2). Similarly, BMDMs infected with the Δ*kasB* released a significantly higher concentration of IL-1β compared to wildtype *M. tuberculosis* CDC1551 (Figure 5.2). Surprisingly, BMDMs also infected with Δ*kasB*C produced higher levels of both TNF-α and IL-1β following a 24-hour infection period, when compared to wildtype *M. tuberculosis* CDC1551. In addition, BMDMs infected with Δ*kasB*C produced significantly higher quantities of TNF-α than Δ*kasB*, with levels of IL-1β produced at similar quantities.

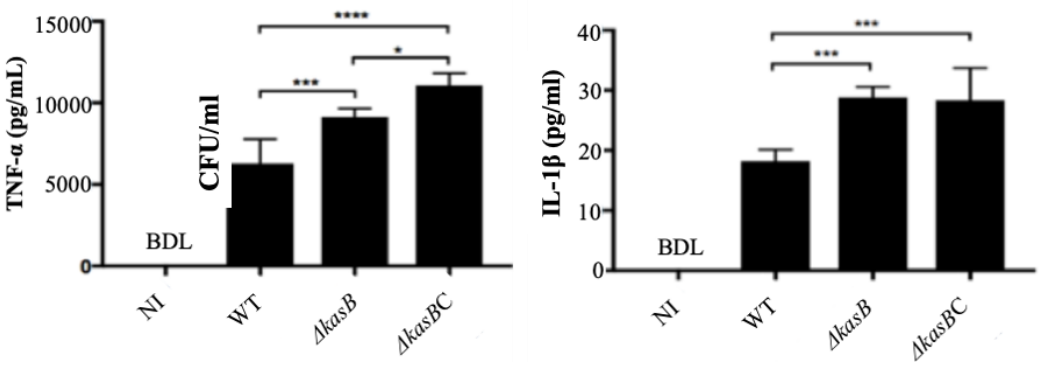

Figure 5.2. Pro-inflammatory cytokine production of murine BMDMs infected with wildtype *M. tuberculosis* CDC1551, Δ*kasB* and Δ*kasB*C. Murine BMDMs were infected with *M. tuberculosis* strains at a MOI of 2, in triplicate, with the means of two technical replicates were used for analysis. Following 24 hours of infection, the supernatants were assayed for TNF-α and IL-1β production by sandwich ELISA. Δ*kasB* infected BMDMs produced TNF-α and IL-1β at significantly greater levels than wildtype *M. tuberculosis*. Values are presented as a mean ± standard deviation. WT, wildtype. *, $p \leq 0.05$. *** $p \leq 0.001$. **** $p \leq 0.0001$. NI, non-infected. BDL, below detection limit.

5.2.3 Expression of pro-inflammatory cytokine mRNA

To determine the specific mechanisms in the initial immune response to infection with the strains included in this study, BMDMs were stimulated over a period of 6 hours with either wildtype *M. tuberculosis* CDC1551, Δ*kasB* or Δ*kasB*C at a MOI of 2. The RNA was extracted from the samples from each time point (3- and 6-hours post infection) and used to synthesise cDNA, which was utilised in RT-PCR to determine cytokine expression during infection. BMDM's were infected with each strain in triplicate, and the means of two technical replicates were compared by means of two-way ANOVA. All three strains induced a peak of TNF-α mRNA expression from BMDMs at 3 hours post infection, with Δ*kasB*C inducing slightly higher levels at this time point (Figure 5.3). This difference however was not significant when compared to the expression levels from BMDMs infected with the wildtype or mutant strain. By 6 hours post infection, TNF-α mRNA expression levels had decreased to similar values for all infection strains. BMDMs infected with the three strains included in this study demonstrated a similar IL-1β mRNA expression following 3 hours post infection (Figure 5.3) with significantly lower levels of IL-1β mRNA expressed in *M. tuberculosis* Δ*kasB* infected BMDMs when compared to the wildtype and complemented strain expression levels, following 6 hours of infection. When studying IL-12 p40 mRNA expression in BMDMs infected with the strains included in this study, Δ*kasB*C surprisingly induced a greater expression at both 3 hours post infection, and 6 hours post-infection, when compared to wildtype and Δ*kasB* (Figure 5.3).

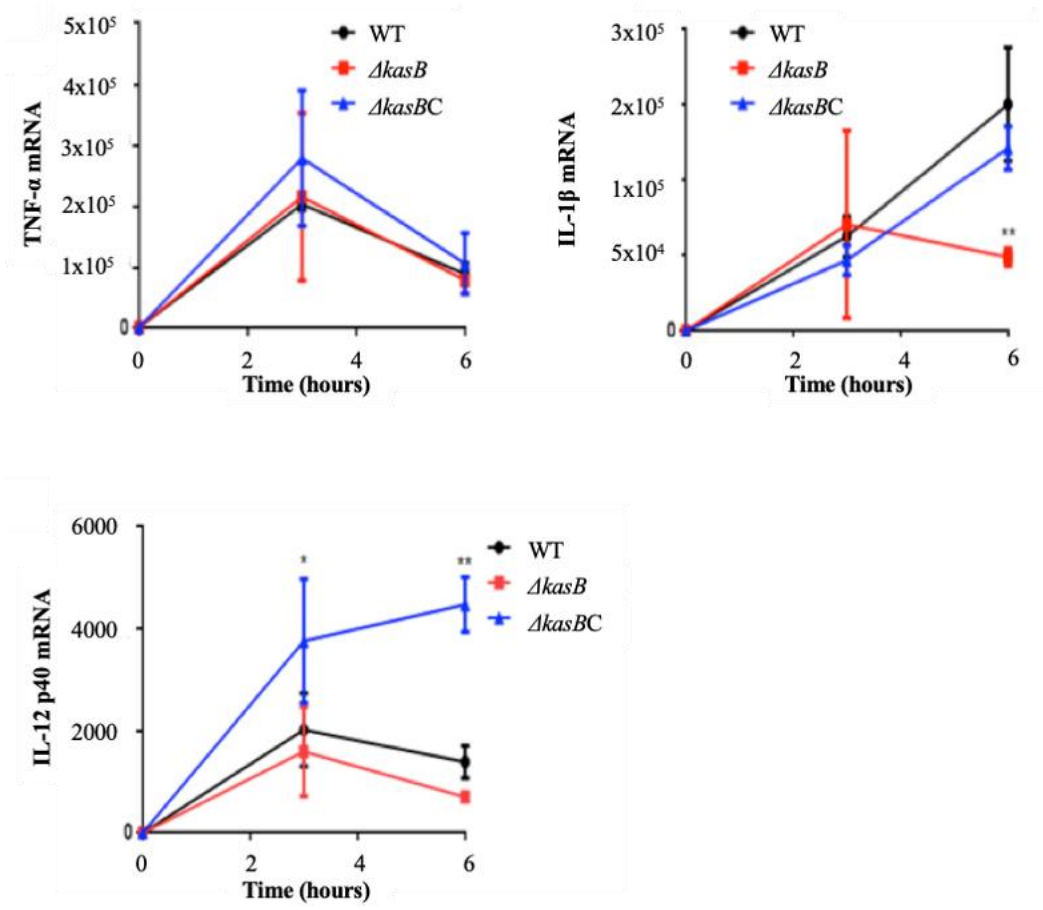

Figure 5.3. Proinflammatory cytokine mRNA expression by murine BMDMs infected with wildtype *M. tuberculosis* CDC1551, Δ*kasB* and Δ*kasB*C. Murine BMDMs were infected with *M. tuberculosis* strains at a MOI of 2:1, in triplicate, with the means of two technical replicates were used for analysis. Following 3 and 6 hours of infection, RNA was extracted, cDNA was synthesised and RT-PCR was carried out using primers specific for the pro-inflammatory cytokines TNF-α, IL-1β and IL-12 p40. Following 6 hours of infection, BMDMs infected with Δ*kasB* displayed significantly greater expression levels of IL-1β when compared to wildtype *M. tuberculosis* and Δ*kasB*C. Values are presented as a mean ± standard deviation. WT, wildtype. *, $p \leq 0.05$. **, $p \leq 0.01$

5.3 DISCUSSION

Latent tuberculosis remains a global burden, with an estimated 1.7 billion latently infected individuals in 2014 (Houben & Dodd, 2016), which serve as a potential reservoir for the development of active disease, if reactivation were to occur. The innate immune response of tuberculosis has been widely studied, and the establishment of the granuloma and its ability to control bacilli replication is understood due to this research. The inability to determine an appropriate model for the study of latent tuberculosis however, has hindered the potential research into the differential innate responses in active and latent tuberculosis. The models which are affordable, require simple handling, and in which work is easy to replicate do not display a true representative of the human granuloma or infection; mice fail to establish a granuloma as complex as that seen in humans, with instead a, non-caseating lung infection that sees an increase in bacterial load, and a decrease in lymphocyte recruitment (Rhoades *et al*., 1997). Additionally, guinea pigs are highly susceptible to low-dose aerosol infection (McMurray, 2001), and are therefore unable to establish latent infection. The availability of an appropriate model of latent tuberculosis that is characteristic to that observed in humans would begin to elucidate the differential innate immune response between active and latent tuberculosis.

The attenuation observed upon *in vivo* mouse infection with the *M. tuberculosis* Δ*kasB* deletion strain (Bhatt *et al*., 2007) mimics the characteristics observed during human latent tuberculosis infection; the reduced severity of granulomatous lesions in the lungs, and the survival of the infected individuals, although bacilli were still present and viable in the lungs conveys strong resemblance to the dormant nature of bacilli during latent infection. Lin *et al*. (2009) studied the differences in the granuloma histology and organisation between those displaying active tuberculosis and those latently infected; for this work, non-human primates

were employed as an infection model, due to the similarity to human tuberculosis infection, in terms of disease progression. It was found that the granulomatous lesions of those latently infected were few in comparison to those with active disease, in addition to being described as less severe in terms of pathology. The granulomatous lesions in the lungs of mice infected with *M. tuberculosis* Δ*kasB* (Bhatt *et al*., 2007) display a high similarity to those that were found in latently infected non-human primates, described by Lin *et al*. (2009). For these reasons, the attenuation of the deletion strain, and the similarity of the lung lesions to non-human primates with latent tuberculosis disease, the *M. tuberculosis* Δ*kasB* deletion strain was employed in this study as a model for latent tuberculosis, in parallel with wildtype *M. tuberculosis*, to begin to delineate differences in the innate immune response.

In this study, it was identified that BMDMs infected with Δ*kasB* produced significantly more IL-1β, when compared with the parental wildtype *M. tuberculosis*. Similarly, TNF-α was produced at a significantly greater quantity when compared to wildtype *M. tuberculosis*. In the previous study by Bhatt *et al*. (2007), it was speculated that the changes observed, in regards to loss of cording ability, attenuation in a mouse model, and the persistence of *M. tuberculosis*, following the loss of *kasB* may be due to the alterations in the mycolic acid profile of TDM. Multiple research studies have concluded that TDM is a potent inflammatory factor of the *M. tuberculosis* cell envelope, and is able to activate macrophages, in addition to inducing a T cell immune response (Ishikawa *et al*., 2009; Schoenen *et al*., 2010). Research has also shown that delipidated *M. tuberculosis* reduces the production of cytokines (TNF-α, IL-1β, IL-12), with restoration to wildtype levels upon TDM reconstitution. TDM is therefore considered a component of the mycobacterial cell wall that drives a response that favours the development of the granuloma (Indrigo *et al*., 2003). It could therefore be hypothesised from the finding in this study, that loss of *kasB* from *M. tuberculosis* induces a greater production of IL-1β and

TNF-α, that the altered mycolic acid profile of TDM may be capable of initiating a greater immunomodulatory influence than wildtype TDM.

To fully determine whether the differential cytokine profile of Δ*kasB* is as a result of the altered mycolic acid profile of TDM, research into the activity of the TDM receptor upon exposure to these *M. tuberculosis* strains would begin to elucidate this hypothesis. The receptor of TDM has long been speculated (Bowdish *et al*., 2009; Werninghaus *et al*., 2009). Ishikawa *et al*. (2009) identified that macrophage inducible C-type lectin (Mincle) is an essential TDM receptor; heat-killed mycobacteria were able to activate Mincle-expressing cells, yet delipidated bacilli were unsuccessful in driving activation. Numerous studies (Schoenen *et al*., 2010; Hansen, M. *et al*., 2019) employed RT-PCR and RNAseq analysis to determine mRNA expression following stimulation with TDM. Employing purified TDM from the strains in this study, wildtype *M. tuberculosis*, Δ*kasB* and Δ*kasB*C, in a similar study would begin to elucidate the role, if any, of TDM in the differential innate immune response observed in this study, and also its role in conveying hypovirulence to Δ*kasB* when employed in the previous *in vivo* study (Bhatt *et al*., 2007).

Study of the mRNA expressions profiles found that IL-1β expression of BMDMs infected with Δ*kasB* was significantly lower when compared to wildtype *M. tuberculosis*, at 6 hours post infection. This data is somewhat contradictory to the results obtained from the IL-1β ELISA results in this study, where IL-1β was produced at significantly greater quantities by Δ*kasB* infected BMDMs, compared to those infected with wildtype *M. tuberculosis*. This differing interpretation of IL-1β production and expression may be as a result of a delay in the cytokine production, as IL-1β is formed by a multi-step process. The interaction of PAMPs with PRRs on phagocytic cells, results in the expression of pro-IL-1β; this interaction, termed the "priming" step is an insufficient stimulus in driving the production of active IL-1β. An additional PAMP or danger associated molecular pattern (DAMP) is required to induce further

processing (Schroder & Tschopp, 2010) and the subsequent activation of the inflammasome. The inflammasome is a multimeric protein complex (Sharma & Kanneganti, 2016) responsible for the activation of pro-caspase-1 into its active form and the subsequent cleavage of pro-IL-1β into the active IL-1β. A study by Herzyk *et al*. (1992) found that IL-1β transcripts in macrophages were 3-fold lower than those in monocytes, as a result of the slower conversion of pro-IL-1β into active IL-1β. This delay in the IL-1β processing would explain the differing results between the IL-1β ELISA study and IL-1β mRNA expression; the mRNA expressions study ceased at 6 hours post infection, whereas the ELISA analysis continued until 24 hours post infection. Due to the differing durations of each experiment, IL-1B mRNA expression may have changed to reflect that of an increased cytokine expression, observed in the ELISA analysis. The mRNA expression study should be extended to collecting the supernatant 24 hours post infection, so that this experiment can be suitably compared with the ELISA study.

The significant findings when studying IL-1β production and IL-1β mRNA expression present as interesting routes for the further investigation into the role of IL-1β following BMDM infection with wildtype *M. tuberculosis* and Δ*kasB*; with Δ*kasB* demonstrating similarities to latent tuberculosis following *in vivo* mouse infection, these further studies may subsequently highlight a difference in the establishment of latent or active tubercular disease. Upon activation of IL-1β, the balance is swayed towards macrophage activation and subsequent elimination of the bacilli by phagosomal maturation (Master *et al*., 2013). This may begin to explain the slight decrease in intracellular survival of Δ*kasB* in BMDMs, observed over the 72-hour study. To determine the cause of the differential production and expression of IL-1β in the *kasB* deletion strain, further investigation into this cytokine should be carried out, including the study of inflammasome activity.

Following *M. tuberculosis* infection, IL-1β secretion depends on the activation of the inflammasome. Two inflammasome sensor molecules responsive to *M. tuberculosis* bacilli are

NOD-, LRR and pyrin domain-containing protein 3 (NLRP3) and absent in melanoma 2 (AIM2) (Mishra *et al*., 2010; Saiga *et al*., 2012), which are components of the NLRP3 and AIM2 inflammasomes, the assembly and activation of which results in IL-1β and IL-18 secretion, both of which drive protective immunity against *M. tuberculosis* (Yamada *et al*., 2000; Okamura *et al*., 1998). Further study into the production of these two inflammasome produced cytokines by BMDMs would begin to delineate differences in inflammasome activity upon infection with wildtype *M. tuberculosis*, Δ*kasB* and Δ*kasB*C. Additionally, it would be interesting to observe the effect of an inflammasome agonist in the production and expression of IL-1β, such as ATP or nigericin, a potassium ionophore, which causes NLRP3 inflammasome activation through K^+ efflux (Perregaux & Gabel, 1994; Muñoz-Planillo *et al*., 2013), following BMDM infection with the strains included in this study; the initiation of inflammasome activation may reflect in changes in IL-1β production and mRNA expression between wildtype *M. tuberculosis* and Δ*kasB* infected BMDMs.

In the previous study by Bhatt *et al*. (2007), it was found that the deletion of Δ*kasB* from *M. tuberculosis* resulted in the inability to synthesise trans-cycloproponated keto mycolic acids with only small amounts of cycloproponated methoxy mycolic acids produced, as a downstream result of this deletion. Glickman *et al*. (2001) identified that the cyclopropane synthase that introduces trans-cyclopropane rings into both keto and methoxy mycolic acids is CmaA2. Rao *et al*. (2006) employed an *M. tuberculosis* Δ*cmaA2* deletion stain in a macrophage infection study, to identify the effect of trans-cycloproponation loss in keto and methoxy mycolic acids, on mediating the host immune response to infection; it was found that the loss of trans-cycloproponation, as a result of *cmaA2* deletion was able to generate an enhanced *M. tuberculosis*-induced macrophage inflammatory response. Their work found that purified TDM, lacking trans-cycloproponate rings was 5-fold more potent in stimulating macrophages following mouse macrophage infection. With the downstream result of Δ*kasB* deletion causing

the loss in the ability to synthesise trans-cyclopropionated keto and methoxy mycolic acids, then a similar hypothesis could be made, taking into account the results of the Δ*cmaA2* study; that a product, as a result of *kasB* deletion, may be considered as a more potent stimulant of macrophages than the wildtype. This may begin to explain why the initial uptake of Δ*kasB* was slightly greater than the uptake of wildtype *M. tuberculosis*, why the intracellular survival of Δ*kasB* decreased over the duration of this study (due to more efficient macrophage activation and bacilli clearing), and why the production of IL-1β and TNF-α was greater by BMDMs infected with Δ*kasB* than wildtype *M. tuberculosis*. It may be hypothesised that the *kasB* deletion strain was able to induce a greater macrophage inflammatory response, potentially due to the inability to incorporate trans-cyclopropionate rings into oxygenated mycolic acids.

Throughout the whole study, the complemented strain did not behave alike to the wildtype strain. In the study of cytokine production, TNF-α production by Δ*kasB*C infected BMDMs, although significantly higher than when infected with Δ*kasB*, was also significantly higher than wildtype *M. tuberculosis* infection. IL-1β production was significantly greater in BMDMs infected with Δ*kasB*C compared to wildtype *M. tuberculosis* infection too. IL-12 p40 mRNA expression was significantly greater in BMDMs infected with Δ*kasB*C compared to both wildtype *M. tuberculosis* and Δ*kasB* infected BMDMs. Complementation of KasB into *M. tuberculosis* Δ*kasB* should revert all experimental results to that seen following BMDM infection with wildtype *M. tuberculosis*, which was expected in this study, due to the seemingly successful complementation of this strain in the previous study by Bhatt *et al*. (2007).

The vector utilised in the complementation of KasB is pMV261, a replicative (multi-copy) vector that introduces the gene extrachromosomally. There is therefore no risk in disrupting the host strain genes through chromosomal integration, and this vector has its own promoter. The differing data when comparing from Δ*kasB*C infected BMDMs with the wildtype *M. tuberculosis* infected BMDMs may be as a result of a regulatory malfunction upon

complementation, which may not have been noticeable in the long-term experiments of the previous study (Bhatt, A. *et al.,* 2007). In the short-term assays included in this study, the differences may be somewhat more prevalent. The study of immunological response, based on cytokine production and cytokine mRNA expression, may be more subtle in their differences, than the previous study, of which the strains were used to infect mice and carried out for a long period of time. For this reason, further work utilising Δ*kasB* should involve a new complemented strain, in which an integrative vector, such as pMV306, is utilised. This would begin to elucidate whether the application of a replicative plasmid in the complemented strain is causing a regulatory malfunction and resulting in the obscure behaviour observed by this strain; in the lack of reversion of the Δ*kasB* knockout to displaying wildtype characteristics during infection.

Whilst providing as a great model for preliminary investigation of pathogen-host interactions during mycobacterial infection, results from *in vitro* experiments should be interpreted with care and should not be extrapolated or assumed to be true for mycobacterial infection *in vivo*. If due care is taken when forming hypotheses, *in vitro* studies can still provide useful information on immune response mechanisms to pathogens. Whilst murine BMDMs are easy and relatively cheap to obtain, there is a difference in humans and mice as hosts of *M. tuberculosis* infection, with humans having co-evolved with *M. tuberculosis* whereas mice have not (Kramnik, I. & Beamer, G., 2016), indicating that constraints may exist in directly translating results obtained from an *in vitro* study using a mouse model to a human model. If care is taken in extrapolating results, these findings may have important implications in further understanding the differential immune response mechanisms observed during active and latent tuberculosis infection. The *in vivo* analysis has previously been carried out by Bhatt *et al.* (2007), highlighting the attenuation of *M. tuberculosis* Δ*kasB*, when compared to wildtype *M. tuberculosis* CDC1551 in a mouse model. The *in vitro* nature of this study is suitably applicable

when focusing solely on the cytokine specific immune response to this attenuated strain. Whilst difficult to further determine the suitability of *M. tuberculosis* Δ*kasB* as a model of latent tuberculosis, the results from this work have begun to provide a solid base, which can be built upon, beginning to identify and elucidate the differing cytokine profiles between wildtype *M. tuberculosis* and the attenuated Δ*kasB* strain.

CHAPTER 6

General Discussion

Whilst effective antibiotics are available for tuberculosis, the BCG vaccine is the world's most widely used vaccine, and global tuberculosis incidence and mortality rates are falling (World Health Organization, 2015), problems remain regarding successful tuberculosis treatment and prevention; the emergence of MDR-TB in over 100 countries worldwide has the potential to reverse progress made so far in the battle against tuberculosis. Research also shows that the efficacy of BCG varies greatly, dependent on factors such as the strain utilised and age of the individual at the time of vaccination. Additionally, with the World Health Organization's End TB Strategy, to reduce tuberculosis incidence by 80% by 2030, research into rapid and accurate diagnostic methods are crucial to identify tubercular infection as early as possible, to ensure appropriate effective treatment. With this in mind, molecular research is pivotal in providing an understanding of mycobacterial growth and virulence, necessary to inform on novel drug targets, potential vaccination candidates and mycobacterial metabolism and survival.

The main objective of this work was to investigate mycobacterial polar growth and cell division, in addition to beginning to elucidate the immunological differences between active tuberculosis and a strain which displayed severe attenuation in a mouse infection model. For this, four projects were carried out; three projects involved potential coiled-coil candidates in mycobacterial polar growth or cell division, and one utilised an attenuated strain, *M. tuberculosis* Δ*kasB*, in parallel with wildtype *M. tuberculosis*, to determine innate immunological differences between these strains, which resemble characteristics to latent and active tubercular disease, respectively, in a mouse infection study (Bhatt *et al.*, 2007).

The first strategy that was used to target the proposed objective was to generate mycobacterial strains, with the deletion of gene candidates, to investigate their roles in polar growth and division. Candidates were identified based on amino acid sequence homology with proteins whose functions have been identified in cell growth and division, or based on the

possession of conserved domains, also identified in these known proteins. Both SepIVA of *M. smegmatis* mc^2 155 and Rv1682 of *M. tuberculosis* possess DivIVA domains. DivIVA, first identified in *B. subtilis*, has a role in septum positioning (Edwards & Errington, 1997), whereas the DivIVA homologue in mycobacteria, Wag31, has a primary essential role in regulating cell shape and cell wall synthesis (Kang *et al*., 2008). This study identified and studied two candidates which possess a DivIVA domain, with the hypothesis that the conservation of this domain may have conserved its function. The aim was to identify proteins involved in cell shape and cell wall synthesis, or in septum positioning and cell division. This strategy, of generating deletion strains, presents as a good starting point in determining both the essentiality of the candidate gene, and also in identifying possible growth defects, based on a resultant change in colony morphology, as a result of the deletion.

The progression from identifying a change in colony morphology to the study of the lipid profile of the deletion mutant is logical, due to the common occurrence of a subtle change in cell envelope composition reflecting in a phenotypic change in the colony characteristics, often due to the differential interactions between cells. Upon inspection of Δ*sepIVA* and Δ*MSMEG_4306*, a change in colony morphology was observed; this was reverted to the wildtype phenotype upon complementation. The lipid profile of Δ*sepIVA*, analysed by TLC, was not altered as a result of *sepIVA* deletion, in terms of polar and apolar lipids of the cell envelope. Based on the conserved DivIVA-domain of this protein, this was not surprising that the deletion of *sepIVA* did not cause a change in lipid profiling or production, as it is suspect that its role is based elsewhere than in lipid metabolism and biosynthesis. The lipid profile of *M. smegmatis* following the loss of *MSMEG_4306* was marginally altered compared to both wildtype and the complemented strain; a lipid species that comigrates with TDM and TAG is produced in greater abundance following the loss of *MSMEG_4306*. Without further lipidomics, it is difficult to determine if this species is increased production of TDM or TAG,

or solely a lipid which comigrates with these. Further work will continue to investigate this alteration in lipid production, through further lipid analysis, and mass spectrometry of the species in question.

If a candidate was proposed to have a role in cell growth or division, the deletion of this gene should reflect in a change in the subsequent cell length; aberrant septation would result in gene deleted cells demonstrating a significant difference in cell length, compared to the wildtype strain, as would a mutant strain that is defective in cell elongation. In this work, it was found that upon the deletion of *SepIVA* and *MSMEG_4306*, cells were significantly longer when compared to wildtype and the complemented cells. Evidence of change in cell length is a good starting point for further study into these candidates being involved in cell elongation and septation.

The deletion of *Mb1709* from *M. bovis* BCG did not associate with any changes in colony morphology, lipid profile or cell length. It is therefore difficult to hypothesise on a potential role of Rv1682 from this lack of differential results and based solely on the conserved domains of the proteins, or based on homology with proteins of known function. Work will continue on the function of this protein, as other research on the *M. bovis* orthologue Mb1709 shows the ability of this protein to self-assemble into filaments in vitro, presenting this protein as an intermediate filament protein (Bagchi et al., 2008); intermediate filament protein often play a structural cellular role, such as in conveying mechanical strength to the cell (Herrmann et al., 2009). For these reasons, it would be interesting to purify Rv1682 to determine a crystal structure for this protein, in addition to identifying interacting partners of Rv1682, through the method utilised in this study. Another point of interest that was not explored in this study was the presence of patchy accumulations along the cell length of *M. bovis* BCG Pasteur upon the deletion of Mb1709, observed during phase contrast microscopy. In addition to the continuation of identifying interacting partners of Rv1682, work will continue to investigate

the nature and cause of these accumulations, through electron microscopy and fluorescence microscopy of lipids.

The significant increase in cell length, as a result of Δ*sepIVA* deletion led to the study of septation and chromosomal segregation, to identify if the cause of an increased cell length was due to aberrant septation. Fluorescence microscopy was employed, along with fluorescent stains to determine septa and chromosomal material. The increased septation in Δ*sepIVA*, leading to the formation of multiple mini-compartments per cell, provides further evidence that SepIVA is involved in appropriate mycobacterial septation.

Another strategy utilised in the delineation the role of numerous candidates in mycobacterial growth and division, was to employ an interaction study, to identify characterised interacting partners; through confirming interactions with proteins of known function may begin to shed light on the potential role of the hypothetical proteins included in this study. For this work, an in vivo crosslinking method was utilised, in which the protein of interest was overexpressed in *M. smegmatis*, crosslinked with its interacting partners, and then purified, utilising the proteins His-tag, prior to mass spectrometry to identify the potential interactors.

During this work, multiple studies focused on SepIVA, identified through its interaction with the cell division protein FtsQ (Wu et al., 2018). The study by Wu et al. (2008), whilst determined the localisation of SepIVA to be at the mid-cell, failed to generate a knockout strain in *M. smegmatis*, concluding the essentiality *sepIVA* for mycobacterial survival. A study by Jain et al. (2018) corroborated the interaction between FtsQ and SepIVA, and confirmed that FtsQ localisation at the septa is independent of SepIVA, suggesting that SepIVA recruitment to the mid-cell occurs following FtsQ recruitment to this site. The results obtained in this study corroborated the pre-existing data that the depletion, and in this case loss, of *sepIVA* resulted

in elongated cells. Results also showed that *sepIVA* is actually a non-essential gene, whose removal resulted in defective septation, furthering the current research on this gene.

Time limitations hindered the progress that could be made in constructing the strains that would allow for each candidate to be utilised in the interaction study. SepIVA was used in the interaction study however, and numerous interesting candidates were identified; these included cell wall synthesis protein Wag31, the cell division protein FtsE, and proteins involved in the biosynthesis of mycolic acids, including the polyketide synthase Pks13, and the long chain fatty acid AMP ligase, FadD32. Further work is required to ensure that these interactions are true, as although *in vivo* crosslinking allows for the capturing of interactions in their native environment, occasionally, partners may present due much higher expression of the protein of interest, or the query protein may pull-down a distant protein, due to its relationship in a larger multi-protein complex, as opposed to a direct interaction. Whilst further investigation is required, such as a co-immunoprecipitation study, to confirm these interactions, this work has provided an excellent base for the further delineation into the role of SepIVA, through the identification of its interacting partners.

The majority of research into KasB, a ketoacyl- acyl carrier protein synthase, have focused on delineating its role in the biosynthesis of mycolic acids, and also the phenotypic changes observed upon *kasB* deletion, including the impaired intracellular growth and the reduced attenuation as a result of the loss of *kasB* (Merrill et al., 2001; Gao et al., 2003; Bhatt et al., 2007), with more recent work focusing on the effect that phosphorylation, by serine-threonine protein kinases, of KasB has on virulence, and on its enzymatic activity and the subsequent control of the FAS-II elongation system (Vilchèze et al., 2014; Alsayed et al., 2019). This work however set out to determine the potential cause of this attenuation, through the study of the immunological response of BMDMs to infection with a *M. tuberculosis kasB* knockout, constructed by Bhatt et al. (2007). Due to the attenuation observed in the study by

Bhatt et al., (2007), *M. tuberculosis* Δ*kasB* bore similarity to latent tubercular infection, with a persistence of bacilli in mice, yet no presentation of disease. Δ*kasB* was therefore utilised as a model of latent tuberculosis, alongside wildtype *M. tuberculosis*, with the aim to determine immunological difference between these strains, to hopefully inform on the innate immune responses which might drive the progression of tubercular infection to the outcome of either latency, or active disease. The strategies utilised in this work included the study of intracellular uptake and survival of Δ*kasB*, alongside wildtype *M. tuberculosis* and Δ*kasB*C, in murine BMDMS, in addition to the cytokine production and expression of these cytokines, during infection. This work began to show differential cytokine production by BMDMs as a result of the loss of Δ*kasB* from *M. tuberculosis*, in addition to distinct differences in the mRNA expression of certain pro-inflammatory cytokines as a result of this loss.

In order to fully understand the importance of these differences in the attenuation, observed as a result of *kasB* loss, and hence the potential immunological differences that drive disease progression to either latency or active disease, further studies should focus on elucidating the activity of the inflammasome, a multiprotein complex involved in the processing and production of IL-1β; the production of which was increased in BMDMs infected with Δ*kasB*, yet mRNA expression was significantly reduced. Due to the suspected altered mycolic acid profile of TDM (Bhatt et al., 2007), future research should also aim to elucidate any potential differences in the immunological response to the immunostimulatory compound, TDM, purified from Δ*kasB*, WT *M. tuberculosis* and Δ*kasB*C. This project has begun an investigation into the immunological differences between LTBI and active tubercular disease, through the application of Δ*kasB*, a potential model for latent tubercular infection; with the suggested future studies, this work will do some way to deciphering the innate immunological differences of tubercular infection that drive disease progression to either

latency or active disease, in addition to furthering evidence of KasB as a potential vaccine candidate against tuberculosis.

The strategies utilised in this work, to achieve the proposed objectives, were appropriate due to the data and results obtained. Whilst objectives may not have been fully achieved, such as characterising and assigning a role of the chosen candidates in mycobacterial growth and division, this work has opened leads for future work to further delineate the role of these genes to gain a better understanding of mycobacterial growth and virulence.

CHAPTER 7

General Materials and Methods

7.1 Bacterial strain growth condition

Escherichia coli were cultured in Luria-Bertani (LB) broth at 37°C, 180rpm, and supplemented with antibiotics where necessary (hygromycin 150µg/ml; kanamycin 50µg/ml). *Mycobacterium smegmatis* mc^2 155 was grown in tryptic soy broth (TSB) at 37°C, 180rpm, and supplemented with 0.05% Tween-80, to prevent bacterial clumping, and with antibiotics where necessary (hygromycin 100µg/ml; kanamycin 25µg/ml). *Mycobacterium bovis* BCG Pasteur was cultured statically in 7H9 broth at 37°C, and supplemented 0.05% Tween-80 and 10% oleic albumin dextrose catalase (OADC) growth supplement, and with antibiotics where necessary (hygromycin 100µg/ml; kanamycin 25µg/ml). All strains used in this thesis are listed in Table 0.1.

7.2 DNA Extraction

7.2.1 Genomic DNA extraction from mycobacterial cells

10ml bacterial culture was centrifuged at 4,000rpm for 10 minutes. The pellet was resuspended in 450µl P1 buffer (50mM Tris-HCl, pH 8.0, 10mM EDTA). 50µl lysozyme (10mg/ml) was also added, and the suspension was incubated at 37°C overnight. 100µl SDS (10%) was added, along with 50µl proteinase K (20mg/ml). The suspension was mixed gently and incubated at 55°C for 20 minutes. 200µl 5M NaCl was added, followed by 750µl chloroform: isoamyl alcohol (24:1). The suspension was mixed and centrifuged at 13,000rpm for 10 minutes. The upper aqueous layer was transferred to a new tube, with a further 750µl chloroform: isoamyl alcohol added. Centrifugation and transfer of upper aqueous layer was repeated. 560µl isopropanol was added to the aqueous extract to allow for DNA precipitation. The solution was inverted briefly until DNA formed, and centrifuged at 13,000rpm for 10

minutes. The DNA pellet was washed with 70% ethanol and allowed to air dry, prior to being resuspended in 50µl EB buffer (10mM Tris-HCl, pH 8.5), pre-heated to 60°C.

Table 0.1. List of bacterial strains used and generated in this work

Bacterial Strain	Description	Source
E. coli		
TOP10	F- *mcrA* Δ(*mrr-hsd*RMS-*mcr*BC) Φ80*lac*ZΔM15 Δ *lac*X74 *rec*A1 *ara*D139 Δ(*araleu*)7697 *gal*U *gal*K *rps*L (StrR) *end*A1 *nup*G	Invitrogen
HB101	F–, *thi*-1, *hsd*S20 (r_B^-, m_B^-), *sup*E44, *rec*A13, *ara*-14, *leu*B6, *pro*A2, *lac*Y1, *gal*K2, *rps*L20 (str^r), *xyl*-5, *mtl*-1.	Promega
BL21 (DE3)	F^- *ompT hsdSB* (r_B^- m_B^-) *gal dcm* (DE3)	ThermoFisher Scientific
M. smegmatis		
M. smegmatis mc^2 155	Parental (WT) strain, Ept mutation	Snapper *et al*., 1990
Δ*sepIVA*	mc^2 155 deletion mutant in which *sepIVA* is replaced with *hyg*	This work
Δ*sepIVA*C	Complemented strain of Δ*sepIVA* containing pMV306-*sepIVA*	This work
Δ*sepIVA*CRv	Complemented strain of Δ*sepIVA* containing pMV306-*Rv2927c*	This work
Δ*sepIVA*V	Δ*sepIVA* transformed with the empty vector pMV306	This work
Δ*MSMEG_4306*	mc^2 155 deletion mutant in which *MSMEG_4306* is replaced with *hyg*	This work
Δ*MSMEG_4306*C	Complemented strain of Δ*MSMEG_4306* containing pMV306-*MSMEG_4306*	This work
Δ*MSMEG_4306*Rv	Complemented strain of Δ*MSME_G4306* containing pMV306-*Rv2229cc*	This work
Δ*MSMEG_4306*V	Δ*MSMEG_4306* transformed with the empty vector pMV306	This work
M. bovis		
M. bovis BCG Pasteur	Parental (WT) strain	
Δ*Mb2254c*	*M. bovis* BCG Pasteur deletion mutant in which *Mb2254c* is replaced with *hyg*	This work
Δ*Mb2254c*C	Complemented strain of Δ*Mb2254c* containing pMV306-*Rv2229c*	This work
Δ*Rv2229c*V	Δ*Mb2254c* transformed with the empty vector pMV306	This work
Δ*Mb1709*	*M. bovis* BCG Pasteur deletion mutant in which *Mb1709* is replaced with *hyg*	This work
Δ*Mb1709*C	Complemented strain of Δ*Mb1709* containing pMV306-*Rv1682*	This work
Δ*Mb1709*V	Δ*Mb1709* transformed with the empty vector pMV306	This work
M. tuberculosis		
M. tuberculosis CDC1551	Parental (WT) strain	
Δ*kasB*	*M. tuberculosis* CDC1551 strain in which *kasB* was replaced by *hyg*	Bhatt, A. *et al*., 2007
Δ*kasB*C	Δ*kasB* complemented with pMV261- *kasB*	Bhatt, A. *et al*., 2007

7.2.2 Plasmid DNA extraction

Plasmid extractions were carried out using QIAGEN QIAprep spin kits. Colonies present on the transformant plates were used to inoculate LB broth, supplemented with appropriate antibiotics, which were cultured overnight at 37°C with agitation. Bacterial cells were harvested by centrifugation and the plasmids were purified according to the manufacturers protocol. Plasmids were confirmed by digestion with corresponding restriction enzymes and sequencing (Eurofins MWG Operon, and Source BioScience). All plasmids and phages used in this study are found in Table 0.2.

Table 0.2. List of plasmids and phages used and generate in this work

Plasmid	Description	Source
p0004s	Vector containing a λ phage *cis* site and a Hyg^R cassette (*hyg*); used in the cloning of allelic exchange constructs to be used for specialised transduction	Bardarov S., *et al*., 2002
p∆*sepIVA*	p0004s derivative designed for allelic exchange of *M. smegmatis sepIVA*	This work
p∆*MSMEG_4306*	p0004s derivative designed for allelic exchange of *M. smegmatis MSMEG_4306*	This work
p∆*Mb2254c*	p0004s derivative designed for allelic exchange of *M. bovis* BCG Pasteur *Mb2254c*	This work
p∆*Mb1709*	p0004s derivative designed for allelic exchange of *M. bovis* BCG Pasteur *Mb1709*	This work
pMV306	Integrative vector for replication in *E. coli*, with a Kan^R cassette (*aph*), and the "gene for the integrase and the ayyP site of phage L5 for integration into the mycobacterial genome" (Stover, C. K. *et al*., 1991)	Stover, C. K. *et al*., 1991
pMV306-*sepIVA*	*sepIVA* cloned into pMV306	This work
pMV306-*Rv2927c*	*Rv2927c* cloned into pMV306	This work
pMV306-*MSMEG_4306*	*MSMEG_4306* cloned into pMV306	This work
pMV306-*Mb2254c*	*Rv2229c* cloned into pMV306	This work
pMV306-*Rv1682*	*Rv1682* cloned into pMV306	This work
pET28b	Bacterial expression vector containing a T7 promoter and an N-terminal His Tag. Kanamycin resistance	Novagen
pET28b- *sepIVA*	*sepIVA* cloned into pET28b	This work
pET28b-*MSMEG_4306*	*MSMEG_4306* cloned into pET28b	This work
pMyNT	Mycobacterial expression vector, containing an acetamidase promoter, and an N-terminal His tag. Kanamycin resistance	Matthias Wilmanns
pMyNT-*sepIVA*	*sepIVA* cloned into pMyNT	This work

Phage		
phAE159	A conditionally replicating temperature sensitive mycobacteriophage TM4 derived shuttle phasmid	Bardarov, S., *et al.*, 2002
ph∆*sepIVA*	phAE159 derivative obtained from cloning sepIVA into its *PacI* site	This work
ph∆*MSMEG_4306*	phAE159 derivative obtained from cloning *MSMEG_4306* into its *PacI* site	This work
ph∆*Mb2254c*	phAE159 derivative obtained from cloning *Mb2254c* into its *PacI* site	This work
ph∆*Mb1709*	phAE159 derivative obtained from cloning *Mb1709* into its *PacI* site	This work

7.3 Polymerase chain reaction (PCR)

PCR was carried out using Q5 High-Fidelity DNA Polymerase (NEB) using the solution mastermix in Table 0.3. The conditions used in these reactions are found in Table 0.4. All primers used in this thesis can be found in Table 0.5

Table 0.3. PCR mastermix for the amplification of genomic DNA using Q5 DNA polymerase

5X Q5 Reaction Buffer	5µl
10mM dNTPs	0.5µl
10µM Forward Primer	1.25µl
10µM Reverse Primer	1.25µl
Template Genomic DNA	xµl
Q5 High-Fidelity DNA Polymerase	0.25µl
5X Q5 High GC Enhancer	5µl
Water	xµl (to 25µl)
Total volume	**25µl**

Table 0.4. Thermocycling conditions for PCR using Q5 DNA polymerase

Step	Temperature	Time	Passes
Initial Denaturation	98°C	1 minute	1
Denaturation	98°C	10 seconds	35
Annealing	50-72°C	30 seconds	35
Extension	72°C	30 seconds/kb	35
Final Extension	72°C	2 minutes	1
Hold	4°C	∞	1

Table 0.5. Primers employed in the construction of allelic exchange, complementation and sequencing

Primer	Sequence
HL	5'-AGGATCCAGGACCTGCCAAT-3'
HR	5'-CTTCACCGATCCGGAGGAAC-3'
OL	5'-CGGCCGATAATACGACTCA-3'
OR	5'-CTGACGCTCAGTCGAACGAA-3'
SepIVA_LL	5'-TTTTTTTTCCATAAATTGGCCTCGAAGAGGAAC ACAAG-3'
SepIVA_LR	5'-TTTTTTTTCCATTTCTTGGGATGTTGCCGTTCTCGATG-3'
SepIVA_RL	5'-TTTTTTTTCCATAGATTGGTTCGTGGCGAGTGCGACATC-3'
sepIVA_RR	5'-TTTTTTTTCCATCTTTTGGGATGGCGGTGGTACAGCTCTTC-3'
SepIVA_Comp_F	5'- GCGTCTAGAGATCGCGCCGACGCGTCCGC-3'
SepIVA_Comp_R	5'- GCGAAGCTTGCGGTGCTTCGCCGCGTTCG-3'
Rv2927c_Comp_F	5'- GCGTCTAGACACGCTCGGGCAAGATCGCC-3'
Rv2927c_Comp_R	5'- GCGAAGCTTGGCCATAAGAGAAATCCTAC-3'
SepIVA_pET28b_F	5'- GCGCATATGGTGTACCGAGTTTTTGAAG-3'
SepIVA_pET28b_R	5'- GCGAAGCTTTCAGCGGGTCACGTAG-3'
SepIVA_pMyNT_F	5'- GCGGGATCCGGTGTACCGAGTTTTTGAAG-3'
SepIVA_pMyNT_R	5'- GCGGAATTCGGTCAGCGGGTCACGTAGTCG-3'
MS4306_LL	5'-TTTTTTTTCCATAAATTGGGGACAAGTGGGTGGTGTTC-3'
MS4306_LR	5'-TTTTTTTTCCATTTCTTGGATCTCGGTGACCTGCTTGG-3'
MS4306_RL	5'-TTTTTTTTCCATAGATTGGGCTCGTCGAGCTCTACGAGAAG-3'
MS4306_RR	5'-TTTTTTTTCCATCTTTTGGTCATACGCACGCTGCAGAGG-3'
Mb2254c_LL	5'-TTTTTTTTCCATAAATTGGCGCGAGAACTCAGAG-3'
Mb2254c_LR	5'-TTTTTTTTCCATTTCTTGGCTGCACCTGCTGGTAAG-3'
Mb2254c_RL	5'-TTTTTTTTCCATAGATTGGCAAGGTCATCGATGTGG-3'
Mb2254c_RR	5'-TTTTTTTTCCATCTTTTGGCGACGACCACGTCC-3'
MS4306_Comp_F	5'- GCGAAGCTTGGTATTCGGCCACGTTGTTG-3'
MS4306_Comp_R	5'- GCGAAGCTTGGTATTCGGCCACGTTGTTG-3'
Mb2254c_Comp_F	5'- GCGTCTAGACCGATCTGCGACATCATCC-3'
Mb2254c_Comp_R	5'- GCGAAGCTTGTGGAGTGATCGGCGGTC-3'
MS4306_pET28b_F	5'-GCGCATATGATGAAAGCTGAAGTAAGCCAAC-3'
MS4306_pET28b_R	5'-GCGAAGCTTTCACTGCTTGACCCGCAAC-3'

Mb1709_LL	5'-TTTTTTTTCCATAAATTGGAACCTGTGCTGCGACTACTG-3'
Mb1709_LR	5'-TTTTTTTTCCATTTCTTGGCTGCCTTGAGCGTTTCAATC-3'
Mb1709_RL	5'-TTTTTTTTCCATAGATTGGACAGCAGGAGTGTGAGAAG-3'
Mb1709_RR	5'-TTTTTTTTCCATCTTTTGGGTGATCGGCCATGAAATCG-3'
Rv1682_Comp_F	5'-GCGAGATCTGTGTTGCCTCAACGCCCAAACT-3'
Rv1682_Comp_R	5'- GCGAAGCTTCTAAATGGCCCGTAGCTCAGCG-3'

7.4 Restriction digest

Plasmids and PCR products were digested using the solution mastermix in Table 0.6. The digestion was carried out for 2 hours at 37°C.

Table 0.6. Restriction digest mastermix for digestion of genomic DNA, plasmid or PCR product.

DNA	1µg
Restriction enzyme (NEB)	1µl
Cutsmart Buffer (NEB)	3µl
Water	xµl
Total volume	**30µl**

7.5 Agarose gel electrophoresis

0.8% agarose gels were prepared using Molecular Biology Grade Agarose (Bioline) dissolved in 1X Tris-acetate EDTA (TAE) buffer (Life Science Products). The solution was boiled to dissolve, and 0.1µl/ml of Midori Green Advance DNA Stain (ThermoFisher) was added once the gel had cooled. Gels were cast, and once set, were immersed in 1X TAE buffer in a gel electrophoresis tank. 1X loading dye (NEB) was added to samples, and ran alongside a 1kb DNA ladder (NEB). Samples were run at 100-140V, 400mA until the dye front had migrated sufficiently for adequate DNA separation. DNA was visualised using an ultraviolet (UV) transilluminator.

7.6 DNA extraction from agarose gel

QIAgen Gel Extraction Kit (Qiagen) was used to extract DNA was extracted from an agarose gel, according to the manufacturers protocol.

7.7 Ligation of digested plasmids and PCR products

Digested plasmids and PCR products were ligated using the solution mastermix in Table 0.7. The ligation was carried out overnight at 4°C or for 3-4 hours at room temperature.

Table 0.7. Ligation mastermix for the ligation of pre-digested plasmid and PCR product.

Plasmid	50ng
PCR product	37.5ng
T4 DNA ligase (NEB)	1µl
T4 DNA ligase buffer (NEB)	2µl
Water	xµl
Total volume	**20µl**

7.8 Preparation of competent cells

7.8.1 *E. coli* chemically competent cells

The required *E. coli* strain was grown (supplemented with 20mM $MgSO_4$) to OD_{600} 0.5-1.0. Cells were harvested by centrifugation (4,000rpm for 15 minutes) and the supernatant was removed. Pelleted cells were resuspended in 0.4 volume of ice-cold transformation buffer 1 (TFB1) (15% glycerol, 30mM CH_3CO_2K, 10mM $CaCl_2$, 50mM $MnCl_2$, 100mM RbCl, pH 5.8; filter sterilised and stored at 4°C) and incubated on ice for 40 minutes. Cells were harvested by centrifugation (4,000rpm for 15 minutes) and the supernatant was removed. Pelleted cells were resuspended in 0.02 volume of transformation buffer 2 (TFB2) (15% glycerol, 75mM

$CaCl_2$, 10mM MOPS, 100mM RbCl, pH 6.5; filter sterilised and stored at 4°C). The cell suspension was incubated on ice for 2 hours, prior to snap freezing and storing at -80°C until future use.

7.8.2 Mycobacterial electrocompetent cells

The required mycobacterial strain was grown until OD_{600} was 0.8-1.0. The cell suspension was incubated on ice for 1-2 hours, followed by harvesting of the cells by centrifugation (4,000rpm for 10 minutes); *M. smegmatis* strains were centrifuged at 4°C whereas slow-growing mycobacterial strains were harvested at room temperature to enhance transformation efficiency. 10% glycerol was used at the original culture volume to wash the cells. Centrifugation was repeated and cells were washed with 10% glycerol, one half of the original culture volume. Centrifugation was repeated and cells were washed with 10% glycerol, one quarter of the original culture volume. Centrifugation was repeated and the cells were resuspended in 10% glycerol, one tenth of the original culture volume. The cell suspension was snap frozen, and stored at -80°C until future use.

7.9 Transformation of bacterial cells

7.9.1 Transformation of competent *E. coli* cells by heat shock method

Chemically competent cells (100µl) were mixed with 5µl of purified plasmid DNA. Cells were transformed by heat-shock at 42°C for 45 seconds, followed by incubation on ice for 5 minutes. Transformed cells were recovered in 1ml LB broth and incubated at 37°C, 180rpm for 1 hour. Transformants were plated onto LB agar plates supplemented with the appropriate antibiotic selection marker, and incubated at 37°C overnight.

7.9.2 Transformation of competent mycobacterial cells by electroporation

Electrocompetent mycobacterial cells (200µl) were mixed with 5µl of the plasmid DNA in a pre-chilled 1mm electroporation cuvette (Cell Projects). Electroporation was carried out at 1800V. The cuvette was returned to ice for 15 minutes, prior to the recovery of the cells in 1ml of media (TSB for *M. smegmatis*, Middlebrook 7H9 broth for slow-growing mycobacteria). Cells were incubated at 37°C, 180rpm for a generation (3-4 hours for *M. smegmatis* and 24 hours for slow-growing mycobacteria) and subsequently plated (TSB agar for *M. smegmatis*, Middlebrook 7H10 agar for slow-growing mycobacteria) with appropriate antibiotics supplemented in the agar. Plates were incubated at 37°C until colonies had formed.

7.10 Generation of gene knockout strains by Specialised Transduction

7.10.1 Construction of an allelic exchange substrate (AES) plasmid

1kb up- and down-stream of the region of interest was PCR amplified using uniquely designed oligonucleotides primers (Eurofins MWG Operon) with Van91I recognition sites located at the 5' ends. Where Van91I was not a suitable restriction enzyme, due to the presence of Van91I cut sites within the region of interest, BstAPI, DraIII or AlwNI were alternatively utilised. Digested PCR products were cloned into the Van91I digested vector, p0004s. This construct was transformed into chemically competent *E. coli* TOP-10 cells, and plated onto LB agar plates supplemented with hygromycin. Plates were incubated at 37°C overnight. Subsequent transformant colonies were screened and recombinant plasmids were confirmed by Van91I digestion and sequencing.

7.10.2 Phasmid construction Phasmid construction

Sequence confirmed AES plasmids were linearised by PacI digestion, alongside phAE159 DNA (a mycobacteriophage vector). 2-4µl of the phage digest and 4-6µl of the AES digest were ligated together in a ligation reaction (total volume of 10µl). 5µl of the ligation reaction was added to a MaxPlax packaging extract tube and incubated at room temperature for 1.5 hours. The reaction was stopped with the addition of 200µl mycobacteriophage (MP) buffer (50mM Tris-HCl, 150mM NaCl, 10mM $MgCl_2$, 2mM $Cacl_2$; filter sterilised and stored at room temperature), followed by further incubation at room temperature for 30 minutes. 100µl of *E. coli* HB101 cell suspension was added directly to the packaging reaction tube, and incubated at 37°C for 1 hour. The cells were harvested by centrifugation at 13,000rpm for 1 minute, the supernatant was discarded and the pelleted cells were re-suspended in 1ml fresh LB broth. The cells were plated onto LB agar plates supplemented with hygromycin, and incubated at 37°C overnight. Colonies that were hygromycin resistant were screened by PacI digestion and agarose gel electrophoresis, with an expected band pattern of approximately 40kb (phage genomic DNA) and approximately 7kb (corresponding to the linearised AES construct).

E. coli HB101 cells were prepared for the previously described transduction from a 50ml LB broth culture, supplemented with 10mM $MgSO_4$ and 0.2% maltose, and inoculated with a fresh overnight culture of *E. coli* HB101 culture. The culture was incubated at 37°C until an OD_{600} 0.8-1.0 was reached. The cells were harvested by centrifugation at 3,000rpm, 4°C for 10 minutes, with the pelleted cells re-suspended in 500µl MP buffer.

7.10.3 Generation of knockout phage

5-10µl of the phasmid DNA (obtained from 7.10.2) was electroporated into 200µl electrocompetent *M. smegmatis* mc^2155 cells. The cells were recovered in 1ml TSB broth, and incubated at 30°C for 1 hour. The following dilutions were prepared:

Dilution 1 – 300µl transformed *M. smegmatis* mc^2155 cells were mixed with 200µl actively growing *M. smegmatis* mc^2155 cells

Dilution 2 – 100µl transformed *M. smegmatis* mc^2155 cells were mixed with 200-300µl actively growing *M. smegmatis* mc^2155 cells

The dilutions were added to 4ml molten top 7H9 agar, which was then mixed via inversion and poured onto pre-warmed 7H9 agar plates. The plates were incubated at 30°C for 3 days until plaques had formed. The plaques were cored and soaked in 200µl MP buffer for 1.5 hours to recover the phage.

7.10.4 Preparation of high titre phage lysate

7H9 basal agar plates were overlaid with 4ml molten top agar containing 400µl actively growing *M. smegmatis* mc^2155 culture. The phage lysate was serially diluted 10-fold, to 10^{-6} in MP buffer, and 10µl of each dilution was spotted onto the overlaid plate. Plates were incubated at 30°C for 3 days until plaques were observed. The plaque forming units (PFU) were calculated by counting the visible plaques for each dilution zone. 7H9 basal agar plates were overlaid with 400µl actively growing *M. smegmatis* mc^2 155 culture mixed with the appropriate phage lysate dilution in 4ml molten top 7H9 agar, which would result in approximately 1,000 plaques per plate. The plates were then incubated at 30°C for 3 days until plaques were observed. The plates were soaked in 3-4ml MP buffer for 4-5 hours at room temperature to recover the phage. The phage lysate was filter sterilised using a 0.22µm filter to

remove the bacterial debris. The phage lysate was stored at 4°C until further use. The ideal titre of phage lysate required for transduction is approximately 10^{10} PFU/ml.

7.10.5 Specialised Transduction

50ml of 7H9 broth, supplemented with 0.2% glycerol, 10% OADC and 0.05% Tween-80, was inoculated with the desired bacterial strain for the Specialised Transduction. The culture was grown until an OD_{600} 0.8-1.0 was reached. The culture was centrifuged at 4,000rpm for 15 minutes followed by re-suspension in 50ml MP buffer. The suspension was centrifuged again at 4,000rpm for 15 minutes, with cells re-suspended in 5ml MP buffer. 1ml of the cell suspension was mixed with 1ml high titre phage lysate, and incubated at 37°C (3-4 hours for *M. bovis* BCG Pasteur, 1 hour for *M. smegmatis*). For a negative control, 1ml cell suspension was mixed with 1ml MP buffer only. Following the incubation period, the cell suspension was centrifuged at 4,000rpm for 15 minutes, with the pellet resuspended in 3ml 7H9 broth and incubated at 37°C again (24 hours for *M. bovis* BCG Pasteur, 3-4 hours for *M. smegmatis*). The cell suspension was centrifuged at 4,000rpm for 15 minutes, and the pellet was re-suspended in 400µl 7H9 broth. 50µl was spread on each 7H10 agar plate, supplemented with 100µg/ml hygromycin. Plates were incubated until transductant colonies were visible. Colonies were verified by confirmatory PCR, Southern Blot analysis or whole genome sequencing (WGS).

7.11 Confirmation of deletion strains

7.11.1 Confirmatory PCR

Genomic DNA was extracted from the strain of interest and was used as the template for PCR amplification with relevantly designed primers. The solution mastermix can be found in Table 0.8, with the conditions used in this reaction found in Table 0.9.

Table 0.8. PCR mastermix for the amplification of genomic DNA using MyTaq DNA Polymerase

5X MyTaq Reaction Buffer	10µl
Template Genomic DNA	xµl
20µM Forward Primer	1µl
20µM Reverse Primer	1µl
myTaq DNA Polymerase	1µl
Water	xµl (to 50µl)
Total volume	**50µl**

Table 0.9. Thermocycling conditions for PCR using MyTaq DNA Polymerase

Step	Temperature	Time	Passes
Initial Denaturation	95°C	1 minute	1
Denaturation	95°C	15 seconds	35
Annealing	50-72°C	15 seconds	35
Extension	72°C	30 seconds/kb	35
Final Extension	72°C	10 seconds	1
Hold	4°C	∞	1

7.11.2 Southern blot analysis

Southern blot analysis was utilised to confirm the knockout of the genes of interest and was carried out as described in the DIG High Prime Labelling and Detection Starter Kit I (Roche). An appropriate restriction enzyme was used to digest genomic DNA obtained from the wild-type and mutant strain. The digested DNA was separated using agarose gel electrophoresis. The gel was soaked in depurination solution (0.25M HCl) for 30 minutes with agitation, then transferred into denaturation solution (1.5M NaCl and 0.5M NaOH) for 30 minutes with agitation. The gel was finally transferred into neutralisation solution (1.5M NaCl, 0.5M Tris-HCl, pH 7.0) for 30 minutes with agitation. The DNA was transferred overnight, from the gel to a positively charged nylon membrane by capillary action using 20X saline-sodium citrate (SSC) (3M NaCl, 0.3M sodium citrate, pH 7.0). Transferred DNA was UV cross-linked to the membrane for 3 minutes, followed by rinsing with ddH_2O.

1µg template DNA (to be used for the DNA probes) was denatured by boiling for 10 minutes, then snap-chilling and labelling with digoxigenin-dUTP, as described in the manufacturers protocol. The membrane was pre-hybridized at 42°C for 30 minutes with the Dig Easy Hyb, followed by the addition of the DIG-labelled probe, which was left on the membrane overnight, with gentle agitation. The membrane was washed twice for 5 minutes in 2X SSC at 25°C under agitation. The membrane was then washed twice for 15 minutes in 0.5X SSC, 0.1% SDS at 68°C under agitation. The membrane was briefly rinsed in washing buffer (0.1M maleic acid, 0.15M NaCl, pH 7.5) supplemented with 0.3% Tween-20, followed by incubation for 30 minutes in 100ml blocking solution (90ml washing buffer + 10ml blocking solution). The membrane was incubated for 30 minutes in 20ml antibody solution (20ml blocking solution + 4µl Anti-Digoxigenin-AP). The membrane was washed twice for 15 minutes in 100ml washing buffer, followed by equilibration for 5 minutes in 20ml detection buffer (0.1M Tris-HCl, 0.1M NaCl, pH 9.5). The membrane was finally incubated with 10ml

colour substrate solution for no longer that 16 hours; the development was stopped by washing of the membrane with 50ml water for 5 minutes.

7.11.3 Whole genome sequencing (WGS)

Genome sequencing was provided by MicrobesNG (http://www.microbesng.uk), which is supported by the BBSRC (grant number BB/L024209/1).

7.12 Lipid extraction and analysis

7.12.1 [^{14}C] labelling of lipids

Bacterial strains were cultured until OD_{600} was 0.5. Cultures were labelled with 10µl acetic acid, sodium salt, [1,2-^{14}C]-, 1mCi (Perkin Elmer) and incubated overnight at 37°C with agitation. Labelled cells were harvested by centrifugation and washed with phosphate buffered saline (PBS), prior to drying at 55°C under nitrogen.

For the study of lipids of bacteria grown on solid media, molten agar was labelled with 10µl acetic acid, sodium salt, [1,2-^{14}C]-, 1mCi. Bacteria were plates at a suitable dilution to give a crowded plate, yet visibly distinct colonies. Plates were incubated for one week at 37°C. Labelled bacterial cells were harvested by scraping colony material, which was resuspended in PBS. Colony material was pelleted and dried at 55°C under nitrogen, prior to lipid extraction.

7.12.2 Extraction of mycobacterial polar and apolar lipids

Cells were centrifuged, washed with PBS and dried under nitrogen at 55°C, prior to lipid extraction. To extract outer and inner apolar lipids, 2ml of CH_3OH:0.3% NaCl (10:1) was

added to the dried pellet, followed by 1ml petroleum ether (60-80°C). The suspension was mixed for 15 minutes, then centrifuged at 3,000rpm for 5 minutes. The upper layer was transferred to a fresh tube, and 2ml of petroleum ether was added to the lower phase of the original tube. This was mixed and centrifuged again. The upper layer was collected with the previous extract and dried at 55°C under nitrogen. The lipids were resuspended in 200µl $CHCl_3$:CH_3OH (2:1).

Polar lipids were then extracted with the addition of 2.3ml $CHCl_3$:CH_3OH:0.3% NaCl (9:10:3) to the lower layer contents which remain in the original sample. The suspension was mixed for 1 hour, then centrifuged at 3,000rpm for 5 minutes. The upper layer was transferred to a fresh tube. 750µl $CHCl_3$:CH_3OH:0.3% NaCl (5:10:4) was used to resuspend the pellet. The cell suspension was mixed for 30 minutes then centrifuged at 3,000rpm for 5 minutes. The upper layer was collected with the previous extract and to this, 1.3ml $CHCl_3$ and 1.3ml 0.3% NaCl was added, forming two phases. The suspension was mixed for 5 minutes then centrifuged for 5 minutes at 3,000rpm. The lower layer was transferred to a fresh tube and dried at 55°C under nitrogen. The lipids were resuspended in 200µl $CHCl_3$:CH_3OH (2:1).

7.12.3 Extraction of mycobacterial mycolic acid methyl esters and fatty acid methyl esters

Fatty acid methyl ester (FAMEs) and mycolic acid methyl esters (MAMEs) could be extracted from delipidated cell pellets and the inner and out apolar lipid extracts. 2ml 5% tetrabutylammonium (TBAH) was added to the dried fractions and heated at 95°C for 24 hours, resulting in fatty and mycolic acid hydrolysis. Tubes were allowed to cool and methyl esterification was carried out with the addition of 2ml water, 4ml dichloromethane and 500µl iodomethane. Samples were mixed for 30 minutes, and separated (organic lower phase and

aqueous upper phase) by centrifugation at 3,000rpm for 5 minutes. The aqueous phase was discarded and the lower organic phase, containing lipids, was transferred to a new tube. 4ml of water was added to the organic phase, and was mixed for 5 minutes. The organic phase was centrifuged at 3,000rpm for 5 minutes, and washed twice more with 4ml of water. The lower organic phase was dried under nitrogen at 55°C. To the dried contents, 4ml of diethyl ether was added, and samples were sonicated for 5 minutes. Samples were centrifuged at 3,000rpm for 5 minutes, the upper FAMEs and MAMEs were transferred to a new tube. Samples were dried under nitrogen at 55°C and resuspended in 200µl chloroform: methanol (2:1).

7.12.4 Thin layer chromatography analysis of mycobacterial lipids

For [^{14}C] labelled samples, 10,000-20,000 counts per minute (cpm) of each sample were spotted onto a silica plate. Thin layer chromatography (TLC) was carried out using the solvent systems in Table 0.10. Following TLC, the plates were exposed to autoradiograph films prior to development.

For extracted FAMEs and MAMEs, approximately 80% of the silica plate was impregnated with 10% AgNO3 dissolved in water. Silica plates were activated by exposure to 100.°C for 25 minutes. FAMEs and MAMEs were analysed exclusively by system F, with the first direction corresponding to the non-impregnated silica plate, and the second direction corresponding to sample exposure to the $AgNO_3$ impregnated portion of the plate. This allows for separation based on the degree of unsaturation, as well as FAME/ MAME size (Ulberth, F. & Achs, E., 1990).

Table 0.10. Solvent systems utilised in the analysis of lipid extracts on 2D-TLCs. 1, solvent system must be ran three times in the first dimension; 2, solvent system ran twice in the first dimension, and three times in the second dimension.

System	1st dimension	2nd dimension
A[1]	Petroleum ether 60-80/ ethyl acetate (98:2)	Petroleum ether 60-80/ acetone (98:2)
B[1]	Petroleum ether 60-80/ acetone (92:8)	Toulene/ acetone (95:5)
C	Chloroform/ methanol (96:4)	Toulene/ acetone (80:20)
D	Chloroform/ methanol/ water (100:14:0.8)	Chloroform/ acetone/ methanol/ water (50:60:2.5:3)
E	Chloroform/ methanol/ water (60:30:6)	Chloroform/ acetic acid (glacial)/ methanol/ water (40:25:3:6)
F[2]	Hexane/ ethyl acetate (19:1)	Petroleum ether 60-80/ diethyl ether (17:3)

7.13 Microscopy

7.13.1 Brightfield microscopy

For cell length analysis, 1ml of bacterial culture (OD_{600} approximately 0.5-1.0) was centrifuged at 13,000rpm for 5 minutes. The supernatant was discarded and the pellet was resuspended in sterile PBS. 10µl of the cell suspension was applied as a drop to a microscope slide, and covered with a coverslip. The coverslip was secured, and cells were visualised using phase contrast microscopy, with a Confocal Nikon A1R. Cell measurements were taken manually using ImageJ.

7.13.2 Fluorescence microscopy

For the study of septation and DNA segregation, a single colony was used to inoculate TSB, which was incubated overnight at 37°C, 180rpm. 1ml of bacterial culture was centrifuged

at 13,000rpm for 5 minutes. The supernatant was discarded and the pellet was resuspended in 1ml ice cold methanol for fixation. The cells were centrifuged at 13,000rpm for 5 minutes, and washed with sterile PBS. The pellet was resuspended in 50µl vancomycin propidium iodide (PI) stain for 90 minutes; the vancomycin PI stain was composed of 2µg/ml vancomycin BODIPY FL Conjugate, 2µg/ml vancomycin (non-fluorescent) and 10µg/ml PI, which was dissolved in sterile PBS supplemented with 0.05% Tween-80. Cell were visualised with a Leica TCS SP2 laser-scanning confocal microscope (vancomycin BODIPY FL Conjugate-Ex/Em 503/512nm; PI-Ex/Em 493/636nm).

7.14 Bacterial adenylate cyclase-based two-hybrid (BACTH) assay

The bacterial adenylate cyclase-based two-hybrid (BACTH) assay was carried out using the kit and protocol from Euromedex. Potential interacting proteins were cloned into the BACTH vectors pKT25 and pUT18, which, when proteins interact with one another, they bring together the constituent components of the adenylate cyclase from *Bordetella pertussis.* This results in cyclic AMP production and the downstream effect of increased expression of the *lac* and *mal* operons. When plated onto selective media, transformants, in which adenylate cyclase is intact and active, are able to utilised lactose or maltose as a carbon source and can be distinguished. Primers utilised in this study can be found in Table 0.11. Sequence confirmed plasmids were co-transformed into *E. coli* BTH101 cells. Resultant co-transformants were utilised in the β-galactosidase assay.

Table 0.11. Primers utilised in the BACTH study

Primers	Sequence
pKT25-SepIVA_F	5'-GCGTCTAGACCGTGTACCGAG-3'
pKT25-SepIVA_R	5'-GCGGAA TTCTCAGCGGGTCAC-3'
pKT25-Rv2927c_F	5'-GCGCTGCAGGTGTACCGAGTCTTTG-3'
pKT25-Rv2927c_R	5'-GCGTCTAGAGCGCACCGCGTAG-3'
pUT18-Wag31_F	5'-GCGAAGCTTATGCCGCTTACAC-3'
pUT18-wag31_R	5'-GCGTCTAGAGTTTTTGCCCCG-3'
pUT18-FtsZ_F	5'-GCGAAGCTTATGACCCCCCC-3'
pUT18-FtsZ_R	5'-GCGTCTAGAGCGGCGCATG-3'
pUT18-FtsI_F	5'-GCGAAGCTTCAGGTGAGCCGCG-3'
pUT18-FtsI_R	5'-GCGTCTAGAGGTGGCCTGCAAGAC-3'

7.14.1 Buffers

7.14.1.1 Z buffer

Z buffer was prepared by dissolving 8.54g/litre Na_2HPO_4, 5.5g/litre $NaH_2PO_4.H_2O$, 0.75g/litre KCl, and 0.25g/litre $MgSO_4.7H_2O$ in distilled water. Prior to use, 2.7ml/litre of β-mercaptoethanol was added.

7.14.1.2 Sodium deoxycholate

1% sodium deoxycholate was prepared by dissolved 1g of sodium deoxycholate in 100ml double distilled H_2O.

7.14.1.3 Orthonitrophenyl-β-galactosidase

0.12g of orthonitrophenyl-β-galactosidase (ONPG) was dissolved in 150ml Z buffer, prior to use.

7.14.1.4 Stop solution

A 1M solution of sodium carbonate was used to stop the reaction.

7.14.2 Assay

Co-transformants were used to inoculate LB broth, and cultures were incubated at 30°C until an OD_{650} 0.4 was reached. Cells were induced with 0.5mM IPTG, and incubated further until OD_{650} 0.6 was reached. Cells were permeabilised with 30µl toluene and 30µl 1% sodium deoxycholate, and incubated at 37°C for 30 minutes, to allow for toluene evaporation. 100µl of the lysate was transferred to a new tube and 2.5ml Z buffer supplemented with ONPG was added. Solutions were incubated at 37°C for a maximum of 20 minutes. Reactions were stopped with the addition of 1ml stop solution, and OD_{420} was recorded for each sample. β-galactosidase activity was determined using the following equation:

$$\beta - \text{galactosidase activity} = \frac{1000 \times \text{OD420} \times 2.5 \times 3.5}{\text{T} \times 4.5 \times \text{V} \times \text{OD650}}$$

2.5 = coefficient factor used to convert absorbance at 650nm into mg dry mass bacteria

3.5 = total reaction volume

T = incubation time for reaction (minutes)

4.5 = molar extinction coefficient for ortho-nitrophenyl at 420nm

V = volume of lysate (ml)

OD420 = absorbance of final reaction at 420nm

OD650 = absorbance of the culture when measured at 650nm

7.15 Protein expression

7.15.1 Protein expression in *E. coli*

A single colony of *E. coli* BL21 transformed with the recombinant plasmid was used to inoculate LB broth, supplemented with the appropriate antibiotic, and incubated at 37°C, 180rpm overnight. 1L of terrific broth was inoculated 1:100 with the overnight inoculum, and incubated at 37°C, 180rpm, until OD_{600} 0.5 was reached. 1mM IPTG was added, and the culture was incubated at 16°C, 180rpm overnight.

Following overnight incubation, the culture was centrifuged at 4,000rpm for 30 minutes at 4°C. The supernatant was discarded and the pellet was washed with PBS. The cell suspension was centrifuged again, at 4,000rpm for 30 minutes at 4°C, and the supernatant was discarded. The pellet was stored at -80°C until further use.

7.15.2 Protein expression in *M. smegmatis*

A single colony of *M. smegmatis* mc^2 155, transformed with the recombinant plasmid, was used to inoculate TSB broth, supplemented with 0.05% Tween-80 and the appropriate antibiotic. The culture was incubated at 37°C, 180rpm for 48 hours. One litre of TSB broth, supplemented with 0.05% Tween-80 and the appropriate antibiotic, was inoculated with the original culture and incubated until OD_{600} 1.0 was reached. Protein expression was induced at this point with 34mM acetamide, and cells were incubated for a further 24 hours at 37°C, with agitation.

7.16 Protein purification

7.16.1 Protein purification from *E. coli*

The pellet (obtained from 7.15.1) was resuspended in lysis buffer (25mM Tris, 250mM NaCl, pH 7, 5% glycerol + protease inhibitor). The cell suspension was lysed by sonication (Soniprep 150, MSE) on ice (30 seconds on, 30 seconds off for 10 cycles). The cell lysate was centrifuged at 18,000rpm for 45 minutes at 4°C.

To prepare for protein purification, a 1ml HiTrap chelating HP column (GE Healthcare) was charged with 0.1M $NiCl_2$, with the excess $NiCl_2$ washed thoroughly with water. The column was equilibrated with lysis buffer prior to exposure to cell lysate.

The clarified lysate was loaded onto the column at a flow rate of 1ml/min. Once the lysate had run through, the column was washed with wash buffer (lysis buffer + 50mM imidazole). This was followed by an imidazole gradient in wash buffer; the gradient concentrations used were 100mM, 200mM, 300mM, 500mM and 1M of imidazole. Fractions were collected from each concentration gradient and boiled for 10 minutes in 1X protein loading buffer (62.5mM Tris-HCl, pH 6.8, 2.5% SDS, 0.002% bromophenol blue, 0.7135M 5% β-mercaptoethanol, 10% glycerol). Protein samples were visualised by sodium dodecyl sulfate polyacrylamide gel electrophoresis (SDS-PAGE), to determine presence of protein and purity.

7.16.2 Protein purification from *M. smegmatis*, and pulldown assay

The bacterial cells from 7.15.2 were harvested by centrifugation at 3,000rpm for 20 minutes, and washed with sterile PBS. The pellet was resuspended in PBS 0.05% Tween-80, 0.13% paraformaldehyde, and incubated at 37°C for 1 hour. The cell suspension was centrifuged at 3,000rpm for 20 minutes, and resuspended in buffer (100mM Tris, 150mM

NaCl, 1mM EDTA, pH 7, protease inhibitor). The cell suspension was lysed by sonication on ice (30 seconds on, 30 seconds off for 12 cycles). The cell lysate was centrifuged at 18,000rpm for 45 minutes at 4°C.

Ni-NTA resin (Thermofisher) was washed with water, and wash buffer (100mM Tris, 150mM NaCl, pH 7) to equilibrate, prior to exposure to the cell lysate. The cell lysate was incubated, on a rotator, with washed resin at 4°C for 2 hours. This was followed by an imidazole gradient in wash buffers; the gradient concentrations used were 100mM, 200mM, 300mM, 500mM and 1M of imidazole, with an initial wash (wash buffer, 50mM imidazole) to remove non-specifically bound protein. Fractions were collected from each concentration gradient and visualised by SDS-PAGE to visualise potential interacting partners of the overexpressed protein. As a control, *M. smegmatis* mc^2 155 only plus the empty vector used to express the protein of interest, was treated as mc^2 155 transformed with the recombinant plasmid for overexpression.

7.17 SDS-PAGE and western blot

Protein samples ran by SDS-PAGE on a gel were transferred to a nitrocellulose blotting membrane. The transfer was carried out in a membrane cassette, completely submerged in transfer buffer (25mM Tris, 190mM glycine, 10% methanol) at 20V, 300mA for 1 hour. The cassette was disassembled and the membrane was transferred to a fresh container, where the membrane was blocked for 1 hour in 5% milk solution in tris buffered saline, Tween-20 (TBST) (20mM Tris, pH 7.5, 150mM NaCl, 0.05% Tween-20). The solution was replaced with 0.1% milk-TBST, with the addition of Penta-His primary antibody (Qiagen) at 1:4,000. Following incubation at room temperature for 30 minutes, the membrane was washed three times with 50ml TBST. The membrane was placed in 0.1% milk-TBST with anti-mouse IgG

alkaline phosphatase (Sigma-Aldrich) at 1:25,000. The membrane was incubated at room temperature for 30 minutes, followed by two washing stages with TBST, and one wash with tris buffered saline (TBS) (20mM Tris, pH 7.5, 150mM NaCl). For visualisation, the membrane was placed in 10ml water in which one tablet of 5-bromo-4-chloro-3'-indolyl phosphate (BCIP) (Sigma-Aldrich) had been dissolved.

7.18 Mass spectrometry of proteins

To analysis protein gels for mass spectrometry, samples were ran by SDS-PAGE, and stained with InstantBlue Protein Stain. The bands of interest were cut out using a sterile scalpel, and placed into sterile eppendorfs; this was carried out in the laminar flow hood. Samples were submitted to the Advanced Mass Spectrometry Facility (School of Biosciences, University of Birmingham), where mass spectrometry was performed.

7.19 Preparation and culture of bone marrow derived macrophages

C57BL/6 mice were euthanized by CO_2 inhalation and hind legs were removed. Tissue was removed from the femur and tibia, and joint ends were removed. Bones were flushed with complete Dulbecco's Modified Eagle Medium (CDMEM), DMEM supplemented with 2mM glutamine and 10% fetal bovine serum (FBS). The bone marrow suspension was passed through a 40μm Nylon cell strainer and centrifuged at 1,200rpm for 6 minutes at 4°C. Bone marrow derived cells were re-suspended in 10ml CDMEM and cells were counted in the presence of trypan blue (0.04%). Bone marrow derived cells were cultured in CDMEM, supplemented with L929-cell conditioned medium (LCCM) (20% v/v) as a source of macrophage colony stimulating factor, in sterile petri dishes at 37°C and 5% CO_2. Following

4 days of incubation, the media was removed and replaced with fresh CDMEM supplemented with LCCM (20% v/v).

7.20 Macrophage infection, bacterial uptake and intracellular survival of *M. tuberculosis* strains in bone marrow derived macrophages

Bone marrow derived macrophages (BMDMs) ($5x10^5$ cells/well) were infected in triplicate in a 24-well plate with wildtype *M. tuberculosis* CDC1551, Δ*kasB* and Δ*kasB*C at a MOI of 2. To assess the bacterial cell uptake, following 3 hours of infection at 37°C, 5% CO2, cells were washed four times with PBS, to remove non-phagocytosed bacterial cells, and lysed with saponin (0.1%). The cell suspension was serially diluted in PBS and dilutions were plated onto 7H9 agar plates, which were incubated at 37°C for 3 weeks. To assess the intracellular survival of *M. tuberculosis* strains, cells were washed four times with PBS and supplemented with fresh CDMEM, prior to further incubation for 3 days at 37°C, 5% CO_2. Cells were lysed with saponin (0.1%), serially diluted in PBS and plated onto 7H9 agar plates. All plates were incubated at 37°C for 3 weeks prior to the calculation of colony forming units (CFU).

7.21 Cytokine production analysis and statistical analysis

Supernatants of infected cells were removed at 24 hours post infection and were filter sterilised using 0.22μm filters. Cytokine concentrations were determined using a sandwich ELISA. 96 well plates were coated with primary antibody, diluted in 1X PBS and incubated overnight at 4°C in humid conditions. The following day, the plates were washed three time with washing buffer (1X PBS + 0.05% Tween-20). Unsaturated surface binding sites were blocked with blocking buffer (1X ELISA/ELISPOT Diluent diluted in double distilled water),

and blocking was carried out for one hour at room temperature. Standards and sample dilutions were prepared in CDMEM. The plate was washed three times with washing buffer. Standards and samples were added to the plate and incubated at room temperature for two hours. The secondary antibody was diluted in 1X ELISA/ELISPOT Diluent, and incubated at room temperature for one hour. The plate was washed five times with washing buffer, and 1X streptavidin, diluted in 1X ELISA/ELISPOT Diluent, was applied. The plate was incubated at room temperature for 30 minutes, protected from the light. The plate was washed seven time with washing buffer, 3, 3',5,5'-Tetramethylbenzidine (TMB) solution was added to each well, and the plate was protected from the light until a colour change was visible (using the standards for monitoring a colour change). Stop solution (H_2SO_4) was added to each well to stop the reaction, and the absorbance was read (at 450nm and 570nm).

ELISA statistical analysis was carried out using a one-way Anova with Tukeys honestly significant difference (HSD) post hoc test (GraphPad, Prism 7).

7.22 mRNA expression quantification

7.22.1 RNA extraction

BMDMs ($5x10^5$ cells/well) were infected in triplicate with *M. tuberculosis* strains (wildtype *M. tuberculosis* CDC1551, Δ*kasB* and Δ*kasB*C), at a MOI of 2. Supernatants were removed at 3- and 6-hours post infection, and 250µl TRIzol Reagent (ThermoFisher) was added to each well. Glycogen was added to act as a carrier to increase RNA yield. 50µl chloroform was added and samples were stored on ice for 15 minutes. Following centrifugation, the upper phase was removed and an equal volume of isopropanol was added. The samples were incubated overnight at -20°C to allow for RNA precipitation. Following centrifugation at 4°C, 13,000rpm for 15 minutes, the RNA pellet was washed with 70%

ethanol. The supernatant was removed and the RNA pellet was allowed to air dry. The pellet was resuspended in RNase/DNase-free water and quantified (Nanodrop 1000, ThermoFisher).

7.22.2 cDNA synthesis

100ng of RNA was used to synthesise cDNA (RevertAid H Minus First Strand cDNA Synthesis Kit, ThermoFisher). The solution mastermix can be found in Table 0.12 with the conditions used in this reaction found in Table 0.13.

7.22.3 RT-PCR and statistical analysis

RT-PCR was performed using SYBR Green PCR Master Mix kit (ThermoFisher) using 100ng of template cDNA. The solution mastermix can be found in Table 0.14. All primers utilised in this study are shown in Table 0.15. RT–PCR was carried out using 7500 Fast Real-Time PCR System (Applied Biosystems, ThermoFisher) for 40 cycles; the conditions used for this reaction can be found in Table 0.16. The mRNA levels of the pro-inflammatory cytokines were calculated relative to the expression of the housekeeping gene ubiquitin.

mRNA expression statistical analysis was carried out using a two-way Anova (GraphPad Prism 7). Data is shown as the mean ± the standard deviation.

Table 0.12. Reaction mastermix for the cDNA synthesis using RevertAid H Minus First Strand cDNA Synthesis Kit

Oligo $(dT)_{18}$	1µl
Nuclease free water	1µl
Reaction buffer	4µl
Ribolock	1µl
dNTP	2µl
RevertAid	1µl
RNA (100ng)	10 µl
Total volume	**20µl**

Table 0.13. Thermocycling conditions for reaction using RevertAid H Minus First Strand cDNA Synthesis Kit

Temperature	**Time**	**Passes**
42°C	60 minutes	1
70°C	15 minutes	1
4°C	∞	

Table 0.14. PCR reaction mastermix for the amplification of cDNA synthesis using SYBR Green PCR Master Mix kit

SYBR Green Mix	5µl
Nuclease free water	3µl
Forward Primer	0.5µl
Reverse Primer	0.5µl
cDNA	1µl
Total volume	**10µl**

Table 0.15. Primer pairs used in the amplification of pro-inflammatory cytokine mRNA.

Primer	Sequence
TNF-α_F	5'-TGGCTATTAATTATTCGGTCTGCAT-3'
TNF-α_R	5'-TGAGGGTCTGGGCCATAGAAC-3'
IL-1β_F	5'-GTGCTGTCGGACCCATATGAG-3'
IL-1β_R	5'-CAGGAAGACAGGCTTGTGCTC-3'
IL-12 p40_F	5'-CAAATTACTCCGGACGGTTC-3'
IL-12 p40_R	5'-AGAGACGCCATTCCACATGTC-3'
Ubiquitin_F	5'-TGGCTATTAATTATTCGGTCTGCAT-3'
Ubiquitin_R	5'-GCAAGTGGCTAGAGTGCAGCGTAA-3'

Table 0.16. Thermocycling conditions for reaction using the SYBR Green PCR Master Mix kit

Step	Temperature	Time	Passes
Initial Denaturation	95°C	15 minutes	1
Denaturation	95°C	15 seconds	40
Annealing	58°C	20 seconds	40
Extension	70°C	15 seconds	40
Melting curve	65-95°C	5 seconds	1
Hold	4°C	∞	1

CHAPTER 8

References

ALDRIDGE, B. B., FERNANDEZ-SUAREZ, M., HELLER, D., AMBRAVANESWARAN, V., IRIMIA, D., TONER, M. & FORTUNE, S. M. 2012. Asymmetry and aging of mycobacterial cells lead to variable growth and antibiotic susceptibility. Science, 335, 100-4

ALEXANDER, D. C., JONES, J. R., TAN, T., CHEN, J. M. & LIU, J. 2004. PimF, a mannosyltransferase of mycobacteria, is involved in the biosynthesis of phosphatidylinositol mannosides and lipoarabinomannan. J Biol Chem, 279, 18824-33

ALSAYED, S. S. R., BEH, C. C., FOSTER, N. R., PAYNE, A. D., YU, Y. & GUNOSEWOYO, H. 2019. Kinase Targets for Mycolic Acid Biosynthesis in *Mycobacterium tuberculosis*. Curr Mol Pharmacol, 12, 27-49

ALVAREZ, H. M., KALSCHEUER, R. & STEINBÜCHEL, A., 2000. Accumulation and mobilization of storage lipids by *Rhodococcus opacus* PD630 and *Rhodococcus ruber* NCIMB 40126. Appl Microbiol Biotechnol, 54, 218-223

APPELBERG, R. & SILVA, M. T. 1989. T cell-dependent chronic neutrophilia during mycobacterial infections. Clin Exp Immunol, 78, 478-83

ARANAZ, A., COUSINS, D., MATEOS, A. & DOMÍNGUEZ, L. 2003. Elevation of Mycobacterium tuberculosis subsp. caprae Aranaz et al. 1999 to species rank as *Mycobacterium caprae* comb. nov., sp. nov. International Journal of Systematic and Evolutionary Microbiology, 53, 1785-1789

ARORA, D., CHAWLA, Y., MALAKAR, B., SINGH, A. & NANDICOORI, V. K. 2018. The transpeptidase PbpA and noncanonical transglycosylase RodA of. J Biol Chem, 293, 6497-6516

AUSMEES, N., KUHN, J. R. & JACOBS-WAGNER, C. 2003. The bacterial cytoskeleton: an intermediate filament-like function in cell shape. Cell, 115, 705-13

AÍNSA, J. A., RYDING, N. J., HARTLEY, N., FINDLAY, K. C., BRUTON, C. J. & CHATER, K. F. 2000. WhiA, a protein of unknown function conserved among gram-positive bacteria, is essential for sporulation in *Streptomyces coelicolor* A3(2). J Bacteriol, 182, 5470-8

BAGCHI, S., TOMENIUS, H., BELOVA, L. M. & AUSMEES, N. 2008. Intermediate filament-like proteins in bacteria and a cytoskeletal function in *Streptomyces*. Mol Microbiol, 70, 1037-50

BANCROFT, G. J. 1993. The role of natural killer cells in innate resistance to infection. Curr Opin Immunol, 5, 503-10

BARANOWSKI, C., REGO, E. H. & RUBIN, E. J. 2019. The Dream of a Mycobacterium. Microbiol Spectr, 7

BARRY, C. E., LEE, R. E., MDLULI, K., SAMPSON, A. E., SCHROEDER, B. G., SLAYDEN, R. A. & YUAN, Y. 1998. Mycolic acids: structure, biosynthesis and physiological functions. Prog Lipid Res, 37, 143-79

BARTA, M. L., BATTAILE, K. P., LOVELL, S. & HEFTY, P. S. 2015. Hypothetical protein CT398 (CdsZ) interacts with σ(54) (RpoN)-holoenzyme and the type III secretion export apparatus in *Chlamydia trachomatis*. Protein Sci, 24, 1617-32

BEHLING, C. A., PEREZ, R. L., KIDD, M. R., STATON, G. W. & HUNTER, R. L. 1993. Induction of pulmonary granulomas, macrophage procoagulant activity, and tumor necrosis factor-alpha by trehalose glycolipids. Ann Clin Lab Sci, 23, 256-66

BEN-YEHUDA, S., RUDNER, D. Z. & LOSICK, R. 2003. RacA, a bacterial protein that anchors chromosomes to the cell poles. Science, 299, 532-6

BERGER, A. 2000. Th1 and Th2 responses: what are they? BMJ, 321, 424

BHATT, A., FUJIWARA, N., BHATT, K., GURCHA, S. S., KREMER, L., CHEN, B., CHAN, J., PORCELLI, S. A., KOBAYASHI, K., BESRA, G. S. & JACOBS, W. R. 2007. Deletion of *kasB* in *Mycobacterium tuberculosis* causes loss of acid-fastness and subclinical latent tuberculosis in immunocompetent mice. Proc Natl Acad Sci U S A, 104, 5157-62

BHATT, A., KREMER, L., DAI, A. Z., SACCHETTINI, J. C. & JACOBS, W. R. 2005. Conditional depletion of KasA, a key enzyme of mycolic acid biosynthesis, leads to mycobacterial cell lysis. J Bacteriol, 187, 7596-606

BLOCH, H., SORKIN, E. & ERLENMEYER, H. 1953. A toxic lipid component of the tubercle bacillus (cord factor). I. Isolation from petroleum ether extracts of young bacterial cultures. Am Rev Tuberc, 67, 629-43

BOWDISH, D. M., SAKAMOTO, K., KIM, M. J., KROOS, M., MUKHOPADHYAY, S., LEIFER, C. A., TRYGGVASON, K., GORDON, S. & RUSSELL, D. G. 2009. MARCO, TLR2, and CD14 are required for macrophage cytokine responses to mycobacterial trehalose dimycolate and *Mycobacterium tuberculosis*. PLoS Pathog, 5, e1000474

BUSH, M. J., CHANDRA, G., BIBB, M. J., FINDLAY, K. C. & BUTTNER, M. J. 2016. Genome-Wide Chromatin Immunoprecipitation Sequencing Analysis Shows that WhiB Is a Transcription Factor That Cocontrols Its Regulon with WhiA To Initiate Developmental Cell Division in *Streptomyces*. MBio, 7, e00523-16

CABEEN, M. T., CHARBON, G., VOLLMER, W., BORN, P., AUSMEES, N., WEIBEL, D. B. & JACOBS-WAGNER, C. 2009. Bacterial cell curvature through mechanical control of cell growth. EMBO J, 28, 1208-19

CAMACHO, L. R., CONSTANT, P., RAYNAUD, C., LANEELLE, M. A., TRICCAS, J. A., GICQUEL, B., DAFFE, M. & GUILHOT, C. 2001. Analysis of the phthiocerol dimycocerosate locus of *Mycobacterium tuberculosis*. Evidence that this lipid is involved in the cell wall permeability barrier. J Biol Chem, 276, 19845-54

CARBALLIDO-LÓPEZ, R. 2006. Orchestrating bacterial cell morphogenesis. Mol Microbiol, 60, 815-9

CARROLL, P., FARAY-KELE, M. C. & PARISH, T. 2011. Identifying vulnerable pathways in *Mycobacterium tuberculosis* by using a knockdown approach. Appl Environ Microbiol, 77, 5040-3

CHA, J. H. & STEWART, G. C. 1997. The *divIVA* minicell locus of *Bacillus subtilis*. J Bacteriol, 179, 1671-83

CHAKRAVARTY, S. D., ZHU, G., TSAI, M. C., MOHAN, V. P., MARINO, S., KIRSCHNER, D. E., HUANG, L., FLYNN, J. & CHAN, J. 2008. Tumor necrosis factor blockade in chronic murine tuberculosis enhances granulomatous inflammation and disorganizes granulomas in the lungs. Infect Immun, 76, 916-26

CHARBON, G., CABEEN, M. T. & JACOBS-WAGNER, C. 2009. Bacterial intermediate filaments: in vivo assembly, organization, and dynamics of crescentin. Genes Dev, 23, 1131-44

CHARRIER, E. E. & JANMEY, P. A. 2016. Mechanical Properties of Intermediate Filament Proteins. Methods Enzymol, 568, 35-57

CHEN, J. M., GERMAN, G. J., ALEXANDER, D. C., REN, H., TAN, T. & LIU, J. 2006. Roles of Lsr2 in colony morphology and biofilm formation of *Mycobacterium smegmatis*. J Bacteriol, 188, 633-41

CHUNG, Y., CHANG, S. H., MARTINEZ, G. J., YANG, X. O., NURIEVA, R., KANG, H. S., MA, L., WATOWICH, S. S., JETTEN, A. M., TIAN, Q. & DONG, C. 2009. Critical regulation of early Th17 cell differentiation by interleukin-1 signaling. Immunity, 30, 576-87

CLAESSEN, D., EMMINS, R., HAMOEN, L. W., DANIEL, R. A., ERRINGTON, J. & EDWARDS, D. H. 2008. Control of the cell elongation-division cycle by shuttling of PBP1 protein in *Bacillus subtilis*. Mol Microbiol, 68, 1029-46

COBURN, B., SEKIROV, I. & FINLAY, B. B. 2007. Type III secretion systems and disease. Clin Microbiol Rev, 20, 535-49

COLDITZ, G. A., BREWER, T. F., BERKEY, C. S., WILSON, M. E., BURDICK, E., FINEBERG, H. V. & MOSTELLER, F. 1994. Efficacy of BCG vaccine in the prevention of tuberculosis. Meta-analysis of the published literature. JAMA, 271, 698-702

COLE, S. T., BROSCH, R., PARKHILL, J., GARNIER, T., CHURCHER, C., HARRIS, D., GORDON, S. V., EIGLMEIER, K., GAS, S., BARRY, C. E., TEKAIA, F., BADCOCK, K., BASHAM, D., BROWN, D., CHILLINGWORTH, T., CONNOR, R., DAVIES, R., DEVLIN, K., FELTWELL, T., GENTLES, S., HAMLIN, N., HOLROYD, S., HORNSBY, T., JAGELS, K., KROGH, A., MCLEAN, J., MOULE, S., MURPHY, L., OLIVER, K., OSBORNE, J., QUAIL, M. A., RAJANDREAM, M. A., ROGERS, J., RUTTER, S., SEEGER, K., SKELTON, J., SQUARES, R., SQUARES, S., SULSTON, J. E., TAYLOR, K., WHITEHEAD, S. & BARRELL, B. G. 1998. Deciphering the biology of *Mycobacterium tuberculosis* from the complete genome sequence. Nature, 393, 537-44

COLLINS, D. M., SKOU, B., WHITE, S., BASSETT, S., COLLINS, L., FOR, R., HURR, K., HOTTER, G. & DE LISLE, G. W. 2005. Generation of attenuated *Mycobacterium bovis* strains

by signature-tagged mutagenesis for discovery of novel vaccine candidates. Infect Immun, 73, 2379-86

COLLINS, M. D., GOODFELLOW, M. & MINNIKIN, D. E. 1982. A survey of the structures of mycolic acids in *Corynebacterium* and related taxa. J Gen Microbiol, 128, 129-49

CONSTANT, P., PEREZ, E., MALAGA, W., LANÉELLE, M. A., SAUREL, O., DAFFÉ, M. & GUILHOT, C. 2002. Role of the pks15/1 gene in the biosynthesis of phenolglycolipids in the *Mycobacterium tuberculosis* complex. Evidence that all strains synthesize glycosylated p-hydroxybenzoic methyl esters and that strains devoid of phenolglycolipids harbour a frameshift mutation in the pks15/1 gene. J Biol Chem, 277, 38148-58

COOPER, A. M. 2009. Cell-mediated immune responses in tuberculosis. Annu Rev Immunol, 27, 393-422

COOPER, A. M., DALTON, D. K., STEWART, T. A., GRIFFIN, J. P., RUSSELL, D. G. & ORME, I. M. 1993. Disseminated tuberculosis in interferon gamma gene-disrupted mice. J Exp Med, 178, 2243-7

COOPER, A. M. & KHADER, S. A. 2008. The role of cytokines in the initiation, expansion, and control of cellular immunity to tuberculosis. Immunol Rev, 226, 191-204

COOPER, A. M., SOLACHE, A. & KHADER, S. A. 2007. Interleukin-12 and tuberculosis: an old story revisited. Curr Opin Immunol, 19, 441-7

COUSINS, D. V., BASTIDA, R., CATALDI, A., QUSE, V., REDROBE, S., DOW, S., DUIGNAN, P., MURRAY, A., DUPONT, C., AHMED, N., COLLINS, D. M., BUTLER, W. R., DAWSON, D., RODRÍGUEZ, D., LOUREIRO, J., ROMANO, M. I., ALITO, A., ZUMARRAGA, M. & BERNARDELLI, A. 2003. Tuberculosis in seals caused by a novel member of the *Mycobacterium tuberculosis* complex: *Mycobacterium pinnipedii* sp. nov. International Journal of Systematic and Evolutionary Microbiology, 53, 1305-1314

COX, J. S., CHEN, B., MCNEIL, M. & JACOBS, W. R. 1999. Complex lipid determines tissue-specific replication of *Mycobacterium tuberculosis* in mice. Nature, 402, 79-83

CRONAN, J. E. & WALDROP, G. L. 2002. Multi-subunit acetyl-CoA carboxylases. Prog Lipid Res, 41, 407-35

CROWE, L. M., SPARGO, B. J., IONEDA, T., BEAMAN, B. L. & CROWE, J. H. 1994. Interaction of cord factor (alpha, alpha'-trehalose-6,6'-dimycolate) with phospholipids. Biochim Biophys Acta, 1194, 53-60

CYKTOR, J. C., CARRUTHERS, B., KOMINSKY, R. A., BEAMER, G. L., STROMBERG, P. & TURNER, J. 2013. IL-10 inhibits mature fibrotic granuloma formation during *Mycobacterium tuberculosis* infection. J Immunol, 190, 2778-90

DAHL, J. L. 2004. Electron microscopy analysis of *Mycobacterium tuberculosis* cell division. FEMS Microbiol Lett, 240, 15-20

DANIEL, J., MAAMAR, H., DEB, C., SIRAKOVA, T. D. & KOLATTUKUDY, P. E. 2011. *Mycobacterium tuberculosis* uses host triacylglycerol to accumulate lipid droplets and acquires a dormancy-like phenotype in lipid-loaded macrophages. PLoS Pathog, 7, e1002093

DANIEL, T. M. 2006. The history of tuberculosis. Respir Med, 100, 1862-70

DATTA, P., DASGUPTA, A., BHAKTA, S. & BASU, J. 2002. Interaction between FtsZ and FtsW of *Mycobacterium tuberculosis*. J Biol Chem, 277, 24983-7

DATTA, P., DASGUPTA, A., SINGH, A. K., MUKHERJEE, P., KUNDU, M. & BASU, J. 2006. Interaction between FtsW and penicillin-binding protein 3 (PBP3) directs PBP3 to mid-cell, controls cell septation and mediates the formation of a trimeric complex involving FtsZ, FtsW and PBP3 in mycobacteria. Mol Microbiol, 62, 1655-73

DE LEEUW, E., GRAHAM, B., PHILLIPS, G. J., TEN HAGEN-JONGMAN, C. M., OUDEGA, B. & LUIRINK, J. 1999. Molecular characterization of *Escherichia coli* FtsE and FtsX. Mol Microbiol, 31, 983-93

DE SOUZA, G. A., LEVERSEN, N. A., MÅLEN, H. & WIKER, H. G. 2011. Bacterial proteins with cleaved or uncleaved signal peptides of the general secretory pathway. J Proteomics, 75, 502-10

DEJESUS, M. A., GERRICK, E. R., XU, W., PARK, S. W., LONG, J. E., BOUTTE, C. C., RUBIN, E. J., SCHNAPPINGER, D., EHRT, S., FORTUNE, S. M., SASSETTI, C. M. & IOERGER, T. R. 2017. Comprehensive Essentiality Analysis of the *Mycobacterium tuberculosis* Genome via Saturating Transposon Mutagenesis. MBio, 8

DESAI, B. B., QUINN, P. M., WOLITZKY, A. G., MONGINI, P. K., CHIZZONITE, R. & GATELY, M. K. 1992. IL-12 receptor. II. Distribution and regulation of receptor expression. J Immunol, 148, 3125-32

DOI, M., WACHI, M., ISHINO, F., TOMIOKA, S., ITO, M., SAKAGAMI, Y., SUZUKI, A. & MATSUHASHI, M. 1988. Determinations of the DNA sequence of the *mreB* gene and of the gene products of the *mre* region that function in formation of the rod shape of *Escherichia coli* cells. J Bacteriol, 170, 4619-24

DOMÍNGUEZ-ESCOBAR, J., CHASTANET, A., CREVENNA, A. H., FROMION, V., WEDLICH-SÖLDNER, R. & CARBALLIDO-LÓPEZ, R. 2011. Processive movement of MreB-associated cell wall biosynthetic complexes in bacteria. Science, 333, 225-8

DU, S., PICHOFF, S. & LUTKENHAUS, J. 2016. FtsEX acts on FtsA to regulate divisome assembly and activity. Proc Natl Acad Sci U S A, 113, E5052-61

DUBNAU, E., CHAN, J., RAYNAUD, C., MOHAN, V. P., LANÉELLE, M. A., YU, K., QUÉMARD, A., SMITH, I. & DAFFÉ, M. 2000. Oxygenated mycolic acids are necessary for virulence of *Mycobacterium tuberculosis* in mice. Mol Microbiol, 36, 630-7

DYE, C. 2013. Making wider use of the world's most widely used vaccine: Bacille Calmette-Guerin revaccination reconsidered. J R Soc Interface, 10, 20130365

DZIADEK, J., RUTHERFORD, S. A., MADIRAJU, M. V., ATKINSON, M. A. & RAJAGOPALAN, M. 2003. Conditional expression of *Mycobacterium smegmatis ftsZ*, an essential cell division gene. Microbiology, 149, 1593-603

EDWARDS, D. H. & ERRINGTON, J. 1997. The *Bacillus subtilis* DivIVA protein targets to the division septum and controls the site specificity of cell division. Mol Microbiol, 24, 905-15

EDWARDS, D. H., THOMAIDES, H. B. & ERRINGTON, J. 2000. Promiscuous targeting of *Bacillus subtilis* cell division protein DivIVA to division sites in *Escherichia coli* and fission yeast. EMBO J, 19, 2719-27

ERICKSON, H. P. 1995. FtsZ, a prokaryotic homolog of tubulin? Cell, 80, 367-70

ESUE, O., RUPPRECHT, L., SUN, S. X. & WIRTZ, D. 2010. Dynamics of the bacterial intermediate filament crescentin in vitro and in vivo. PLoS One, 5, e8855

FABRE, M., KOECK, J. L., LE FLÈCHE, P., SIMON, F., HERVÉ, V., VERGNAUD, G. & POURCEL, C. 2004. High genetic diversity revealed by variable-number tandem repeat genotyping and analysis of *hsp65* gene polymorphism in a large collection of "*Mycobacterium canettii*" strains indicates that the *M. tuberculosis* complex is a recently emerged clone of "*M. canettii*". J Clin Microbiol, 42, 3248-55

FAY, A., CZUDNOCHOWSKI, N., ROCK, J. M., JOHNSON, J. R., KROGAN, N. J., ROSENBERG, O. & GLICKMAN, M. S. 2019. Two Accessory Proteins Govern MmpL3 Mycolic Acid Transport in Mycobacteria. MBio, 10

FIGGE, R. M., DIVAKARUNI, A. V. & GOBER, J. W. 2004. MreB, the cell shape-determining bacterial actin homologue, co-ordinates cell wall morphogenesis in *Caulobacter crescentus*. Mol Microbiol, 51, 1321-32

FILIPE-SANTOS, O., BUSTAMANTE, J., CHAPGIER, A., VOGT, G., DE BEAUCOUDREY, L., FEINBERG, J., JOUANGUY, E., BOISSON-DUPUIS, S., FIESCHI, C., PICARD, C. & CASANOVA, J. L. 2006. Inborn errors of IL-12/23- and IFN-gamma-mediated immunity: molecular, cellular, and clinical features. Semin Immunol, 18, 347-61

FLYNN, J. L., CHAN, J., TRIEBOLD, K. J., DALTON, D. K., STEWART, T. A. & BLOOM, B. R. 1993. An essential role for interferon gamma in resistance to *Mycobacterium tuberculosis* infection. J Exp Med, 178, 2249-54.

FLÄRDH, K. 2003. Essential role of DivIVA in polar growth and morphogenesis in *Streptomyces coelicolor* A3(2). Mol Microbiol, 49, 1523-36

FORMSTONE, A. & ERRINGTON, J. 2005. A magnesium-dependent *mreB* null mutant: implications for the role of *mreB* in *Bacillus subtilis*. Mol Microbiol, 55, 1646-57.

GAMSJAEGER, R., LIEW, C. K., LOUGHLIN, F. E., CROSSLEY, M. & MACKAY, J. P. 2007. Sticky fingers: zinc-fingers as protein-recognition motifs. Trends Biochem Sci, 32, 63-70

GANDE, R., DOVER, L. G., KRUMBACH, K., BESRA, G. S., SAHM, H., OIKAWA, T. & EGGELING, L. 2007. The two carboxylases of *Corynebacterium glutamicum* essential for fatty acid and mycolic acid synthesis. J Bacteriol, 189, 5257-64

GAO, L. Y., LAVAL, F., LAWSON, E. H., GROGER, R. K., WOODRUFF, A., MORISAKI, J. H., COX, J. S., DAFFE, M. & BROWN, E. J. 2003. Requirement for *kasB* in Mycobacterium mycolic acid biosynthesis, cell wall impermeability and intracellular survival: implications for therapy. Mol Microbiol, 49, 1547-63

GINDA, K., BEZULSKA, M., ZIÓŁKIEWICZ, M., DZIADEK, J., ZAKRZEWSKA-CZERWIŃSKA, J. & JAKIMOWICZ, D. 2013. ParA of *Mycobacterium smegmatis* co-ordinates chromosome segregation with the cell cycle and interacts with the polar growth determinant DivIVA. Mol Microbiol, 87, 998-1012

GLICKMAN, M. S., CAHILL, S. M. & JACOBS, W. R. 2001. The *Mycobacterium tuberculosis* cmaA2 gene encodes a mycolic acid trans-cyclopropane synthetase. J Biol Chem, 276, 2228-33

GLICKMAN, M. S., COX, J. S. & JACOBS, W. R. 2000. A novel mycolic acid cyclopropane synthetase is required for cording, persistence, and virulence of *Mycobacterium tuberculosis.* Mol Cell, 5, 717-27

GOEHRING, N. W. & BECKWITH, J. 2005. Diverse paths to midcell: assembly of the bacterial cell division machinery. Curr Biol, 15, R514-26

GOLA, S., MUNDER, T., CASONATO, S., MANGANELLI, R. & VICENTE, M. 2015. The essential role of SepF in mycobacterial division. Mol Microbiol, 97, 560-76

GOREN, M. B., D'ARCY HART, P., YOUNG, M. R. & ARMSTRONG, J. A. 1976. Prevention of phagosome-lysosome fusion in cultured macrophages by sulfatides of *Mycobacterium tuberculosis*. Proc Natl Acad Sci U S A, 73, 2510-4

GRIFFIN, J. E., GAWRONSKI, J. D., DEJESUS, M. A., IOERGER, T. R., AKERLEY, B. J. & SASSETTI, C. M. 2011. High-resolution phenotypic profiling defines genes essential for mycobacterial growth and cholesterol catabolism. PLoS Pathog, 7, e1002251

GROHMANN, U., BELLADONNA, M. L., VACCA, C., BIANCHI, R., FALLARINO, F., ORABONA, C., FIORETTI, M. C. & PUCCETTI, P. 2001. Positive regulatory role of IL-12 in macrophages and modulation by IFN-gamma. J Immunol, 167, 221-7

GUEIROS-FILHO, F. J. & LOSICK, R. 2002. A widely conserved bacterial cell division protein that promotes assembly of the tubulin-like protein FtsZ. Genes Dev, 16, 2544-56

GUILLEMARD, E., GENITEAU-LEGENDRE, M., KERGOT, R., LEMAIRE, G., GESSANI, S., LABARRE, C. & QUERO, A. M. 1998. Simultaneous production of IFN-gamma, IFN-alpha/beta and nitric oxide in peritoneal macrophages from TDM-treated mice. J Biol Regul Homeost Agents, 12, 106-11

GUPTA, S., BANERJEE, S. K., CHATTERJEE, A., SHARMA, A. K., KUNDU, M. & BASU, J., 2015. Essential protein SepF of mycobacteria interacts with FtsZ and MurG to regulate cell growth and division. Microbiology, 161, 1627-1638

GUZMAN, L. M., BARONDESS, J. J. & BECKWITH, J. 1992. FtsL, an essential cytoplasmic membrane protein involved in cell division in *Escherichia coli.* J Bacteriol, 174, 7716-28

HALE, C. A. & DE BOER, P. A. 1997. Direct binding of FtsZ to ZipA, an essential component of the septal ring structure that mediates cell division in *E. coli.* Cell, 88, 175-85

HALL, T. M. 2005. Multiple modes of RNA recognition by zinc finger proteins. Curr Opin Struct Biol, 15, 367-73

HAMOEN, L. W., MEILE, J. C., DE JONG, W., NOIROT, P. & ERRINGTON, J. 2006. SepF, a novel FtsZ-interacting protein required for a late step in cell division. Mol Microbiol, 59, 989-99

HANSEN, M., PELTIER, J., KILLY, B., AMIN, B., BODENDORFER, B., HÄRTLOVA, A., UEBEL, S., BOSMANN, M., HOFMANN, J., BÜTTNER, C., EKICI, A. B., KUTTKE, M., FRANZYK, H., FOGED, C., BEER-HAMMER, S., SCHABBAUER, G., TROST, M. & LANG, R. 2019. Macrophage Phosphoproteome Analysis Reveals MINCLE-dependent and -independent Mycobacterial Cord Factor Signaling. Mol Cell Proteomics, 18, 669-685

HARRISON, R. E., BUCCI, C., VIEIRA, O. V., SCHROER, T. A. & GRINSTEIN, S. 2003. Phagosomes fuse with late endosomes and/or lysosomes by extension of membrane protrusions along microtubules: role of Rab7 and RILP. Mol Cell Biol, 23, 6494-506

HEALY, C., GOUZY, A. & EHRT, S. 2020.Peptidoglycan hydrolases RipA and Ami1 are critical for replication and persistence of *Mycobacterium tuberculosis* in the host. mBio, 11, e03315-19

HEDBERG, K. K. & CHEN, L. B. 1986. Absence of intermediate filaments in a human adrenal cortex carcinoma-derived cell line. Exp Cell Res, 163, 509-17

HEICHLINGER, A., AMMELBURG, M., KLEINSCHNITZ, E. M., LATUS, A., MALDENER, I., FLÄRDH, K., WOHLLEBEN, W. & MUTH, G. 2011. The MreB-like protein Mbl of *Streptomyces coelicolor* A3(2) depends on MreB for proper localization and contributes to spore wall synthesis. J Bacteriol, 193, 1533-42

HEMPEL, A. M., WANG, S. B., LETEK, M., GIL, J. A. & FLÄRDH, K. 2008. Assemblies of DivIVA mark sites for hyphal branching and can establish new zones of cell wall growth in *Streptomyces coelicolor.* J Bacteriol, 190, 7579-83

HERRMANN, H. & AEBI, U. 2004. Intermediate filaments: molecular structure, assembly mechanism, and integration into functionally distinct intracellular Scaffolds. Annu Rev Biochem, 73, 749-89

HERRMANN, H., STRELKOV, S. V., BURKHARD, P. & AEBI, U. 2009. Intermediate filaments: primary determinants of cell architecture and plasticity. J Clin Invest, 119, 1772-83.

HERZYK, D. J., ALLEN, J. N., MARSH, C. B. & WEWERS, M. D. 1992. Macrophage and monocyte IL-1 beta regulation differs at multiple sites. Messenger RNA expression, translation, and post-translational processing. J Immunol, 149, 3052-8.

HOEFSLOOT, W., VAN INGEN, J., ANDREJAK, C., ANGEBY, K., BAURIAUD, R., BEMER, P., BEYLIS, N., BOEREE, M. J., CACHO, J., CHIHOTA, V., CHIMARA, E., CHURCHYARD, G., CIAS, R., DAZA, R., DALEY, C. L., DEKHUIJZEN, P. N., DOMINGO, D., DROBNIEWSKI, F., ESTEBAN, J., FAUVILLE-DUFAUX, M., FOLKVARDSEN, D. B., GIBBONS, N., GÓMEZ-MAMPASO, E., GONZALEZ, R., HOFFMANN, H., HSUEH, P. R., INDRA, A., JAGIELSKI, T., JAMIESON, F., JANKOVIC, M., JONG, E., KEANE, J., KOH, W. J., LANGE, B., LEAO, S., MACEDO, R., MANNSÅKER, T., MARRAS, T. K., MAUGEIN, J., MILBURN, H. J., MLINKÓ, T., MORCILLO, N., MORIMOTO, K., PAPAVENTSIS, D., PALENQUE, E., PAEZ-PEÑA, M., PIERSIMONI, C., POLANOVÁ, M., RASTOGI, N., RICHTER, E., RUIZ-SERRANO, M. J., SILVA, A., DA SILVA, M. P., SIMSEK, H., VAN SOOLINGEN, D., SZABÓ, N., THOMSON, R., TÓRTOLA FERNANDEZ, T., TORTOLI, E., TOTTEN, S. E., TYRRELL, G., VASANKARI, T., VILLAR, M., WALKIEWICZ, R., WINTHROP, K. L., WAGNER, D. & GROUP, N. M. N. E. T. 2013. The geographic diversity of nontuberculous mycobacteria isolated from pulmonary samples: an NTM-NET collaborative study. Eur Respir J, 42, 1604-13

HOLMES, N. A., WALSHAW, J., LEGGETT, R. M., THIBESSARD, A., DALTON, K. A., GILLESPIE, M. D., HEMMINGS, A. M., GUST, B. & KELEMEN, G. H. 2013. Coiled-coil protein Scy is a key component of a multiprotein assembly controlling polarized growth in *Streptomyces*. Proc Natl Acad Sci U S A, 110, E397-406

HOUBEN, R. M. & DODD, P. J. 2016. The Global Burden of Latent Tuberculosis Infection: A Re-estimation Using Mathematical Modelling. PLoS Med, 13, e1002152

HUNTER, R. L., VENKATAPRASAD, N. & OLSEN, M. R. 2006. The role of trehalose dimycolate (cord factor) on morphology of virulent *M. tuberculosis* in vitro. Tuberculosis (Edinb), 86, 349-56

HUYNH, K. K., ESKELINEN, E. L., SCOTT, C. C., MALEVANETS, A., SAFTIG, P. & GRINSTEIN, S. 2007. LAMP proteins are required for fusion of lysosomes with phagosomes. EMBO J, 26, 313-24

INDRIGO, J., HUNTER, R. L. & ACTOR, J. K. 2002. Influence of trehalose 6,6'-dimycolate (TDM) during mycobacterial infection of bone marrow macrophages. Microbiology, 148, 1991-8

INDRIGO, J., HUNTER, R. L. & ACTOR, J. K. 2003. Cord factor trehalose 6,6'-dimycolate (TDM) mediates trafficking events during mycobacterial infection of murine macrophages. Microbiology, 149, 2049-59

ISHIKAWA, E., ISHIKAWA, T., MORITA, Y. S., TOYONAGA, K., YAMADA, H., TAKEUCHI, O., KINOSHITA, T., AKIRA, S., YOSHIKAI, Y. & YAMASAKI, S. 2009. Direct recognition of the mycobacterial glycolipid, trehalose dimycolate, by C-type lectin Mincle. J Exp Med, 206, 2879-88

JAIN, P., MALAKAR, B., KHAN, M. Z., LOCHAB, S., SINGH, A. & NANDICOORI, V. K. 2018. Delineating FtsQ-mediated regulation of cell division in. J Biol Chem, 293, 12331-12349

JANI, C., EOH, H., LEE, J. J., HAMASHA, K., SAHANA, M. B., HAN, J. S., NYAYAPATHY, S., LEE, J. Y., SUH, J. W., LEE, S. H., REHSE, S. J., CRICK, D. C. & KANG, C. M. 2010. Regulation of polar peptidoglycan biosynthesis by Wag31 phosphorylation in mycobacteria. BMC Microbiol, 10, 327

JENSEN, S. O., THOMPSON, L. S. & HARRY, E. J. 2005. Cell division in *Bacillus subtilis*: FtsZ and FtsA association is Z-ring independent, and FtsA is required for efficient midcell Z-Ring assembly. J Bacteriol, 187, 6536-44

JONES, L. J., CARBALLIDO-LÓPEZ, R. & ERRINGTON, J. 2001. Control of cell shape in bacteria: helical, actin-like filaments in Bacillus subtilis. Cell, 104, 913-22

JOYCE, G., WILLIAMS, K. J., ROBB, M., NOENS, E., TIZZANO, B., SHAHREZAEI, V. & ROBERTSON, B. D. 2012. Cell division site placement and asymmetric growth in mycobacteria. PLoS One, 7, e44582

JUFFERMANS, N. P., FLORQUIN, S., CAMOGLIO, L., VERBON, A., KOLK, A. H., SPEELMAN, P., VAN DEVENTER, S. J. & VAN DER POLL, T. 2000. Interleukin-1 signaling is essential for host defense during murine pulmonary tuberculosis. J Infect Dis, 182, 902-8

KAN-SUTTON, C., JAGANNATH, C. & HUNTER, R. L. 2009. Trehalose 6,6'-dimycolate on the surface of *Mycobacterium tuberculosis* modulates surface marker expression for antigen presentation and costimulation in murine macrophages. Microbes Infect, 11, 40-8

KANG, C. M., ABBOTT, D. W., PARK, S. T., DASCHER, C. C., CANTLEY, L. C. & HUSSON, R. N. 2005. The *Mycobacterium tuberculosis* serine/threonine kinases PknA and PknB: substrate identification and regulation of cell shape. Genes Dev, 19, 1692-704

KANG, C. M., NYAYAPATHY, S., LEE, J. Y., SUH, J. W. & HUSSON, R. N. 2008. Wag31, a homologue of the cell division protein DivIVA, regulates growth, morphology and polar cell wall synthesis in mycobacteria. Microbiology, 154, 725-35.

KARLSON, A. G. & LESSEL, E. F. 1970. *Mycobacterium bovis* nom. nov. International Journal of Systematic and Evolutionary Microbiology, 20, 273-282

KEANE, J., BALCEWICZ-SABLINSKA, M. K., REMOLD, H. G., CHUPP, G. L., MEEK, B. B., FENTON, M. J. & KORNFELD, H. 1997. Infection by *Mycobacterium tuberculosis* promotes human alveolar macrophage apoptosis. Infect Immun, 65, 298-304

KIESER, K. J., BOUTTE, C. C., KESTER, J. C., BAER, C. E., BARCZAK, A. K., MENICHE, X., CHAO, M. C., REGO, E. H., SASSETTI, C. M., FORTUNE, S. M. & RUBIN, E. J. 2015. Phosphorylation of the Peptidoglycan Synthase PonA1 Governs the Rate of Polar Elongation in Mycobacteria. PLoS Pathog, 11, e1005010

KIESER, K. J. & RUBIN, E. J. 2014. How sisters grow apart: mycobacterial growth and division. Nat Rev Microbiol, 12, 550-62

KLUG, A. 1999. Zinc finger peptides for the regulation of gene expression. J Mol Biol, 293, 215-8

KOCH, R. 1882. Die Ätiologie der Tuberkulose (1882). Robert Koch : Zentrale Texte. Berlin, Heidelberg: Springer Berlin Heidelberg

KOCH, R. 1982. Classics in infectious diseases. The etiology of tuberculosis: Robert Koch. Berlin, Germany 1882. Rev Infect Dis, 4, 1270-4

KREMER, L., DOUGLAS, J. D., BAULARD, A. R., MOREHOUSE, C., GUY, M. R., ALLAND, D., DOVER, L. G., LAKEY, J. H., JACOBS, W. R., BRENNAN, P. J., MINNIKIN, D. E. & BESRA, G. S. 2000. Thiolactomycin and related analogues as novel anti-mycobacterial agents targeting KasA and KasB condensing enzymes in *Mycobacterium tuberculosis.* J Biol Chem, 275, 16857-64

KRISHNAN, N., ROBERTSON, B. D. & THWAITES, G. 2013. Pathways of IL-1β secretion by macrophages infected with clinical *Mycobacterium tuberculosis* strains. Tuberculosis (Edinb), 93, 538-47

KUMAR, A. & KARTHIKEYAN, S. 2018. Crystal structure of the *MSMEG_4306* gene product from *Mycobacterium smegmatis*. Acta Crystallogr F Struct Biol Commun, 74, 166-173

LAY, G., POQUET, Y., SALEK-PEYRON, P., PUISSEGUR, M. P., BOTANCH, C., BON, H., LEVILLAIN, F., DUTEYRAT, J. L., EMILE, J. F. & ALTARE, F. 2007. Langhans giant cells from *M. tuberculosis*-induced human granulomas cannot mediate mycobacterial uptake. J Pathol, 211, 76-85

LEA-SMITH, D. J., PYKE, J. S., TULL, D., MCCONVILLE, M. J., COPPEL, R. L. & CRELLIN, P. K. 2007. The reductase that catalyzes mycolic motif synthesis is required for efficient attachment of mycolic acids to arabinogalactan. J Biol Chem, 282, 11000-8

LEE, D. S., KIM, P., KIM, E. S., KIM, Y. & LEE, H. S. 2018. *Corynebacterium glutamicum* WhcD interacts with WhiA to exert a regulatory effect on cell division genes. Antonie Van Leeuwenhoek, 111, 641-648

LEE, J. J., KAN, C. M., LEE, J. H., PARK, K. S., JEON, J. H. & LEE, S. H. 2014. Phosphorylation-dependent interaction between a serine/threonine kinase PknA and a putative cell division protein Wag31 in *Mycobacterium tuberculosis.* New Microbiol, 37, 525-33.

LENARCIC, R., HALBEDEL, S., VISSER, L., SHAW, M., WU, L. J., ERRINGTON, J., MARENDUZZO, D. & HAMOEN, L. W. 2009. Localisation of DivIVA by targeting to negatively curved membranes. EMBO J, 28, 2272-82

LETEK, M., ORDÓÑEZ, E., VAQUERA, J., MARGOLIN, W., FLÄRDH, K., MATEOS, L. M. & GIL, J. A. 2008. DivIVA is required for polar growth in the MreB-lacking rod-shaped actinomycete *Corynebacterium glutamicum*. J Bacteriol, 190, 3283-92

LEWIS, A. G., JR., LASCHÉ, E. M., ARMSTRONG, A. L. & DUNBAR, F. P. 1960. A clinical study of the chronic lung disease due to nonphotochromogenic acid-fast bacilli*†. Annals of Internal Medicine, 53, 273-285

LIMA, V. M., BONATO, V. L., LIMA, K. M., DOS SANTOS, S. A., DOS SANTOS, R. R., GONÇALVES, E. D., FACCIOLI, L. H., BRANDÃO, I. T., RODRIGUES-JUNIOR, J. M. & SILVA, C. L. 2001. Role of trehalose dimycolate in recruitment of cells and modulation of production of cytokines and NO in tuberculosis. Infect Immun, 69, 5305-12

LIN, P. L. & FLYNN, J. L. 2010. Understanding latent tuberculosis: a moving target. J Immunol, 185, 15-22

LIN, P. L., RODGERS, M., SMITH, L., BIGBEE, M., MYERS, A., BIGBEE, C., CHIOSEA, I., CAPUANO, S. V., FUHRMAN, C., KLEIN, E. & FLYNN, J. L. 2009. Quantitative comparison of active and latent tuberculosis in the cynomolgus macaque model. Infect Immun, 77, 4631-4

LIU, J., ZHENG, Q., DENG, Y., CHENG, C. S., KALLENBACH, N. R. & LU, M. 2006. A seven-helix coiled coil. Proc Natl Acad Sci U S A, 103, 15457-62

LOGSDON, M. M. & ALDRIDGE, B. B. 2018. Stable Regulation of Cell Cycle Events in Mycobacteria: Insights From Inherently Heterogeneous Bacterial Populations. Front Microbiol, 9, 514

LOPEZ-CASTEJON, G. & BROUGH, D. 2011. Understanding the mechanism of IL-1β secretion. Cytokine Growth Factor Rev, 22, 189-95

LUPAS, A., VAN DYKE, M. & STOCK, J. 1991. Predicting coiled coils from protein sequences. Science, 252, 1162-4

LUPAS, A. N. & GRUBER, M. 2005. The structure of alpha-helical coiled coils. Adv Protein Chem, 70, 37-78

LUTKENHAUS, J. 1993. FtsZ ring in bacterial cytokinesis. Mol Microbiol, 9, 403-9

MAHAIRAS, G. G., SABO, P. J., HICKEY, M. J., SINGH, D. C. & STOVER, C. K. 1996. Molecular analysis of genetic differences between *Mycobacterium bovis* BCG and virulent *M. bovis*. J Bacteriol, 178, 1274-82

MASTER, S. S., RAMPINI, S. K., DAVIS, A. S., KELLER, C., EHLERS, S., SPRINGER, B., TIMMINS, G. S., SANDER, P. & DERETIC, V. 2008. *Mycobacterium tuberculosis* prevents inflammasome activation. Cell Host Microbe, 3, 224-32

MATTHEWS, J. M. & SUNDE, M. 2002. Zinc fingers--folds for many occasions. IUBMB Life, 54, 351-5

MAWUENYEGA, K. G., FORST, C. V., DOBOS, K. M., BELISLE, J. T., CHEN, J., BRADBURY, E. M., BRADBURY, A. R. & CHEN, X. 2005. *Mycobacterium tuberculosis* functional network analysis by global subcellular protein profiling. Mol Biol Cell, 16, 396-404

MAZANDU, G. K. & MULDER, N. J. 2012. Function prediction and analysis of *Mycobacterium tuberculosis* hypothetical proteins. Int J Mol Sci, 13, 7283-302

MCMURRAY, D. N. 2001. Disease model: pulmonary tuberculosis. Trends Mol Med, 7, 135-7

MEHLA, J., CAUFIELD, J. H., SAKHAWALKAR, N. & UETZ, P, 2017. A comparison of two hybrid approaches for detecting protein-protein interactions. Methods Enzymol, 586, 333-358

MENDELSON, N. H. 1975. Cell division suppression in the *Bacillus subtilis* div IC-A1 minicell-producing mutant. J Bacteriol, 121, 1166-72

MENICHE, X., OTTEN, R., SIEGRIST, M. S., BAER, C. E., MURPHY, K. C., BERTOZZI, C. R. & SASSETTI, C. M. 2014. Subpolar addition of new cell wall is directed by DivIVA in mycobacteria. Proc Natl Acad Sci U S A, 111, E3243-51

MIDDLEBROOK, G., COLEMAN, C. M. & SCHAEFER, W. B. 1959. Sulfolipid from virulent tubercle bacilli. Proc Natl Acad Sci U S A, 45, 1801-4

MIR, M. A., RAJESWARI, H. S., VEERARAGHAVAN, U. & AJITKUMAR, P. 2006. Molecular characterisation of ABC transporter type FtsE and FtsX proteins of *Mycobacterium tuberculosis.* Arch Microbiol, 185, 147-58

MISHRA, B. B., MOURA-ALVES, P., SONAWANE, A., HACOHEN, N., GRIFFITHS, G., MOITA, L. F. & ANES, E. 2010. *Mycobacterium tuberculosis* protein ESAT-6 is a potent activator of the NLRP3/ASC inflammasome. Cell Microbiol, 12, 1046-63

MOHANTY, D., SANKARANARAYANAN, R. & GOKHALE, R. S. 2011. Fatty acyl-AMP ligases and polyketide synthases are unique enzymes of lipid biosynthetic machinery in *Mycobacterium tuberculosis.* Tuberculosis (Edinb), 91, 448-55

MORSE, D., BROTHWELL, D. R. & UCKO, P. J. 1964. Tuberculosis in ancient Egypt. Am Rev Respir Dis, 90, 524-41

MUKHERJEE, P., SUREKA, K., DATTA, P., HOSSAIN, T., BARIK, S., DAS, K. P., KUNDU, M. & BASU, J. 2009. Novel role of Wag31 in protection of mycobacteria under oxidative stress. Mol Microbiol, 73, 103-19

MUÑOZ-PLANILLO, R., KUFFA, P., MARTÍNEZ-COLÓN, G., SMITH, B. L., RAJENDIRAN, T. M. & NÚÑEZ, G. 2013. K^+ efflux is the common trigger of NLRP3 inflammasome activation by bacterial toxins and particulate matter. Immunity, 38, 1142-53

MÅLEN, H., PATHAK, S., SØFTELAND, T., DE SOUZA, G. A. & WIKER, H. G. 2010. Definition of novel cell envelope associated proteins in Triton X-114 extracts of *Mycobacterium tuberculosis* H37Rv. BMC Microbiol, 10, 132

NAGARAJAN, S. N., UPADHYAY, S., CHAWLA, Y., KHAN, S., NAZ, S., SUBRAMANIAN, J., GANDOTRA, S. & NANDICOORI, V. K. 2015. Protein kinase A

(PknA) of *Mycobacterium tuberculosis* is independently activated and is critical for growth in vitro and survival of the pathogen in the host. J Biol Chem, 290, 9626-45

NAGAYAMA, H., SATO, K., KAWASAKI, H., ENOMOTO, M., MORIMOTO, C., TADOKORO, K., JUJI, T., ASANO, S. & TAKAHASHI, T. A. 2000. IL-12 responsiveness and expression of IL-12 receptor in human peripheral blood monocyte-derived dendritic cells. J Immunol, 165, 59-66

NEHRT, N. L., CLARK, W. T., RADIVOJAC, P. & HAHN, M. W. 2011. Testing the ortholog conjecture with comparative functional genomic data from mammals. PLoS Comput Biol, 7, e1002073

NEWPORT, M. J., HUXLEY, C. M., HUSTON, S., HAWRYLOWICZ, C. M., OOSTRA, B. A., WILLIAMSON, R. & LEVIN, M. 1996. A mutation in the interferon-gamma-receptor gene and susceptibility to mycobacterial infection. N Engl J Med, 335, 1941-9

NÚÑEZ MARTÍNEZ, O., RIPOLL NOISEUX, C., CARNEROS MARTÍN, J. A., GONZÁLEZ LARA, V. & GREGORIO MARAÑÓN, H. G. 2001. Reactivation tuberculosis in a patient with anti-TNF-alpha treatment. Am J Gastroenterol, 96, 1665-6

OKAMURA, H., TSUTSUI, H., KASHIWAMURA, S., YOSHIMOTO, T. & NAKANISHI, K. 1998. Interleukin-18: a novel cytokine that augments both innate and acquired immunity. Adv Immunol, 70, 281-312

OLUKOSHI, E. R. & PACKTER, N. M., 1994. Importance of stored triacylglycerols in *Streptomyces*: possible carbon source for antibiotics. Microbiology, 140, 931-943

ONWUEME, K. C., VOS, C. J., ZURITA, J., FERRERAS, J. A. & QUADRI, L. E. 2005. The dimycocerosate ester polyketide virulence factors of mycobacteria. Prog Lipid Res, 44, 259-302

ORGANIZATION, W. H. 2015. Global Tuberculosis Report 2015. Geneva, Switzerland: World Health Organization

ORGANIZATION, W. H. 2016. Global Tuberculosis Report 2016. Geneva, Switzerland: World Health Organization

ORGANIZATION, W. H. 2018. Tuberculosis Fact Sheet. World Health Organization

ORTALO-MAGNÉ, A., LEMASSU, A., LANÉELLE, M. A., BARDOU, F., SILVE, G., GOUNON, P., MARCHAL, G. & DAFFÉ, M. 1996. Identification of the surface-exposed lipids on the cell envelopes of *Mycobacterium tuberculosis* and other mycobacterial species. J Bacteriol, 178, 456-61

OSHIMI, Y., ODA, S., HONDA, Y., NAGATA, S. & MIYAZAKI, S. 1996. Involvement of Fas ligand and Fas-mediated pathway in the cytotoxicity of human natural killer cells. J Immunol, 157, 2909-15

OTTENHOFF, T. H., VERRECK, F. A., HOEVE, M. A. & VAN DE VOSSE, E. 2005. Control of human host immunity to mycobacteria. Tuberculosis (Edinb), 85, 53-64

PABST, M. J., GROSS, J. M., BROZNA, J. P. & GOREN, M. B. 1988. Inhibition of macrophage priming by sulfatide from *Mycobacterium tuberculosis.* J Immunol, 140, 634-40.

PATRICK, J. E. & KEARNS, D. B. 2008. MinJ (YvjD) is a topological determinant of cell division in Bacillus subtilis. Mol Microbiol, 70, 1166-79

PAWELCZYK, J., BRZOSTEK, A., KREMER, L., DZIADEK, B., RUMIJOWSKA-GALEWICZ, A., FIOLKA, M. & DZIADEK, J. 2011. AccD6, a key carboxyltransferase essential for mycolic acid synthesis in *Mycobacterium tuberculosis*, is dispensable in a nonpathogenic strain. J Bacteriol, 193, 6960-72

PERREGAUX, D. & GABEL, C. A. 1994. Interleukin-1 beta maturation and release in response to ATP and nigericin. Evidence that potassium depletion mediated by these agents is a necessary and common feature of their activity. J Biol Chem, 269, 15195-203

PETERSEN, H. J. & SMITH, A. M. 2013. The role of the innate immune system in granulomatous disorders. Front Immunol, 4, 120

PEYRON, P., VAUBOURGEIX, J., POQUET, Y., LEVILLAIN, F., BOTANCH, C., BARDOU, F., DAFFÉ, M., EMILE, J. F., MARCHOU, B., CARDONA, P. J., DE CHASTELLIER, C. & ALTARE, F. 2008. Foamy macrophages from tuberculous patients' granulomas constitute a nutrient-rich reservoir for *M. tuberculosis* persistence. PLoS Pathog, 4, e1000204

PLOCINSKA, R., PURUSHOTHAM, G., SARVA, K., VADREVU, I. S., PANDEETI, E. V., ARORA, N., PLOCINSKI, P., MADIRAJU, M. V. & RAJAGOPALAN, M. 2012. Septal localization of the *Mycobacterium tuberculosis* MtrB sensor kinase promotes MtrA regulon expression. J Biol Chem, 287, 23887-99

PLOCINSKI, P., ARORA, N., SARVA, K., BLASZCZYK, E., QIN, H., DAS, N., PLOCINSKA, R., ZIOLKIEWICZ, M., DZIADEK, J., KIRAN, M., GORLA, P., CROSS, T. A., MADIRAJU, M. & RAJAGOPALAN, M. 2012. *Mycobacterium tuberculosis* CwsA interacts with CrgA and Wag31, and the CrgA-CwsA complex is involved in peptidoglycan synthesis and cell shape determination. J Bacteriol, 194, 6398-409

PLOCINSKI, P., ZIOLKIEWICZ, M., KIRAN, M., VADREVU, S. I., NGUYEN, H. B., HUGONNET, J., VECKERLE, C., ARTHUR, M., DZIADEK, J., CROSS, T. A., MADIRAJU, M. & RAJAGOPALAN, M. 2011. Characterization of CrgA, a new partner of the *Mycobacterium tuberculosis* peptidoglycan polymerization complexes. J Bacteriol, 193, 3246-56

PORTEVIN, D., DE SOUSA-D'AURIA, C., HOUSSIN, C., GRIMALDI, C., CHAMI, M., DAFFÉ, M. & GUILHOT, C. 2004. A polyketide synthase catalyzes the last condensation step of mycolic acid biosynthesis in mycobacteria and related organisms. Proc Natl Acad Sci U S A, 101, 314-9

PORTEVIN, D., DE SOUSA-D'AURIA, C., MONTROZIER, H., HOUSSIN, C., STELLA, A., LANÉELLE, M. A., BARDOU, F., GUILHOT, C. & DAFFÉ, M. 2005. The acyl-AMP ligase FadD32 and AccD4-containing acyl-CoA carboxylase are required for the synthesis of mycolic acids and essential for mycobacterial growth: identification of the carboxylation

product and determination of the acyl-CoA carboxylase components. J Biol Chem, 280, 8862-74

QUIGLEY, J., HUGHITT, V. K., VELIKOVSKY, C. A., MARIUZZA, R. A., EL-SAYED, N. M. & BRIKEN, V. 2017. The Cell Wall Lipid PDIM Contributes to Phagosomal Escape and Host Cell Exit of. MBio, 8

QURESHI, N., SATHYAMOORTHY, N. & TAKAYAMA, K. 1984. Biosynthesis of C30 to C56 fatty acids by an extract of *Mycobacterium tuberculosis* H37Ra. J Bacteriol, 157, 46-52

RAIN, J. C., SELIG, L., DE REUSE, H., BATTAGLIA, V., REVERDY, C., SIMON, S., LENZEN, G., PETEL, F., WOJCIK, J., SCHÄCHTER, V., CHEMAMA, Y., LABIGNE, A. & LEGRAIN, P. 2001. The protein-protein interaction map of *Helicobacter pylori.* Nature, 409, 211-5

RAO, V., FUJIWARA, N., PORCELLI, S. A. & GLICKMAN, M. S. 2005. *Mycobacterium tuberculosis controls* host innate immune activation through cyclopropane modification of a glycolipid effector molecule. J Exp Med, 201, 535-43

REDDY, B. K., LANDGE, S., RAVISHANKAR, S., PATIL, V., SHINDE, V., TANTRY, S., KALE, M., RAICHURKAR, A., MENASINAKAI, S., MUDUGAL, N. V., AMBADY, A., GHOSH, A., TUNDUGURU, R., KAUR, P., SINGH, R., KUMAR, N., BHARATH, S., SUNDARAM, A., BHAT, J., SAMBANDAMURTHY, V. K., BJÖRKELID, C., JONES, T. A., DAS, K., BANDODKAR, B., MALOLANARASIMHAN, K., MUKHERJEE, K. & RAMACHANDRAN, V. 2014. Assessment of *Mycobacterium tuberculosis* pantothenate kinase vulnerability through target knockdown and mechanistically diverse inhibitors. Antimicrob Agents Chemother, 58, 3312-26

REED, M. B., DOMENECH, P., MANCA, C., SU, H., BARCZAK, A. K., KREISWIRTH, B. N., KAPLAN, G. & BARRY, C. E. 2004. A glycolipid of hypervirulent tuberculosis strains that inhibits the innate immune response. Nature, 431, 84-7

REGO, E. H., AUDETTE, R. E. & RUBIN, E. J. 2017. Deletion of a mycobacterial divisome factor collapses single-cell phenotypic heterogeneity. Nature, 546, 153-157

REHREN, G., WALTERS, S., FONTAN, P., SMITH, I. & ZÁRRAGA, A. M. 2007. Differential gene expression between *Mycobacterium bovis* and *Mycobacterium tuberculosis.* Tuberculosis (Edinb), 87, 347-59

RHOADES, E. R., FRANK, A. A. & ORME, I. M. 1997. Progression of chronic pulmonary tuberculosis in mice aerogenically infected with virulent *Mycobacterium tuberculosis*. Tuber Lung Dis, 78, 57-66

RICHARDSON, K., BENNION, O. T., TAN, S., HOANG, A. N., COKOL, M. & ALDRIDGE, B. B. 2016. Temporal and intrinsic factors of rifampicin tolerance in mycobacteria. Proc Natl Acad Sci U S A, 113, 8302-7

RIGDEN, D. J. 2011. Ab initio modeling led annotation suggests nucleic acid binding function for many DUFs. OMICS, 15, 431-8

ROGALL, T., WOLTERS, J., FLOHR, T. & BÖTTGER, E. C. 1990. Towards a phylogeny and definition of species at the molecular level within the genus *Mycobacterium.* Int J Syst Bacteriol, 40, 323-30

RYAN, K. A., KARIM, N., WORKU, M., MOORE, S. A., PENN, C. W. & O'TOOLE, P. W. 2005. HP0958 is an essential motility gene in *Helicobacter pylori*. FEMS Microbiol Lett, 248, 47-55

SAIGA, H., KITADA, S., SHIMADA, Y., KAMIYAMA, N., OKUYAMA, M., MAKINO, M., YAMAMOTO, M. & TAKEDA, K. 2012. Critical role of AIM2 in *Mycobacterium tuberculosis* infection. Int Immunol, 24, 637-44

SANTI, I., DHAR, N., BOUSBAINE, D., WAKAMOTO, Y. & MCKINNEY, J. D. 2013. Single-cell dynamics of the chromosome replication and cell division cycles in mycobacteria. Nat Commun, 4, 2470

SASSETTI, C. M., BOYD, D. H. & RUBIN, E. J. 2003. Genes required for mycobacterial growth defined by high density mutagenesis. Mol Microbiol, 48, 77-84

SCHAEFFER, M. L., AGNIHOTRI, G., VOLKER, C., KALLENDER, H., BRENNAN, P. J. & LONSDALE, J. T. 2001. Purification and biochemical characterization of the *Mycobacterium tuberculosis* beta-ketoacyl-acyl carrier protein synthases KasA and KasB. J Biol Chem, 276, 47029-37

SCHMIDT, K. L., PETERSON, N. D., KUSTUSCH, R. J., WISSEL, M. C., GRAHAM, B., PHILLIPS, G. J. & WEISS, D. S. 2004. A predicted ABC transporter, FtsEX, is needed for cell division in *Escherichia coli.* J Bacteriol, 186, 785-93

SCHOENEN, H., BODENDORFER, B., HITCHENS, K., MANZANERO, S., WERNINGHAUS, K., NIMMERJAHN, F., AGGER, E. M., STENGER, S., ANDERSEN, P., RULAND, J., BROWN, G. D., WELLS, C. & LANG, R. 2010. Cutting edge: Mincle is essential for recognition and adjuvanticity of the mycobacterial cord factor and its synthetic analog trehalose-dibehenate. J Immunol, 184, 2756-60

SCHRODER, K. & TSCHOPP, J. 2010. The inflammasomes. Cell, 140, 821-32

SCHWEIZER, E. & HOFMANN, J. 2004. Microbial type I fatty acid synthases (FAS): major players in a network of cellular FAS systems. Microbiol Mol Biol Rev, 68, 501-17, table of contents

SEREBRIISKII, I. G. & GOLEMIS, E. A. 2000. Uses of *lacZ* to study gene function: Evaluation of β-galactosidase assays employed in the yeast two-hybrid system. Analytical Biochemistry, 285, 1-15

SHARMA, A. K., ARORA, D., SINGH, L. K., GANGWAL, A., SAJID, A., MOLLE, V., SINGH, Y. & NANDICOORI, V. K. 2016. Serine/Threonine Protein Phosphatase PstP of *Mycobacterium tuberculosis* Is Necessary for Accurate Cell Division and Survival of Pathogen. J Biol Chem, 291, 24215-24230

SHARMA, D. & KANNEGANTI, T. D. 2016. The cell biology of inflammasomes: Mechanisms of inflammasome activation and regulation. J Cell Biol, 213, 617-29

SHI, L., SOHASKEY, C. D., PHEIFFER, C., DATTA, P., PARKS, M. & MCFADDEN, J., 2010. Carbon flux rerouting during *Mycobacterium tuberculosis* growth arrest. Mol Microbiol, 78, 1199-1215

SHIH, Y. L., LE, T. & ROTHFIELD, L. 2003. Division site selection in *Escherichia coli* involves dynamic redistribution of Min proteins within coiled structures that extend between the two cell poles. Proc Natl Acad Sci U S A, 100, 7865-70

SINGH, B., NITHARWAL, R. G., RAMESH, M., PETTERSSON, B. M., KIRSEBOM, L. A. & DASGUPTA, S. 2013. Asymmetric growth and division in *Mycobacterium spp*.: compensatory mechanisms for non-medial septa. Mol Microbiol, 88, 64-76

SINSIMER, D., HUET, G., MANCA, C., TSENOVA, L., KOO, M. S., KUREPINA, N., KANA, B., MATHEMA, B., MARRAS, S. A., KREISWIRTH, B. N., GUILHOT, C. & KAPLAN, G. 2008. The phenolic glycolipid of *Mycobacterium tuberculosis* differentially modulates the early host cytokine response but does not in itself confer hypervirulence. Infect Immun, 76, 3027-36

SMYTH, M. J., CRETNEY, E., KELLY, J. M., WESTWOOD, J. A., STREET, S. E., YAGITA, H., TAKEDA, K., VAN DOMMELEN, S. L., DEGLI-ESPOSTI, M. A. & HAYAKAWA, Y. 2005. Activation of NK cell cytotoxicity. Mol Immunol, 42, 501-10

SNAPPER, S. B., MELTON, R. E., MUSTAFA, S., KIESER, T. & JACOBS, W. R. 1990. Isolation and characterization of efficient plasmid transformation mutants of *Mycobacterium smegmatis*. Mol Microbiol, 4, 1911-9

SPARGO, B. J., CROWE, L. M., IONEDA, T., BEAMAN, B. L. & CROWE, J. H. 1991. Cord factor (alpha,alpha-trehalose 6,6'-dimycolate) inhibits fusion between phospholipid vesicles. Proc Natl Acad Sci U S A, 88, 737-40

SREEVATSAN, S., PAN, X., STOCKBAUER, K. E., CONNELL, N. D., KREISWIRTH, B. N., WHITTAM, T. S. & MUSSER, J. M. 1997. Restricted structural gene polymorphism in the *Mycobacterium tuberculosis* complex indicates evolutionarily recent global dissemination. Proc Natl Acad Sci U S A, 94, 9869-74

STOVER, C. K., DE LA CRUZ, V. F., FUERST, T. R., BURLEIN, J. E., BENSON, L. A., BENNETT, L. T., BANSAL, G. P., YOUNG, J. F., LEE, M. H. & HATFULL, G. F. 1991. New use of BCG for recombinant vaccines. Nature, 351, 456-60

SVITKINA, T. M. & BORISY, G. G. 1999. Arp2/3 complex and actin depolymerizing factor/cofilin in dendritic organization and treadmilling of actin filament array in lamellipodia. J Cell Biol, 145, 1009-26

TAKAYAMA, K., WANG, C. & BESRA, G. S. 2005. Pathway to synthesis and processing of mycolic acids in *Mycobacterium tuberculosis*. Clin Microbiol Rev, 18, 81-101

TAKAYAMA, K., WANG, L. & DAVID, H. L. 1972. Effect of isoniazid on the in vivo mycolic acid synthesis, cell growth, and viability of *Mycobacterium tuberculosis*. Antimicrob Agents Chemother, 2, 29-35

THOMAIDES, H. B., FREEMAN, M., EL KAROUI, M. & ERRINGTON, J. 2001. Division site selection protein DivIVA of *Bacillus subtilis* has a second distinct function in chromosome segregation during sporulation. Genes Dev, 15, 1662-73

TILNEY, L. G. & PORTNOY, D. A. 1989. Actin filaments and the growth, movement, and spread of the intracellular bacterial parasite, *Listeria monocytogenes*. J Cell Biol, 109, 1597-608

TOMIYASU, I. 1982. Mycolic acid composition and thermally adaptative changes in *Nocardia asteroides*. J Bacteriol, 151, 828-37

TORTOLI, E. 2009. Clinical manifestations of nontuberculous mycobacteria infections. Clin Microbiol Infect, 15, 906-10

TRIVEDI, O. A., ARORA, P., SRIDHARAN, V., TICKOO, R., MOHANTY, D. & GOKHALE, R. S. 2004. Enzymic activation and transfer of fatty acids as acyl-adenylates in mycobacteria. Nature, 428, 441-5

TSANG, M. J. & BERNHARDT, T. G. 2015. A role for the FtsQLB complex in cytokinetic ring activation revealed by an ftsL allele that accelerates division. Mol Microbiol, 95, 925-44

TURK, J. L. & NARAYANAN, R. B. 1982. The origin, morphology, and function of epithelioid cells. Immunobiology, 161, 274-82

ULBERTH, F. & ACHS, E. 1990. Argentation chromatography of fatty acid methyl esters using silver-loaded solid-phase extraction columns. Journal of Chromatography

VAN DULLEMEN, H. M., VAN DEVENTER, S. J., HOMMES, D. W., BIJL, H. A., JANSEN, J., TYTGAT, G. N. & WOODY, J. 1995. Treatment of Crohn's disease with anti-tumor necrosis factor chimeric monoclonal antibody (cA2). Gastroenterology, 109, 129-35.

VANKAYALAPATI, R., WIZEL, B., WEIS, S. E., SAFI, H., LAKEY, D. L., MANDELBOIM, O., SAMTEN, B., PORGADOR, A. & BARNES, P. F. 2002. The NKp46 receptor contributes to NK cell lysis of mononuclear phagocytes infected with an intracellular bacterium. J Immunol, 168, 3451-7

VARMA, A. & YOUNG, K. D. 2009. In Escherichia coli, MreB and FtsZ direct the synthesis of lateral cell wall via independent pathways that require PBP 2. J Bacteriol, 191, 3526-33.

VENETIANER, A., SCHILLER, D. L., MAGIN, T. & FRANKE, W. W. 1983. Cessation of cytokeratin expression in a rat hepatoma cell line lacking differentiated functions. Nature, 305, 730-3

VERSCHOOR, J. A., BAIRD, M. S. & GROOTEN, J. 2012. Towards understanding the functional diversity of cell wall mycolic acids of *Mycobacterium tuberculosis*. Prog Lipid Res, 51, 325-39

VICENTE, M., RICO, A. I., MARTÍNEZ-ARTEAGA, R. & MINGORANCE, J. 2006. Septum enlightenment: assembly of bacterial division proteins. J Bacteriol, 188, 19-27

VILCHÈZE, C., MOLLE, V., CARRÈRE-KREMER, S., LEIBA, J., MOUREY, L., SHENAI, S., BARONIAN, G., TUFARIELLO, J., HARTMAN, T., VEYRON-CHURLET, R., TRIVELLI, X., TIWARI, S., WEINRICK, B., ALLAND, D., GUÉRARDEL, Y., JACOBS, W. R. & KREMER, L. 2014. Phosphorylation of KasB regulates virulence and acid-fastness in *Mycobacterium tuberculosis.* PLoS Pathog, 10, e1004115

VILCHÈZE, C., MORBIDONI, H. R., WEISBROD, T. R., IWAMOTO, H., KUO, M., SACCHETTINI, J. C. & JACOBS, W. R. 2000. Inactivation of the inhA-encoded fatty acid synthase II (FASII) enoyl-acyl carrier protein reductase induces accumulation of the FASI end products and cell lysis of *Mycobacterium smegmatis.* J Bacteriol, 182, 4059-67

WAGSTAFF, J. & LÖWE, J. 2018. Prokaryotic cytoskeletons: protein filaments organizing small cells. Nat Rev Microbiol, 16, 187-201

WAKIL, S. J., STOOPS, J. K. & JOSHI, V. C. 1983. Fatty acid synthesis and its regulation. Annu Rev Biochem, 52, 537-79

WANG, R., PRINCE, J. T. & MARCOTTE, E. M. 2005. Mass spectrometry of the *M. smegmatis proteome*: protein expression levels correlate with function, operons, and codon bias. Genome Res, 15, 1118-26

WELLS, A. Q. 1937. Tuberculosis in wild voles. The Lancet, 229, 1221

WERNINGHAUS, K., BABIAK, A., GROSS, O., HÖLSCHER, C., DIETRICH, H., AGGER, E. M., MAGES, J., MOCSAI, A., SCHOENEN, H., FINGER, K., NIMMERJAHN, F., BROWN, G. D., KIRSCHNING, C., HEIT, A., ANDERSEN, P., WAGNER, H., RULAND, J. & LANG, R. 2009. Adjuvanticity of a synthetic cord factor analogue for subunit *Mycobacterium tuberculosis* vaccination requires FcRgamma-Syk-Card9-dependent innate immune activation. J Exp Med, 206, 89-97

WHITE, C. L. & GOBER, J. W. 2012. MreB: pilot or passenger of cell wall synthesis? Trends Microbiol, 20, 74-9

WILK, K. E., JAMES, V. J. & AMEMIYA, Y. 1995. The intermediate filament structure of human hair. Biochim Biophys Acta, 1245, 392-6

WOLF, E., KIM, P. S. & BERGER, B. 1997. MultiCoil: a program for predicting two- and three-stranded coiled coils. Protein Sci, 6, 1179-89

WOODRUFF, P. J., CARLSON, B. L., SIRIDECHADILOK, B., PRATT, M. R., SENARATNE, R. H., MOUGOUS, J. D., RILEY, L. W., WILLIAMS, S. J. & BERTOZZI, C. R. 2004. Trehalose is required for growth of *Mycobacterium smegmatis.* J Biol Chem, 279, 28835-43

WU, K. J., ZHANG, J., BARANOWSKI, C., LEUNG, V., REGO, E. H., MORITA, Y. S., RUBIN, E. J. & BOUTTE, C. C. 2018. Characterization of Conserved and Novel Septal Factors in *Mycobacterium smegmatis.* J Bacteriol, 200

XU, W. X., ZHANG, L., MAI, J. T., PENG, R. C., YANG, E. Z., PENG, C. & WANG, H. H. 2014. The Wag31 protein interacts with AccA3 and coordinates cell wall lipid permeability and lipophilic drug resistance in *Mycobacterium smegmatis.* Biochem Biophys Res Commun, 448, 255-60

YAMADA, H., MIZUMO, S., HORAI, R., IWAKURA, Y. & SUGAWARA, I. 2000. Protective role of interleukin-1 in mycobacterial infection in IL-1 alpha/beta double-knockout mice. Lab Invest, 80, 759-67

ZHANG, L., RU, H. W., CHEN, F. Z., JIN, C. Y., SUN, R. F., FAN, X. Y., GUO, M., MAI, J. T., XU, W. X., LIN, Q. X. & LIU, J. 2016. Variable Virulence and Efficacy of BCG Vaccine Strains in Mice and Correlation With Genome Polymorphisms. Mol Ther, 24, 398-405

ZHANG, W., ZHANG, Y., ZHENG, H., PAN, Y., LIU, H., DU, P., WAN, L., LIU, J., ZHU, B., ZHAO, G., CHEN, C. & WAN, K. 2013. Genome sequencing and analysis of BCG vaccine strains. PLoS One, 8, e71243

ZOU, J. J., SCHOENHAUT, D. S., CARVAJAL, D. M., WARRIER, R. R., PRESKY, D. H., GATELY, M. K. & GUBLER, U. 1995. Structure-function analysis of the p35 subunit of mouse interleukin 12. J Biol Chem, 270, 5864-71